Università Degli Studi Di Pavia

Dottorato In Scienze Chimiche E Farmaceutiche E Innovazione Industriale
(XXXIV Ciclo)

Coordinatore: Chiar.mo Prof. Giorgio Colombo

Sensors designed for analytical determinations and practical applications

Ph.D. candidate:

Lisa Rita Magnaghi

Tutor:

Prof.ssa Raffaela Biesuz

A.A. 2020/2021

“One never notices what has been done;

one can only see what remains to be done”

Maria Salomea Skłodowska Curie

Contents

Abstract (ITA)

Lo sviluppo di array di sensori differenziali rappresenta una delle più promettenti linee di ricerca in ambito sensoristico. [1, 2] In particolare, la possibilità di coniugare misure colorimetriche, basate su immagini digitali, con un'elaborazione multivariata dei dati consente sia la misura facile, rapida ed efficace di un numero anche elevato di analiti sia il monitoraggio di processi, anche complessi. [3, 4]

Fra le diverse applicazioni, il monitoraggio della freschezza degli alimenti rappresenta una delle sfide più interessanti, sia per la complessità dei processi degradativi, che per i requisiti fondamentali richiesti per questi dispositivi e per l'impatto sociale e ambientale. Il crescente interesse dei consumatori per alimenti freschi, di qualità e senza additivi e conservanti ha spinto diversi gruppi di ricerca di tutto il mondo ad esplorare varie strategie per lo sviluppo di sensori per il monitoraggio della freschezza, comunemente chiamati *intelligent packaging* o *smart labels.* [5, 6] Fra i diversi alimenti, una particolare attenzione è stata posta sugli alimenti a base proteica. [5, 6]

Sulla base del background del gruppo di ricerca e dei risultati preliminari ottenuti nel corso della mia Tesi di Laurea Magistrale, abbiamo individuato un approccio vincente per lo sviluppo di questo genere di sensori. Come dispositivo sensibile, abbiamo utilizzato degli array di sensori generalizzati che, posti all'interno delle confezioni alimentari, mostrassero delle variazioni cromatiche nel corso della degradazione indicative della freschezza in tempo reale. L'elaborazione dei dati prevede l'acquisizione delle fotografie degli array a tempi prestabili ed in condizioni di illuminazione costanti, l'acquisizione delle terne RGB selezionando manualmente l'area del sensore e la loro successiva analisi tramite opportune tecniche chemiometriche a supporto dell'analisi visiva. A seconda delle applicazioni, sono state applicate tecniche *unsupervised* o *supervised* finalizzate allo sviluppo di modelli *soft* descrittivi o predittivi del processo di degradazione.

Basandoci sullo studio dei meccanismi chimici e microbiologici alla base della degradazione degli alimenti e delle caratteristiche dei sottoprodotti target, abbiamo costruito un panel di recettori commerciali adatti al monitoraggio della freschezza e abbiamo operato la selezione dei più efficaci direttamente con esperimenti di monitoraggio di alimenti proteici conservati in frigorifero. Abbiamo inoltre testato diversi supporti solidi, disponibili in commercio, di basso costo e di facile implementazione nel packaging.

Dopo un primo screening condotto usando come supporto solido l'Acchiappacolore©, commercializzato in Italia da Grey, [7, 8, 9] abbiamo messo a punto e brevettato [10, 11, 12, 13] una procedura per l'attacco tramite legame covalente dei recettori a diversi materiali, fra cui l'alcol etilenvinilico (EVOH), polimero plastico in uso nel packaging alimentare come film barriera, [14, 15, 16] e la carbossimetilcellulosa (CMC), derivato cellulosico usato come additivo alimentare. Entrambi questi materiali sono stati investigati come supporto solido per *smart labels*, mettendo a punto un'opportuna strategia di produzione e applicazione.

La preparazione dei sensori è stata messa a punto applicando tecniche di Disegno Sperimentale, ove possibile, e definendo in ogni dettaglio procedure di preparazione riproducibili ed affidabili. Sono state testate diverse tipologie di alimenti, fra cui carni bianche e rosse, pesci e latte, e, per ognuno di essi è stata verificata la possibilità di monitoraggio della freschezza in condizioni di conservazione quanto più possibile vicine a quelle domestiche. Ove possibile, il funzionamento del dispositivo è stato validato tramite opportune analisi strumentali di riferimento.

I risultati ottenuti nel corso della ricerca sono stati decisamente incoraggianti e rappresentano un importante passo in avanti nel campo delle *smart labels* non solo in ambito accademico ma anche industriale. Per questo motivo, abbiamo dato grande importanza non solo alla partecipazione a congressi nazionali ed internazionali e alla pubblicazione di lavori su riviste di settore ma anche al deposito dei brevetti e all'industrializzazione dei dispositivi più promettenti attraverso la costituzione della start-up innovativa SAFER Smart Labels.

Abstract (ENG)

In the sensing field, the development of differential sensors arrays represents one of the most promising trends. [1, 2] In particular, the possibility of jointly exploiting digital images colorimetric analysis and multivariate data elaboration allows the easy, fast and efficient analysis of a high number of analytes or even complex processes monitoring. [3, 4]

Among the various applications, food freshness monitoring poses an interesting challenge due to the spoilage processes complexity, the key requirements for this kind of devices and the environmental and social impact. The consumers increasing interest for fresh, high-quality, minimally processed, foods has encouraged many research groups around the world to explore various strategies for the development of freshness monitoring devices, usually called *intelligent packaging* or *smart labels*. [5, 6]

Based on our research group's background and on the preliminary results collected during my Master Degree Thesis, we identified a winning approach for the *smart labels* development. As sensing device, we used different arrays of generalised sensors that, located inside food packages, show colour transitions during food spoilage according to the actual food freshness. Data elaboration includes the first acquisition of arrays' photographs at given times and in constant lighting conditions, the following RGB triplets acquisition manually selecting the region of interest and the final multivariate analysis to support the naked-eye evaluation. Depending on the applications, both unsupervised and supervised techniques were exploited to develop either descriptive or predictive soft models for spoilage process rationalisation.

Starting from a deep investigation of the chemical and microbiological mechanisms responsible for food degradation and of the main features of target by-products, we built a panel of commercial receptors suitable for freshness monitoring and we selected the most effective ones directly performing freshness monitoring experiments on chilled stored protein foods. Furthermore, we tested different solid supports, cheap, commercially available and easy to be implemented in food packaging.

The first screening was performed using Colour Catcher©, sold in Italy by Grey [7, 8, 9]. Then we developed and patented [10, 11, 12, 13] a synthetic pathway for the covalent anchoring of the receptors to various solid materials, such as ethylenvinyl alcohol (EVOH), plastic copolymer used in food packaging industry as film barrier, [14, 15, 16] and carboxymethylcellulose (CMC), cellulose-based derivative employed as food additive. Both these materials were tested as solid supports for the *smart labels*, developing a suitable strategy for their production and application.

In any case, the sensors' preparation was developed applying Design of Experiments, when possible, and specifically defining reproducible and reliable preparation procedures. Various protein foods were tested, such as meats, fishes and milk, and for each one the devices applicability as *smart labels* in domestic conditions was verified. When possible, sensors performances were validated by independent instrumental methods.

The results obtained during this project were definitely encouraging and represents a significant step forward in the field of *smart labels* both in academia and industry. For this reason, we gave great attention, on one hand, to contributions in national and international congresses and to publications on peer review journals while, on the other hand, to patents deposition and to industrial scale-up of the most promising devices, through the constituition of the innovative start-up SAFER Smart Labels.

1. Introduction

The introductive part of this thesis has been organised in three sections. In the first section, a general discussion on sensing devices is conducted, starting from basic definition to more complex application, highlighting the key points for this project. In the second part, the topic of food freshness is discussed, considering both the chemical and microbiological mechanisms related to protein foods degradation and the most recent literature on devices for spoilage monitoring. In the last part, the aim of the project is described, summarising the general features characterising the experimental work, the key points of our freshness sensing approach and the main characteristics of the developed devices.

1.1 Sensing devices: from definitions to applications

1.1.1 Sensors: definition and classification

A chemical sensor is a device that transforms chemical information, ranging from the concentration of a specific sample component to total composition analysis, into an analytically useful signal. Chemical sensors contain two basic functional units: receptor and transducer. In the receptor, the chemical information is transformed into a form of energy which may be measured by the transducer. The transducer is a device capable of transforming the energy converting the chemical information into a useful analytical signal. [17]

Chemical sensors may be classified according to the operating principle of the transducer: [17]

- Optical devices transform changes of optical phenomena, which are the result of an interaction of the analyte with the receptor part. This group may be further subdivided according to the type of optical properties which have been applied in chemical sensors: absorbance, reflectance, luminescence, fluorescence and others.
- Electrochemical devices transform the effect of the electrochemical interaction analyte-electrode
  into a useful signal.
- Electrical devices are based on measurements, where no electrochemical processes take place, but the signal arises from the change of electrical properties caused by the interaction of the analyte.
- Mass sensitive devices transform the mass change, caused by the accumulation of the analyte at a specially modified surface into a change of a property of the support material.
- Magnetic devices are based on the change of paramagnetic properties of gas being analysed.
- Thermometric devices are based on the measurement of the heat effects of a specific chemical reaction or adsorption which involves the analyte.

Among the various sensing devices, colourimetric sensors provide desirable features for many applications because of the potential for high sensitivity, good selectivity, rapidity of analysis, portability of instrumentation and overall cost-effectiveness. [2]

Colourimetric sensors detect the change in colour of a pigment upon interaction with an analyte vapour or solution. The dyes most commonly used are solvatochromic, Lewis base sensitive, pH-sensitive, or redox reactive. This colour change can be either detected visually for rapid qualitative analysis or measured by a suitable instrument for quantitative detection. [2]

1.1.2 Selective vs. generalised devices

In addition to the previously discussed classifications, sensors are distinguished in specific or selective and differential or generalised, referring to receptors' different binding characteristics. Selective receptors exhibit high selectivity towards specific analytes, while differential ones have different binding characteristics, none of which are necessarily specific or even very selective. [1]

This difference is well depicted in Figure 1.1 reported by J. J. Lavigne and E. J. Anslyn. [1] Selective receptors mimic the lock-and-key approach to molecular recognition, typical of several biological systems, as represented in the upper part of Figure 1.1. This high specificity approach has been used successfully in some cases, but it has several drawbacks that limit its applicability to many sensing challenges. Firstly, the rational design of receptors is impractical for analytes that have not been fully characterized; secondly, the synthetic work required to actually make the receptor can be an overwhelming task in itself. Last but not least, analysing complex mixtures of analytes using a lock-and-key approach requires the design and synthesis of receptors for each component in the mixture, which is often an incredibly time-consuming undertaking. [2]

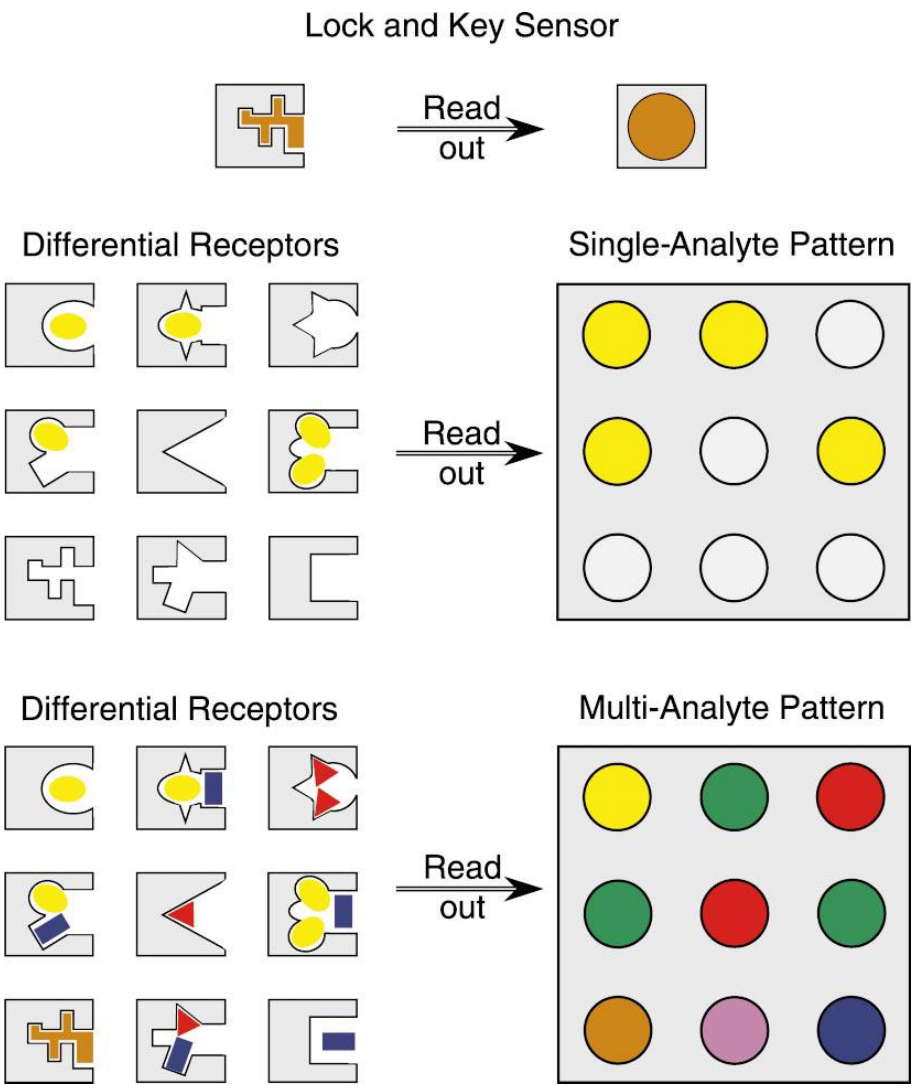

Figure 1.1: Schematic representation of receptors and transducer operating principle in selective and differential receptors. In the top part, a specific binding event (the lock and key paradigm), which exhibits a large degree of complementarity between the host and guest. In the bottom part an array of generalized receptors interacting with one or multiple analytes. [1]

Opposite, differential receptors, represented in the lower part of Figure 1.1, mimic the binding scenario used in the mammalian senses of taste and smell; they require an array of sensors to be created and a composite signal to be evaluated and interpreted, usually exploiting multivariate tools. [1] These receptors need neither to be designed nor to be highly specific for any one analyte and allow the discrimination of analytes or analyte mixtures that have not been exhaustively characterized. [2]

The last years scientific production of our research group includes several selective sensing devices for environmental and biomedical applications [18, 19, 20, 21, 22, 23, 24, 25, 26, 27]. Preliminary investigations were performed on differential sensing devices which were studied in deep during this project.

1.1.3 Multivariate approach to generalised sensors arrays

The differential sensing is accomplished using sets of cross-reactive receptors and pattern recognition algorithms to process the large amount of data generated which is not usually interpretable by visual inspection of the data set or by basic calibrations like a simple linear regression. Therefore, chemometric methods are routinely used to reduce the dimensionality of the data and present it in graphical form for visual interpretation. [2]

Among the unsupervised chemometric techniques, Principal Component Analysis (PCA) is definitely the most commonly employed for the first data rationalisation, visualisation and preliminary pattern recognition. In fact, when a visual inspection of a PCA plot detects not only close clustering between data points, representing repetitions of the same analyte class, but also good separation between data points, referring to different analyte classes, as shown in Figure 1.2, preliminary discrimination of the analytes has been successfully achieved. Furthermore, analysing the loading values for each receptor, which represent the contribution of that receptor to each PC axis, the most informative ones in the array can be identified. [2, 4]

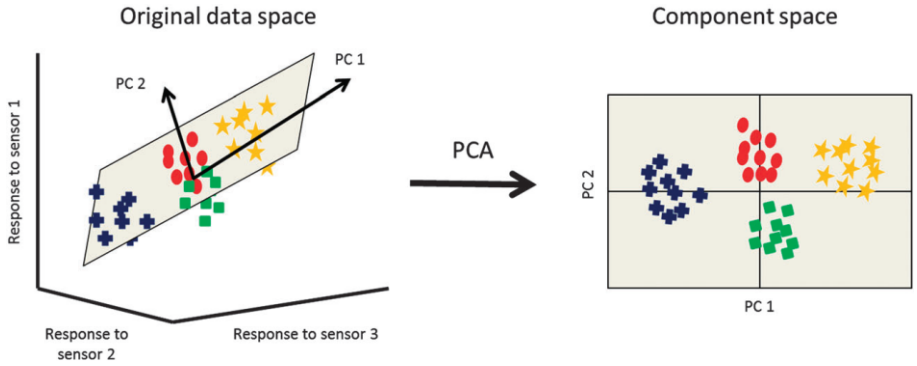

Figure 1.2: PCA displays the variance in the data set with PC 1 representing the largest variance. [2]

After the exploratory data analysis, suitable supervised chemometric tools are usually applied both for qualitative and quantitative analysis when an independent reference method is available.

In the first case, the most common supervised classification and modelling techniques employed are linear discriminant analysis (LDA), partial least squares discriminant analysis (PLS-DA), K-nearest neighbours (KNN) and soft independent modelling by class analogy (SIMCA). [4] Thanks to these methods, a mathematical rule or model is built, allowing to characterize a sample with respect to a peculiar qualitative property, which can be coded as class membership. The main importance of multivariate classification methods is given by the possibility of predicting the class membership based on some experimentally measurable predictors. It is mandatory to build and validate classification rules/models on a suitable and representative training set. [28]

In the second case, multivariate calibration models should be developed, evaluated and validated. Multiple Linear Regression (MLR), Principal Component Regression (PCR) and Partial Least Square regression (PLS) are the most commonly employed tools in sensing applications. [4] Multivariate calibration finds relationships between one or more response variables *y* and measurable predictors *x* and, also in this case, once built and validated the model on a suitable training set, it can be exploited to predict the *y* values for unknown samples. [29]

1.1.4 Sensors' development challenges

From a practical point of view, there are many challenges involved in developing an effective sensor since an ideal sensor should satisfy certain characteristics like selectivity, sensitivity, robustness, accuracy, precision, minimal error, reproducibility, linearity and others. [30] To fulfil these requirements, several features have to be defined during sensors' development.

Firstly, the best receptors have to be identified, choosing from either selective or generalised molecules, synthetic or natural and commercially available or innovative. Secondly, the ideal solid support has to be investigated, also in this case, ranging from natural or synthetic materials, commercial or innovative but also plastic-based or biocompatible. The choice of receptors and the solid support is strongly related to the linkage mechanisms exploited to fix the sensing unit to the support: the most commonly employed are ion exchange, H bond, anchoring by covalent or ionic bonds.

Once defined the main components of the device, operating features has to be defined according to the final application meant for the sensors. The best operating principle of the transducer and detection technique is selected among those listed in Section 1.1.1 while the data elaboration approach depends on the receptors selected and the final purpose. Whether selective or generalised receptors are used, and qualitative or quantitative analyses are performed, the most suitable univariate or multivariate approach to data elaboration has to be identified.

Last but not least, the preparation procedure, namely all the steps required to prepare and apply the device, and all the parameters involved have to be defined and its reproducibility, efficiency and reliability have to be verified. The winning strategy to optimise and validate the preparation procedure involves the employment of Design of Experiments, a versatile chemometric tool that allows to investigate a large number of variables of different nature and to calculate their effect on one or more selected responses of interest.

1.1.5 Colourimetric sensors arrays, digital imaging and chemometrics

To sum up the topics discussed above, colourimetric sensors arrays, in which different generalised receptors are exploited, represent one of the hottest research topics in the last years, thanks to their versatility, wide applicability and ideal features. Colourimetric sensor arrays generally provide naked eye analysis, overcoming some limitations of traditional array-based sensors, i.e., electronic-noses, such as the generally low selectivity and the need for electrochemical instrumentation and statistical tools for data analysis. [7]

As an alternative, thanks to digital imaging colourimetry (DIC), colourimetric sensor arrays provide a simple and efficient approach for the rapid detection and identification of several analytes. [3] DIC refers to a colourimetric analysis method based on digitizing images collected by some image acquisition tools such as mobile phones, digital cameras, webcams, scanners, and so on. [3] DIC is becoming a powerful, fast and low-cost tool for analysing the concentration of target analyte with visual assessment of colour changes of an obtained digital image, especially for users who want to perform colourimetric analyses with little effort, low costs and independently from the location. [3] The use of digital images could replace the naked eyes, eliminating the subjective error of the naked-eye observation and, to promote a standardized specification, different colour systems were used to define a three-dimensional coordinate space, where each colour is represented by a single point. The commonly used colour spaces (colour models) include RGB, CMYK, XYZ, L*a*b* and HSV. [3]

These three-dimensional coordinates represent the eligible input dataset for multivariate approach, both applying unsupervised and supervised techniques, depending on the type of application. The so-called Chemometrics-assisted colour histogram-based analytical systems (CACHAS), have been widely tested for various applications, applying both pattern recognition and multivariate calibration, among which food accounts for the main part, as summarised in Figure 1.3. [4]

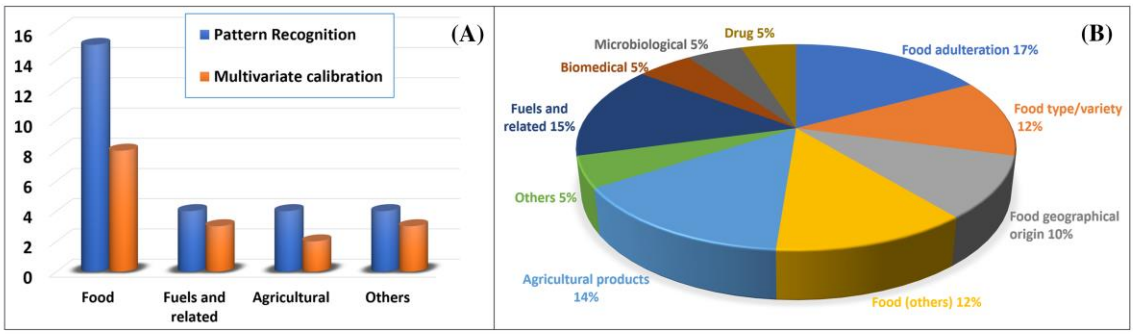

Figure 1.3: Distribution of the publications employing CACHAS by means of (A) pattern recognition and multivariate calibration techniques for analysis of (B) food, agricultural, fuels (and related), biomedical, microbiological, and drug samples [4]

1.2 Freshness of protein foods: from spoilage mechanisms to intelligent packaging prototypes

1.2.1 Chemical composition and bacterial degradation

The term “protein foods” or “high protein foods” commonly refers to protein-rich foodstuffs both of vegetable and animal origin such as meat, fish, dairy products, legumes and others. Focusing our attention on animal-based products, their spoilage mechanism is a very complex combination of processes, related to the activity of different bacteria, which, depending on food composition and external conditions, are responsible for the oxidation of glucose, lactic acid, fatty acid and, eventually, the degradation of proteins. [31] Despite the wide biodiversity of microorganisms, the spoilage process of all proteinaceous foods is similar and it is caused by one predominant group, termed the specific spoilage organism (SSO). [32]

Meat and fish spoilage process

A consortium of bacteria, commonly dominated by *Pseudomonas spp*., is in most cases responsible for spoilage of meat and fish stored aerobically at different temperatures. [33, 34] The population of pseudomonads to the arbitrary level of $10^{7\text{-}8}$ CFU/g, has been attributed to slime and off-odours formation. [33] However, in practice, both these characteristics become evident when the pseudomonads have exhausted the glucose and lactate present in meat and begin to metabolise nitrogenous compounds such as amino acids. [33]

In fact, for these foodstuffs, two different spoilage steps can be identified: early spoilage and spoilage [35]. During the early spoilage, the chemical spoilage index (CSI) is associated with the consumption of glucose, lactic acid and their derivatives and the consequent production of EtOH, 3-methyl-1-butanol, and free fatty acids, mainly acetic acid, which are definitively the dominant VOCs. [35, 36] It must be underlined that any meat or fish at this stage is still a safe product since no toxic by-products are released by bacteria. [8]. Only when no more glucose and none of its direct metabolites are left, the catabolism of proteins starts, and the production of amines and thiols is manifested as off-odours and discolouration. [35] Due to the toxicity of these classes of by-products, [37] consumption of meat at this stage could be a severe hazard. For this reason, the presence of the so-called “biogenic amines” (putrescine, cadaverine, histamine, tyramine, spermidine, spermine, and ethylamine) is an important indicator of food quality and hygiene. [8]

Milk spoilage

Spoilage microorganisms or their enzymes (e.g., oxidases, polymerases, proteases, esterases, lipases) are capable of milk components degradation such as proteins, fat and carbohydrates in order to yield compounds suitable for their growth. [38] The quality of milk for human consumption is determined by the number of bacteria present in milk at a given time: depending on the specific nature of spoilage and microbial types, the spoilage detection level can range from 10^6 to 10^8 cells/ml. [38] The bacteria mainly involved in the milk spoilage are acid-forming bacteria (Lactic acid bacteria LAB) which ferment lactose to lactic acid. [38]

In general, the pH of raw milk decreases with time due to bacterial growth, hydrolysis of fat and protein, and the production of lactic acid from lactose. [38, 39] The pH value of raw milk is around 6.5–6.7, making it slightly acidic, but during spoilage, many of the bacteria create lactic acid as a by-product, which causes a gradual and slight decrease in the pH value. [38, 39, 40] The standard for "spoiled" milk is subjective and can be interpreted in many ways. Nevertheless, there is a general consensus among consumers and manufacturers that characteristics such as off-flavours, colour changes, and loss of consistent texture can signal spoilage. [41]

1.2.2 Spoilage during distribution and the role of smart packaging

In the last years, the control of food quality has risen in its importance and it is of great concern in our daily life because of the ever-increasing demand for good quality and hygienic food products. [33, 42, 43] Consumers' requests for mildly preserved, minimally processed, easily prepared and ready-to-eat "fresher" foods, together with the globalization of the food business, and the logistics of distribution from processing centres make food quality control a significant challenge. [44, 45, 46] In this scenario, both the regulations about expiration dates and the traditional methods for determining food freshness, based on physical, chemical, microbiological measurement and human sensory evaluation, have proven insufficient and need to be updated or even replaced by rapid, low cost and non-destructive techniques to be implemented directly on food packaging. [8, 5]

The efforts made in recent years have led to a promising emerging field, comprised of innovative packaging technologies showing the potential to substitute conventional materials. [5] Traditionally, common packaging technologies consist of the use of passive, inactive, and inert barriers with the function to prevent moisture, oxygen, and contaminants from becoming in contact with the food products. On the contrary, innovative food packages, usually defined as "smart packaging", may present one or multiple active functions able to play an active role in food preservation and quality indication. [5]

Smart packaging systems are commonly divided into active and intelligent packaging. Active packaging systems contain active agents (antimicrobial, antioxidant, emitters, nanoparticles) that absorb or release ingredients into or from the packed food or environment surrounding the food package to elongate its shelf-life. On the other hand, intelligent food packaging is defined as a packaging system that can monitor the quality of food in real-time and inform food conditions to consumers by emitting a signal (colourimetric, optical, chemical, electric, etc.) in response to changes in the packaging environment and food quality in real-time. [47]

We will focus our attention on intelligent packaging, alternatively called *smart labels*, and on the most relevant sensors proposed in literature for this application.

1.2.3 Intelligent packaging systems

Since this theme has been on the front burner in the last years, a large variety of devices have been proposed so far to monitor to comply with market demand. We can include in this category mainly biosensors, electronic devices (e-nose and e-tongue) and colourimetric sensors but we will focus our attention on the last group. [9]

Intelligent packaging systems can be classified according to the target Food Quality Indicator (FQI), namely specific indicators able to indicate the quality state of food products, connected to physical or chemical modifications that occur in a certain product. Table 1.1 summarizes the main food quality indicators and their applications in real-time monitoring. [5]

Table 1.1: Summary of the main FQI and their main applications in food packages.

FQI	Working Principle	Main Applications
O_2	Luminescence-based Redox-based Colourimetric assay-based	Modified atmosphere packages
CO_2	Luminescence-based Colourimetric assay-based	Modified atmosphere packages
Humidity	Inductor and capacitor-based Colourimetric assay-based Photonic crystal-based	Modified atmosphere packages Dry food products
pH	Colourimetric assay-based Electrochemical assay-based Photonic crystal-based	Meat, fish and dairy products (aerobic storage)
Temperature	Colourimetric assay-based	Frozen food products
Nitrogen	Antibodies-based Colourimetric assay-based	Meat and fish products

Among all, those relying on pH as food quality indicator and pH indicators as the sensing unit, seem to be highly promising for intelligent packaging systems. In fact, the use of several pH indicators with bright colours, having different $\log K_a$ values to cover a wide pH range, ensures a reliable methodology for food degradation evaluation by the naked eye. [14]

The various smart labels proposed in literature in the last years for industrial application are well summarised in several recent reviews. [38, 5, 47, 48, 6, 49, 50, 51] It must be underlined that the proposed devices have some limitations in common: firstly, they are mainly developed in experimental conditions far from the actual domestic ones, using synthetic samples, enriched foods or foodstuffs stored at RT. Secondly, when one or two sensors are included in the device, naked-eye analysis is not so clear, and the final users are expected to distinguish between very similar colour shades. [7, 8, 9, 14, 15, 52]

1.3 Aim of this project

1.3.1 General features

In this scenario, we aimed to develop a panel of colourimetric sensors arrays, coupled with multivariate data elaboration, to be used as an intelligent packaging solution for real-time monitoring of protein foods freshness. To be actually suitable for industrial application, these devices must exhibit some key requirements listed below:

- Low cost
- Naked-eye detection
- Suitability for untrained operators
- Wide applicability
- Biocompatibility or compostability
- Efficiency during chilled storage
- Scalable production
- Ease to implement in packaging

To fulfil these requirements, we produced our devices exploiting commercially available and cheap materials, we tested them directly on various real samples, chilled stored in a domestic fridge, we coupled naked eye evaluation, always verified, with various chemometric tools for spoilage visualisation and modelling and, last but not least, we validated the devices' responses by independent instrumental analyses.

Despite the different receptors and solid support tested, a common approach in freshness sensing was applied, derived from a precise analysis of spoilage processes and by-products released and verified directly on real samples.

1.3.2 Freshness sensing approach

Meat and fish products

As discussed in Section 1.2.1, the early spoilage and the spoilage are characterised by the bacterial release of by-products with different acid-base behaviour and volatility. In the early spoilage, a large amount of volatile fatty acids is released in the package headspace. The most sensitive strategy to detect these molecules is using as receptor one or more pH indicators with logK_a value above 7, equilibrated at alkaline form, which show a complete transition from the alkaline to the neutral or acidic form after the reaction with these by-products. [7, 8, 9, 14, 52]

Opposite, during spoilage, thiols and amines are the main by-products. Thiols are mainly small volatile molecules that distribute in the headspace and can be detected by a specific receptor for molecules containing the -SH group. [32, 35, 45, 53] As for amines, an assortment of these molecules is produced, characterised by different dimensions, molecular weights, acid-base behaviours and, therefore, volatilities. The most significant class of amines, in terms of toxicity, is

represented by biogenic amines (BA) and, in fact, the overwhelming majority of papers on this topic have stubbornly focused on sensing BAs in the headspace. [52]

Undoubtedly, the presence of BAs in meat has been widely proven by instrumental methods [54, 55] and could be quantified by the standard methods to determine TVB-N. [56] Nevertheless, their existence in the solid does not imply finding them into the headspace: BAs are weak bases and many of them are involved in one or more protonation equilibria. Considering that only neutral molecules can pass into the headspace and in all biological matrices the pH is buffered at a value around seven, it must be observed that, at these pH values, all the amines present a positively charged protonated form and cannot pass into the vapour phase. [52] As an example, in Figure 1.4 the acid-base speciation of some BAs calculated on their logK_a values is reported. In each diagram, the grey area corresponds to the pH range in which BAs are present over 10% in the fully deprotonated and actually volatile form, which is always much higher than 7. [52]

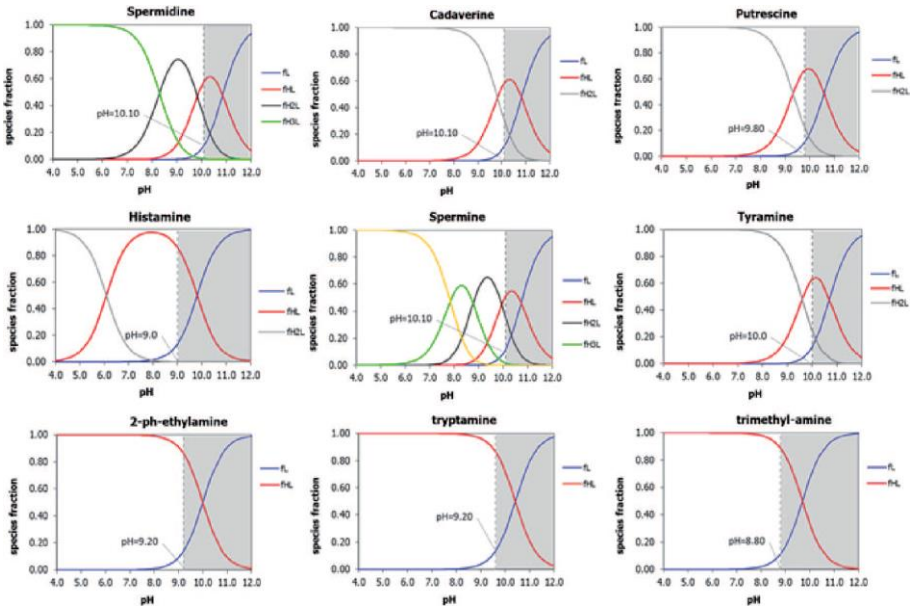

Figure 1.4: Acid-base speciation scheme of some BAs calculated from logKa values found in the literature. The vertical line corresponds with the pH values at which the fraction of the fully deprotonated form (L) is 10%. The shadow area represents the L domain, where the L fraction is above 0.1. [52]

Having this in our mind, the most sensitive strategy to detect these molecules is using as receptor one or more pH indicators with logK_a value much below 7, equilibrated at acidic form, which show a complete transition from the acidic to the neutral or alkaline form. The choice of pH indicators that turns its colour at acidic pH is fundamental to detect the very slight increase in the headspace pH related to the end of acidic by-products release and the presence of alkaline molecules in the meat or fish.

Milk

As discussed in Section 1.2.1, the decrease in the pH of raw milk with time is a direct consequence of bacterial growth, hydrolysis of fat and protein, and production of lactic acid from lactose. [15] Differently from meat and fish, milk is no longer eatable when a certain acidity threshold is crossed and the easiest technique to evaluate this parameter is represented by Soxhlet-Henkel titration, reference method for titratable acidity determination. [57, 15] Alongside the case of BAs in meat and fish, it must be underlined that also milk is a buffer solution thus a considerable amount of acid should be produced before these pH changes will be detectable and the actual pH decrease, corresponding to threshold crossing, is definitely small. Therefore, the most accurate sensing strategy to detect the threshold crossing is using as receptor one or more pH indicators with logK_a value around 7, equilibrated at alkaline form, which show a complete transition from the alkaline to the neutral or acidic form. In this case, the selection of the ideal receptor must be performed directly on milk samples during chilled storage and validated by a reference method to assure that the colour change occurs in correspondence with the threshold crossing.

1.3.3 Chemometric approach to sensors development and data elaboration

Together with the sensitive freshness sensing approach, previously described, the extensive application of various chemometric tools played a crucial role in our sensors arrays development. During this project, chemometrics was applied in two different steps of sensors development. Upstream, Design of Experiments (ED) was exploited to investigate the influent factors and their effect and to define the experimental procedures. Downstream, Multivariate Analysis was used to extract information from the raw data extracted from sensors pictures or by other measurements. All the techniques exploited are widely discussed in literature [58, 59] therefore I will not go into details of the theoretical aspects, but I will only generally describe how and when we applied these techniques.

For the multivariate data treatment, we always used the open-source program Chemometric Agile Tool (CAT), that has proved to be a robust and implementable tool, for the easy management of matrixes, even of big dimensions, clarity of output and data portability. [60]

Design of Experiments

Design of Experiments was applied several times during this project and, for brevity's sake, here only the most interesting applications are reported. It must be underlined that, in this thesis, every time ED was applied the term "optimisation" was used: from a strictly theoretical point of view, this term should be used only when quadratic models are applied and thus our use of this term is wrong. Nevertheless, being this thesis for a wider readership, we used the term "optimisation" to distinguish from the most common "one variable at time" approach.

Design of Experiments was exploited to investigate several types of variables, ranging from quantitative, to qualitative at two or more levels and mixture variables. When possible, Full Factorial Design was applied while, for more complex cases, tailored Designs were developed. Eventually, the models were always validated performing the experiments at the centre point and comparing the average experimental response, usually on three replicates, with the predicted value.

Multivariate Analysis

Multivariate Analysis tools were the eligible techniques to extract information from the data acquired during freshness monitoring experiments. As already discussed in Section 1.1.5, the colour of colourimetric sensors can be described by exploiting different colour models with different characteristics, pros and cons that I will not describe in detail.

In all the applications, we used the RGB colour model to describe sensors' colouration and the lighting conditions were kept constant and well-defined to avoid undesirable variability between the pictures. The open-source GIMP software [61] was used to acquire the RGB triplets from the .jpg files straight from the camera, manually selecting the region of interest, exploiting the "Intelligent Scissors" tool.

The RGB values matrixes, properly organised depending on the specific application, were then submitted to multivariate analysis, always applying only centring as data pretreatment, being the RGB values intrinsically scaled from 0 to 255.

The two main unsupervised techniques employed were Principal Component Analysis (PCA) and 3-Way Principal Component Analysis. PCA was used to deal with 2-dimensional dataset which means dataset made by the sensors' RGB acquired during spoilage. Therefore, PCA allows to visualise and rationalise the results of freshness monitoring experiments of replicates of the same food. 3-Way PCA was exploited to deal with 3-dimensional data set which means dataset made by the sensors' RGB (*variables*) acquired during the spoilage (*conditions*) of various foods or, in general, different types of samples (*objects*). This 3-Way PCA allows to compare the results of freshness monitoring experiments of different foods, always analysed in replicates, or on synthetic samples. It must be underlined that PCA can be applied to every dataset, of any dimension, while 3-Way PCA can be run only on completely symmetrical matrixes in which the *variables* are acquired for each *object* at each *condition* and vice versa.

When possible, also supervised techniques are exploited both for classification and multivariate calibration purposes. Among all the classification techniques, Linear Discriminant Analysis was preferred for the specific application for milk freshness prediction since it gave the best results compared to k-NN and QDA, which were also tested. As for multivariate calibration, Partial Least Square regression was preferred among the various techniques. This tool was exploited in milk freshness sensing, to build a soft model able to calculate °SH from the sensors' colour, and in pH measurement, to predict pH from the most informative sensors' colouration.

1.3.4 Summary of developed devices

To conclude, the previously described sensing strategy and chemometric tools are applied in the development of four main classes of devices, distinguished by the solid support exploited:

- Colour Catcher-based devices, described in Chapter 2
- EVOH (32%)- based devices, described in Chapter 3
- EVOH (29%)- based devices, described in Chapter 4
- CMC- based devices, described in Chapter 5

Per each solid support, the state of art is presented, the selection of the receptors and the experimental procedures are described, the results obtained are presented and conclusions are drive together with the patent deposited, the congress contributions and the published papers.

2. CC-based devices

In this chapter, the Colour Catcher-based devices are discussed. Firstly, the state of art is presented providing a brief description of the recent literature on this topic. The selection of the receptors and the experimental procedures are described; the results obtained are presented. Eventually, the main conclusions are driven, the publications on this topic are summarised and the insights for further development are discussed.

2.1 State of art

The employment of commercially available and ready to use supports represents a common trend in sensing devices development. In the last years, Colour Catcher®, distributed in Italy by Grey, in England by Dylon (Figure 2.1**a**), partners of Henkel Company, has been widely exploited as low-cost support for devices for environmental applications. [26, 27, 62, 25, 63] This support is a soft sheet of paper (Figure 2.1**b** and **c**), insoluble and stable in water solution for days, under stable conditions. It is a commercial product of the washing powder market, distributed in Italy by Grey, that exhibits sequestration properties towards molecules and ions when they are released by clothes. [25] For its peculiar property as ionic exchanger, our research group has widely exploited this material as low-cost and disposable support for several anionic dyes, like Ellman reagent [26], Eriochrome Black T (EBT) and 1-(2-pyridylazo)-2-naphthol (PAN) [27] and Alizarine Red S [25], to develop colourimetric sensors for environmental analysis.

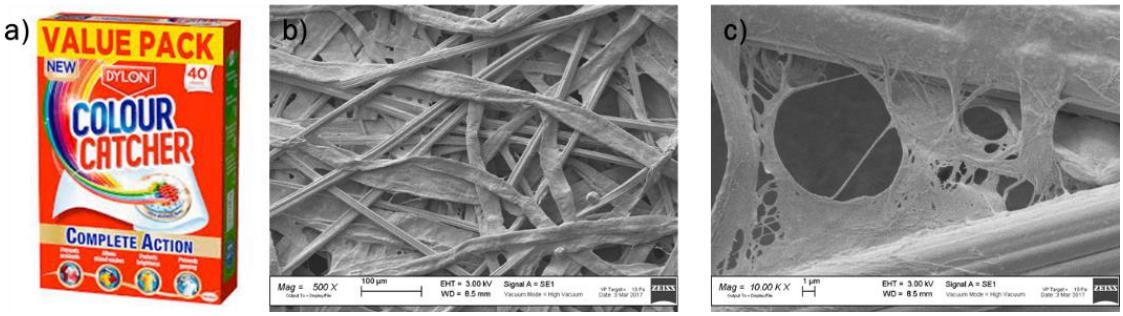

Figure 2.1: Colour Catcher® packaging (a) and SEM images at increasing magnitude (b and c).

Colour Catcher® was also used as solid support in the very first part of the development of colourimetric sensors for protein foods monitoring. [7, 8] Having selected a panel of pH indicators with logK_a values around neutrality, the amount of sorbed dye was defined, sorption kinetic and reproducibility were investigated, the miniaturisation and preparation procedure were developed. [7] The final sensors array was tested for freshness monitoring of chicken breasts samples, stored at different temperatures, both by naked-eye evaluation and chemometric-assisted modelling, and sensors attribution were validated by independent instrumental analysis. [8]

Based on the encouraging results, it seemed worthwhile to extend the application of the device to other protein foods, like fish, pork and beef, and to explore the sensitivity of the array, in terms of the minimum amount of samples suitable for freshness monitoring. [9]

2.2 Materials and methods

2.2.1 Receptors

The panel of reactive dyes used is composed of six different molecules. The first five sensing moieties are acid-base indicators, belonging to the class of sulphonphtaleins: *m*-cresol purple (**1**), *o*-cresol red (**2**), bromothymol blue (**3**), thymol blue (**4**) and chlorophenol red (**5**). The chemical formula of these dyes and their logK_a values, as reported in literature, [64, 65, 66] are shown in Figure 2.2.

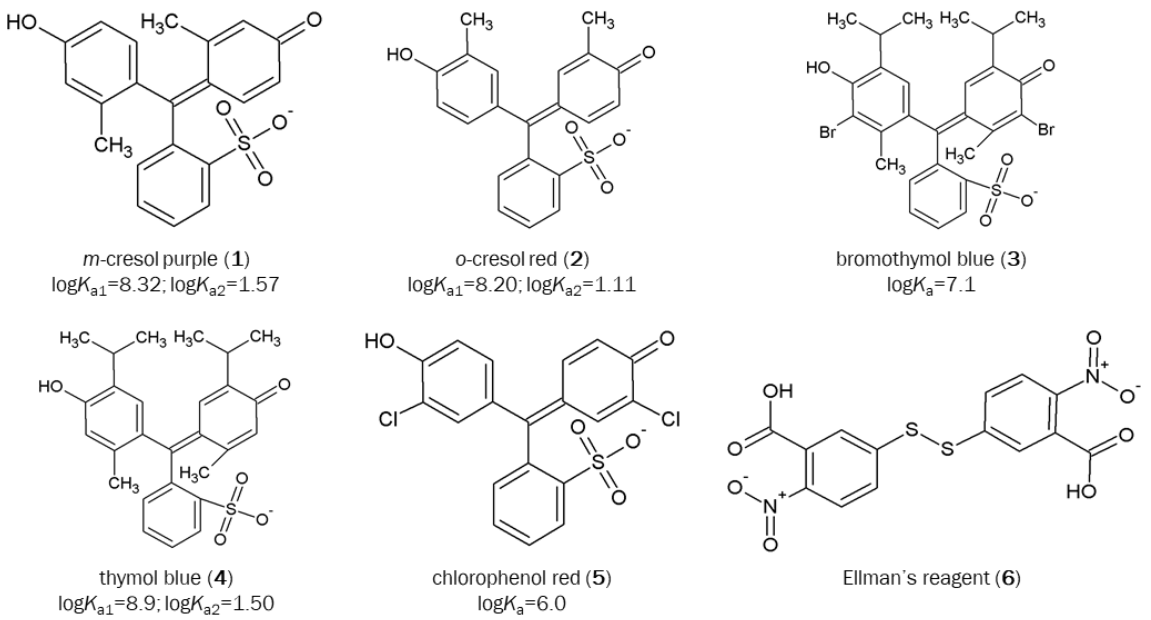

Figure 2.2: Chemical formula of the six dyes employed as sensing moieties and their log K_a values.

The sixth receptor is the 5,5'-dithiobis(2-nitrodibenzoic acid) (**6**) (DTNB), generally called Ellman's reagent: it is a molecule with two electron-deficient phenyl groups linked by a sulphydryl bridge. In the presence of thiols, it readily undergoes a trans-sulforation reaction with the reduction of the sulfhydryl group that releases a highly chromogenic product, the 5-thio-2-nitrobenzoate (TNB), with an intense absorption band at 412 nm. [53] All these molecules present one or two, in the case of Ellman's reagent, permanent negative charges and can thus be easily linked to CC® via ion exchange mechanism to obtain the final sensors.

2.2.2 Preparation of Dye-CC@

The preparation of the Dye-CC@ follows the same procedure presented in previous works. [7, 8] The CC® is cut in circles of 0.4 cm diameter of approximatively 0.0015(3) g (average weight calculated by weighting 20 CC® spots), obtained with a hole punch for paper. The acid-base form of the dye is of paramount importance since the ion exchange sorption reaction on CC® causes the dyes to change into their basic colour. Table 2.1 reports the defined conditions to prepare the final sensors.

Table 2.1: Experimental conditions for the preparation of the Dye-CC@ sensors.

Dye	Dye concentration (μM)	μL HNO_3 10^{-3} M
m-cresol purple (**1**)	7	20
o-cresol red (**2**)	4	40
bromothymol blue (**3**)	9	40
thymol blue (**4**)	8	10
chlorophenol red (**5**)	7	500
Ellman's reagent (**6**)	24	100

An amount of 1 mL of the dye solution, at the concentration reported in the second column of Table 2.1, is placed in an Eppendorf tube. After adding the proper amount of acid (reported in the third column), one CC® spot is added per each Eppendorf tube and the samples are left to equilibrate overnight at ambient temperature, on a stirring plate. Subsequently, the CC spots are dried and kept ready for use. When needed, they are placed on a stripe of Scotch 3M Magic Tape in order **1** to **6** (from left to right) and put over the tray to offer the free side to the inner part of the packaging.

2.2.3 Protein foods freshness monitoring

Experimental setup

The protein foods used for these experiments are chicken breast slices, beef slices, pork slices and codfish fillets. Food samples are purchased in a local supermarket. The trays are taken from the shelf on the day of the delivery from the producer to ensure the homogeneous lifetime of all samples. Within ten minutes, the samples are in the lab, the plastic film is removed, the stripes with sensors are placed over the tray and a new plastic film is fixed around the tray. The samples are stored at RT for 2 or 3 days, depending on the type of protein food. Figure 2.3 shows a picture of the experimental setup for different food samples.

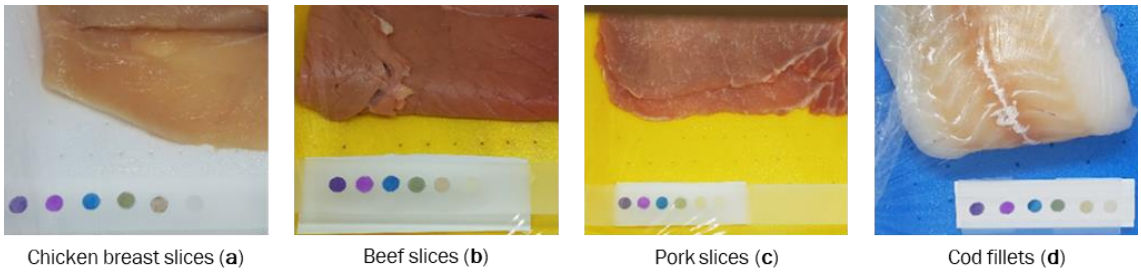

Chicken breast slices (**a**) Beef slices (**b**) Pork slices (**c**) Cod fillets (**d**)

Figure 2.3: An example of the array placed over trays containing chicken breast slices (a), beef slices (b) and pork slices (c) and codfish fillets (d).

Colour analysis & Chemometrics

At given times, photos of the array are acquired by a Smartphone Samsung Galaxy S7 in a lightbox to ensure a constant and reproducible light exposition. To extract the RGB triplets for each sensing unit during freshness monitoring, GIMP software is employed which allows defining the area of the photo to be analysed, usually the entire spot, and gives the average values of RGB triplets for each selected area [61].

A multivariate approach is employed for the data treatment. Firstly, Principal Component Analysis (PCA) is performed to model the spoilage of each food type and to evaluate sensors array sensitivity. RGB triplets are used as input dataset, applying only centring as transformation, but not scaling the data since the RGB triplets are intrinsically scaled (RGB values vary from 0 to 255). Moreover, for each food, the most informative receptors, which are the ones with the highest contributions in the loading plot, are individuated.

Then, 3-Way PCA is employed to compare the spoilage processes of different protein foods, stored in the same conditions. This data elaboration aims to demonstrate that different protein foods undergo a typical spoilage process, characterized by the same steps, in terms of nutrients attacked and by-products released; what differs among them is the spoilage timing. Again, RGB triplets of the sensors are employed as *variables*, centred but not scaled, to study the degradation process, taking into account the composition of different foods, labelled as *objects*, over time, referred to as *conditions*. For this comparison, we have to use a few tricks: firstly, the entire array is used because the selection of the most informative receptors depends on the food under investigation. Secondly, for the difference in perishability and spoilage timing, the shortest timeline must be used, which is in this case the codfish fillets timeline.

The open-source Chemometric Agile Tool (CAT) program is employed both for PCA and later for 3-Way PCA analysis [60], as for other chemometric tools employed in this thesis project.

Training and test sets

To model each spoilage process, the training set is composed of five samples of similar mass per food type. Therefore, the input matrixes have 18 columns (3 RGB indexes per 6 Dye-CC@ sensors) and respectively 40, 50 and 70 rows in the case of chicken breast slices, beef and pork slices and codfish fillets (8, 10 or 14 acquisition times per 5 replicates). The average masses of foods are reported in the first column of Table 2.2. The average mass amount is selected as the most commonly used in the supermarket for each type of food. The training set is also used in the comparison of spoilage processes by 3-Way PCA.

To validate the PCA models, two samples of similar mass amounts, reported in the second column of Table 2.2, are projected as external test set.

Table 2.2: Mass of samples of different foods, employed as the training and test set.

Food type	Training set Av. mass (g)	Test set Av. mass (g)
*Chicken breast slices (**a**)*	333(18)	338(3)
*Beef slices (**b**)*	157(6)	160(4)
*Pork slices (**c**)*	138(5)	141(4)
*Codfish fillets (**d**)*	200(6)	215(7)

Dataset for sensitivity test

Once developed and validated the models, an evaluation of sensors array sensitivity is performed for meat samples. In fact, from everyday life experience, we noticed that the amount of meat in the selling tray could widely vary, depending on the type of meat, the quality and even the supermarket. When decreasing the amount of sample on the same tray, the analytes dilute progressively and it is relevant to estimate the lowest amount of meat or fish that produces an equal colour evolution. For this reason, decreasing fractions of meat mass used for the model development (100%; 50%; 25%; 12.5% and 6.75%), are sealed in the common tray and analysed following the procedure explained before. In this case, PCA input matrixes have 18 columns (3 RGB indexes per 6 Dye-CC@ sensors) and respectively 36 rows (6 acquisition times per 6 decreasing fractions of meat).

2.3 Results and discussion

2.3.1 Dye-CC@ sensors array colour evolution over protein foods

Being our final aim a smart label for naked-eye reading, the first step of the monitoring always consists of a naked-eye analysis of the colour evolution, shown by the sensors array during the degradation process. As an example, in Figure 2.4, the colour evolution of sensors array during spoilage monitoring, when exposed over one of the samples in the training set, per each food type, is displayed.

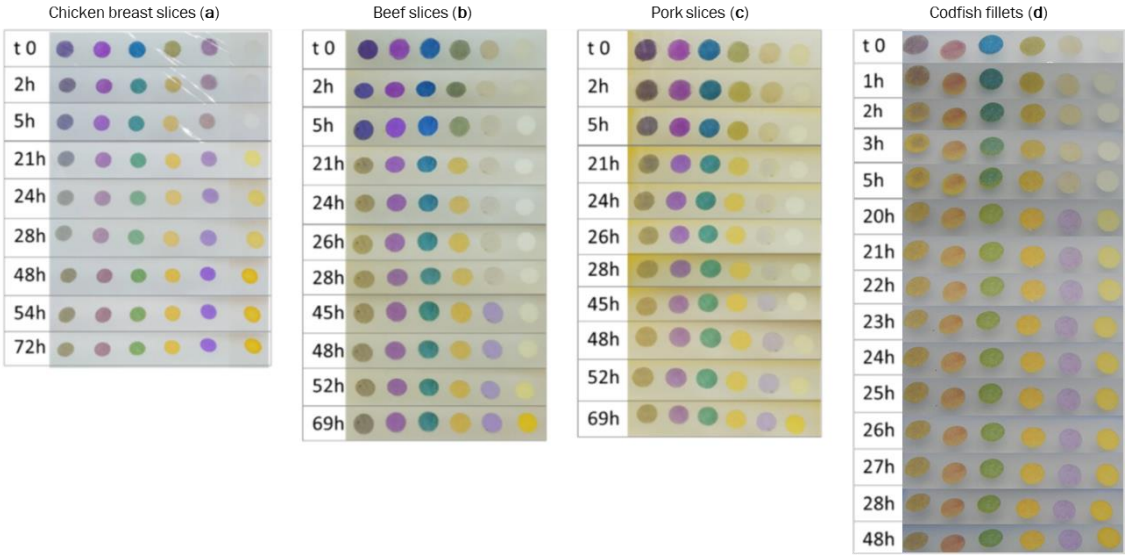

Figure 2.4: Dye-CC@ sensors array colour evolution over chicken breast slices (a), beef slices (b), pork slices (c) and codfish fillets (d), stored at RT.

At first glance, we can notice that similar behaviour is detected in all the food, despite the different timelines, because, as already highlighted, the same spoilage process is occurring. In particular, two clear steps can be identified. Firstly, the evolution of alcohol and acids arises from sugar catabolism by bacteria, as discussed above, detected by pH indicators that turn their colour from the violet/blue basic form into the yellow acidic one. For this purpose, four dyes (from **1** to **4**) with logK_a higher than seven have been included in the array.

When sugars and their derivates are eventually depleted, the bacteria attack the proteins, releasing amines and thiols. Both these classes of molecules are definitively unwanted and dangerous. However, they differ widely in their volatility, especially in the buffered pH typical of the biological matrix: in fact, amines are present in their protonated form, and can pass into the headspace only at an insignificant amount, as discussed before; on the other hand, thiols are neutral and volatile molecules that are present in great abundance in the headspace. For this reason, during the second step, only a slight increase in the pH is expected, while thiols can be easily detected. Chlorophenol red-CC@ (**5**), whose logK_a = 6.0, exposed in the acidic yellow form, shows an appreciable colour

change to violet (basic form) in all the samples, at different times. However, the other receptors with higher logK_a, even if in their acidic colour and form, remain unchanged.

Meanwhile, Ellman's reagent (**6**), which has been included in the array to detect the presence of thiols, reacts in all the foods tested but with very different timings: in chicken and fish samples, intense yellow colour is observed after 21 h, while in beef and pork meat, the detection occurs only after 48 h.

To rationalize these preliminary findings and to model the entire spoilage process, PCA is performed on all the RGB data of the samples, as described in Section 2.2.3.

2.3.2 Spoilage modelling by PCA models

As explained before, PCA is employed in this case to visualise and model the degradation process of different meats, without claims of classification. After model development, two independent samples of similar mass are used as test set to be projected in the score plot to preliminarily validate the model.

Figure 2.5 shows the score plots on the first two components for all the foods, reporting both the training set (coloured spots) and the test set (blue squares).

Figure 2.5: The score plots of the PCA models on the first two principal components, built on the training set and validated by projection of the test set, for chicken breast slices (a), beef slices (b), pork slices (c) and codfish fillets (d). The ellipsoids are exclusively added as a simplification of the different groups: SAFE, WARNING and HAZARD.

In all the score plots of the first two components, which explain a variance from 95.1% to 72.7%, a clear evolution is observed during monitoring and the samples form quite evident clusters.

For meat samples (Figure 2.5 from **a** to **c**), three groups can be detected, called SAFE, WARNING and HAZARD. In the case of chicken breast slices (Figure 2.5**a**), the clusters are well separated while, for beef (Figure 2.5**b**) and pork slices (Figure 2.5**c**), the WARNING and HAZARD zones are partially overlapped. In general, samples in the first hours are located in the lower-left part of the score plot; then, during the spoilage process, the samples move to the right side. As a consequence, we can assess that, here, the first component explains the spoilage, but PC2 is still the fundamental component for the separation of the clusters. During the WARNING step, the score of PC2, generally increases, while it decidedly decreases for samples that fall into the HAZARD zone.

The score plot of codfish fillets (Figure 2.5**d**) is utterly different compared to other meat, a diversity much more evident in these graphs rather than in the spot evolution of Figure 2.4. It is common knowledge that fish is an extremely perishable food and its spoilage process is very fast, even if stored in appropriate conditions. The PCA model on the RGB triplets makes it manifest: only two clusters are identified, corresponding to SAFE and HAZARD zone, without any intermediate step. In

particular, the SAFE cluster is in the lower part of the graph; as the spoilage goes on, the samples move to the higher part of the graph, i.e., at the high value of PC2, which definitively give a significant contribution to the cluster separation.

As for model validation, we can observe that all the samples in the test set are located in the right cluster, near training samples with similar times. This evidence is essential both to assure the reproducibility of the sensors' responses and to validate the models developed by PCA.

After the development and validation of PCA models, a preliminary selection of the most informative dye for each food can be performed, analysing the colour evolution and the loading plots, reported in Figure 2.6.

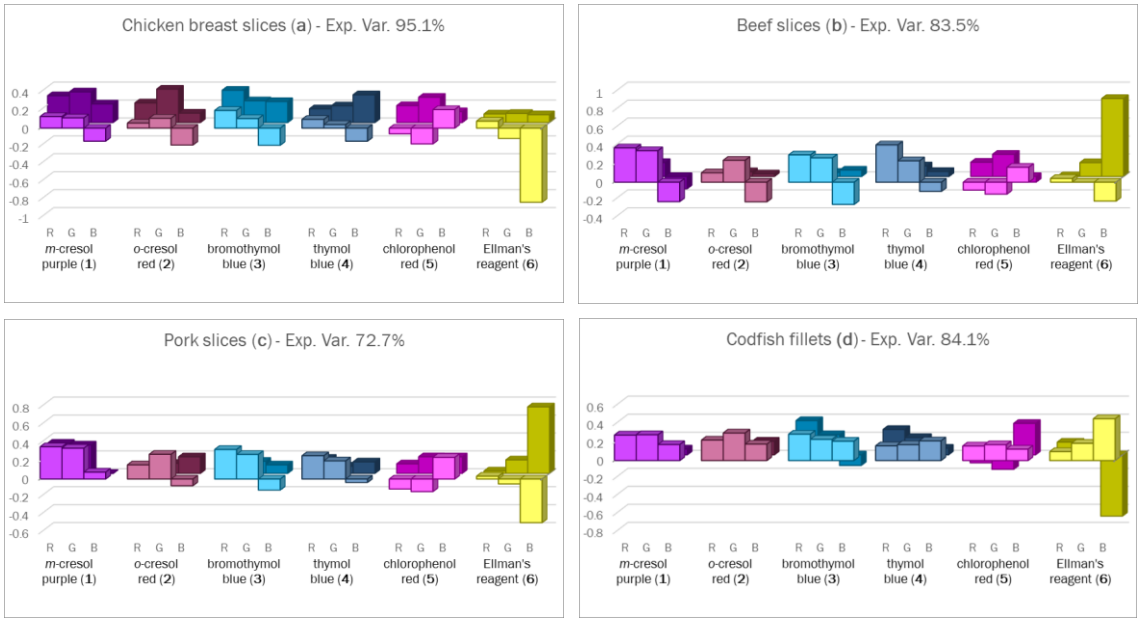

Figure 2.6: The loading values of the PCA models on PC1 (in foreground) and PC2 (in background) for chicken breast slices (a), beef slices (b), pork slices (c) and codfish fillets (d).

The most informative receptors are the ones that give the highest contribution in the loading plots. It is interesting to note that some dyes are significant for each food, such as bromothymol blue (**3**) and Ellman's reagent (**6**); conversely, the other pH indicators can be informative or not, depending on the type of food.

2.3.3 Sensitivity evaluation

The goal of these experiments is to estimate the minimum mass of food characterized by an evident and similar colour evolution as that previously observed in training and test samples. Such estimation cannot be performed by a simple naked-eye analysis of the colour evolutions with sufficient certainty, but PCA can be useful, at least for a preliminary estimation. For this reason, for each food, we run PCA on the RGB triplets of sensors array exposed over subsamples of reduced mass, as reported in Section 2.2.3, and we analyse the resulting score plots, which are reported in Figure 2.7. The loading plots are reported in Figure 8.1 in Appendix III: Loading and score plots.

Figure 2.7: The score plots of the PCA models on the first two principal components, built on the sensitivity dataset for chicken breast slices (a), beef slices (b) and pork slices (c).

The trays with similar mass to training and test samples, i.e., 100%, are considered the reference tray and their degradation process was used as the “reference pathway” in the score plot. We notice that, down to a certain amount of mass, colour evolution overlaps that of the reference. It means that samples in the score plot fall near the reference ones, following the same “pathway”.

Below this mass value, the colour evolution significantly differs, resulting in a different allocation in the score plot. In Figure 2.7, for each food, only reference points and samples above critical mass are highlighted and labelled with the corresponding reference mass percentage; the critical mass percentage corresponds to 50% in the case of chicken and pork, and 25% for beef. As previously argued, this is not an absolute value since the analyte concentration depends on both the amount of food and headspace volume. For this reason, the sensitivity of the array, in terms of meat mass, can be sharply improved by using smaller trays with lower volume.

2.3.4 Spoilage processes comparison by 3-Way PCA

To conclude, we perform a comparison between the spoilage processes of the different protein foods, as described above, using 3-Way PCA. Five samples for each food under investigation, already defined as training set, are employed as *objects* (20 in all), the acquisition times are identified as *conditions* (six in all), while the RGB triplets of the entire array are used as *variables* (18 in all).

Table 2.3: Cumulative % variance explained after unfolding.

Mode	PC1	PC1&2
Objects	37.92%	63.93%
Variables	42.67%	69.40%
Conditions	53.56%	84.49%

The variance explained by the [2 2 2] Tucker3 model (50.81%) is somehow lower than the lowest variance explained by the PCA on the three unfolded matrices (63.93%). This means that part of the information contained in the dataset is lost when the common degradation process is taken into account. In our opinion, this loss is mainly due to the significant difference in spoilage duration for the considered types of meat. As already observed, after 48 h, codfish fillets were in an advanced state of decomposition, while spoilage was still ongoing for the other samples. This information is inevitably lost by analysing the common degradation. Nevertheless, the percentage of explained variance is fully satisfying, considering the high variability of the system, the types of data employed for the analysis, and the necessary reduction in the data set.

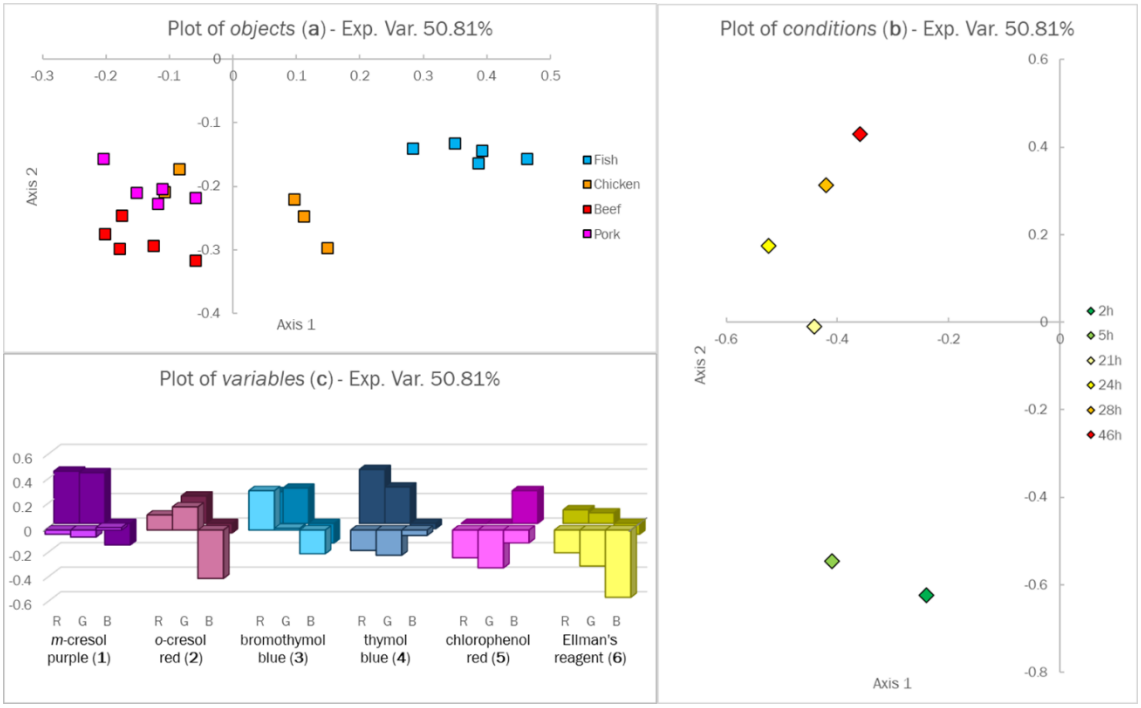

Figure 2.8: The loading plots of the 3-Way PCA model on the first two axes: objects (a), conditions (b) and variables (c) loading plots. In graph c, the variables loadings on Axis 1 are in foreground, the ones on Axis 2 in background.

Moving to results interpretation, in the plot of *objects* (Figure 2.8**a**), different protein foods are separated along the *x*-axis (Axis 1). In particular, fish samples occupy the right part of the graph; chicken samples are in the centre, while beef and pork are on the left. These last two have slightly different loading values on the *y*-axis (Axis 2), but they are too near to be distinguished with sufficient certainty. Comparing this graph with the plot of *variables* (Figure 2.8**c**) we can conclude that the most informative receptors in *objects* separation are the ones with a higher loading value on Axis 1, in the foreground, and therefore are *o*-cresol red (**2**), bromothymol blue (**3**) and Ellman's reagent (**6**). This conclusion is in good agreement with what was previously observed during the analysis of each degradation: both these pH indicators, namely (**2**) and (**3**), do not turn completely to an acidic colour. However, they show a different behaviour according to the food under investigation. At the same time, Ellman's reagent (**6**) reacts at different times depending on the type of meat or fish.

In the plot of *conditions* (Figure 2.8**b**), times follow a well-defined trajectory from negative to positive loadings along Axis 2: the very first degradation steps are located in the lower part of the graph, while, during the spoilage process, the loading values on Axis 2 increase. Again, from the plot of *variables* (Figure 2.8**c**), the most critical receptors in conditional separation are identified, based on the value of the loading on Axis 2, in the background, which are *m*-cresol purple (**1**), bromothymol blue (**3**) and thymol blue (**4**). We compared the spoilage profile of protein foods with widely different compositions and perishability. Even if the number of *conditions* is reduced, even if we are well aware that these results are only an indication, they are profoundly coherent and have a precise sense.

First, the order of perishability is maintained as fish, chicken, beef and pork (Figure 2.8**a**) secondly, the *conditions*, even if compressed, clearly show a clear difference between the early stage and the subsequent stages.

2.4 Conclusions

The Dye-CC@ sensors array was developed and tested on various protein foods as “proof of concept” to demonstrate not only that our monitoring strategy can be applied to a wide variety of protein foods but, even more, that the array can be adapted and optimized for the food of interest by selecting the proper receptors.

It must be underlined that, to develop the prototype of an intelligent label, suitable for industrial production and large-scale application, this solid support would no longer be suitable, both for its physical characteristics and for the reversible linkage mechanism that allows dye release when in contact with solutions or even humidity.

For this reason, new materials were tested as solid supports, both plastic-based, described in Chapter 3 and 4, and bio-based, described in Chapter 5, and covalent linkage between solid phase and receptors was investigated.

To conclude, the results discussed in this Chapter, together with those reported in my Master Degree Thesis, were presented as oral communication at the “International Symposium on MEtal Complexes” (Florence, 2018), at the “XXVII Congresso della Divisione di Chimica Analitica” (Bologna, 2018) and at “Merck Young Chemists’ Symposium” (Rimini, 2019). The publication of these results on Journal of Agricultural and Food Chemistry (ACS) [7, 8] and on Foods (MDPI) [9] was possible only after the first patent deposition in March 2019 [10].

3. EVOH (32%)-based devices

In this chapter, the EVOH(32%)-based devices are discussed. Firstly, the state of art is presented providing a brief description of the recent literature on this topic. The selection of the receptors, the physicochemical and optical characterization and the experimental procedures are described; the results obtained are presented. Eventually, the main conclusions are driven, the publications on this topic are summarised and the insights for further development are discussed

3.1 State of art

In the field of sensing devices for food application, a large number of linkage mechanisms are commonly exploited and, in particular, immobilization strategies are preferred mainly on inorganic supports, [67, 68, 69] filter paper [31] and different mixtures of cellulose derivatives and polyethylene glycol (PEG) [44, 70]. All these reversible anchoring strategies have in common the risk of dye release, as already argued in the case of CC®, that would provoke unwanted changes like coloured spots, drops or halos on food samples or even health risks for the consumers. To avoid dye release and related issues, we investigated the possibility of covalently binding our receptors to a polymeric plastic-based material, an approach seldomly followed in literature. [14]

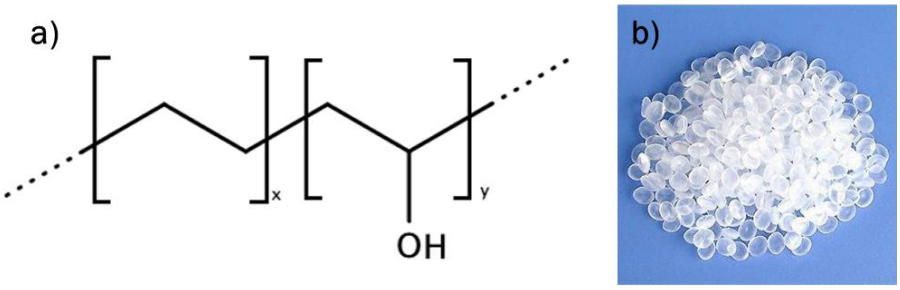

Figure 3.1: Chemical structure of EVOH (a) and EVOH beads, as commercially available.

As polymeric support, ethylene vinyl alcohol copolymers (EVOH), composed of hydrophilic (vinyl alcohol) and hydrophobic (ethylene) segments in a single macromolecule (Figure 3.1**a**), were selected. These unique copolymers are biocompatible, insoluble in water and have excellent barrier properties, which made them suitable for food packaging films, especially for those foods that are sensitive to certain levels of oxygen or carbon dioxide. [71, 72] The presence of quite reactive hydroxyl moieties in polymer structure makes EVOH an excellent candidate for covalent anchoring of different classes of molecules, as reported in recent papers by our and other research groups [71, 72, 73] and, eventually, EVOH-based materials are usually extrudable, which, in principle, is much more convenient for a practical application. [74, 75, 76, 77, 78]

This copolymer is commercially available in form of beads (Figure 3.1**b**) with different monomers ratios, ranging from 29% to 44% of ethylene content. Among all, EVOH (32% ethylene) is the most commonly employed in food packaging and was first selected as solid support for our sensing device,

to facilitate the industrial scale-up and the implementation in typical food packaging, significantly reducing the costs.

The Dye-EVOH@ sensors array was synthesised, characterised from a physicochemical and analytical point of view and tested for freshness monitoring of protein foods both solid, like chicken breast slices and codfish fillets [14], and liquid, like whole, semi-skimmed and skimmed milk. [15]

3.2 Materials and methods

3.2.1 Receptors

The panel of reactive dyes used is composed of six different pH indicators, belonging to the class of sulphonphtaleins: *m*-cresol purple (**1**), *o*-cresol red (**2**), bromothymol blue (**3**), thymol blue (**4**), chlorophenol red (**5**) and bromophenol blue (**6**). The chemical formula of these dyes and their logK_a values, as reported in literature, [64, 65, 66] are shown in Figure 2.2.

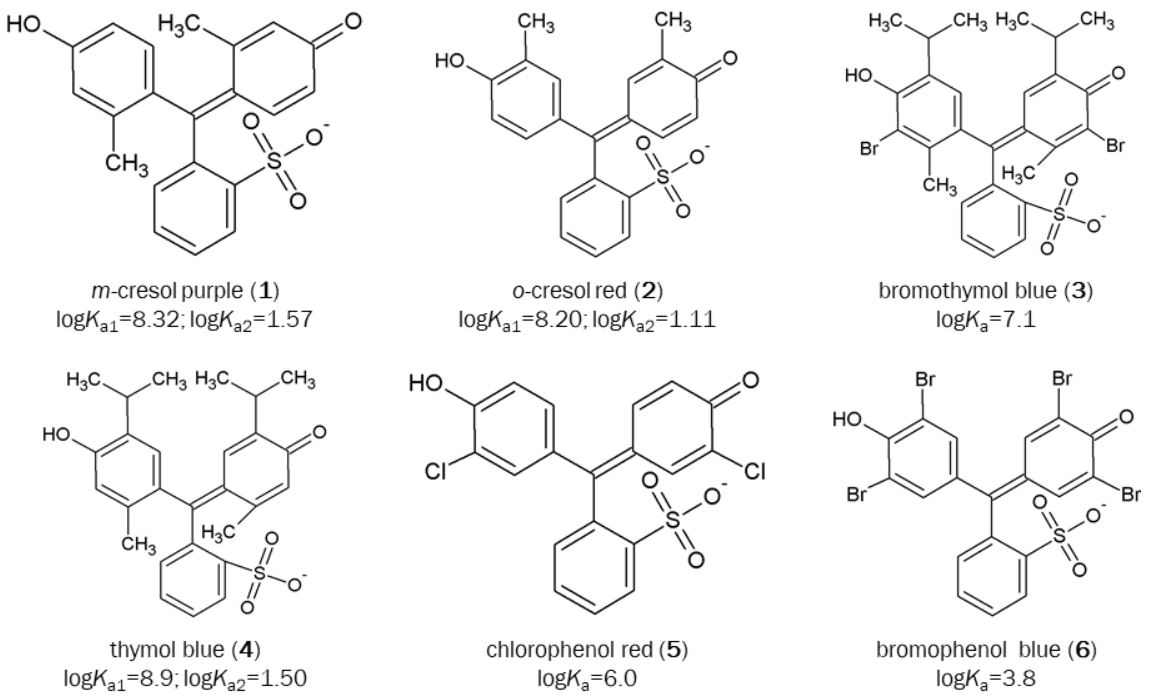

Figure 3.2: Chemical formula of the six dyes employed as sensing moieties and their log K_a values.

All these molecules present one sulphonic group, not involved in the protonation and deprotonation equilibria, that can be exploited to link the reactive dyes to the polymeric support, following the synthetic pathway described below.

3.2.2 Synthesis and pressing of Dye-EVOH@

The synthesis of the reactive polymeric material, internationally patented, [10, 11, 13, 12] consists of two reaction steps: (i) dye activation through chlorination and (ii) polymer functionalization by nucleophilic substitution.

In the first step, a selected dye is dissolved in $SOCl_2$ and the mixture is heated at reflux for some time; the chlorinated dye can be stored by leaving it under the $SOCl_2$ solution for 18 h before use. The $SOCl_2$ excess is evaporated just before the second step.

In the second step, EVOH is poured in DMA at 110 °C, under stirring and a nitrogen atmosphere, and solid NaOH is added as the catalyst. When the polymer is completely dissolved, a freshly prepared sulfonyl chloride DMA solution is added dropwise to the polymer solution. After 4 h at 110 °C, the reaction mixture is cooled at room temperature and then in an ice bath. The functionalized polymer is precipitated in cooled DCM under stirring, and the temperature is kept around 0 °C because the process is strongly exothermic; this procedure helps to increase the final yield.

The solid material is then filtered under vacuum, washed with DCM to remove the unreacted dye excess, and left to dry overnight. A further drying step is conducted under vacuum at 60 °C for 24 h in an Abderhalden apparatus.

After the synthesis, the functionalized polymer comes in the form of small blocks of irregular shapes (Figure 3.3**a**) and needs to be pressed to have the final sensitive films (Figure 3.3**b**), from which the miniaturised sensors (Figure 3.3**c**) are obtained.

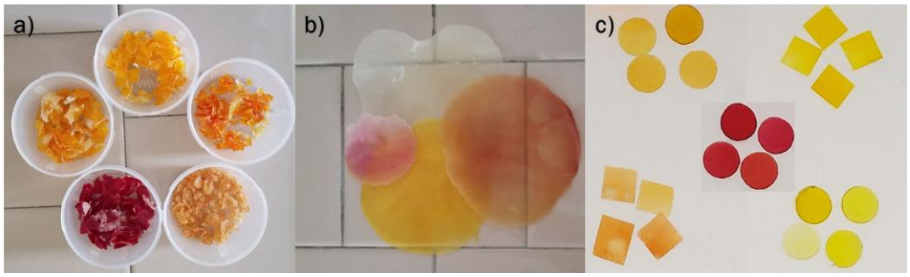

Figure 3.3: Dye-EVOH@ small blocks after synthesis (a), thin films after pressing (b) and miniaturised sensors of different shapes (c).

A dual heated plate manual press is employed, and pressing parameters are optimised by Full Factorial Experimental Design 2^4, using EVOH functionalised with thymol blue, (**4**)-EVOH@. The experimental matrix is reported in Table 8.1 in Appendix IV, where the variables taken into account are time (x_1), pressure (x_2), polymer mass (x_3) and temperature (x_4) and the responses analysed are film quality (y_1) and n° sensors obtained (y_2).

3.2.3 Dye-EVOH@ characterization

The characterization is performed on different samples of each synthesized Dye-EVOH@. Apart from DSC analyses, all of the other measurements are taken on the final films, obtained after pressing.

Physicochemical measurements

Differential scanning calorimetry (DSC) analyses are performed by heating the samples (~5 mg) from −80 to 250 °C at a rate of 5 °C/min under a N_2 atmosphere. For selected samples, a second heating−cooling cycle is appended to verify the reversibility of the processes.

Fourier transform infrared (FT-IR) spectra are acquired using a spectrometer equipped with an attenuated total reflectance (ATR) sampling accessory by co-adding 32 scans in the range from 4000 to 650 cm^{-1} with the resolution set at 4 cm^{-1}.

Elemental analyses of the films are performed by energy dispersive X-ray analysis (EDX) by an X-max 50 mm^2 probe connected to an EVO MA10 scanning electron microscope (SEM). The films are supported on graphite bi-adhesives fixed on Al stubs and subsequently transferred into the SEM chamber. EDX measurements are performed under ultrahigh vacuum at a working distance of 8.5 mm and with an electron generation voltage of 20 kV.

The thickness of three samples for each Dye-EVOH@ film is measured by a profilometer, applying 2 mg force.

Optical measurements

UV−vis spectra of Dye-EVOH@ films are recorded at different pH, after equilibration for 24 h in 0.1 M HNO_3, phosphate buffer at pH 7.00, and 0.1 M NaOH and compared with the corresponding spectra of the dye dissolved in aqueous solutions (~10 μM).

3.2.4 Dye-EVOH@ sensing performances

Apart from the physicochemical characterization of sensitive films, sensing performances of Dye-EVOH@ sensors array need to be evaluated before testing the device for real samples freshness monitoring. For these experiments, miniaturised sensors, circular (diameter 0.5cm) or squared (0.5x0.5 cm) of Dye-EVOH@ of approximately 0.0025(2) g (average weight calculated by weighting 20 Dye-EVOH@ sensors), cut with a hole punch for paper of different shapes, are used.

Reproducibility

Reproducibility of the final sensors, which includes, in this case, the variability of both the functionalised material and the pressing procedure, is firstly investigated. In our research, the term "reproducibility" could refer also to the image acquisition method, but this parameter was already studied in previous researches [7] and is kept unchanged. To evaluate sensors reproducibility, for each Dye-EVOH@, 10 independent sensing spots, obtained from different films, are equilibrated by 2-hours immersion in 10 mL of proper solutions, as reported in Table 3.1, and analysed by photo acquisition. The reproducibility is assessed, based on the RGB values collected and compared.

Table 3.1: Equilibration conditions used to test sensors reproducibility for each Dye-EVOH@

Dye-EVOH@	Equilibration A	Equilibration B	Equilibration C
1-EVOH@	HNO_3 0.1M	NaOH 0.1M	Phosphate buffer pH=7
2-EVOH@	HNO_3 0.1M	NaOH 0.1M	Phosphate buffer pH=7
3-EVOH@	HNO_3 0.1M	NaOH 0.1M	---
4-EVOH@	HNO_3 0.1M	NaOH 0.1M	Phosphate buffer pH=7
5-EVOH@	HNO_3 0.1M	NaOH 0.1M	---
6-EVOH@	HNO_3 0.1M	NaOH 0.1M	---

Colour change kinetic in solution and vapour

As for colour change kinetic, from preliminary experiments, 2-hours immersion in 1 mL of 0.1M solutions of strong acids or bases per sensor is sufficient to assure homogeneous colouration of sensors and this methodology is thus followed to equilibrate the sensors before every analysis.

To better estimate colour change rate at lower analyte's concentrations, kinetic experiments in solution are performed; dilute solutions of nitric acid and sodium hydroxide are used to test extremely acidic and basic pH while phosphate buffer is used to mimic neutral buffered biological matrices, like milk. Dye-EVOH@ sensors array, made of 6 miniaturised sensors, one per pH indicator, are immersed in 10 mL of different solutions, always previously equilibrating the sensors at the proper pH, acidic or basic depending on test solution pH. A summary of kinetic experiments in solution is reported in the first four rows of Table 3.2.

Being the final aim of these sensors the detection of acidic or basic volatile by-products, also kinetic in the vapour phase is tested. Acetic acid is used to simulate volatile acid by-products released during spoilage process, ammonia to mimic volatile bases, following the procedure already used for Dye-CC@ sensors optimization. [7] Opposite, phosphate buffer is used as "blank analysis" to evaluate the stability of sensors colours, in absence of specific acidic or basic analytes. Dye-EVOH@ sensors array is equilibrated at the proper pH, as discussed before, and located in a sealed box (V=1 L) over 20 mL of various test solutions. A summary of kinetic experiments and "blank analyses" in the vapour is reported in the last eight rows of Table 3.2

Table 3.2: Test solutions and equilibration conditions for kinetic experiments in solutions (rows 1-4), in vapour (rows 5-10) and for blank analysis (rows 11-12).

	Name	Test solution	Equilibration conditions
1	*Solution A*	HNO_3 0.01M	NaOH 0.1M
2	*Solution B*	NaOH 0.01M	HNO_3 0.1M
3	*Solution C*	Phosphate buffer pH=7	NaOH 0.1M
4	*Solution D*	Phosphate buffer pH=7	HNO_3 0.1M
5	*Vapour A*	CH_3COOH 0.1M	NaOH 0.1M
6	*Vapour B*	CH_3COOH 0.01M	NaOH 0.1M
7	*Vapour C*	CH_3COOH 0.001M	NaOH 0.1M
8	*Vapour D*	NH_3 0.1M	HNO_3 0.1M
9	*Vapour E*	NH_3 0.01M	HNO_3 0.1M
10	*Vapour F*	NH_3 0.001M	HNO_3 0.1M
11	*Blank Analysis A*	Phosphate buffer pH=7	NaOH 0.1M
12	*Blank Analysis B*	Phosphate buffer pH=7	HNO_3 0.1M

3.2.5 Protein foods freshness monitoring

Experimental setup

First, the sensors are equilibrated at the proper pH by being immersed for 2 h in 10 mL of 0.1 M HNO_3 or 0.1 M NaOH, to be able to detect both acidic and basic by-products released during spoilage process. Subsequently, the Dye-EVOH@ spots are dried, placed on a stripe of Scotch 3M Magic Tape, and taped over the selling tray.

The chicken breast slices and codfish fillets are purchased in a local supermarket. The trays are taken from the shelf, a few minutes after the preparation to ensure a homogeneous lifetime of all samples. Within 10 min, the samples are in the lab, the plastic film is removed, the stripes with sensors are placed over the tray, and a new plastic film is fixed around the tray. The samples are stored at RT for 2 days.

The same procedure is applied for the analysis of both protein foods except for the preliminary equilibration step: for chicken breast slices, dyes **1**–**5** are dipped in a basic solution and only dye **6** is immersed in an acidic solution; for fish samples, also dye **5** is previously equilibrated at acidic pH.

Colour analysis & Chemometrics

At given times, photos of the array are acquired by a Smartphone Samsung Galaxy S7 in a lightbox to ensure a constant and reproducible light exposition. To extract the RGB triplets for each sensing unit during freshness monitoring, GIMP software is employed [61], as previously commented.

Principal component analysis (PCA) is performed on RGB triplets, only centring the data because these indexes are intrinsically scaled from 0 to 255, to rationalize the colour evolution and visualize spoilage process.

The open-source Chemometric Agile Tool (CAT) program was employed for PCA [60].

Training and test sets

For each protein food, the training set consists of two samples used to monitor the spoilage process at room temperature (around 22 °C). Therefore, the input matrixes have 18 columns (3 RGB indexes per 6 Dye-EVOH@ sensors) and respectively 22 and 18 rows in the case of chicken breast slices and codfish fillets (11 or 9 acquisition times per 2 replicates). The average masses of foods are 300(15) g for chicken breast slices and 206(13) g for codfish fillets, both amounts in good agreement with what is argued in Section 2.2.3.

Then, for each food, one new sample of similar mass (309 g of chicken breast meat and 220 g of codfish fillets) is projected as external test set.

Validation by independent instrumental analyses

For each test sample, almost the entire quantity is left in the tray with the array and kept as a reference, while the rest is divided into subsamples for instrumental analyses, performed to corroborate the assumptions derived from PCA.

Each analysis is performed in triplicate, and each sample is split into two parts, one for the solid analysis and one for the identification of the volatile in the headspace.

For the analysis of the solid, we follow the procedure suggested in the literature [55, 54]. In the case of chicken meat, each piece of meat is cut in a blender, 4 g is extracted with a homogenizer and 5% TCA and then centrifuged. On the contrary, for codfish fillets, the first part of the procedure is slightly modified to improve amine extraction. 20 g is chopped, using a common kitchen mixer, left to equilibrate in 20 mL of 10% TCA at the proper temperature, and centrifuged.

For both protein foods, after the centrifugation step, the supernatants are collected and purified on SPE STRATA X cartridges (conditioned with 4 mL of methanol followed by 4 mL of Milli-Q water). Then, 2 mL of the sample (supernatant), with a pH adjusted to around 11 upon addition of 200 µL of 28% NH_4OH, is passed through the cartridges. After sample loading has reached completion, cartridges are rinsed with 2 mL of a MeOH/H_2O mixture [5:95 (v/v)] and dried under vacuum to remove the excess of water. Analytes are eluted from the STRATA X sorbents with 2 + 2 mL of a solution of a methanol/acetic acid mixture [99:1 (v/v)]. The eluting solution is dried with nitrogen gas, and the residue is collected with 2 mL of 0.1 M HCl, filtered, and injected into the LC-MS/MS instrument.

On the contrary, for volatile analysis, samples (~5 g) are placed in the vials equipped with the solid phase, kept under the same storage conditions of samples, and then analysed. The analyses are performed directly using headspace solid phase microextraction (HSSPME) coupled with gas chromatography and mass spectrometry (GC/MS). The following experimental parameters are used: polydimethylsiloxane/divinylbenzene (PDMS/DVB) fibre, 65 µm; extraction temperature, 35 °C; extraction time, 20 min; desorption temperature, 250 °C; desorption time, 4 min. GC/MS analysis is performed on a single-quadrupole GC/MS system equipped with a MS capillary column [30 m, 0.25 mm (inside diameter), 0.25 µm film thickness], with helium as the carrier gas at a constant flow rate of 1.0 mL/min. The injector temperature is set at 250 °C, and the injector is operated in splitless mode. The oven is held at 35 °C for 2 min, and then the temperature is increased to 80 °C at a rate of 5 °C/min, ramped to 300 °C at a rate of 10 °C/min, and finally held at 300 °C for 2 min. The GC transfer line temperature is 270 °C.

All mass spectra are acquired in electron impact mode (ionization energy of 70 eV and source temperature of 250 °C), with spectra acquired in full scan mode (mass range of m/z 15−650 and scan speed of 832 amu/s). Assignment of chemical structures to chromatographic peaks is based on the comparison with the databases for the GC/MS NIST Mass Spectral Library (NIST 08) and the Wiley Registry of Mass Spectral Data (8th edition). Xcalibur MS Software version 2.1 (Thermo Scientific Inc.) and the AMDIS Program for the automated deconvolution of mass spectra are used for GC/MS data interpretation.

3.2.6 Milk freshness monitoring

Experimental setup

In the case of milk, microbial spoilage process results in an increasing acidity therefore Dye-EVOH@ sensors are tested to select the most informative one, which is, in principle, the one that turns its colour when milk is no longer eatable. The sensors are equilibrated at basic pH by 2-hours immersion in 10 mL NaOH 0.1 M and, after the drying step, they are ready to be employed for milk monitoring.

Different types of fresh milk, whole, semi-skimmed or skimmed, are purchased in a local supermarket the day of the dairy's delivery to ensure a homogeneous lifetime of all samples and monitor the entire degradation process. Within ten minutes, the bottles are carried in the lab and divided into subsamples of 20 mL in sterile plastic containers, in which the Dye-EVOH@ sensors array is dipped.

Colour analysis & Chemometrics

At given times, during storage at a different temperature, photos of the array are acquired by a Smartphone Samsung Galaxy S7 in a lightbox to ensure a constant and reproducible light exposition and sensing spots RGB triplets are extracted using GIMP software [61].

Being the sensors dipped in milk, they must be separated from the white liquid to acquire the photographs. For facilitating this step, all the sensors are poked with a needle (Figure 3.4**a**) and a thread was put through the hole of each sensor (Figure 3.4**b**). When dipping the sensors in the milk, both the thread ends are kept out of the liquid (Figure 3.4**c**) and used to collect the sensors to acquire the photographs. The sensors are fixed in the thread in order **1** to **6** starting from the left.

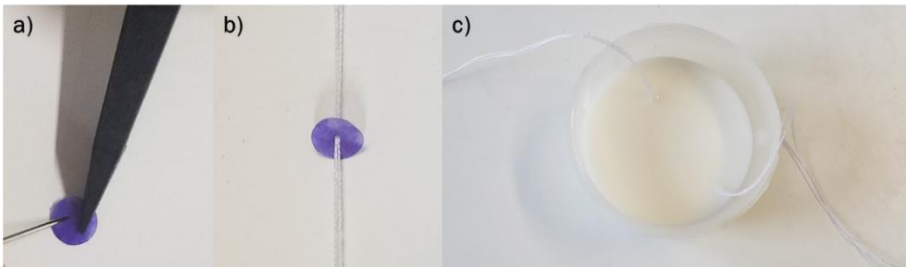

Figure 3.4: Example of one sensor immobilization to facilitate separation from milk: poking with a needle (a), immobilization using a thread (b) and immersion in milk (c).

Different chemometric techniques are employed in the data treatment. Firstly, Principal Component Analysis, PCA, is performed on RGB triplets of the most informative sensors, only centring the data, to visualise the degradation process.

Then, 3-Way PCA is employed to compare the spoilage processes of whole, semi-skimmed and skimmed milk. The aim of this is to demonstrate the versatility of the sensing device, which could be applied to different milk types with no need for further modification. Following the same approach of Section 2.2.3, RGB triplets of the sensors are employed as *variables*, centred but not scaled, to study

the degradation process, taking into account the different types of milk, labelled as *objects*, over time, referred to as *conditions*.

Eventually, a very first attempt of classification is performed on the RGB indexes of the most informative sensors, using Linear Discriminant Analysis, LDA. Two classes are identified, SAFE for fresh milk suitable for human consumption and HAZARD for uneatable milk, according to their location in PCA score plot. The pictures of Dye-EVOH@ sensors array at different times compose the overall data set; the training set is built using 60 samples whose attribution is sure while the remaining 84 samples are used as a test set.

The open-source Chemometric Agile Tool (CAT) program is employed for data elaboration [60].

Training and test sets

For each type of milk, the training set consists of two samples stored at RT (around 22°C) and two in the fridge (around 4°C). Therefore, the input matrixes have 9 columns (3 RGB indexes per 3 Dye-EVOH@ informative sensors) and 48 rows (9 acquisition times at 22°C per 2 replicates and 15 acquisition times at 4°C per 2 replicates).

Validation by independent analyses

Several techniques are employed to validate the degradation models obtained from Dye-EVOH@ sensors colours.

Firstly, at each test time, milk pH is measured by the mean of a pH meter. Secondly milk acidity, after 24-hours storage at 22°C and 4°C, is determined by titration, according to the Soxhlet-Henkel methodology with slight modifications: 50 mL of milk sample is added of 2 mL of phenolphthalein solution (1% w/v in ethanol) and the mixture is titrated with standardized 0.1 M NaOH until the colour change to pink. The determination is performed on three replicates and the results are expressed as °SH/100 mL, calculated as reported in Equation 3.1 [15, 40, 57, 79]

$$°SH = \frac{M_{NaOH} \times V_{vir} \times 2}{0.25M}$$

Equation 3.1: °SH calculation

Eventually, we perform an instrumental analysis to identify volatile by-products in the headspace at each degradation step, similarly to other research groups in the literature. [80] This analysis is done using 10 mL samples stored for 24 hours at 22°C and 4°C, in triplicate per each milk type, following the same procedure used for solid protein foods (Section 3.2.5).

3.3 Results and discussion

3.3.1 Pressing optimisation by Full Factorial Design 2^4

The same synthesis is successfully performed for all of the dyes, and no differences are observed among the dyes. Moreover, yields are sufficiently high for our purpose in all of the syntheses, with more than 4.5 g of the functionalized polymer obtained after the last drying step.

The optimisation of the pressing procedure, performed using Full Factorial Design 2^4, is crucial to obtain suitable sensitive films. In Table 3.3 the parameters under investigation and the corresponding upper and lower levels are reported.

Table 3.3: Level definitions for the parameters under investigation

Parameter		Upper level (+)	Lower level (-)
Time (s)	x_1	60	30
Pressure (psi)	x_2	2000	1000
Polymer mass (mg)	x_3	300	150
Temperature (°C)	x_4	180	160

After parameters selection and level definition, we identified a suitable response that represents the characteristics of the obtained film and the possibility to use it as source of sensing units. Since a representative measurable parameter is not available, we select two different responses. The first one (Y_1) is the judgment of film quality on a scale from 1 to 5, always given blindly by the same trained judge. The second one (Y_2) is the number of usable sensing spots (diameter 0.5 cm) obtained by the film. This Experimental Design aims to increase both the responses to obtain films with better quality and more productive, in terms of sensors derived. The general model equation, calculated for both responses, is reported below while the experimental matrix and the responses under investigation are reported in Table 8.1 in Appendix IV.

$$Y = b_0 + b_1X_1 + b_2X_2 + b_3X_3 + b_4X_4 + b_{12}X_1X_2 + b_{13}X_1X_3 + b_{14}X_1X_4 + b_{23}X_2X_3 + b_{24}X_2X_4 + b_{34}X_3X_4$$

Equation 3.2: General model equation for Full Factorial Design 2^4

In Table 3.4, the main statistics for the models are reported. The models have in common both the maximum leverage value in the experimental domain (0.6875) and the number of degrees of freedom (5), being these figures determined by the number and location of the experimental points. As for response Y_1, % explained variance is quite low due to by the subjectivity of the response parameter employed, specifically a judgment given by one single judge. Opposite, for response Y_2, better results are obtained in terms of % explained variance.

Table 3.4: Statistics for pressing model

Statistic parameters	Value	
	Y_1	Y_2
Maximum leverage	0.6875	0.6875
Degrees of freedom	5	5
% Explained Variance	34.15%	86.39

In Figure 3.5 the coefficients plots for both responses are shown while, in Table 3.5, the numerical values, semi-amplitude of confidence intervals and significance are listed. Analysing the coefficients calculated for the first response, film quality, shown in Figure 3.5**a**, the significant parameters are highlighted: the polymer mass has a positive effect on response Y_1 and has to be set at upper value to improve film quality. Conversely, temperature has a negative effect on the response, therefore, has to be put at lower value. Eventually, the interaction between time and polymer mass presents a significant positive effect on the response Y_1 thus, setting polymer mass at upper value, also time has to be set at the highest value. As for the second response, N°sensors, the only significant parameter is polymer mass, with a positive effect, thus it has to be set at the upper value. (Figure 3.5**b**) As a general comment, the two responses under investigation are correlated since from better films a higher number of sensors is obtained; as a consequence, the two coefficients plots are very similar and the variables have the same effect on both responses.

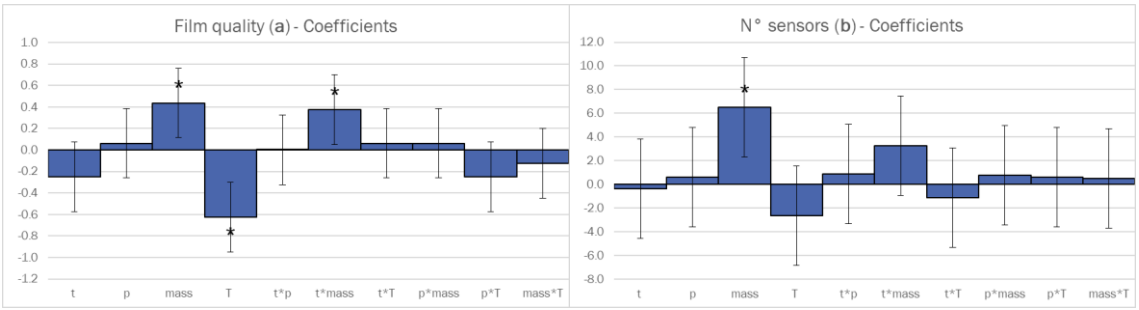

Figure 3.5: Coefficients plot for Y_1, film quality, (a) and Y_2, N°sensors, (b).

Table 3.5: Coefficients and significance (* p≤0.05, ** p≤0.01, *** p≤0.001) calculated for Y_1, film quality, and Y_2, N°sensors. Conficence interval is reported in the headers between brackets.

Coefficients		Y_1		Y_2	
		Value (±0.32)	Significance	Value (±4.2)	Significance
	b_0	3.56		16.9	
Time (t)	b_1	-0.25		-0.4	
Pressure (p)	b_2	0.06		0.6	
Pol. mass (mass)	b_3	0.44	*	6.5	*
Temperature (T)	b_4	-0.63	*	-2.6	
*t*p*	b_{12}	0.00		0.9	
*t*mass*	b_{13}	0.38	*	3.3	
*t*T*	b_{14}	0.06		-1.1	
*p*mass*	b_{23}	0.06		0.8	
*p*T*	b_{24}	-0.25		0.6	
*mass*T*	b_{34}	-0.13		0.5	

For both responses, three replicates at the point [0 0 0 0] are prepared and the average value, standard deviation and confidence interval (CI) at 95% confidence level are reported in Table 3.6. In both cases, the predicted value fits into the confidence interval, thus the models are validated.

Table 3.6: Model validation by three replicates at point [0 0 0 0]

	Y_1	Y_2
Average value	3.2	17
Standard deviation	0.3	4
Upper bound CI	3.9	26
Lower bound CI	2.5	8
Predicted response	3.6	17

Since the aim of the design is to increase both responses, analysing the coefficients plots (Figure 3.5), we selected the pressing parameters reported in Table 3.7. Since pressure was never found significant, the value was set at the upper value since it was easier to be set in the dual heated plate manual press employed.

Table 3.7: Optimized parameters for Dye-EVOH@ pressing.

Parameter		Optimized level
Time (s)	x_1	30
Pressure (psi)	x_2	2000
Polymer mass (mg)	x_3	300
Temperature (°C)	x_4	160

3.3.2 Characterization: physicochemical measurements

DSC analyses are performed on the irregular blocks obtained after the synthesis and the profiles per each Dye-EVOH@ sensor are reported in Figure 8.10 in Appendix V. The calorimetric profile shows for all of the samples, after a second-order transition (evident for only some of them), an endothermic melting peak upon being heated. The process is fully reversible, as evidenced in the cooling part of the calorimetric curve. In Table 3.8, the onset and peak temperature for the melting process of all of the investigated polymeric materials are reported.

The thermal behaviour of Dye-EVOH@ affects the temperature required for pressing the functionalised polymers. To obtain the final sensitive films, melting temperature has to be reached but not exceeded, in fact, for **4**-EVOH@, 160°C is set as optimized temperature for pressing (see Table 3.7) which corresponds to the peak temperature. Based on this evidence, all Dye-EVOH@ polymers are pressed at a temperature equal to or slightly higher than the peak temperature, reported in the third column of Table 3.8.

Table 3.8: Onset, peak and pressing temperatures for the melting of each Dye-EVOH@.

Dye-EVOH@	Onset T (°C)	Peak T (°C)	Pressing T (°C)
***1**-EVOH@*	125.69	152.17	160
***2**-EVOH@*	152.00	170.16	170
***3**-EVOH@*	147.50	170.68	170
***4**-EVOH@*	137.85	160.19	160
***5**-EVOH@*	148.74	168.43	170
***6**-EVOH@*	145.59	167.97	170

The remaining part of the characterization is performed on the films obtained after pressing, following the procedure described in Section 3.3.1.

FT-IR spectra of the pH indicator powders, starting EVOH copolymer, and Dye-EVOH@ films are reported in Figure 8.11 in Appendix V. The same signals characterize the spectra of EVOH before and after the functionalization; the only difference is the presence of a band at 1615 cm^{-1}, due to the formation of a sulphonic ester from the reaction between the receptor's sulphonic group, previously activated, and the polymer's hydroxyl group, demonstrating the successful modification of the starting copolymer.

Electron images of the films are acquired, and elementary analysis is performed. In Figure 3.6, the SEM images acquired on the surface of the polymeric film at increasing magnitudes, in secondary electron mode, and the results of EDX analysis are displayed in the case of **3**-EVOH@. The SEM images show a compact and homogeneous surface, with no pores and no holes on it, while from the elemental analysis, it is possible to evidence the presence of S in the sample. Because S is present only in the receptor's structure, from the atomic per cent of this element (~0.3%) we can estimate the millimoles of the receptor, successfully bonded to the polymer matrix, per sensor (~0.2 µmol per

spot of 0.5 cm diameter). Because the weight of one spot is~2.5 mg, this means a roughly estimated capacity of 0.1 mmol g^{-1}.

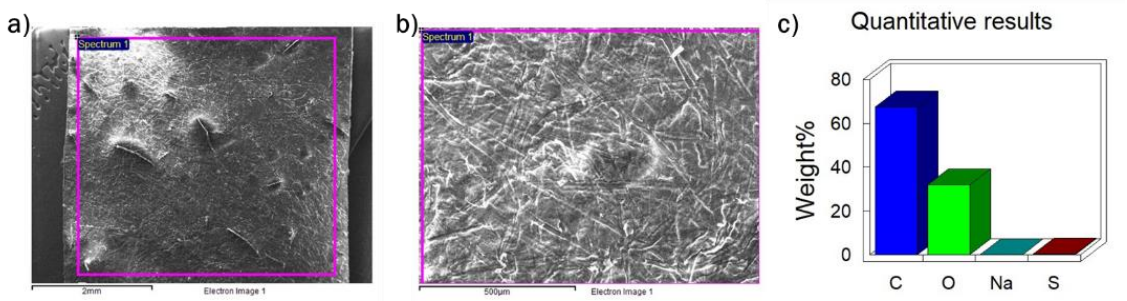

Figure 3.6: SEM images of 3-EVOH@ at different magnifications (a,b) and quantitative results of elemental analysis of 3-EVOH@ (c).

Eventually, the film thickness is measured multiple times on samples functionalized with different receptors. This physical parameter is crucial in the development of new sensors. On one hand, thinner sensors ensure both higher sensitivity and homogeneity in colour shade and colour changes. On the other hand, the thickness must be reproducible to guarantee the same sensing performances for all of the spots and to minimize the differences among the sensors. From these measurements, we observe that no significant differences were highlighted, in films containing different pH indicators, and 168(11) µm is found to be the medium thickness value. This result is satisfying in terms of both thickness and reproducibility.

3.3.3 Characterization: optical measurements

The optical behaviour of Dye-EVOH@ films is first investigated by UV–Vis spectroscopy. Rectangles (2 cm × 2.5 cm) are cut and employed to register UV-Vis spectra. For each receptor under investigation, we want to compare the optical behaviour of the molecule in an aqueous solution and after functionalization at different pH values. In Figure 3.7, the results for all dyes in solution (~10 µM) and Dye-EVOH@ are displayed: UV–Vis spectra and corresponding photographs after equilibration at acidic, basic, and neutral pH.

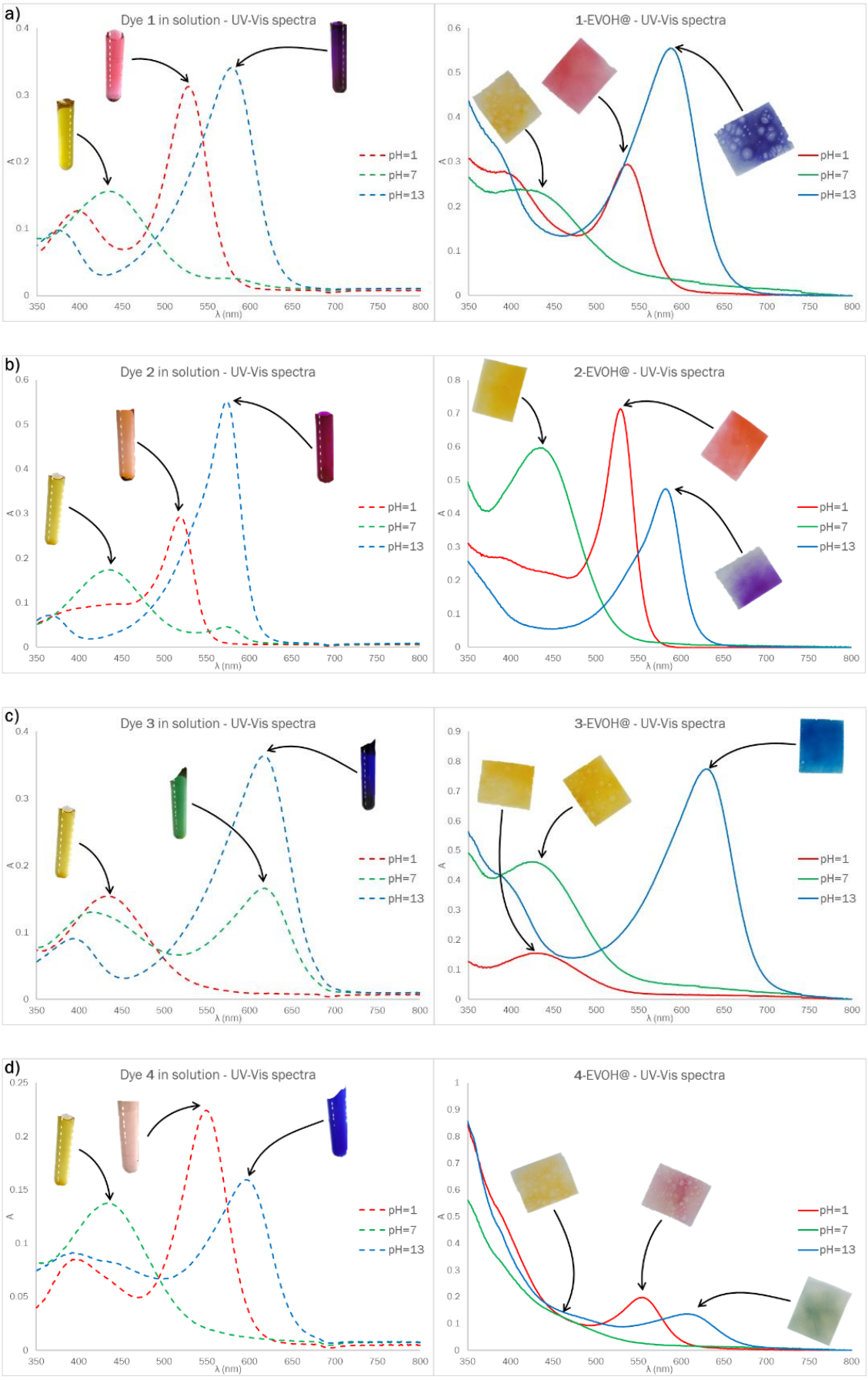
a)
Dye 1 in solution - UV-Vis spectra
1-EVOH@ - UV-Vis spectra
b)
Dye 2 in solution - UV-Vis spectra
2-EVOH@ - UV-Vis spectra
c)
Dye 3 in solution - UV-Vis spectra
3-EVOH@ - UV-Vis spectra
d)
Dye 4 in solution - UV-Vis spectra
4-EVOH@ - UV-Vis spectra
pH=1
pH=7
pH=13
A
λ (nm)

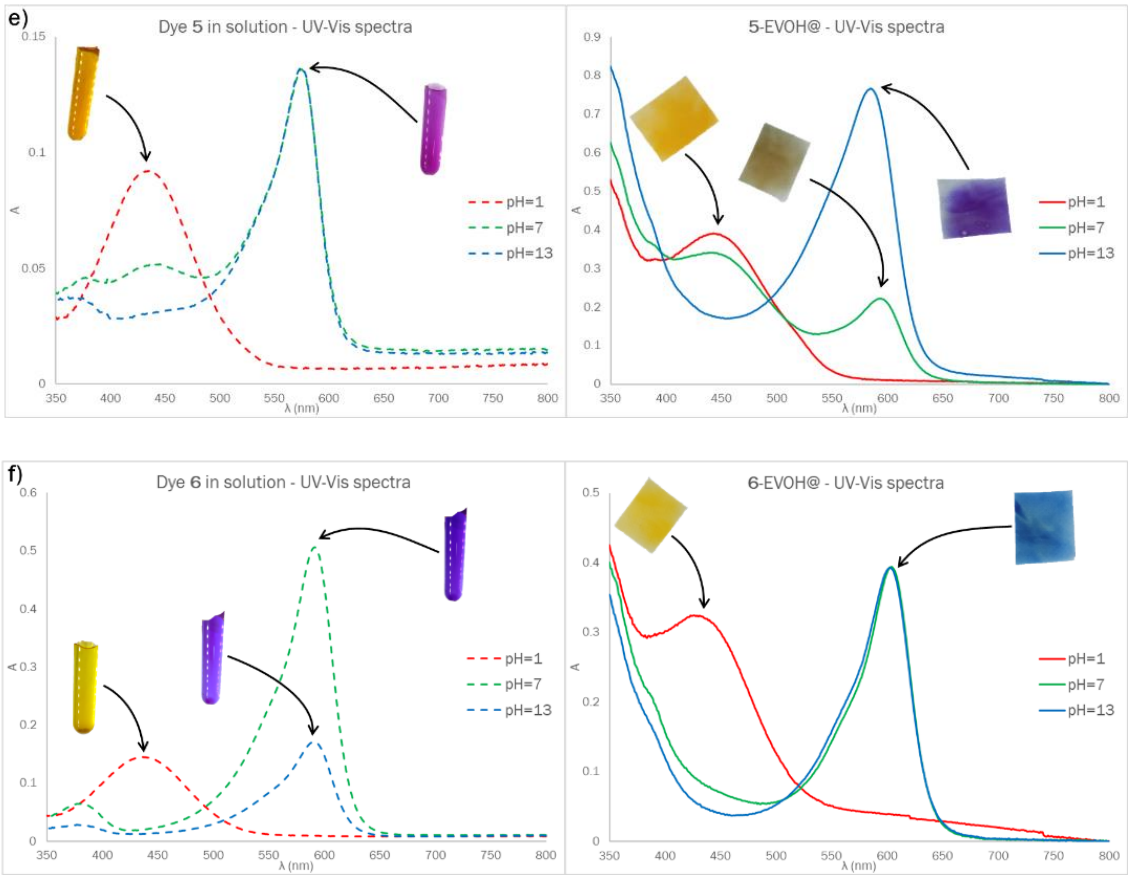

Figure 3.7: UV–Vis spectra and corresponding photographs of a ~10 µM dye solution (graphs on the left, dashed lines) and Dye-EVOH@ (graphs on the right, solid lines) in order from dye 1 to 6.

Many conclusions can be drawn from these experiments. First, the maximum of the absorbance band, for acid and alkaline forms of the indicators, is located at a very similar wavelength in solution and films and only a small shift is observed. Consequently, from the naked-eye analysis of the photographs, the colours of solutions and films are similar at extremely acidic and alkaline pH. The spectra present a different absorbance value at the maximum due to the different amounts of dye in the solution and film, but this is not relevant for the qualitative investigation of the optical behaviour of the polymers.

As for the samples at pH=7, the optical behaviour of dye n°3 and n°5 is particularly interesting. These pH indicators have logK_a values respectively of 7.1 and 6.0 and the UV-Vis spectra in solution confirm this evidence. Opposite, after covalent binding to EVOH, completely different behaviour is observed. For dye n°3, the main absorbance peak was the one related to the acidic form, while the peak at 628 nm was not even visible and, indeed, the sensing film is completely yellow. For dye n°5, both the peaks are visible, with similar absorbance value, and the film shows a brownish colour, from the mixture of yellow and violet forms. Because, after the preparation, a sufficiently long time is set to ensure the equilibration of the reactive material with the buffered solution, the only possible explanation for this behaviour is that, together with the functionalization, a shift toward higher logK_a

values occurs, with respect to the values of the receptors in solution [64, 65], as suggested by other research groups. [81, 82, 83, 84]

A rough estimation of logK_a values shift is about 1 pH unit but this point will be further discussed in the next Chapter. To avoid misunderstandings, the apparent logK_a values after functionalisation, even if not systematically calculated but only experimentally estimated, are labelled as logK_a' to be distinguished from protonation constant in solution.

This aspect is of paramount importance in the choice of the Dye-EVOH@ sensors selected for building the sensing device since it is expected that different receptors can be employed in EVOH-based devices, compared to CC-based devices.

3.3.4 Sensing performances: reproducibility

The reproducibility of the sensing material, in terms of colour shade and homogeneity, is of paramount importance for colourimetric sensors since the differences in the starting material must not influence the sensing performances and the evaluation of colour changes. To assess this parameter, 10 independent sensors, obtained from different films, are equilibrated in different conditions, photos of the sensors are acquired and RGB triplets analysed.

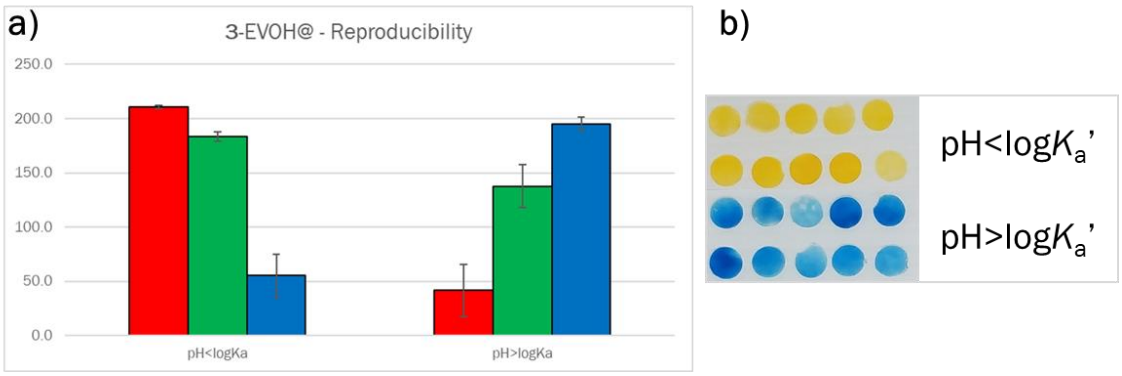

Figure 3.8: Bar plots representing the average value of RGB triplets for both acidic and basic form (a) and corresponding sensors picture (b) in the case of 3-EVOH@.

Dye n°3, 5 and 6, which have only one logK_a' value and thus only two different forms, are equilibrated at acidic and basic pH to evaluate the reproducibility of both the acidic (yellow) and basic (blue/violet) form. In Figure 3.8, the results for **3**-EVOH@ are reported as an example: the bar plots shows the average value and confidence interval of RGB triplets and the picture of the original sensor is presented.

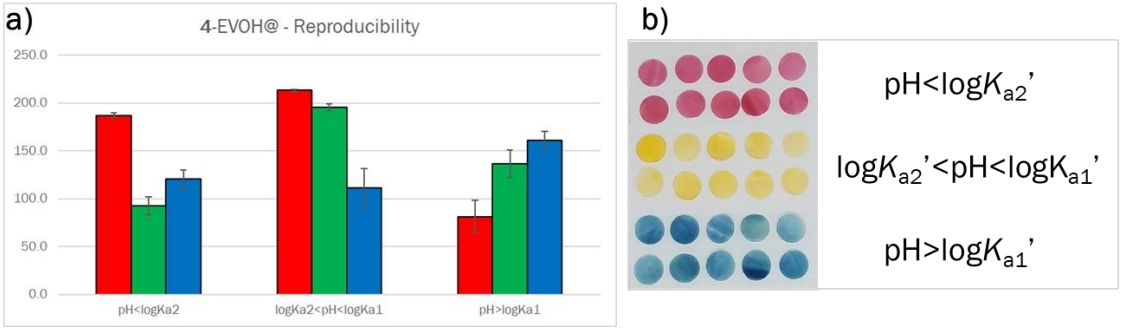

Figure 3.9: Bar plots representing the average value of RGB triplets acidic, neutral and basic form (a) and corresponding sensors picture (b) in the case of 4-EVOH@.

The other dyes, n°1, 2 and 4, have two logK_a' values and thus three different forms, acid, neutral and basic, whose reproducibility is tested. As an example, in Figure 3.9, the results for **4**-EVOH@ are presented.

For all Dye-EVOH@, the RGB reproducibility is judged to be satisfactory and no differences of colour shade are observed by naked-eye evaluation.

3.3.5 Sensing performances: colour change kinetic

From kinetic experiments in solution, we observe that complete protonation of Dye-EVOH@ sensors is very fast also in 0.01 M H^+ solution and it is completed in less than 1 minute while deprotonation in 0.01 M OH^- solution is much slower and it took 3 hours. The equilibrium in buffered solution at pH=7 is reached in 2 hours both starting from the acidic and basic form of Dye-EVOH@ sensors array.

From kinetic experiments in vapour, we observe that, exposed over acetic acid 0.1 M, all Dye-EVOH@ sensors turn their colour into the acidic or neutral form, depending on their logK_a' value, within 4 hours. The same occurs for Dye-EVOH@ sensors exposed over acetic acid 0.01 M within 22 hours while, for acetic acid 0.001 M, only dye n°4, which had the higher logK_a' value, partially turns to the neutral colour. As for basic volatile analytes, the equilibrium is reached in 30 minutes, when Dye-EVOH@ sensors are exposed to ammonia 0.1 M, and all the sensors turn into their basic form, apart from dye n°4 which remained neutral. Decreasing ammonia concentration to 0.01 M, the equilibrium is reached in 2 hours and only dye n°5 and 6 turn into their basic colour. Eventually, the lowest ammonia concentration, 0.001 M, is detected only by dye n°6 turning into the blue form in 22 hours.

Finally, from the "blank analyses", no significant changes are observed by naked-eye evaluation in Dye-EVOH@ sensors colour after equilibration of sensors either in acidic or basic form for 96 hours.

3.3.6 Protein foods: Dye-EVOH@ sensors array colour evolution

Having equilibrated the sensing spots at the proper pH value and having prepared the samples, as reported in Section 3.2.5, we register the evolution of Dye-EVOH@ sensors array colour over chicken breast slices, Figure 3.10**a**, and codfish fillets, Figure 3.10**b**.

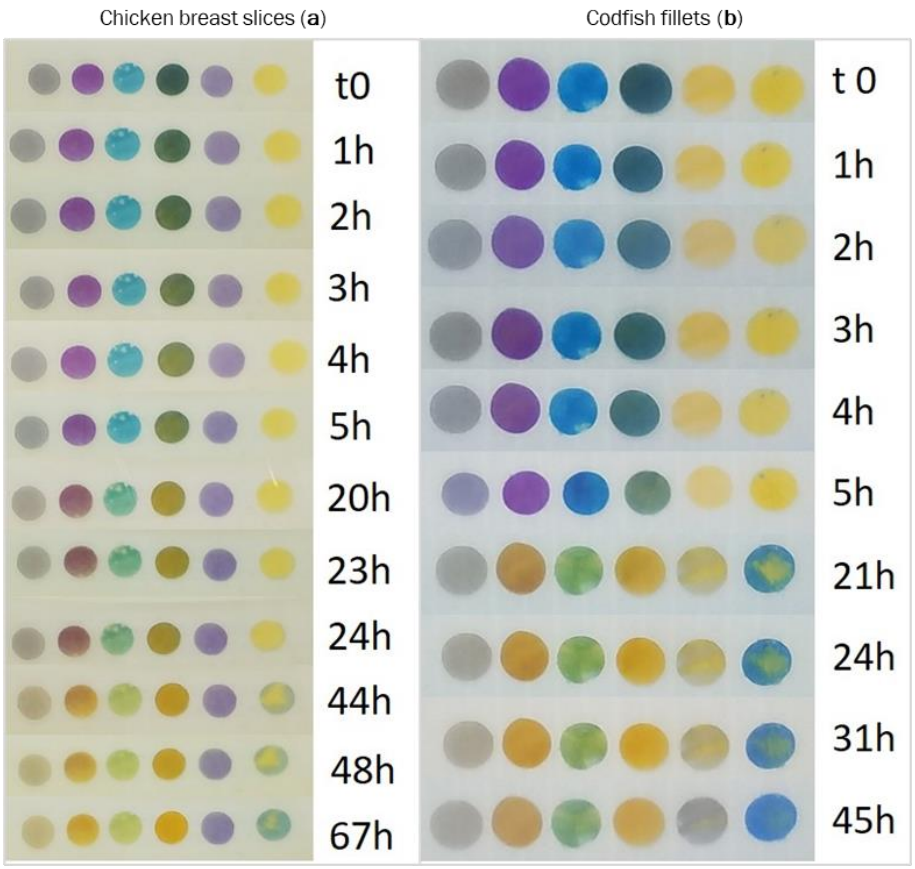

Figure 3.10: Dye-EVOH@ sensors array colour evolution over chicken breast slices (a), and codfish fillets (b), stored at RT.

The behaviour of the sensing units is very similar in both cases. In the first part of the degradation process, the receptors with logK_a' values of >7 (Dyes 1 to 4), previously equilibrated at basic pH, partially turn to the acid form due to the reaction with acid volatiles released by bacteria.

Then, in the second part of the spoilage process, the pH of the headspace undergoes a slight increase, due to the end of acid production and the formation of amines in the meat, and thus, the receptor with the lowest logK_a' value, dye n°6, turns into the blue basic form. This reaction starts after 44 hours, for chicken breast slices, and after 21 hours, for codfish fillets which is much more perishable. Dye n°5 turns out to be unreactive, and therefore useless, after basic equilibration in spoilage monitoring of chicken samples and can be discarded for a future large-scale implementation. In codfish fillets samples, it partially turns to the basic colour in the last monitoring hours.

This means that the resulting pH in the headspace is higher in the case of fish than in the case of chicken, and the spoilage process of this food is much faster, according to common knowledge. Nevertheless, even in the case of fish, we cannot consider the pH of the headspace "alkaline" because the other receptors, with slightly higher logK_a' values remain in the acid form (see sensors from **1**-EVOH@ to **4**-EVOH@).

3.3.7 Protein foods: spoilage modelling by PCA

PCA is then performed on the RGB triplets of the sensors during degradation to visualise the degradation process of the two samples. Both the loading plots are displayed in Figure 8.2 in Appendix III: Loading and score plots. For chicken breasts slices, analysing the score plot reported in Figure 3.11**a**, we notice that the score value on PC1, which accounts for 61.80% variability, increased during time and could be correlated to degradation while PC2 accounted for the variability among samples. Moreover, three different clusters, called SAFE, WARNING, and HAZARD, can be identified, with widely different values on PC1.

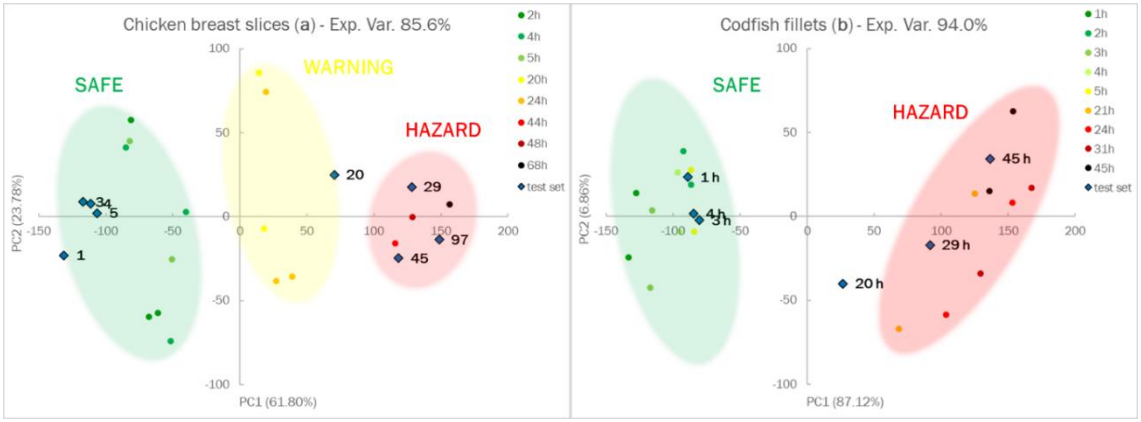

Figure 3.11: The score plots of the PCA models on the first two principal components, built on the training set and validated by projection of the test set, for chicken breast slices (a) and codfish fillets (b). The ellipsoids are exclusively added as a simplification of the different groups.

As for codfish fillets, the score plot is reported in Figure 3.11**b.** PC1 (87.12% variability) is correlated with the spoilage process, and PC2 (6.86% variability) with the differences between the samples analysed. On PC1, two well-separated clusters, called SAFE and HAZARD, can be identified since, at room temperature, one night is enough to observe the complete spoilage of the food,

For both foods, new samples are projected in the PCA model to verify the degradation pathway and the correct allocation, labelled as test set in Figure 3.11**a** and **b**. Test samples show the same degradation pathway of the training set and are located in the right clusters.

For both chicken and fish samples, these analyses are a proof of concept to demonstrate that the polymer-based device can be employed in food freshness monitoring because the colour evolution observed is in line with CSI and volatile by-products released during spoilage.

3.3.8 Protein foods: validation by instrumental analysis

To demonstrate that the clusters are not artefacts, but are characterised by significant differences in the solid and headspace composition, qualitative analyses are performed both on the solid food, to extract and identify BAs, and on the headspace, to analyse the volatile composition.

As for the analysis of the solid, the results are displayed in Figure 3.12. For chicken meat (Figure 3.12**a**), qualitative identification of BAs present in the solid is enough to clearly distinguish the samples belonging to different clusters. In the SAFE zone, no amines are detected; in the WARNING zone, four of seven are found, while all of the BAs under investigation are detected in the HAZARD zone.

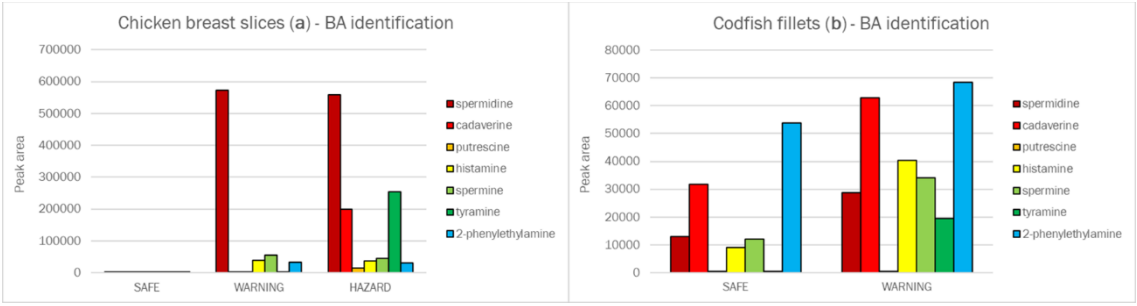

Figure 3.12: Bar plots representing peak area of BA identified in chicken (a) and codfish (b) samples at different degradation steps through HPLC-ESI/MS analysis.

On the contrary, in the case of codfish fillets (Figure 3.12**b**), almost all of the BAs can be detected even in the SAFE zone. It is well known that fish samples contain a large number of amines, even when it is fresh, and even the fishy odour is due to volatile amines, in particular trimethylamine. Moreover, this food is highly perishable, and for this reason, the production of BA is very fast and significant even in the small time required for the analysis. Nevertheless, a substantial difference between the SAFE and HAZARD zones in the amount of BAs was detected: from the peak areas we notice that the entire quantity of each amine is much higher, in the HAZARD zone rather than in the SAFE one.

Eventually, the headspace composition is analysed, and the results are reported below in Table 3.9.

Table 3.9: Classes of substances detected in chicken (column 1-3) and codfish (column 4-5) samples at different degradation steps using HSSPME coupled with GC/MS.

	Chicken breast slices			Codfish fillets	
	SAFE	WARNING	HAZARD	SAFE	HAZARD
Alcohols	✓	✓	✓	✓	✓
Aldehydes	✓	✓	✓	✓	✓
Ethanol	✓	✓	✓	✓	✓
Acids	✓	✓	✓	✓	✓
Ketones	-	✓	✓	✓	✓
Esters	-	✓	✓	✓	✓
Thiols	-	✓	✓	✓	✓
Volatile amines	-	-	-	-	✓
Biogenic amines	-	-	-	-	-
Indole	-	-	✓	-	✓

The case of chicken meat is easier to interpret because in the SAFE zone very few classes are detected and, above all, a large number of acid compounds are found, as suggested by the colour evolution of Dye-EVOH@ sensors array. In the WARNING zone, ketones and esters are released after the bacterial catabolism of sugars and their derivatives, but no amines are detected even if, at this stage, they are present in the meat. In the HAZARD cluster, when all of the BAs were detected in large amounts in the solid, amines are not found in the headspace, confirming our previous assumption about this topic. [7, 8, 9, 52] The main qualitative difference between these two last clusters is the presence of indole in the HAZARD zone.

As for codfish fillets, the composition of the headspace in the two clusters is very similar, but important details are nevertheless observed. At first, small volatile amines are present only in the HAZARD step, but BAs are again never detected; second, indole is revealed in the second part of the degradation process, which is similar to what is observed in chicken meat samples.

In conclusion, the instrumental analysis of the headspace during degradation confirms Dye-EVOH@ sensors array behaviour. BAs are produced, even in large quantities, in the solid when food is no longer eatable, but due to the buffered pH of the solid phase, they are present in their protonated form so they do not fly and, consequently, can not be detected in the headspace at any step. Therefore, only a very slight increase in the headspace pH is observed and only the receptor with a very low logK_a value shows a complete reaction to the basic form due to the reduction of acid volatile by-products released or, only for fish samples, to the presence of small volatile amines.

3.3.9 Milk: Dye-EVOH@ sensors array colour evolution

Having equilibrated the sensing spots at basic pH and having prepared the samples, as reported in Section 3.2.6, we register the evolution of Dye-EVOH@ sensors array colour dipped in different types of milk. Firstly, the evolution during storage at RT is displayed in the case of whole, semi-skimmed and skimmed milk, reported in Figure 3.13.

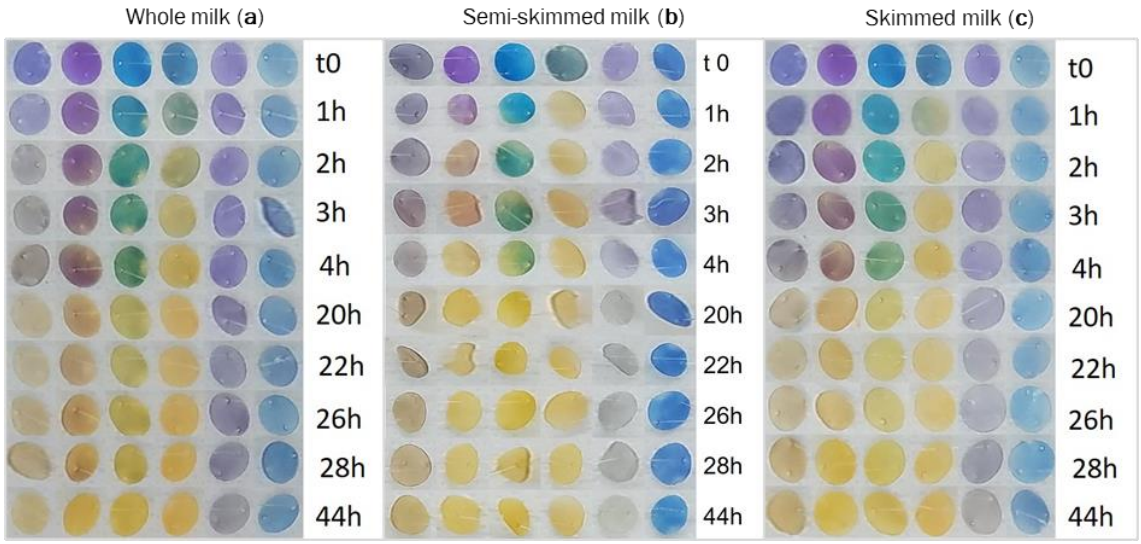

Figure 3.13: Dye-EVOH@ sensors array colour evolution dipped in whole (a), semi-skimmed (b) and skimmed (c) milk, stored at RT.

The colour evolution is similar between different types of milk. Moreover, only the first three sensors on the left, in each array, turn out to be informative to follow the spoilage, namely **1**-EVOH@, **2**-EVOH@ and **3**-EVOH@, which show a clear conversion from the alkaline to the acidic form between 4 and 20 hours. As for the others, **4**-EVOH@ is useless since it showed complete conversion to the yellow acidic form in the first hour of monitoring, having the highest logK_a' value both, while, on the contrary, **5**-EVOH@ and **6**-EVOH@ remain in their alkaline form, respectively violet and blue, during the entire time length, having lower logK_a' values than the other receptors.

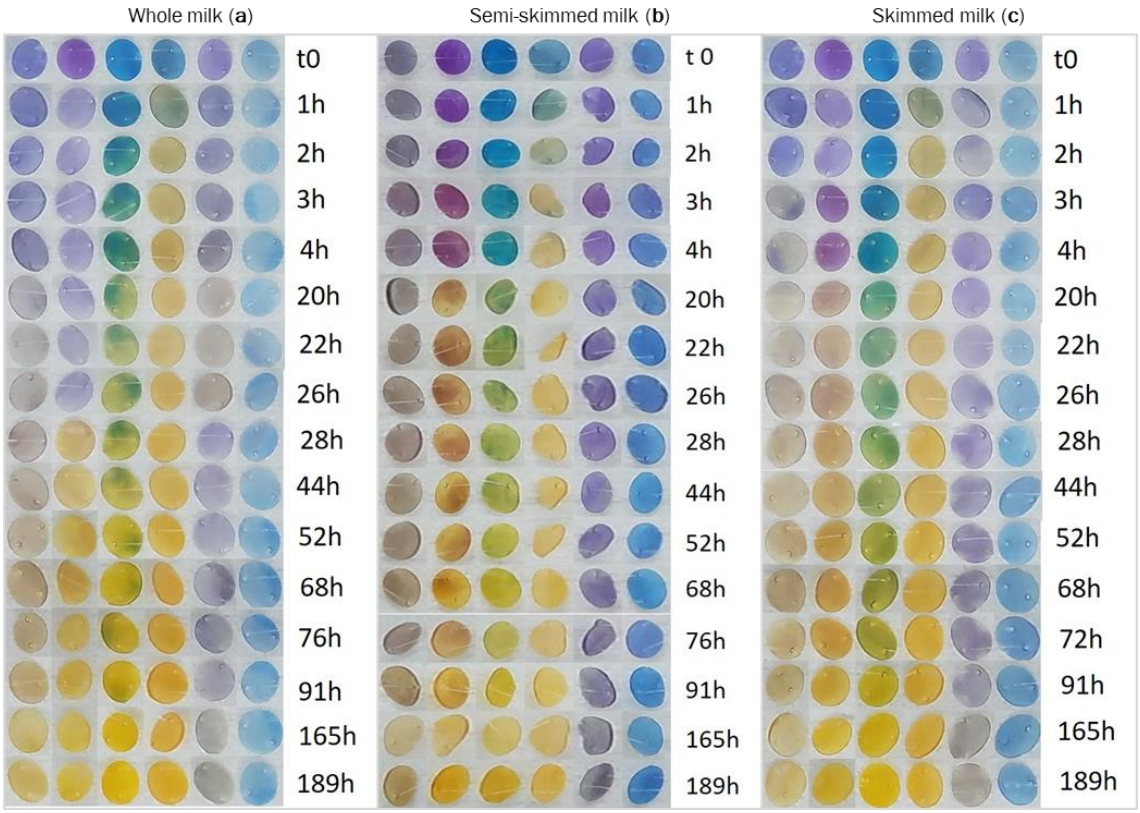

Figure 3.14:The colour evolution of the sensors array dipped in whole (a), semi-skimmed (b) and skimmed (c) milk, stored at 4°C.

Very similar conclusions are drawn analysing the colour evolution during storage at 4°C, displayed in Figure 3.14. Slight differences are observed between the three types of milk under investigation, mainly for long storage times. Again, the last three sensors, starting from the left, are not suitable to follow the degradation process, being either too alkaline or too acid for the overall acidity of the samples, and are thus discarded from the following multivariate analysis. The first three sensors are much more informative, showing the gradual conversion mentioned above from basic to acidic form gradually during the degradation. The starting and the final colours are equal for all milk types while a different time evolution is observed, depending on sample composition. This evidence is of paramount importance to set the following chemometrics investigation.

3.3.10 Milk: spoilage modelling by PCA

PCA is applied on the RGB triplets of the three selected sensors per each milk type, during storage both at RT and at 4°C. In each case, the overall percentage variance explained by the first two components is sufficient, considering the intrinsic variability of the system under investigation.

In Figure 8.3 in Appendix III: Loading and score plots the loading plots are shown. The score plots, reported in Figure 3.15, are analysed to visualise and model the degradation process occurring at the different temperatures. For facilitating the interpretation of the score plots, the samples kept at room temperature are represented as circles of three different colours: GREEN for the first day of

monitoring, YELLOW for the second day and RED for the third; instead, the samples chilled stored are represented as X icons of different colours: GREEN before the expiry date reported on the bottle, YELLOW around the expiry date and RED after the expiry date.

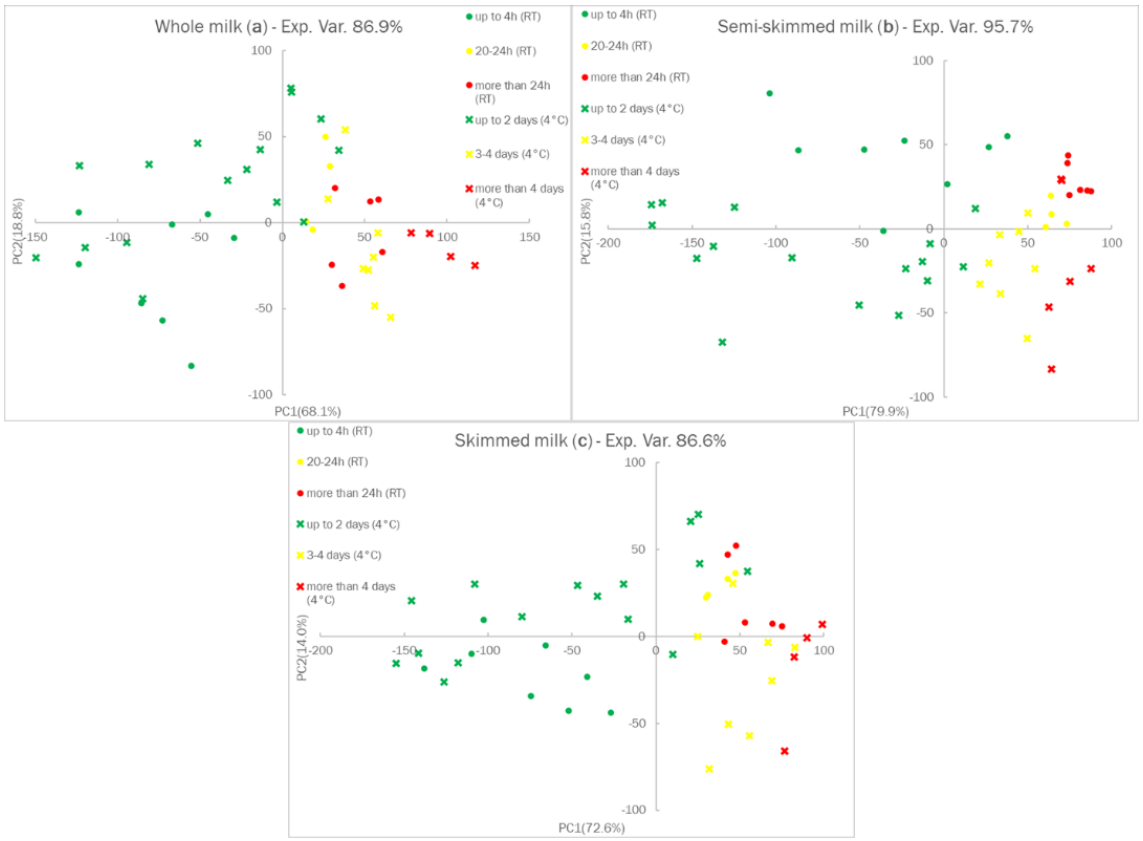

Figure 3.15: The score plots of the PCA models on the first two principal components, for whole (a), semi-skimmed (b) and skimmed (c) milk.

For all milk types, the score value on PC1 increased during the monitoring: for samples stored at room temperature, an evident increase is observed during the first 4 hours (green circles), suggesting a fast bacterial degradation promoted by the high temperature, and after the first night (yellow circles). After that, no great differences are further observed even after 2 days of storage: at this stage, milk is no longer suitable for human consumption and the matrix pH is acid enough to provoke the complete conversion of our sensors to the acidic yellow form, but still around neutrality due to the presence of several natural buffering agents.

As for the samples chilled stored, the score value on PC1 increases much more slowly and gradually since the refrigeration reduces the bacterial degradation rate but, around (yellow X) and after (red X) the expiry date, the samples are located in the same region of the spoiled samples stored at room temperature (RT) suggesting that milk is no longer eatable.

3.3.11 Milk: milk types comparison by 3-Way PCA

As highlighted before, no significant difference is observed between the three milk types under investigation, thus suggesting us to exploit 3-Way PCA to compare the three spoilage processes. The variance percentage explained after unfolding, reported in Table 3.10, is slightly lower than the Tucker model's value (77.1%). This result suggests that, considering the common degradation process, only a small part of the overall information contained in the dataset is lost and thus the degradation is very similar in the three milk types. Moreover, the percentage of explained variance is fully satisfying, considering the high variability of the system and the types of data employed for the analysis.

Table 3.10: Cumulative % variance explained after unfolding.

Mode	PC1	PC1&2
Objects	70.67%	86.41%
Variables	68.44%	88.09%
Conditions	66.85%	83.47%

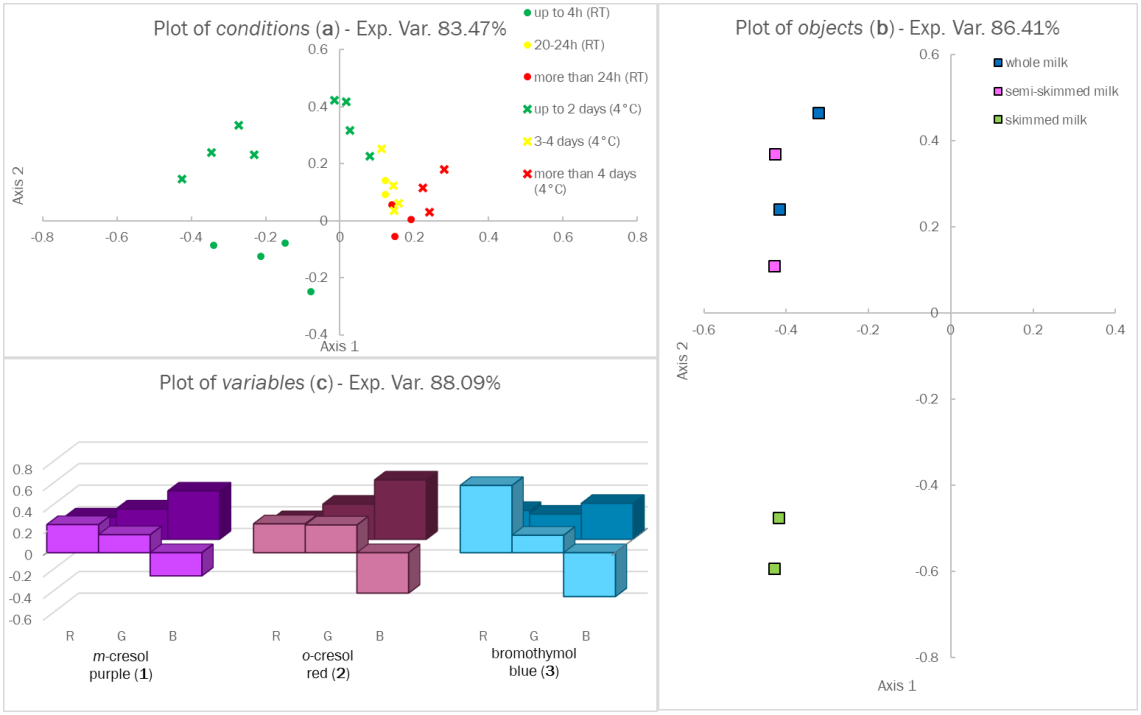

Figure 3.16: The loading plots of the 3-Way PCA model on the first two axes: conditions (a), objects (b) and variables (c) loading plots. In graph c, the variables loadings on Axis 1 are in foreground, the ones on Axis 2 in background.

Moving to results interpretation, in the plot of *conditions* (Figure 3.16a), times are well separated along the x-axis: the very first degradation steps are located in the left part of the graph, while, during the spoilage process, the loading values on Axis 1 increase, with different spoilage rates depending

on the storage temperature. In contrast, in the plot of *objects* (Figure 3.16**b**), different milk types are separated along the *y*-axis (Axis 2). Considering the low value of explained variance associated with this axis, we can affirm that the difference between the three types is not evident and, much more important, our device shows promising results in monitoring all the types of milk. Finally, from the *variables* loadings, shown in Figure 3.16**c**, the most informative sensor in *conditions* separation, which is the ones with a higher loading value on Axis 1, in the foreground, turns out to be **3**-EVOH@, while the other sensors are more informative in *objects* separation.

3.3.12 Milk: preliminary classification by LDA

Having demonstrated that our sensing device can be successfully used to monitor and model the degradation of milk, regardless of milk type and temperature storage, a very first attempt of classification using LDA on RGB indexes is performed. Two classes are identified, SAFE for fresh milk suitable for human consumption and HAZARD for uneatable milk, according to their location in PCA score plot. The overall dataset is split in two groups. Samples whose attribution is sure, which means at the very beginning and at the end of the monitoring, are used as training samples while samples located in the central part of PCA score plot are exploited as test set. We are well aware that this approach is not rigorous and, in fact, it was exploited only as proof of concept, nevertheless the results are worth of attention. A more systematic approach will be followed in the next Chapter, working with the final device

In cross-validation, the prediction is 100% satisfactory and thus the prediction of the unknown samples of the test set is performed. The software CAT gives, as an output, the Mahalanobis distance from the two classes of each sample. To aid interpretation, in Figure 8, the reciprocal of the distance is reported for each sample of the test set, so for each sample, the highest bar represents the class closest to that sample, so the assigned one. [8]

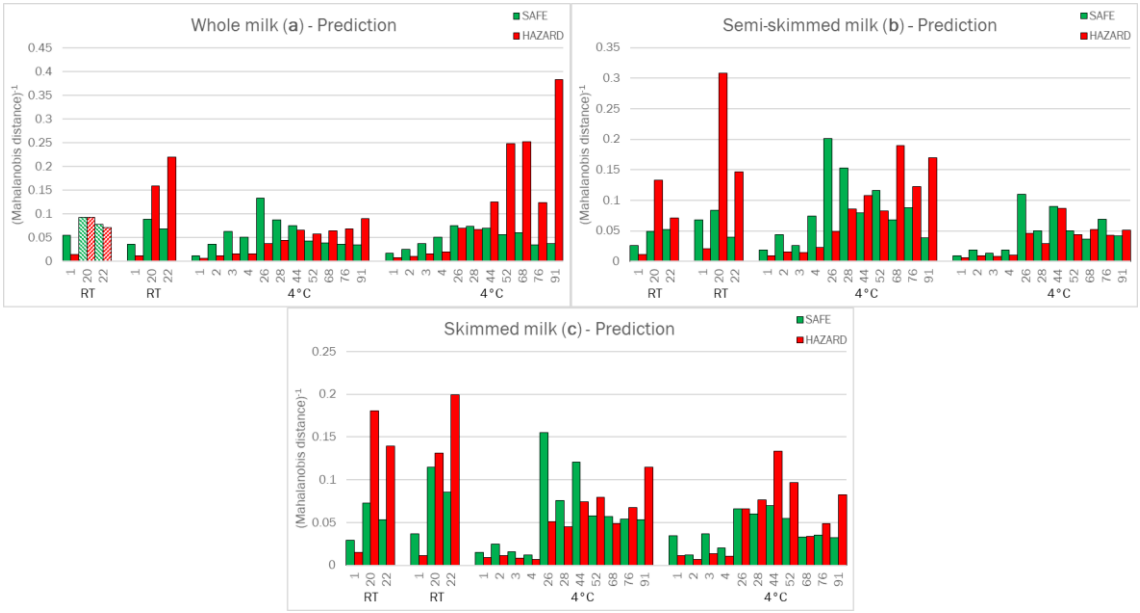

Figure 3.17: Results of prediction of test samples for whole (a), semi-skimmed (b) and skimmed (c) milk, stored at different temperatures, reporting storage time and temperature on the *x*-axis and the inverse of Mahalanobis distance from each of the two classes on the *y* axis.

In 2 cases out of 84, highlighted with the striped bars, the samples are wrongly assigned to the SAFE class but, remembering that LDA gives a dichotomic answer (a sample is or in or out of the class) without uncertainty, it is worth noting that the distance between these samples and the two classes is more or less equal. In all the other samples, during the spoilage process, the distance from the SAFE class increases while that from the HAZARD class decreases; at a certain point, slightly different among the milk types and in quite good agreement with the expiry date, the sample is nearer to the HAZARD class than to the SAFE one and is thus labelled as uneatable.

3.3.13 Milk: validation procedures

From the multivariate analysis of sensors colours during milk degradation, the presence of two main spoilage steps arises, the so-called SAFE and HAZARD steps. Verifying this assumption by an independent method is of paramount importance to validate our models and demonstrate the device's applicability to milk freshness detection. For fulfilling this goal, several methods have been tested based on different chemical principles.

On the one hand, we want to independently measure the increasing milk acidity during monitoring time to confirm the accuracy of sensors' responses. For this reason, at each test time, milk pH is measured but this approach reveals unfruitful since the measured pH remains almost constant at room temperature and a slight decrease is observed during chilled storage. These results are probably strongly affected by the electrode used, and the calibration performed.

Better results are obtained using the Soxhlet-Henkel methodology to determine milk acidity in the two identified classes, SAFE and HAZARD, following the procedure reported in Section 3.2.6. Table

3.11 reports, the titration results, expressed as average °SH/100 mL on three replicates, are reported, with standard deviations between parenthesis.

Table 3.11: Average milk acidity (°SH/100 mL) for SAFE and HAZARD class, determined by Soxhlet-Henkel methodology

Milk type	Acidity in SAFE (°SH/100 mL)	Acidity in HAZARD (°SH/100 mL)
Whole milk	8.01 (5)	9.08 (8)
Semi-skimmed milk	7.88 (8)	8.12 (8)
Skimmed milk	7.80 (8)	8.12 (8)

Different reference values are reported for this methodology, but the value of 8°SH/100 mL is commonly considered the dividing line between eatable and uneatable milk. In this case, an increase in the acidity is observed per each milk type moving from the SAFE to the HAZARD class identified by the sensors array. The °SH values are below or equal to the threshold for SAFE samples and above for the HAZARD. From this preliminary investigation, it is clearly evident that Soxhlet-Henkel titration is preferable to pH measurements as an independent method to validate multivariate models, in our case. Therefore, the reliable results obtained with Soxhlet-Henkel titration will be used in the following Chapter in applying in a more systematic way supervised chemometric tools as LDA and PLS.

Another interesting aspect is the possibility of relating the sensors' responses to the different classes of by-products released during spoilage, not only in solution but also in the headspace. The results of analyses obtained with the Headspace Solid-Phase Microextraction (HSSPME), coupled with gas chromatography–mass spectrometry (GC/MS), performed on the headspace of the same samples used for Soxhlet-Henkel titration are summarized in Table 3.12

. For this qualitative analysis, no evident difference between different milk types is observed while a clear difference between the two classes arises. Alkanes, aromatic compounds and ketones are detected in samples belonging to the SAFE class while, at the HAZARD steps, acids and esters appear and aromatic compounds are no longer identified. This qualitative investigation thus reveals a significantly different headspace composition in correspondence of different spoilage steps.

Table 3.12: Classes of substances detected in milk samples at different degradation steps using HSSPME coupled with GC/MS.

	SAFE	HAZARD
Alkanes	✓	✓
Aromatic compounds	✓	-
Acids	-	✓
Ketones	✓	✓
Esters	-	✓

3.4 Conclusions

The synthetic pathway to obtain Dye-EVOH@ sensing material, starting from commercially available EVOH (32% ethylene) was successfully developed. From physicochemical characterization, information about material characteristics was acquired and, from optical measurements, pH indicators behaviour after covalent anchoring to EVOH was investigated.

Once defined the sensing performances of the device, it was tested on both solid and liquid protein foods with promising results. The application of Dye-EVOH@ device as smart label for milk freshness monitoring was definitely the most successful since also monitoring during chilled storage was possible. Opposite, in the case of solid protein foods, promising results were obtained during storage at RT but, in the case of chilled storage, the device turned out to be not enough sensitive. In fact, at a lower temperature, both bacterial activity and by-products volatility were reduced, resulting in a slower spoilage process and lower analytes' concentration in the headspace. In this condition, Dye-EVOH@ sensors array was still able to detect the HAZARD step but with a delay of around 24 hours, revealed by instrumental analysis.

To overcome the sensitivity issue, two main improvements were made, as described in Chapter 4. Firstly, EVOH copolymers with different ethylene content, and thus different permeability and hydrophilicity, were tested. Secondly, a more efficient sensing approach was used, aiming at reducing both the number of sensing units required and the delay of detection, in the case of chilled storage.

To conclude, the results discussed in this Chapter were presented as oral communication at the "International Symposium on Dyes and Pigments" (Sevilla, 2019) and, as poster communication, at "Merck Young Chemists' Symposium" (Rimini, 2019). The synthetic procedure for Dye-EVOH@ sensors and their application as smart labels has been patented in Italy, Europe and USA [10, 11, 13, 12]. All these data were finally collected in two papers published on ACS Food Science and Technology [14, 15].

4. EVOH (29%)-based devices

In this chapter, the EVOH(39%)-based devices are discussed. Firstly, the preliminary experiments performed for the selection of the most suitable EVOH copolymer and receptors are presented providing a brief description of the most relevant results. Then selected receptors are listed and the experimental procedures and data elaboration approach for each specific application are described. The results obtained are divided according to the final application and presented. Eventually, the main conclusions are driven, the publications on this topic are summarised and the insights for further development are discussed.

4.1 Preliminary experiments

As discussed in Section 3.4, EVOH (32%)-based device successfully detects the spoilage of milk and RT stored protein foods but, in the case of chilled storage, its sensitivity turned out to be too low to real-time detect the spoilage onset. To improve the device sensitivity and large-scale applicability, we followed two strategies, discussed in the following sections:

1. Selection of the best EVOH copolymer
2. Selection of the most informative receptors for the specific application

The final version of Dye-EVOH@ device was then tested for freshness monitoring of various protein foods [85] and milk types [16] but also as a plastic-based chemometrics-assisted litmus test.

4.1.1 EVOH copolymer selection

As hinted in Section 3.1, EVOH copolymers commercially available differs from each other by both ethylene content and melt flow rate (MFR). As deeply discussed in literature [78, 86], higher ethylene content results in higher oxygen permeability, lower water vapour permeability and lower T_m and T_g, thus easier processability. Opposite, MFR influence is never investigated in literature, up to our knowledge.

Aiming at increasing our device sensitivity towards weakly acid or alkaline spoilage by-products, four different commercial EVOHs, provided by Nippon Goshei, were tested as solid support. In Table 4.1 ethylene content and MFR of commercial EVOHs under investigation are reported.

Table 4.1: Ethylene content and melt flow rate (MFR) of commercial EVOHs under investigation

Commercial name	Ethylene content (mol%)	Melt Flow Rate (MFR)
DT2904	29%	3.8
D2908	29%	8
AT4403	44%	3.5
A4412	44%	12

For this first screening, three pH indicators out of six were selected as more informative, bromothymol blue (**1**), thymol blue (**2**) and bromophenol blue (**3**), and were covalently bound to the four EVOHs, following the experimental procedure described in Section 3.2.2.

Sensing performances of the different Dye-EVOH@ devices were tested firstly on synthetic samples, according to the procedures described in Section 3.2.4, and then real ones. Codfish fillets were selected as test protein food and the freshness monitoring was performed at 4°C, according to the previously described procedure (Section 3.2.5). In Figure 4.1, the colour evolution of Dye-EVOH@ devices over codfish fillets during chilled storage is displayed, with sensors in order from **1**-EVOH@ to **3**-EVOH@ for each device.

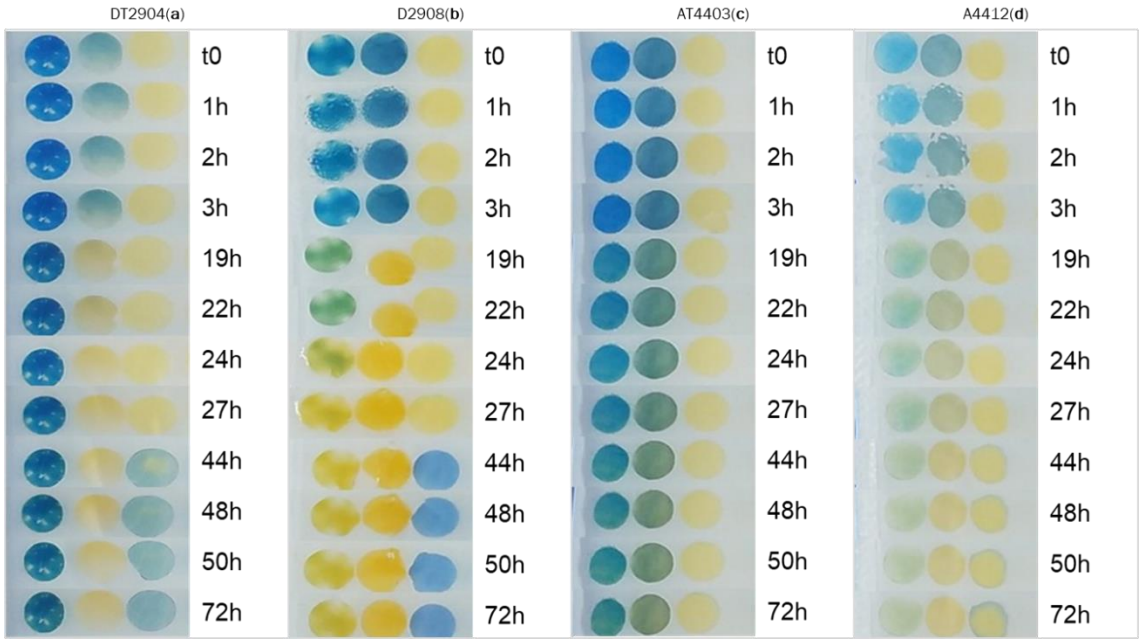

Figure 4.1: Dye-EVOH@ sensors array colour evolution over codfish fillets, stored at 4°C, using DT2904 (a), D2908 (b), AT4403 (c) and A4412 (d) as solid support

As clearly visible, the same pH indicators covalently bound to different EVOHs showed the same colour evolution but with different timing. In particular, EVOHs with 29% ethylene content (Figure 4.1**a** and Figure 4.1**b**) were able to detect both the WARNING step after 19h and the HAZARD step after 44 h, while EVOHs with 44% ethylene content (Figure 4.1**c** and Figure 4.1**d**) showed almost no colour changes during the entire monitoring. In addition, D2908 (Figure 4.1**b**) colour transitions were more glaring than DT2904 (Figure 4.1**a**) therefore this EVOH was selected as the best solid support.

4.1.2 Receptors' selection

In Chapters 2 and 3, a panel of reactive dyes was tested for various applications. This approach is suitable for screening experiments but, aiming at large-scale application, the large number of dyes results in higher production costs and harder naked-eye evaluation, due to the large number of sensing units and reference colour. Consequently, in the final version of the device described in this

Chapter, for each application only the essential receptors were selected, reducing the number of sensing units with a preference for glaring colour transitions or “traffic-light” sensing mechanism. As for EVOH selection previously described, also receptors selection was always performed directly on real samples under investigation, in the same storage conditions of the final application.

4.2 Materials and methods

4.2.1 Receptors

Protein foods

The selection of the receptor, performed directly on real samples, has led to o-cresol red (CR) as the best receptor, already used in EVOH (32%)-based devices (Chapter 3) labelled as **2**-EVOH@.This pH indicator is involved in two protonation equilibria, one at alkaline and one at acid pH, and thus could detect both weakly acid and alkaline spoilage by-products. In Figure 4.2, the protonation equilibria and the correspondent log K_a values in solution are reported [64, 65]; it must be underlined that, after the covalent linkage to EVOH, an increase of around 1 unit for each logK_a' value is observed, as already discussed in Section 3.3.3.

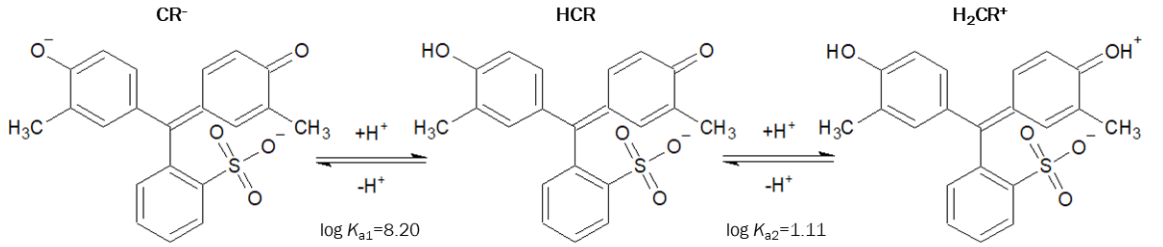

Figure 4.2: Protonation equilibria of o-cresol red and correspondent log K_a, as found in literature [64, 65].

CR-EVOH@ assures an enhanced sensitivity towards alkaline spoilage by-products, characteristics of the HAZARD spoilage step, compared to bromophenol blue (logK_a'~5), used in Chapter 3, having a logK_a' value more than 2 units lower (logK_a'~2). Therefore, an even lower concentration of weak bases is required to obtain the complete conversion from H_2CR^+ to HCR.

Milk

Testing the sulphonphtaleins with logK_a around neutrality, after covalent linkage to EVOH, directly on milk freshness monitoring at 4°C, bromocresol purple (BCP) turned out to be the most informative dye for the present application, showing a glaring colour transition from green to yellow. The chemical structure of the dye and its logK_a value in solution are reported in Figure 4.3; [64] after functionalisation, a logK_a'~7 is expected for this receptor that was not used in EVOH (32%)-based devices described in Chapter 3.

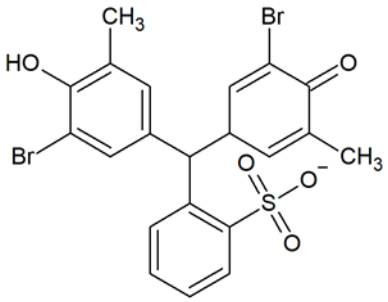

bromocresol purple (**BCP**)
logK_a = 6.05

Figure 4.3: Chemical formula of bromocresol purple and its log K_a value [64].

Chemometric-assisted litmus test

The extremely high variety of possible pH indicators and the versatility of our synthetic pathway suggest the possibility to create a Chemometric-assisted litmus test (CLT). To cover the widest pH range, ideally, from 0 to 14, a panel of commercially available pH indicators, belonging to different classes, has been selected. All these molecules have in common the presence of either sulphonic or carboxylic groups in their structure, fundamental for covalent linkage to EVOH, and bright colours at both protonated and deprotonated forms. In Table 4.2 the pH indicators and their logK_a values in solution, as found in literature, are reported. Among them, the previous labels of the receptors already employed in EVOH (32%)-based devices, described in Chapter 3, are reported in the last column.

Table 4.2: pH indicators selected for the chemometric-assisted litmus test, corresponding logK_a values and previously assigned labels in Chapter 3.

n	pH indicator	logK_a	logK_{a1}	logK_{a2}	Reference	EVOH (32%)-based sensors
1	phenol red	--	8.32	1.57	[64, 65]	
2	*o*-cresol red	--	8.20	1.11	[64, 65]	**2**-EVOH@
3	thymol blue	--	8.9	1.50	[64, 65]	**4**-EVOH@
4	*m*-cresol purple	--	8.32	1.57	[64, 65]	**1**-EVOH@
5	methyl orange	3.42	--	--	[87]	
6	Congo red	4.1	--	--	[66]	
7	bromocresol green	4.35	--	--	[64]	
8	chlorophenol red	6.0	--	--	[64]	**5**-EVOH@
9	bromothymol blue	7.1	--	--	[64]	**3**-EVOH@
10	alizarin red S	--	11.0	4.5	[66]	
11	alizarin yellow R	11.5	--	--	[66]	
12	Clayton yellow	12	--	--	[66]	

4.2.2 Dye-EVOH@ sensors preparation

For Dye-EVOH@ sensors preparation, the same procedures described in Section 3.2.2 are applied. Dye-EVOH@ raw materials are synthesised following the internationally patented procedure [10, 11, 13, 12], Dye-EVOH@ films are obtained by pressing under heating, setting the previously optimised parameters, reported in Section 3.3.1. Physicochemical measurements confirm similar results to those obtained for EVOH (32% ethylene)-based device.

Dye-EVOH@ sensors of 0.5 cm diameter are cut from the polymeric films by the means of a hole punch for paper and used as final sensing unit for different applications. The main difference between EVOH (32%) and EVOH (29%) lies in functionalised films thickness: Dye-EVOH(29%)@ films present a less homogeneous thickness therefore, cutting the sensors from different areas of the film, different sensors thickness is obtained. This parameter is of paramount importance for final device sensitivity, in particular for real samples monitoring, and has to be controlled, ideally on every sensor.

4.2.3 Dye-EVOH@ sensors thickness selection

For both **CR**-EVOH@ and **BCP**-EVOH@, a rapid method to verify sensors thickness is developed. For brevity's sake, only the case of **BCP**-EVOH@ is presented. 72 sensors with various thicknesses are equilibrated at alkaline pH by 2-hours immersion in 100 mL NaOH 0.1M. The pictures of the sensors are then acquired. RGB triplets of each sensor are extrapolated [61] and used as input dataset for PCA, only centring the data [60]. Then 8 sensors, representative of the various thicknesses, are selected and tested on real samples to evaluate the most effective thickness for the final application.

4.2.4 Protein foods freshness monitoring

Experimental setup

For this application, a dual sensors device is used, made of two **CR**-EVOH@ previously equilibrated one at the completely deprotonated form (CR^-), from now called b-**CR**-EVOH@, and one at the completely protonated one (H_2CR^+), from now defined a-**CR**-EVOH@. Equilibrations are performed by 1 h immersion in 2 mL NaOH (b-**CR**-EVOH@) or HNO_3 (a-**CR**-EVOH@) 0.1 M, resulting respectively in violet and pink sensors. In the absence of spoilage markers, the stability of both b-**CR**-EVOH@ and a-**CR**-EVOH@ has been verified for up to five days. [85]

Chicken breast slices and various fish products fillets are purchased at the local supermarket, choosing tray containing similar weights of food, and are carried to the lab within 10 minutes. The plastic film is removed, the **CR**-EVOH@ device is taped to the bottom of the PP tray using 3M Magic Tape, as already discussed, and a new plastic film is fixed to seal the package. Samples are stored in a domestic fridge at 4 °C for 10 days, in the case of chicken, or for 5 days, for fish products.

Colour analysis & Chemometrics

At given times, photos of the device are acquired by a Nikon COOLPIX S6200 in a lightbox to ensure a constant and reproducible light exposition. To extract the RGB triplets for each sensing unit during freshness monitoring, GIMP software is employed [61].

For each food under investigation, Principal component analysis (PCA) is performed on RGB triplets, only centring the data because these indexes are intrinsically scaled from 0 to 255, to rationalize the colour evolution and visualize spoilage process.

3-Way PCA is also applied to evaluate the effect on spoilage of source and dimension of fish fillets, being the eligible technique to deal with a 3-dimensional dataset.

The open-source Chemometric Agile Tool (CAT) program was employed for multivariate data elaboration [60].

Training and test sets

For chicken breast slices, the training set consists of five samples of similar mass, purchased the same day of the delivery from the supplier. Therefore, the input matrix has 6 columns (3 RGB indexes per 2 **CR**-EVOH@ sensors) and 135 rows (27 acquisition times per 5 replicates).

Then, to preliminary validate the model, two new samples of similar mass are projected as external test set, one purchased the same day of the delivery and the other one two days after. This test aims to verify the correct device behaviour even if implemented in foods already under degradation.

As for fish products, this class includes a wide variety of foods that differ in fish characteristics, like dimension, meat composition and nutritional values, and transformation and distribution procedures. To explore the widest panel, we select four types of fish fillets that are commonly frozen, delivered to the supermarket, defrosted and sold in sealed packages. The fish products under investigation, the average fish and fillets weight and the type of sales package are reported in the first four rows of Table 4.3. For each fish product, five samples are used as training set and an independent sample is exploited as test-set. Therefore, the training set input matrixes have 6 columns (3 RGB indexes per 2 **CR**-EVOH@ sensors) and 60 rows (12 acquisition times per 5 replicates).

Table 4.3: The fish products under investigation, the average fish and fillets weight and type of sales package.

Fish product	Av. Fish weight (kg)	Av. Fillet weight (g)	Sales package
Swordfish	250	200	Sealed
Codfish	40	150	Sealed
Plaice	4	150	Sealed
Scorpionfish	2	150	Sealed
Gurnard	<1	30	Unsealed

In addition, gurnard fillets are also tested to evaluate the device applicability towards fish products directly filleted in the supermarket, with small fillets and sold in an unsealed package. The characteristics of this food are reported in the last row of Table 4.3. Three gurnard fillets package of the same foods' weight but different fillets dimension and weight are purchased and monitored,

inserting three devices per each package. Therefore, the input matrix has 6 columns (3 RGB indexes per 2 **CR**-EVOH@ sensors) and 99 rows (11 acquisition times per 9 replicates).

4.2.5 Milk freshness monitoring

Experimental setup

For this application, **BCP**-EVOH@ sensor is equilibrated at basic pH by 1-hour immersion in 2 mL NaOH 0.1 M and, after drying step, dipped in 100 mL milk sample.

Fresh milk bottles, whole, semi-skimmed or skimmed, are purchased in a local supermarket the day of the dairy's delivery to ensure a homogeneous lifetime of all samples and monitor the entire degradation process. Within ten minutes, the bottles are carried in the lab and divided into subsamples of 100 mL in sterile plastic containers, in which **BCP**-EVOH@ sensor is dipped. Samples are stored at 4 °C per ten days in a domestic fridge.

Colour analysis & Chemometrics

At given times during storage, photos of the array are acquired by a Nikon COOLPIX S6200 in a lightbox to ensure a constant and reproducible light exposition and sensing spots RGB triplets are extracted using GIMP software [61].

To facilitate and speed up this step, similarly to what was previously described in Section 3.2.6, all the sensors are poked with a needle, and a thread is put through the hole of each sensor. When dipping the sensors in the milk, both thread ends are kept out of the liquid; in this way, it is simple to extract the sensors and acquire the photographs. Furthermore, before shooting the picture, the sensors are dried using common adsorbent paper to remove the white milk residue on the surface that would affect the RGB index.

As for chemometric data treatment, firstly unsupervised techniques are exploited to visualize and rationalize the overall data set: Principal Component Analysis was applied separately to each type of milk and 3-Way PCA jointly to the entire dataset, always applying the only centring as data pre-treatment.

Then supervised techniques are used to develop predictive models, both qualitative (Linear Discriminant Analysis, LDA) and quantitative (Partial Least Square regression, PLS), based on °SH measurement by Soxhlet-Henkel titration, described below. For these techniques, a stepwise approach is used to develop the final models, here described.

- Step 1: Milk types are analysed separately. Each dataset is split into training and test set (10:7 ratio). Models are built on the training set and validated by the prediction of the test set. If validation is successful, a total model is built per each milk type.
- Step 2: Total models are used to predict the overall training set of both the other milk types, repeating this operation per each milk type. If the prediction is correct, a general model is built on the entire dataset, including different milk types.

- Step 3: General model was validated by predicting unknown samples, totally independent from the first dataset.

The open-source Chemometric Agile Tool (CAT) program is employed for data elaboration [60].

Training and test sets

For each type of milk, the training set consists of five milk samples stored at 4°C in which one BCP-EVOH@ sensor is dipped. Therefore, the input matrixes have 3 columns (3 RGB indexes per 1 **BCP**-EVOH@ sensors) and 95 rows (19 acquisition times per 5 replicates).

As already pointed out in the previous Chapter, °SH values can be successfully exploited for a proper validation of this sort of sensing devices. Therefore, each **BCP**-EVOH@ sensor picture has to be correlated to the actual correspondent °SH value. To avoid volume changes during monitoring, per each replicate, per each milk type, 1.5 L of milk, homogenized in a sterile bottle, 100 mL sample is used for **BCP**-EVOH@ monitoring, and the remaining part is gradually consumed to measure °SH. The two portions are stored at the same temperature and kept out of the fridge only for the minimum time required for picture acquisition and titration.

This entire procedure is repeated for the first dataset for 5 samples of each milk type (whole W, semi-skimmed SS and skimmed S) while, for the test set, for 2 replicates of each milk type, measured only once a day.

Validation by independent analyses

Milk titratable acidity is usually measured by Soxhlet-Henkel methodology and expressed as °SH/100 mL, according to the procedure reported in Section 3.2.6. To systematically apply supervised chemometric tools, at every picture shot the titration was performed on each one of the replicates.

Dye release in simulated conditions

To check BCP release in water, UV-Vis spectroscopy can be used, exploiting the intense absorption of the deprotonated form of BCP at 589 nm. In this case, dye release can not be measured directly on milk samples due to the white colour of milk but is tested in two different conditions, using phosphate buffer 0.1M at pH=7 [88] to mimic milk.

- Concentrated samples: around 100 mg **BCP**-EVOH@ sensors, equilibrated at alkaline pH likewise monitoring experiments, are dipped in 25 mL phosphate buffer 0.1M at pH=7, stored at 22°C for 10 days
- Simulated samples: one **BCP**-EVOH@ sensor, equilibrated at alkaline pH likewise monitoring experiments, is dipped in 100 mL phosphate buffer 0.1M at pH=7, stored at 4°C for 10 days

In both cases, UV-Vis spectra are acquired once per day starting from Day 2 and the amount of dye released is calculated.

4.2.6 Chemometrics-assisted Litmus Test (CLT)

Experimental setup

In this case, Dye-EVOH@ sensors are used without previous equilibration since buffered solutions are used as samples and there is no need to enhance sensors sensibility.

The twelve Dye-EVOH@ sensors are poked with a needle and fixed to inert plastic support by the means of a thread to obtain the 3x4 sensing array shown in Figure 4.4. The arrays are then dipped in 100 mL samples of solutions at different pH, ranging from 1 to 13 and are left equilibrating overnight.

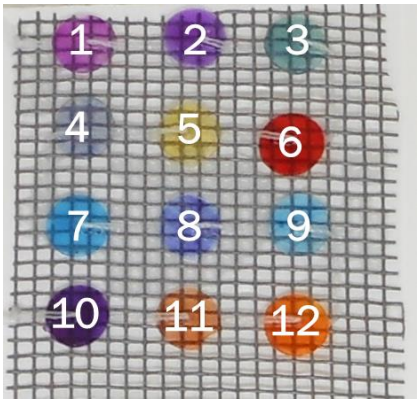

Figure 4.4: Example of 3x4 sensing array used as chemometrics-assisted litmus test. Dye-EVOH@ sensors are numbered from 1 to 12, according to the numbering in Table 4.2

Colour analysis & Chemometrics

After the equilibration, Dye-EVOH@ arrays are removed from the solution, dried by common adsorbent paper and photos of the array are acquired by a Nikon COOLPIX S6200 in a lightbox to ensure a constant and reproducible light exposition. Dye-EVOH@ sensors RGB triplets are used as experimental data while pH value, measured after equilibration by the means of a pH-meter, is used as reference value for the following multivariate data treatment.

From preliminary investigations, a two-step approach, combining Principal Component Analysis (PCA) and Partial Least Square regression (PLS) has proven to be the best data elaboration method, in terms of model robustness and predictive performances. PCA is firstly run on the entire data set and, from the resulting score plot, three pH subintervals partially overlapped are highlighted, characterised by the same informative Dye-EVOH@ sensors. Then, PLS is applied separately for each pH subinterval, developing a tailored model from the RGB triplets of the Dye-EVOH@ sensors that turn their colour in the pH range under investigation. This approach allows to improve accuracy and to avoid gross predictive errors, sometimes occurring due to those Dye-EVOH@ sensors with similar colours, in terms of RGB values, at extremely acid and alkaline pHs.

Training and test set

Both for the training and the test set, 1 L stock solution at defined composition and pH are prepared and then divided into 100 mL samples. For the training set, 4 replicates are prepared from each solution, for the test set, only 1. Therefore, the training input matrix has 36 columns (3 RGB indexes per 12 Dye-EVOH@ sensors) and 56 rows (14 stock solutions per 4 replicates) while the test set matrix has 36 columns (3 RGB indexes per 12 Dye-EVOH@ sensors) and 36 rows (9 stock solutions per 4 replicates).

In Table 4.4 the solutions used for training set samples are listed. For extremely acid and alkaline pH, dilute strong acid and base are exploited while, in the other cases, common buffers are used, avoiding buffering agents with one or more volatile species involved in the acid-base equilibria which may evaporate during the analysis and modify the samples' composition. Furthermore, ionic strength was buffered at 0.1M adding $NaNO_3$ in the solution with lower content of acid-base species (from B to O).

Table 4.4: Solutions used for the training set samples

Solution	Acid-base species	Concentration (M)	I buffer	Concentration (M)	Exp. pH
A	HNO_3	0.1	--	--	1.12
B	HNO_3	0.01	$NaNO_3$	0.1	2.06
C	NaH_2PO_4	0.01	$NaNO_3$	0.1	2.19
D	NaH_2PO_4	0.01	$NaNO_3$	0.1	3.07
E	Citric acid	0.01	$NaNO_3$	0.1	3.97
F	Citric acid	0.01	$NaNO_3$	0.1	4.97
G	Citric acid	0.01	$NaNO_3$	0.1	6.02
H	Na_2HPO_4	0.01	$NaNO_3$	0.1	7.01
I	Na_2HPO_4	0.01	$NaNO_3$	0.1	8.05
L	$NaHCO_3$	0.01	$NaNO_3$	0.1	8.99
M	$NaHCO_3$	0.01	$NaNO_3$	0.1	10
N	$NaHCO_3$	0.01	$NaNO_3$	0.1	11.06
O	NaOH	0.01	$NaNO_3$	0.1	12.13
P	NaOH	0.1	--	--	13.04

In Table 4.5 the solutions used for test set samples are listed. We aim to test the model robustness in the case of different ionic strength and buffering agents. Therefore, solutions from a to f are prepared using already employed buffering agents but with I=1M (a-c) and I=0.01M (d-f) while solutions from g to i are prepared using Good's buffers at I=0.1M.

Table 4.5: Solutions used for test set samples

Solution	Acid-base species	Concentration (M)	I buffer	Concentration (M)	Exp. pH
a	Citric acid	0.01	$NaNO_3$	1	4.04
b	Na_2HPO_4	0.01	$NaNO_3$	1	6.95
c	HCO_3	0.01	$NaNO_3$	1	9.82
d	Citric acid	0.01	$NaNO_3$	0.01	4.08
e	Na_2HPO_4	0.01	$NaNO_3$	0.01	7.08
f	HCO_3	0.01	$NaNO_3$	0.01	9.97
g	MES	0.01	$NaNO_3$	0.1	5.52
h	PIPES	0.01	$NaNO_3$	0.1	7.00
i	EPPS	0.01	$NaNO_3$	0.1	8.45

Dye release

In this case, dye release is checked only for two out of twelve Dye-EVOH@, having demonstrated that no significant differences are observed changing the dye. UV-Vis spectroscopy is used, as already argued in Section 4.2.5, registering the spectra at alkaline pH to exploit the intense absorption of the deprotonated form of the test dyes, which are Dye n°3 (596 nm) and n°7 (617 nm). Dye release is tested dipping around 100 mg Dye-EVOH@ sensors in 25 mL NaOH 0.1M, registering UV-Vis spectra after 2, 5, 8 and 10 days and calculating the amount of dye released.

Evaluation on logK_a shift after functionalisation

In order to evaluate the logK_a shift, occurring after dye covalent linkage to EVOH, a collaboration with Prof. Remelli's group from the University of Ferrara is established, having as purpose the potentiometric titration of dyes in solution and Dye-EVOH@ by the means of an automated titration system (pH meter Orion EA 940; combined microelectrode Metrohm 6.0234.100, automatic burette Hamilton with 500 µL microsyringe Hamilton; titration vessel with thermostat jacket Metrohm and circulation thermostat Lauda L100). This investigation is performed by selecting the same test sensors used for release experiments: **3**-EVOH@ and **7**-EVOH@.

Dye logK_a value is calculated both in solution (0.002mmol dye) and after functionalisation (10 Dye-EVOH@ sensors, around 20 mg), in 5 mL of 10% EtOH aqueous solution I=0.1M (KCl), starting from acid pH and adding NaOH. The equilibration kinetic is unknown and thus two different modes are firstly tested:

- variable times: $\Delta V/t$ = 0.002 mV/s and t_{max}= 2 hours per each titrant addition
- fixed times: t = 15–18 min after each titrant addition

Considering that, from the variable times' mode, quite rapid titrations are performed, the results obtained by the fixed times' mode are considered reliable.

Furthermore, the exact amount of dye linked to EVOH is not known. From the EDX results, reported in Section 3.3.2, a rough estimation of 0.1 mmol/g has been performed, which means around 0.002 mmol per 10 Dye-EVOH@ sensors, but this value is inaccurate. For this reason, to calculate the logK_a' value, both the theoretical and refined dye amount is used in the data elaboration, performed using Hyperquad [89].

4.3 Results and discussion

4.3.1 Sensors thickness selection

A rapid method is developed to verify sensors thickness and select the most effective thickness range. Neither weighing each sensor, having a very low average mass of 0.002(1) g (average weight calculated by weighting 20 Dye-EVOH@ sensors), nor measuring each one's thickness using a profilometer, requiring too much experimental effort, can be exploited for this purpose. Exploiting the relationship between thickness and colour intensity turns out to be a more suitable approach in this context.

Here below the results for **BCP**-EVOH@ are described while the results for **CR**-EVOH@ are reported in Appendix VI: CR-EVOH@ sensors thickness selection. 72 **BCP**-EVOH@ sensors, obtained from one batch synthesis exhibiting different thicknesses, are equilibrated at alkaline pH both to enhance the colour intensity and to mimic the sensor preparation for real sample monitoring. This batch of sensors is used as the training set to map the entire experimental domain. RGB triplets are used as input dataset for PCA to reduce the data's dimensionality and obtain a single parameter representative of sensors thickness. The loading plot is reported in Figure 8.4 in Appendix III: Loading and score plots.

From the score plot, shown in Figure 4.5**a**, important assumptions are driven. More than 96% of the dataset variance is explained by PC1, which is oppositely related to sensors thickness: the lower the score value on PC1, the higher the sensor thickness. Thus, the score value on PC1 can be used to estimate sensor thickness, both for the training set and any other following sensor, by projection in the score plot.

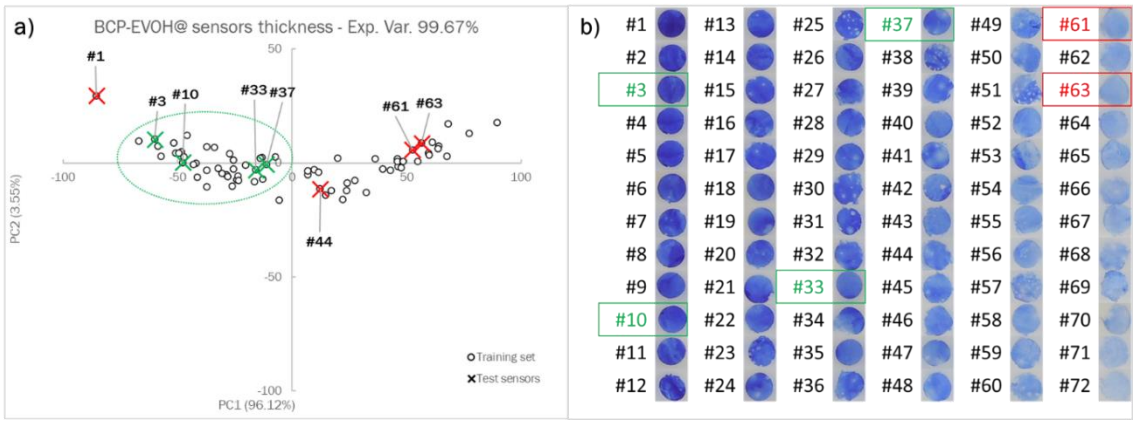

Figure 4.5: PCA score plot on the first two components based on RGB triplets of 72 sensors of various thicknesses (white circles); the sensors tested for real samples monitoring are highlighted with green and red x, and the suitable thickness range is identified by the green oval (a). Pictures of the 72 sensors used to build the PCA model. The sensors tested for milk monitoring are highlighted in green and red (b).

Once this parameter is measured, the most effective thickness range has to be identified, bearing in mind that too thin sensors show faded colours, difficult to be analysed by naked-eye, opposite thick sensors have lower sensing rate, resulting in a delay in spoilage monitoring. Therefore, from the 72 sensors, reported in Figure 4.5**b** ordered by increasing score on PC1, thus by decreasing thickness, 8 sensors, representative of various thicknesses are selected and used in preliminary real samples monitoring. 4 out of 8 sensors, highlighted in green in Figure 4.5, present a suitable colour transition during milk freshness monitoring. In comparison, the remaining 4 sensors were either too thick (sensor #1) or too faded (sensors #44, #61 and #63) to be used.

In conclusion, only sensors within the thickness range identified by the green circle in Figure 4.5**a** will be used for real samples monitoring. The same analysis is performed also for **CR**-EVOH@ sensors selecting the suitable thickness range for real samples monitoring, using chicken breast slices as test food.

4.3.2 Protein foods: CR-EVOH@ dual sensors device colour evolution

After thickness selection and sensors equilibration, we register **CR**-EVOH@ dual sensors device colour evolution during spoilage process of chicken breast slices, codfish fillets, swordfish fillets, plaice fillets, scorpionfish fillets and gurnard fillets, stored at 4 °C. All these foods present very similar colour evolution, apart from gurnard fillets discussed below, thus only the training sets of chicken breast slices and codfish fillets are shown in Figure 4.6.

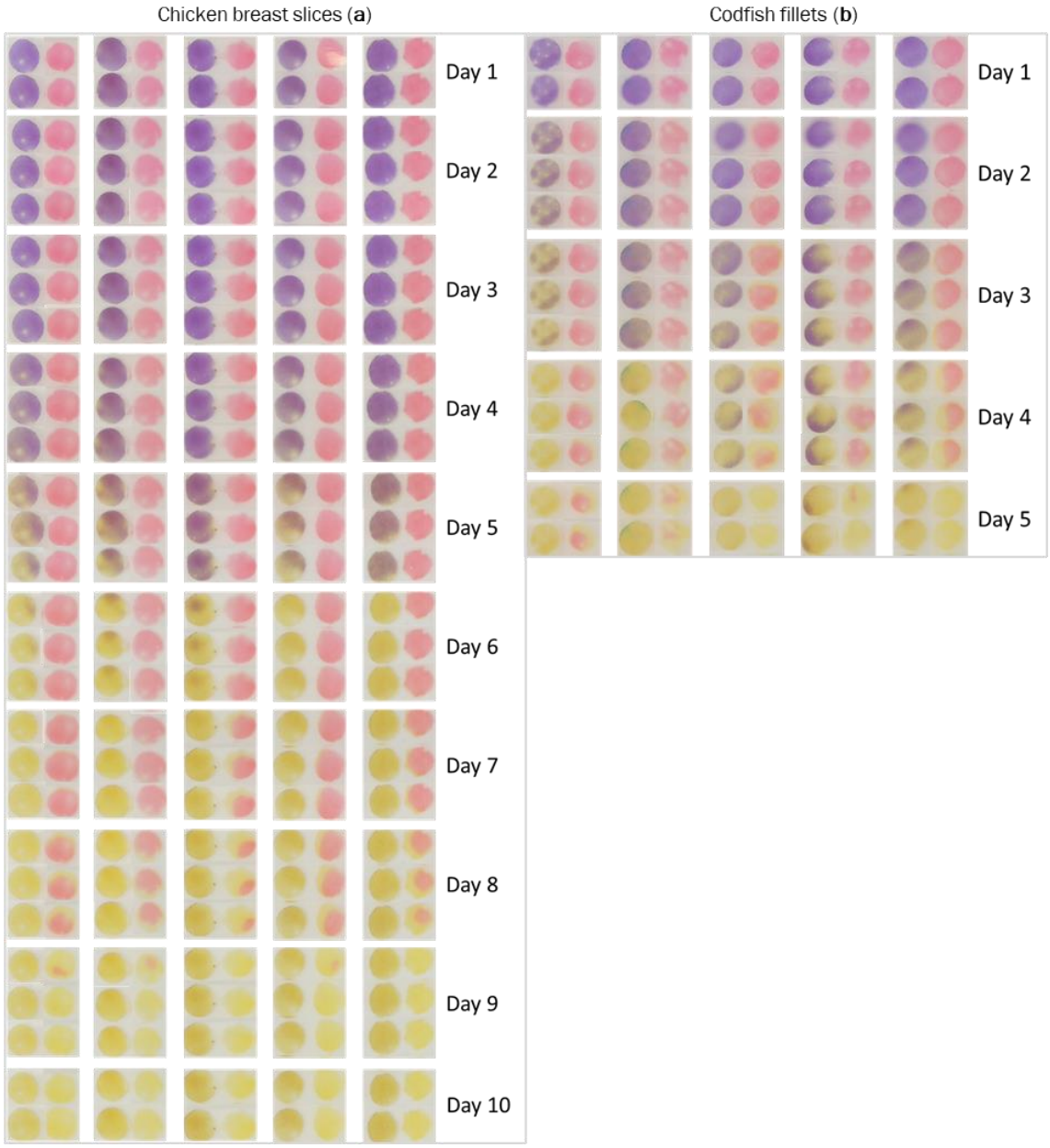

Figure 4.6: CR-EVOH@ dual sensors device colour evolution over chicken breast slices (a) and codfish fillets (b), stored at 4 °C.

As hinted before, naked-eye analysis of colour evolution represents a crucial step in the device development since, in the final application, the device has to work like a traffic light for protein foods freshness and should be readable for untrained consumers. Therefore, the device has to show a clear and glaring colour transition according to headspace composition and thus food freshness.

Analysing Figure 4.6, we can observe that, for both foods, in the first spoilage step, the so-called "early spoilage", weak acid volatile by-products released by bacteria, are detected by b-**CR**-EVOH@ that turns its colour from violet (CR^-) to yellow (HCR). The conversion occurs between Day 4 and Day

6 for chicken breast slices and between Day 2 and 4 for codfish fillets, with a slightly different timing between the replicates due to the high intrinsic variability of foods under investigation.

Then, in the second spoilage step, the so-called “spoilage”, bacterial proteins degradation begins with the consequent release of thiols and amines. As deeply discussed in the literature [52], only a few of these by-products are volatile at buffered pH typical of biological matrixes; thus, only a slight increase of pH could be observed. a-**CR**-EVOH@ detects this headspace atmosphere modification by changing its colour from pink (H_2CR^+) to yellow (HCR). This colour change occurs within Day 7 and 9 for chicken breast slices and within Day 4 and Day 5 for codfish fillets. The other fish products share the same colour evolution but with slightly different timing.

Finally, gurnard fillets are selected to prove the applicability of our device also for fish products filleted directly in the supermarket, or the fishery, presenting various fillets dimensions and sold in an unsealed package. In Figure 4.7, the colour evolution of the dual sensors device during spoilage monitoring is reported. Considering the even higher experimental variability associated with this kind of food, three gurnard fillets package of the same whole fillets weight are monitored, inserting three devices per package.

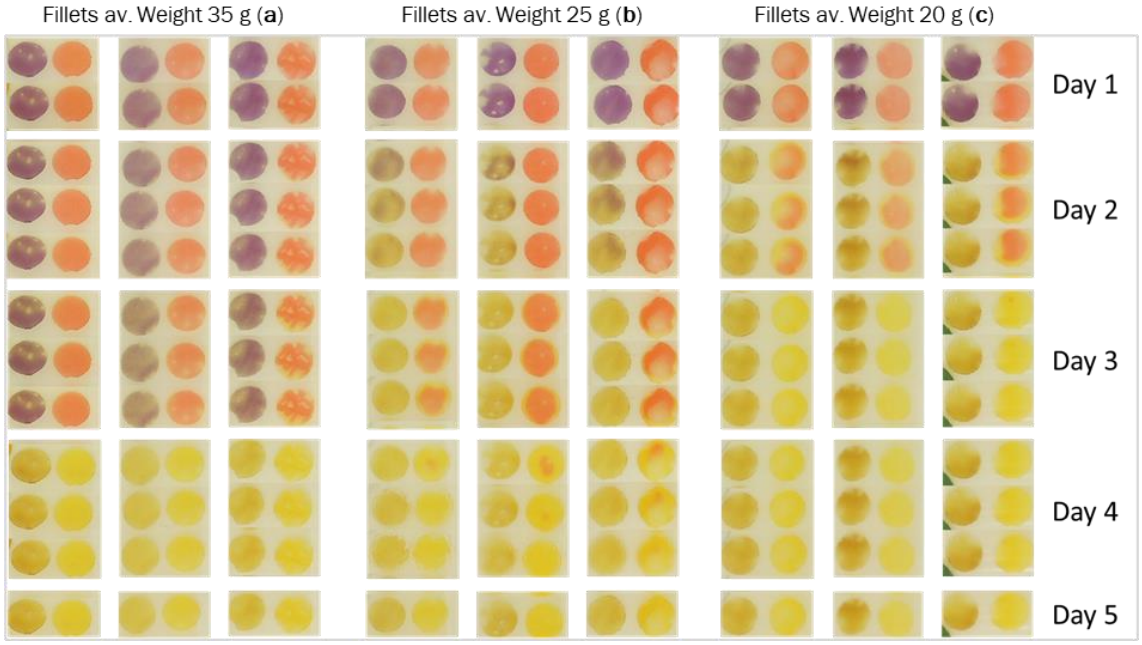

Figure 4.7: CR-EVOH@ dual sensors device colour evolution over gurnard fillets packages containing fillets with an average weight of 35 g (a), 25 g (b) and 20 g (c), stored at 4 °C.

Even from naked-eye analysis, it is visible that not only storage time but also the average weight, or dimension, of the fillets inside the package influence the spoilage rate. The colour evolution of the device corresponds to that shown in Figure 4.6 but the timing is different in the package with different fillets dimensions. Bigger fillets (Figure 4.7**a**) present slower spoilage than smaller fillets

(Figure 4.7**c**) probably due to the lower surface area. A similar effect is observed for the different spoilage rates of minced meat, compared to thick steaks, for instance, as it is well-known in daily life experience.

4.3.3 Protein foods: spoilage modelling by PCA

Naked-eye analysis of colour evolution allows qualitative information about spoilage process, which can be visualized and modelled by multivariate elaboration of **CR**-EVOH@ dual sensors RGB triplets. Therefore, PCA is then performed on the RGB triplets of the sensors during degradation to visualise the degradation process of each food training set. In Table 4.6, the % explained variance on the first two components per protein food under investigation is reported.

Table 4.6: % Explained variance on PC1, PC2 and PC1+PC2 per protein food.

Protein food	% Exp. Var PC1	% Exp Var PC2	% Exp Var PC1+PC2
Chicken breast slices	85.43%	8.26%	93.7%
Swordfish fillets	78.01%	16.53%	94.5%
Codfish fillets	89.57%	5.23%	94.8%
Plaice fillets	81.13%	11.53%	92.7%
Scorpionfish fillets	65.44%	20.67%	86.1%

In all cases, the % explained variance on the first two components is very high thus, these two components are selected for the final models. All the loading plots are reported in Figure 8.5 in Appendix III: Loading and score plots. Being all the plots very similar, in Figure 4.8, only the score plots, built on the training set and preliminarily validated by projecting the test set, for chicken breast slices and codfish fillets are reported while the other score plots are displayed in Figure 8.6 in Appendix III: Loading and score plots.

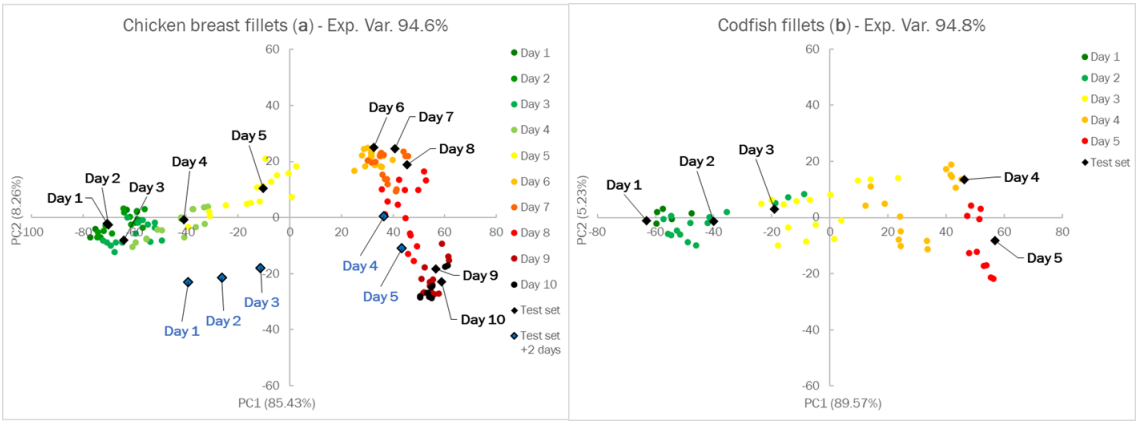

Figure 4.8: The score plots of the PCA models on the first two principal components, built on the training set and validated by projection of the test set, for chicken breast slices (a) and codfish fillets (b).

In both cases, PC1, which accounts for the main % explained variance, represents the ongoing spoilage process, and the samples' score values on the x-axis increase during spoilage. PC2 meaning, instead, slightly differs in the two cases: for chicken breast slices (Figure 4.8**a**), it can be specifically related to the "spoilage" step, occurring between Day 6 and Day 10. In this time lapse, samples' score values on PC1 continue to increase while the PC2 values significantly decrease.

Opposite, for codfish fillets (Figure 4.8**b**) and the other fish products, PC2 accounts for the experimental variability, both in terms of sensors and fish products, and the higher variability results in the higher % explained variance on this component. Therefore, for the different fish products, the overall experimental variability increases in the following order: codfish < plaice < swordfish < scorpionfish fillets. It must be underlined that in samples chilled stored the spoilage process is slower and progressive thus the well-defined clusters, observed in the previous sections, are replaced by a gradual transition of the samples in the plot during degradation.

As for test set projection, the new samples acquired the same day of the delivery from the supplier show a similar degradation process and are correctly located in the score plots in both cases. Much more interesting is the case of the test sample acquired two days after the delivery: Dye-EVOH@ sensors device can detect the lower freshness of the food and, as spoilage goes on, a shift of two days is observed in the location of the sample in the score plot, with test sample at Day 3 aligned on PC1 to training samples at Day 5 and so on.

4.3.4 Protein foods: evaluation of source and dimension of fish fillets' effect on spoilage by 3-Way PCA

As already hinted before, 3-Way PCA represents the eligible tool to deal with 3-dimensional datasets; in our case, this technique is of paramount importance to evaluate the effect of various parameters on the spoilage process. In these cases, **CR**-EVOH@ RGB triplets (labelled as *variables*) of fish fillets of different source or dimensions (named as *objects*) are acquired at given times during degradation (labelled as *conditions*) and are analysed jointly to evaluate the cumulative effect of time and the other specific parameter on the spoilage process registered by the device.

As for the first case, the source of fillets represents the parameter of interest and the training sets of swordfish, codfish, plaice and scorpionfish fillets (five replicates per each) are used as input dataset. Therefore, the overall matrix has 6 columns (3 RGB indexes per 2 **CR**-EVOH@ sensors) and 300 rows (12 acquisition times per 25 samples). The cumulative % explained variance after unfolding for each mode is reported in the first two columns of Table 4.7, while the Tucker 3 model value is 76.8%. The % explained variance is generally satisfactory, and the small difference between the Tucker 3 model value and the cumulative values after unfolding means that very little information is lost in considering the common spoilage process rather than the single ones.

Table 4.7: Cumulative % explained variance after unfolding for each mode for 3-Way PCA models of fish fillets of different sources (Columns 1 and 2) or dimension (Column 3 and 4).

Mode	Fillets source		Fillets dimension	
	PC1	PC1&2	PC1	PC1&2
Conditions	79.56%	97.58%	58.56%	91.15%
Objects	58.18%	79.96%	59.78%	85.17%
Variables	60.92%	80.91%	79.46%	89.49%

In Figure 4.9**a**, 3-Way PCA triplot, showing the loading values for *conditions*, *objects* and *variables*, is reported. Acquisition times (*conditions*) show a decreasing loading value on the y-axis during storage time, and a clear separation between the first two and the last three days is observed. Opposite, replicates of fish products (*objects*) are located in well-defined clusters, except for scorpionfish fillets which present a higher variability. As for the *variables*, a-**CR**-EVOH@ Green and Blue, associated with the pink-yellow transition, have the higher loading value on Axis 1 while b-**CR**-EVOH@ Blue, related to violet-yellow turn, is the main effect on Axis 2. We could assume that the a-**CR**-EVOH@, which detects the final spoilage, has the main influence in objects separation alongside Axis 1, while b-**CR**-EVOH@, which detects the early spoilage, determines the conditions' distribution alongside Axis 2.

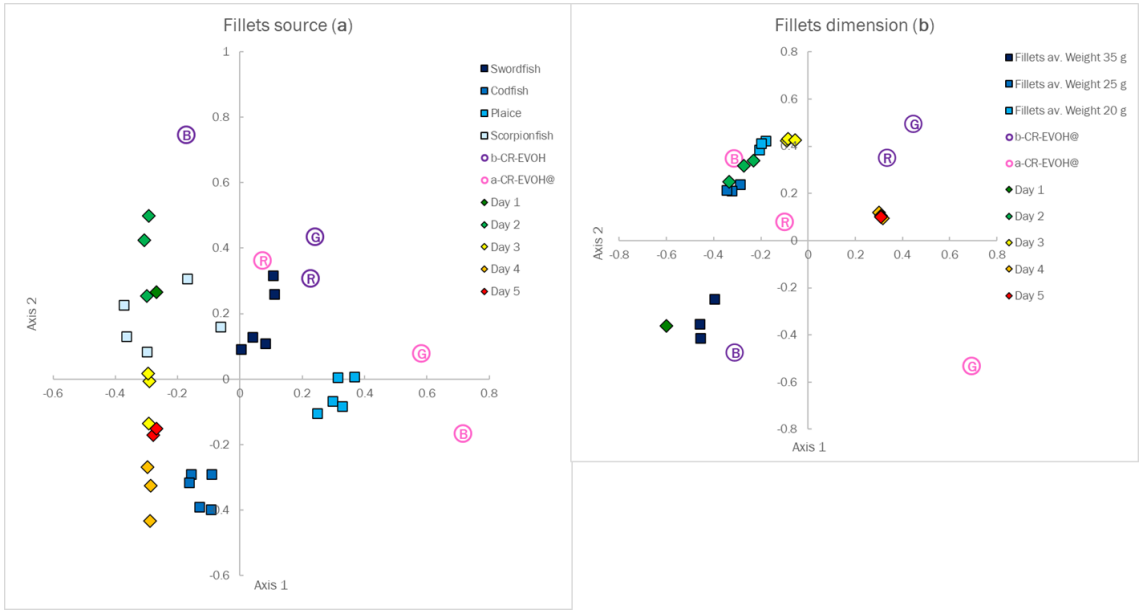

Figure 4.9: 3-Way PCA triplot reporting the loading values for *conditions* (diamonds), *objects* (square) and *variables* (spots) for fillets of different source (a) and dimension (b).

In the second case, the average dimension, or weight, of small fish fillets on spoilage rate is investigated. As discussed before, the RGB triplets of nine **CR**-EVOH@ dual sensors devices, inserted three per each fish package, containing gurnard fillets of different average weights, represent the

input dataset for this analysis. Therefore, the overall matrix has 6 columns (3 RGB indexes per 2 **CR**-EVOH@ sensors) and 99 rows (11 acquisition times per 9 samples). The difference between the cumulative % explained variance after unfolding, reported in the last two columns of Table 4.7, and the Tucker 3 model value (81.6%) is even lower than before since the *objects* are much more similar to each other and thus even less information is lost in considering the overall spoilage process.

In Figure 4.9**b**, 3-Way PCA triplot is displayed. As for *conditions*, the loading value on the x-axis increases during storage time while on the y-axis, it has a maximum on Day 3; opposite, as for *objects*, the loading value on both axes increases for lower average fillets weight. The *variables* loading values interpretation is very interesting. b-**CR**-EVOH@ presents a violet colour, which means high Blue value, in the bottom left of the plot, i.e., at the beginning of storage and for heavier fillets, while opposite it turns to yellow at the top right, i.e., at the end of the storage. As for a-**CR**-EVOH@, it remains pink (high value of Red and Blu, low value of Green) up to Day 3, and then it turns to yellow while the average fillets mass is much less related to this sensor colour evolution. From this plot, we could confirm that the difference in the average fillets weight mainly influences b-**CR**-EVOH@ behaviour, and thus the detection of the early spoilage, while it slightly influences a-**CR**-EVOH@ colour evolution, which means the final spoilage recognition.

4.3.5 Milk: BCP-EVOH@ sensor colour evolution

We register **BCP**-EVOH@ sensor colour evolution during spoilage process of whole, semi-skimmed and skimmed milk, stored at 4 °C. In Figure 4.10, the pictures of two out of five replicates per each milk type are displayed. A very similar behaviour, with slightly different timing, is observed for the three milk types and three steps can be highlighted. During Day 1, **BCP**-EVOH@ sensors equilibration at neutral pH is observed, with the colour transition from blue to green. A stable green colour is registered from Day 2 to Day 8-9 with no appreciable change in the sensor's hue. During Day 9-10, sensors showed a transition from light green to yellow corresponding to pH decrease after milk spoilage. Further information can be extracted by multivariate analysis of the pictures, considering that pictures during Day 1 have to be excluded from multivariate analysis because the colour transition, showed by the sensors, depends on the equilibration at milk pH rather than on milk freshness monitoring.

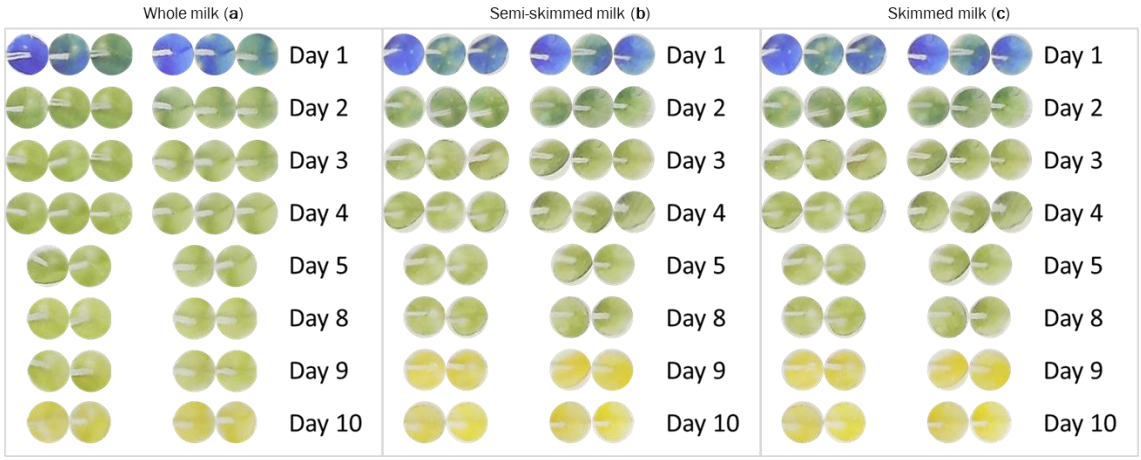

Figure 4.10: Colour evolution of two out of five sensors dipped in whole (a), semi-skimmed (b) and skimmed (c) milk during 10-days storage at 4°C, followed by photo acquisition 3 (Day 1-4) or 2 (Day 5-10) times per day.

4.3.6 Milk: spoilage modelling and comparison by PCA and 3-Way PCA

Firstly, PCA is applied separately to each milk type to visualize the spoilage process but, due to the large number of samples, the score plots required a laborious interpretation. In Appendix III: Loading and score plots, the loading (Figure 8.7) and score (Figure 8.8) plots are reported. In this case, the output of 3-Way PCA is much easier to analyse and more informative. Similarly to the previous case, described in Section 4.3.4, acquisition times (17), milk samples (15) and sensors RGB indexes (3) are labelled respectively as *conditions*, *objects* and *variables*. Therefore, the input matrix has 3 columns (3 RGB indexes per 1 **BCP**-EVOH@ sensors) and 255 rows (17 acquisition times per 15 milk types). The first step in 3-Way PCA interpretation consists of comparing the cumulative % explained variance after unfolding, reported in Table 4.8, and the Tucker 3 model value (87.71%).

Table 4.8: Cumulative % explained variance after unfolding

Mode	PC1	PC1&2
Conditions	60.51%	92.95%
Objects	60.13%	89.31%
Variables	76.89%	99.38%

The Tucker 3 model value is slightly lower than the other values, meaning that, considering the common spoilage process, only a small part of the overall information is lost, and the spoilage process presents no significant differences in the three milk types. Moreover, all the values related to the % explained variance are definitively high, considering the variability of the system.

As interpretation is concerned, the loading values of each mode are jointly displayed in the triplot, reported in Figure 4.11. As for the *objects*, they are located alongside the x-axis, no clear separation is observed among different milk types, but whole and semi-skimmed samples are located at lower

x values than skimmed samples, suggesting similar spoilage. Opposite, a clear separation is observed for the *conditions* loadings alongside the *y*-axis: the *y* value increases with time, but times from Day 2 to Day 8 are separated by the final two days when almost all milk samples are spoilt. As for the *variables*, they all have a positive loading value on the x-axis, with a B value higher than the others, which means that they all play a similar role in *objects*' location. Opposite, on the *y*-axis, R and G have positive loading values, and B has a negative value, suggesting that, during spoilage, R and G indexes increase while B index decreases, which correspond to the numerical effect of transition from green to yellow on the variables.

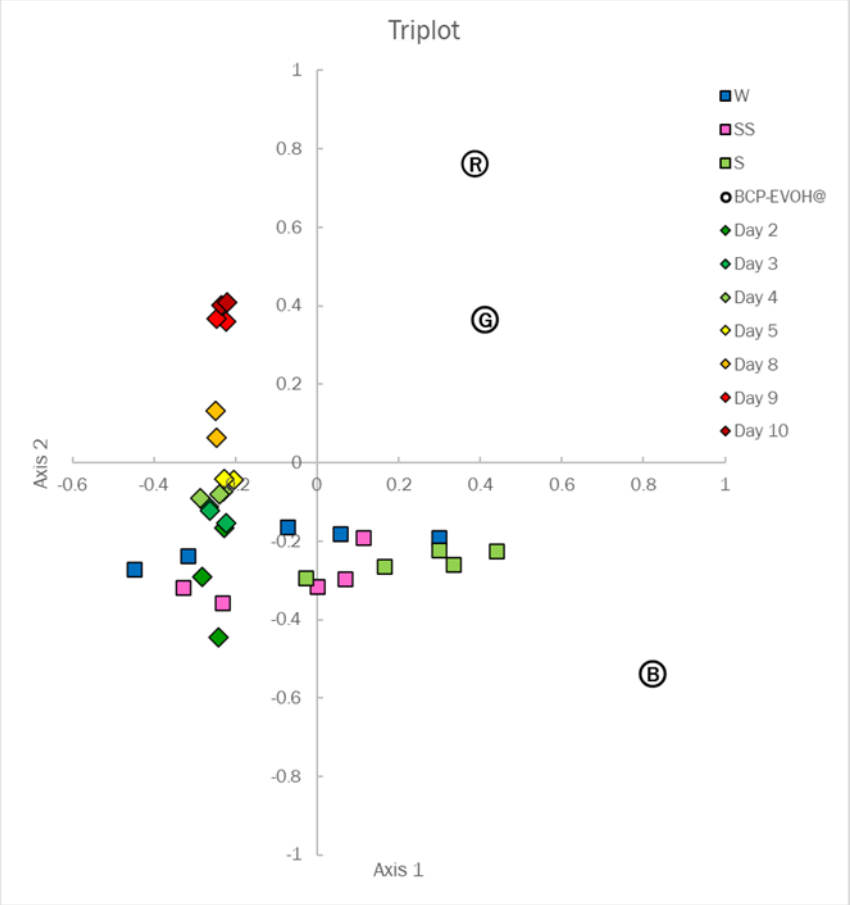

Figure 4.11: 3-Way PCA triplot reporting the loading values for *conditions* (diamonds), *objects* (square) and *variables* (spots) for different milk types

4.3.7 Milk: titratable acidity determination by Soxhlet-Henkel method

Unsupervised chemometric techniques, like PCA and 3-Way PCA, are suitable for visualizing the spoilage process monitored by **BCP**-EVOH@. Nevertheless, to develop qualitative or quantitative predictive models, supervised methods are needed, and a reference value, independently measured, is required. For this purpose, we use the Soxhlet-Henkel titration to determine the titratable acidity of milk samples during spoilage, expressed as °SH/100 mL. The value °SH=8 is commonly referred

to as the threshold value for milk suitable for human consumption: milk samples with °SH<8 are safe while °SH>8 identifies spoilt milk.

In Figure 4.12, the average °SH values and the related standard deviations are reported. In the histogram the different spoilage rate of the milk types is displayed: whole milk presents °SH>8 at Day 10, semi-skimmed milk from Day 9 and skimmed milk from Day 8. Moreover, after threshold crossing, °SH value remains between 8 and 8.5 for whole and semi-skimmed milk, while it reaches values between 9.5 and 10 for skimmed milk. This behaviour is probably due to the different matrix compositions of the samples: skimmed milk undergoes more processing steps, resulting in a matrix with lower buffering capacity. Consequently, when spoilage is ongoing, the acidic by-products are less buffered than in the other milk types and provoke a higher pH decrease.

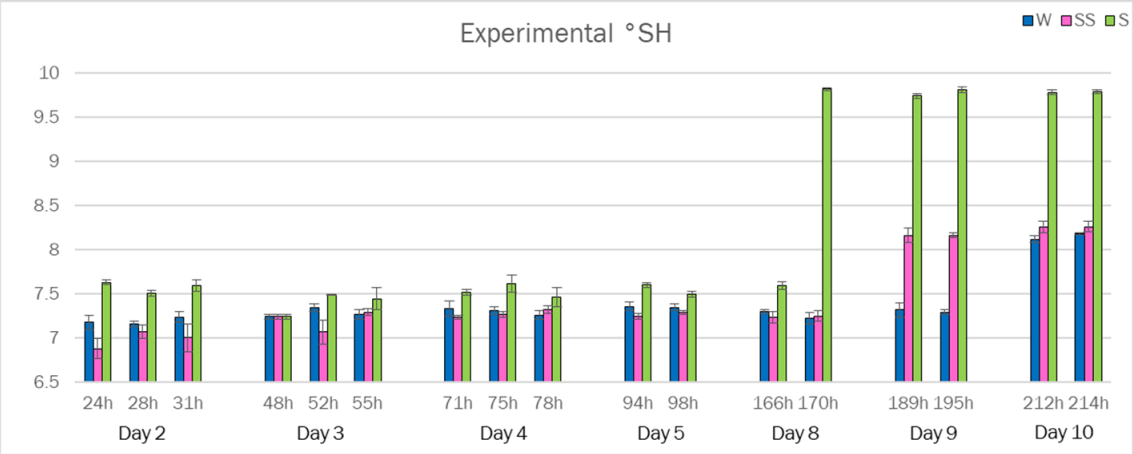

Figure 4.12: Average °SH and standard deviation measured 3 or 2 times per day by Soxhlet-Henkel titration for the three milk types (W, SS and S) during 10-days storage at 4°C.

4.3.8 Milk: samples classification by LDA

Aiming at the final application as smart labels, developing a classification model that discriminates between fresh and spoilt milk is paramount. For this purpose, LDA is applied to the dataset, identifying 2 classes, fresh and spoilt, and selecting °SH=8 as the delimiter [28]. Indeed, differently from the first classification attempt with EVOH (32%)-based device, described in the previous Chapter, here an independent measure is always associated with the sensor's photo making possible a rigorous application of this chemometric technique.

As described in detail in the previous section, a stepwise approach is used, and LDA is applied three times on a dataset progressively bigger and more complex. In Step 1, each milk type is analysed separately. The dataset, consisting of the RGB indexes of the 5 **BCP**-EVOH@ during 10-days acquisition, is split into training and test (10:7). The model is developed on the training set and exploited to predict the test set. This step aims to verify the correct location of samples of the same type and with the same sensors. The % correct prediction in cross-validation (CV) and prediction (P)

are reported in Table 4.9: for whole and semi-skimmed milk, both values are 100%, while a bit lower percentage is observed for skimmed milk.

Table 4.9: % correct predictions in cross-validation and prediction for LDA (Step 1)

Milk type	% Correct prediction CV	% Correct predictions P
Whole	100%	100%
Semi-skimmed	100%	100%
Skimmed	98.8%	96.7%

In Step 2, the total model is developed per each milk type, exploiting as input data the entire dataset, and they are used to predict the dataset of the two other milk types. This step aims to verify the location of samples of different milk types but with sensors of the same batch. The % correct prediction in cross-validation (CV) and prediction (P) are reported in Table 4.10: the value referring to cross-validation is similar to Step 1 while, in prediction, the percentage value ranges from 94 to 100%.

Table 4.10: % correct predictions in cross-validation and prediction using different milk type datasets as test samples for LDA (Step 2)

Milk type	% Correct prediction CV	% Correct predictions P		
		Whole milk	*Semi-skimmed milk*	*Skimmed milk*
Whole	100%	--	94.6%	97.2%
Semi-skimmed	100%	100%	--	94%
Skimmed	98.3%	100%	100%	--

Finally, in Step 3, a general model is developed, including the three datasets of all milk types. It is exploited to predict an unknown test set, completely independent from the first dataset. This step aims to verify the location of samples of different milk types and to observe the effect of sensors obtained from a different batch. For this model, the % correct prediction in CV is 97.7% while in P is 91.7%. In Figure 4.13, the reciprocal of the Mahalanobis distance from each class for the unknown samples is displayed: for each sample, the highest bar represents the class closest to that sample, so the assigned one. The only wrong location is the sample labelled as W_7 at Day 8, highlighted with the striped bars.

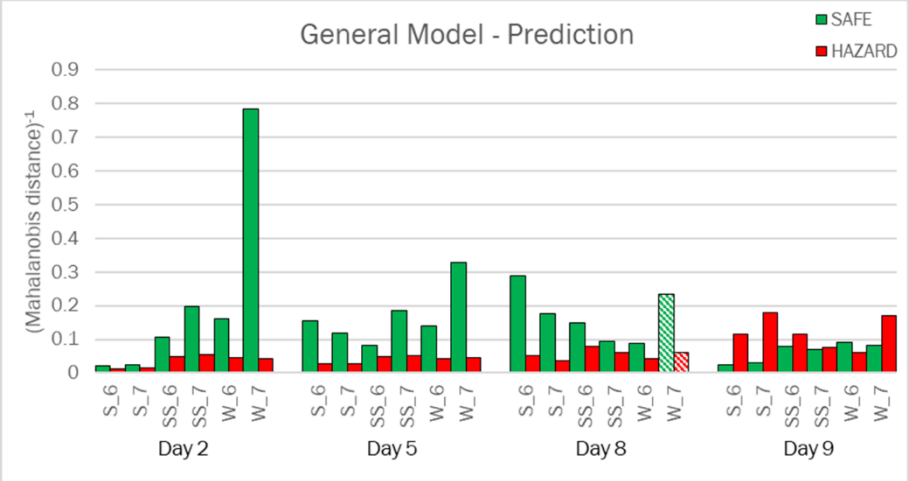

Figure 4.13: Prediction of the unknown test set by general LDA model (Step 3). On the *y*-axis, the inverse of each sample's Mahalanobis distance from each of the two classes is reported

To conclude, only one cheap sensor, the **BCP**-EVOH@, allows a definitely satisfying classification of any type of milk with a very simple, easy and rapid analysis.

4.3.9 Milk: °SH calculation by PLS

A further possible level of interpretation consists of developing a regression model able to calculate °SH during spoilage, based on **BCP**-EVOH@ sensor colour. For this purpose, PLS is applied to the dataset, using as a reference value, for each sensor acquisition, the correspondent °SH measured by Soxhlet-Henkel titration. Also, for PLS, the previously described stepwise approach is followed to gradually increase the complexity of the system under investigation. It must be underlined that, in all the cases, starting from 3 variables, the best performances are obtained with 3-components models, so no variables reduction is performed but, being the number of variables very low, this is not considered a problem further analysis.

In Table 4.11, the % explained variance in CV, Root Mean Square Error in CV (RMSECV) and P (RMSEP) for the Step 1 models are reported. The whole and semi-skimmed milk models present similar errors, while the skimmed milk model is characterized by definitely higher RMSECV and RMSEP, suggesting a worse performance for this milk type.

Table 4.11: % explained variance in CV, RMSECV and RMSEP for PLS (Step 1)

Milk type	% Exp. Var. CV	RMSECV	RMSEP
Whole	66.51%	0.1619	0.1438
Semi-skimmed	83.54%	0.1810	0.1805
Skimmed	74.19%	0.4562	0.6665

Moving on to Step 2, whose statistics are reported in Table 4.12, the total model developed per each milk type presents very similar RMSECV but, in the prediction of samples of different nature, very different performances are found. When semi-skimmed milk samples are predicted by the whole milk model and vice versa, RMSEP is around 0.3, slightly higher than the error in prediction in Step 1, consequently not so different from predicting the same milk employed for the training set. Opposite, predicting skimmed milk samples or exploiting the skimmed milk model to predict the other two, RMSEP is always around 1 or even higher. Based on this evidence, a general model including skimmed milk can not be developed; thus, only the whole and semi-skimmed milk samples are modelled jointly in Step 3.

Table 4.12: % Explained variance in CV, RMSECV and RMSEP, using different milk type datasets as test samples, for PLS (Step 2)

Milk type	%Exp. Var. CV	RMSECV	RMSEP		
			W	*SS*	*S*
Whole	68.84%	0.1620	--	0.3049	1.067
Semi-skimmed	83.28%	0.1886	0.2903	--	1.109
Skimmed	74.36%	0.5206	0.9349	1.041	--

Finally, in Step 3, the general model for whole and semi-skimmed milk samples is developed and exploited to predict an unknown test set, completely independent from the first dataset. For this model, the % of explained variance was 69.54%, and RMSECV was 0.2129, both values similar to those reported in Table 4.12 for these milk types. As for the prediction, RMSEP was 0.6526, definitively higher than the previous one, but it must be underlined that, in this set of unknown samples, also the variability of sensors from different synthetic procedures is taken into account, in addition to the food samples intrinsic variability. In Figure 4.14**a**, the comparison between experimental and fitted values, referred to the training set, is displayed: despite the intrinsic variability of the system, already discussed before, the distinction between samples before and after spoilage is clear.

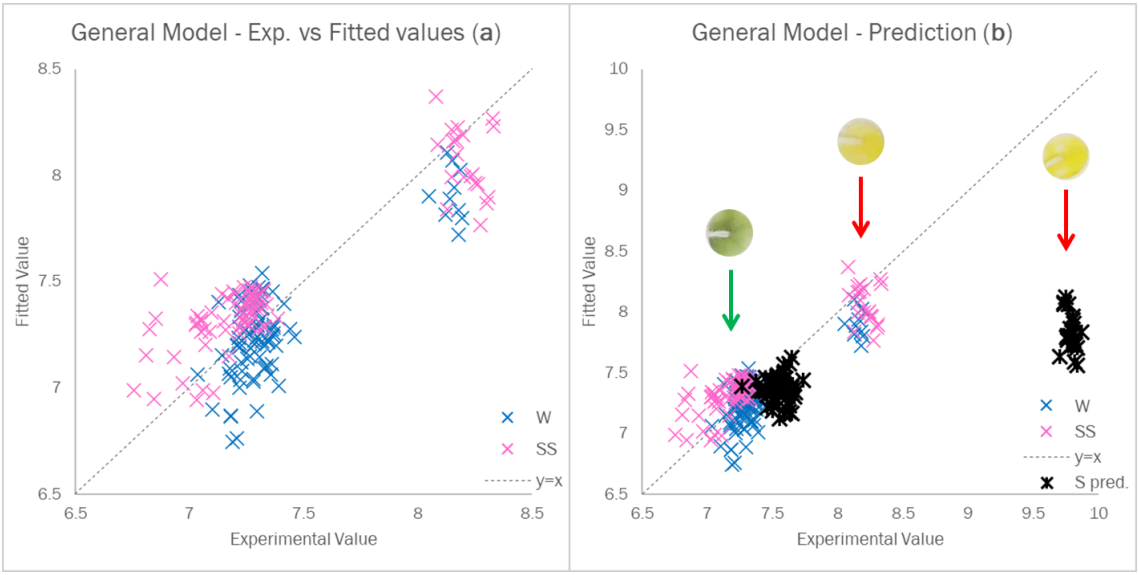

Figure 4.14: Experimental vs. Fitted plot for samples of whole and semi-skimmed milk, used as a training set for general PLS model (Step 3) (a) and for skimmed milk samples, used as test set, with an example of sensors colour in the different spoilage steps (b).

In Figure 4.14**a**, it appears evident that there are clusters of samples in some regions since milk °SH do not increase gradually during spoilage but present a neat gap before and after spoilage. From a strictly theoretical point of view, this model is biased since the training samples are not homogeneously distributed in the experimental domain. On the other hand, to obtain a homogeneous distribution, naturally spoiling milk samples can not be exploited but spoilage should be simulated by the gradual addition of acidic compounds. Since a compromise must be found between these two issues, we preferred to avoid any samples manipulation and to work on real spoiling milk, even if this approach leads to formally biased models, having in mind the final application as an intelligent packaging prototype.

In conclusion, the case of skimmed milk is evaluated more in detail. Exploiting the general model to predict °SH of skimmed milk dataset, the location of the samples in the Exp. Vs. Fitted values plot makes the matter clearer. Before spoilage (°SH<8), samples are predicted with errors similar to that of the training set. Opposite, samples after spoilage (°SH>8) are affected by a negative bias. There are two possible explanations: firstly, skimmed milk after spoilage presents °SH values much higher than the other milk types due to different matrix composition and lower buffering capacity, as already hinted above, and thus the model is used to predict sample out of the experimental domain mapped by the training set. Secondly, and much more influential, the sensor relies on one single pH indicator, BCP, able to detect pH changes in a defined pH range: at fresh milk pH, the equilibrium between blue deprotonated and yellow protonated forms results in the green colour. After spoilage, when °SH value rises to 8, pH decrease causes the complete protonation of BCP and the consequent yellow colouration, but any further pH decrease, or °SH increase, can not be detected since the sensor

colour remains unchanged. For these reasons, °SH values of skimmed milk samples after spoilage, typically between 9.5 and 10, can not be correctly calculated by the **BCP**-EVOH@ sensor.

4.3.10 Milk: comparison between BCP-EVOH@ sensor and reference method

The results of Figure 4.14 can be visualised plotting the average values of measured °SH and PLS output per each acquisition time, as shown in Figure 4.15, to perform an easier comparison between the two methods. The case of the whole milk is presented in Figure 4.15**a** and the one of semi-skimmed milk in Figure 4.15**b**. As it is visible, both the methods allow to clearly identify the threshold value crossing, which means the complete spoilage, and a good agreement between the average values is observed during the entire monitoring. Standard deviations are generally higher for the PLS model than for the reference method, but it is obvious because the PLS model is built relying on the Soxhlet-Henkel titration reference value. It means that it takes into account the errors of both the reference model and the colourimetric sensor. Nevertheless, this encouraging result suggests the prospective capability of measuring milk spoilage with this cheap, easy and rapid sensor as an alternative to laborious and time-consuming Soxhlet-Henkel titration.

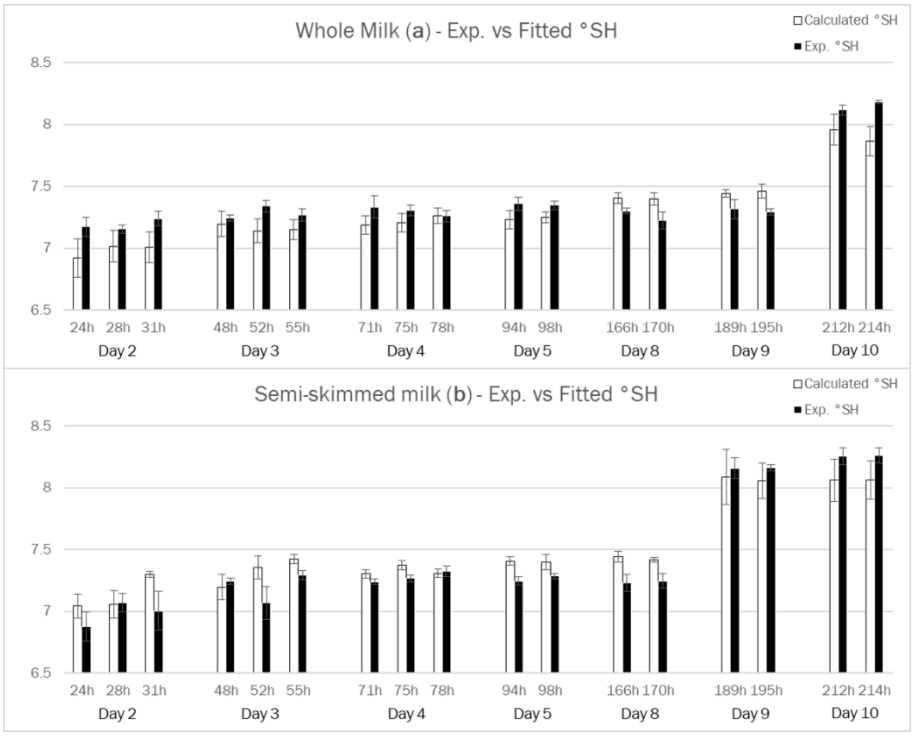

Figure 4.15: Average value and standard deviation of °SH calculated by PLS and measured by the reference method for whole (a) and semi-skimmed (b) milk

4.3.11 Milk: BCP-EVOH@ sensor dye release

In Figure 4.16, UV-Vis spectra registered for concentrated (Figure 4.16**a**) and simulated (Figure 4.16**b**) samples are reported. In concentrated samples, BCP is released in solution at increasing amounts from Day 2 to Day 8, while dye concentration in solution is only slightly increased in the last two days.

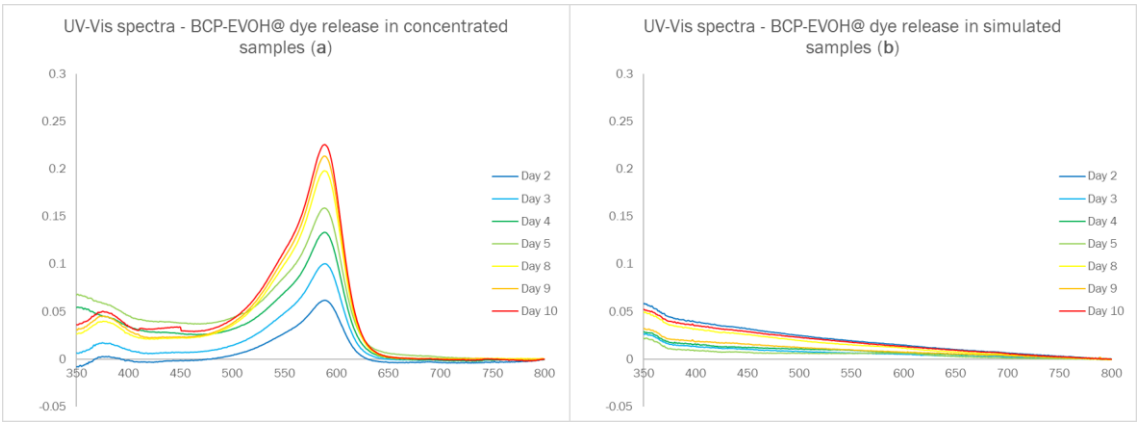

Figure 4.16: UV-Vis spectra of solutions from release experiments in concentrated (a) and simulated (b) samples

In Table 4.13, BCP concentration in solution (µM) and BCP release, expressed as µmol per **BCP**-EVOH@ g, are reported. Considering the estimated value of 0.1 mmol/g of BCP content in **BCP**-EVOH@, dye release ranges from 0.6% to 2% of total BCP content in 10 days. Taking into account the low amount of dye released, even in concentrated conditions, the slow release kinetic and the equilibrium reached in the last days we can assume that, during the synthetic procedure, the washing step is not efficient enough and, during **BCP**-EVOH@ polymerisation, some BCP not linked to the polymer matrix is not washed away and remains within the polymeric chains. These BCP molecules are then slowly released after immersion in aqueous solutions.

Table 4.13: Absorbance value at 589nm, BCP concentration in solution (µM) and BCP release (mmol/g) for release experiments in concentrated and simulated samples

Time (d)	Concentrated samples			Simulated samples	
	A (589nm)	[BCP] (µM)	BCP release (µmol/g)	A (589nm)	[BCP] (µM)
Day 2	0.062	2.3	0.57	0.016	<LOD
Day 3	0.101	3.6	0.91	0.006	<LOD
Day 4	0.134	4.8	1.20	0.007	<LOD
Day 5	0.159	5.7	1.43	0.006	<LOD
Day 8	0.198	7.1	1.78	0.013	<LOD
Day 9	0.214	7.7	1.92	0.008	<LOD
Day 10	0.226	8.1	2.03	0.014	<LOD

As for simulated samples, the concentration of BCP released is below the LOD for UV-Vis measurements, as clearly visible from the spectra reported in Figure 4.16**b**, but, assuming the same release process, after 10 days of equilibration in milk of one **BCP**-EVOH@ sensor (estimated average weight 2.5 mg), the amount of BCP released in milk is around 5 nmol or 3 µg.

In conclusion, the amount of BCP released is definitely low, considering that this material has not been found to be a carcinogen nor produce genetic, reproductive, or developmental effects, and could be further reduced by improving the washing step during the synthetic procedure. Moreover, the device can be employed, not only as intelligent label, but also, possibly with easier implementation, as control device in dairy industry.

4.3.12 CLT: Dye-EVOH@ sensors array colour evolution

As for the training set, pictures of Dye-EVOH@ sensors arrays are acquired for each replicate and each test solution described in Table 4.4. Contrary to the previous cases, the large number of Dye-EVOH@ sensors in the array makes impossible the direct naked-eye analysis of the arrays' pictures. For this reason, the pictogram, displayed in Figure 4.17, is built as following. For each Dye-EVOH@ sensor at each experimental pH, the average R, G and B values for the 4 replicates are calculated. Then, using PowerPoint, 12 rectangles of constant dimensions, one per each Dye-EVOH@ sensor in the array, labelled according to the numbering in Table 4.2, are coloured using the "Gradient fill" and setting, at each experimental pH, the average RGB triplet as "Gradient stop". The final pictogram well summarises the colour evolution of Dye-EVOH@ sensors array in a pH range from 0 to 14

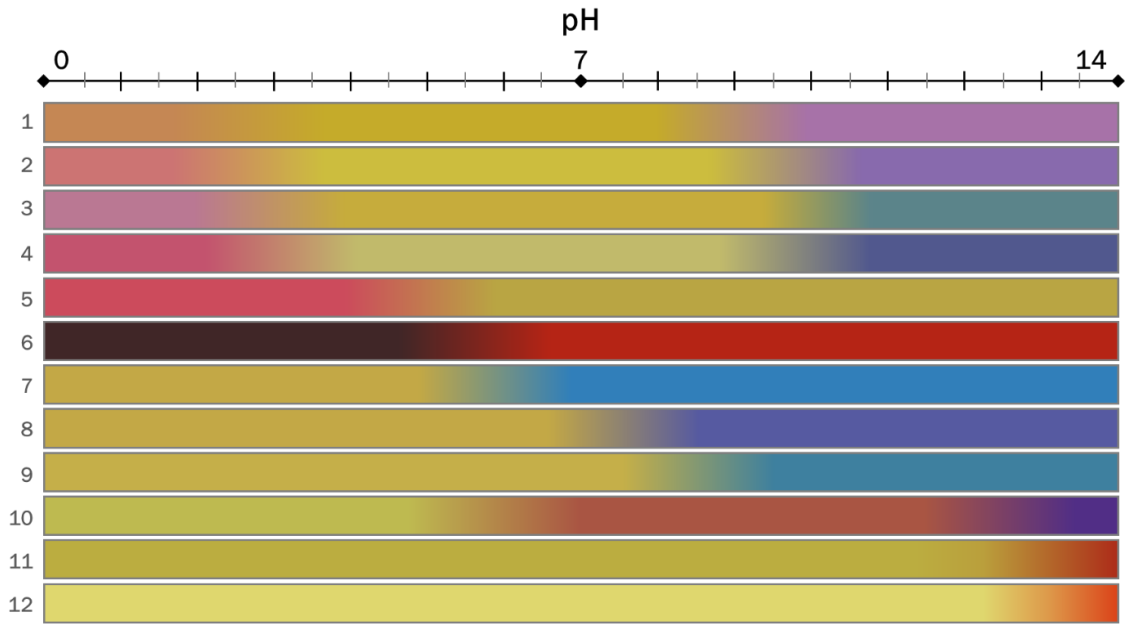

Figure 4.17: Pictogram reporting the colour evolution of Dye-EVOH sensors in a pH range from 0 to 14. Coloured rectangles are labelled on the left according to the numbering in Table 4.2 while pH values are reported in the axis above the pictogram.

At a glance, we can observe that Dye-EVOH@ sensors colour changes are equally distributed within the pH range and, at acidic pH, sensors from **1**-EVOH@ to **6**-EVOH@ are the most informative, at neutral pH, sensors from **7**-EVOH@ to **10**-EVOH@ and, at basic pH, sensors from **1**-EVOH@ to **4**-EVOH@ and from **10**-EVOH@ to **12**-EVOH@. Furthermore, comparing the pH values of colour turning of Dye-EVOH@ sensors to those of dyes in solution, the logK_a value increase of around 1 unit is again observed, as discussed below.

4.3.13 CLT: pH screening by PCA

As hinted in Section 4.2.6, PCA is firstly applied on the RGB triplets of Dye-EVOH@ sensors array of training set to visualise the colour evolution and to identify the main clusters. This 2-steps approach allows identifying pH subintervals in which the same Dye-EVOH@ sensors are informative and thus to develop tailored PLS models, relying only on the informative receptors for the specific pH subinterval. Also direct application of PLS on the entire pH range is possible but two main problems arise. Firstly, some dyes present similar colours, in terms of RGB values, at extremely acidic and alkaline pH, which compromises the accuracy and makes gross predictive errors possible. Secondly, working on the entire pH range, all the Dye-EVOH@ sensors are needed while, in many applications, the attention is focused only on a specific pH interval and thus the number of Dye-EVOH@ sensors can be reduced to the actual informative ones for the specific application.

The PCA model is built considering only the first two components, which explain the 69.1% of the experimental variance, and the resulting score plot is reported in Figure 4.18**a.** The samples display an arch-shaped distribution in the plot, from the lower right to the lower left at increasing pH values and three main clusters, partially overlapped, can be identified:

- Cluster A: for pH below 4, samples are separated alongside PC2 and their score value on this component is directly related to pH (red ellipsoid)
- Cluster B: for pH between 4 and 9: samples are mainly separated alongside PC1 and their score value on this component is directly related to pH (green ellipsoid)
- Cluster C: for pH above 9: samples are separated alongside both PC1 and PC2, with PC1 score value increasing and PC2 score value decreasing at increasing pH (violet ellipsoid)

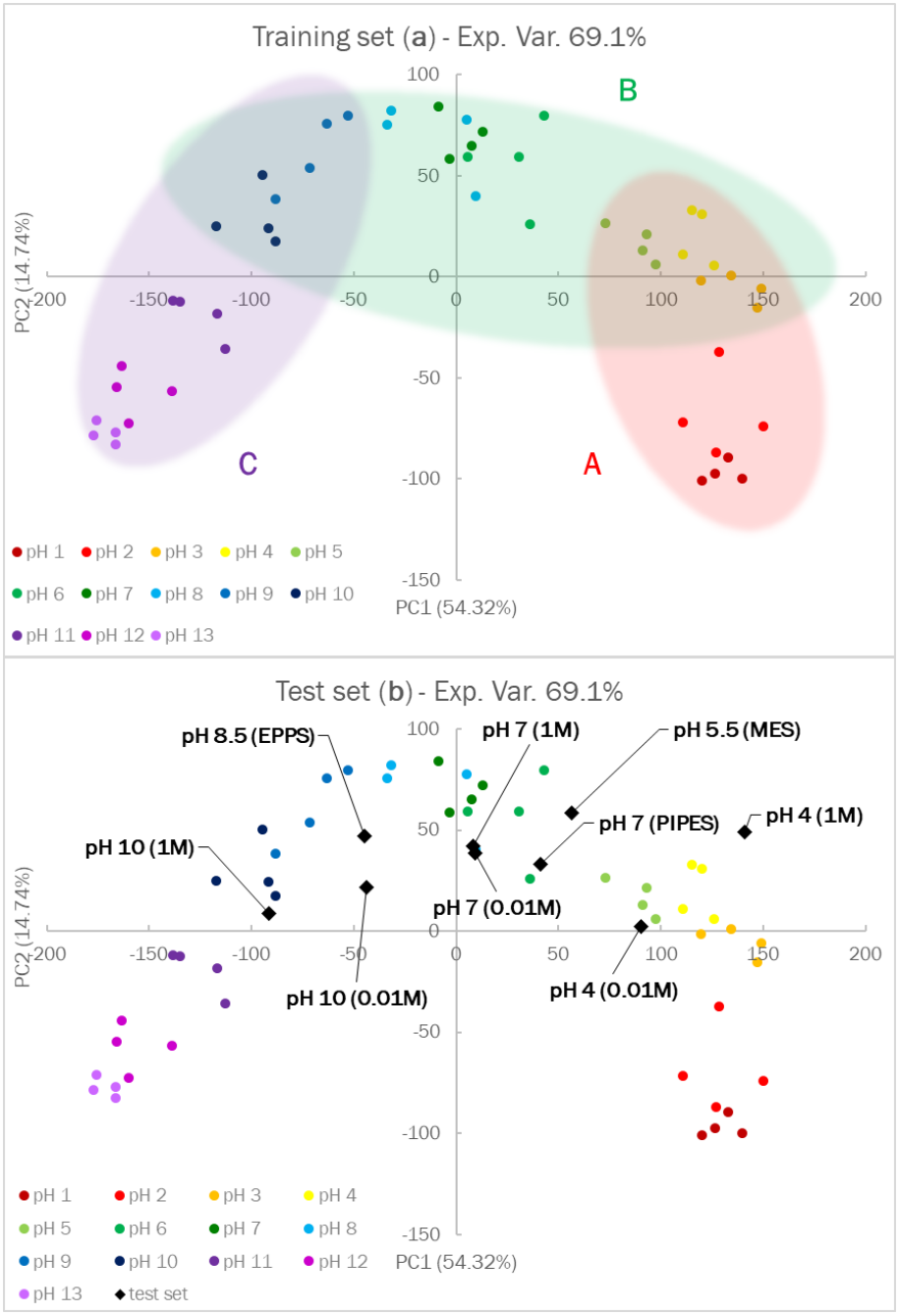

Figure 4.18: The score plot of the PCA model on the first two principal components, built on the training set (a) and validated by projection of the test set (b). The ellipsoids in (a) are added to identify the cluster A, B and C used for the PLS models described below.

The PCA model is firstly validated by projection of the test set, as reported in Figure 4.18**b**: both samples with a different buffering agent and ionic strength are correctly located in the score plot.

After validation, the PCA model is exploited to divide the entire pH range into subintervals for the following PLS application and to identify the corresponding reactive Dye-EVOH@ sensors. These subintervals correspond to the clusters described before and are highlighted in the plot by the

coloured ellipsoids while, for the informative Dye-EVOH@ sensors selection, the loading values, displayed in Figure 4.19, has to be analysed.

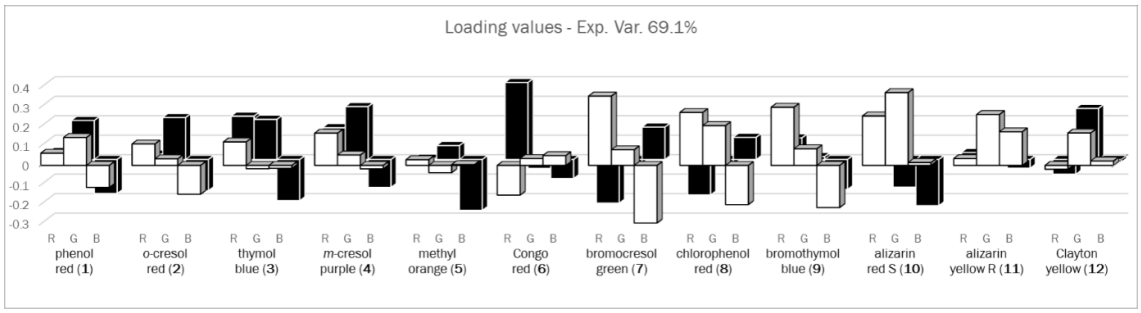

Figure 4.19: The loading values of the PCA model on PC1 (white, in foreground) and PC2 (black, in background)

Analysing the loading values, we can observe that Dye-EVOH@ sensors which turn their colour at neutral pH present a high loading value on PC1 while Dye-EVOH@ sensors which react at both acidic and alkaline pH give the highest contribution on PC2, in good agreement with what was argued before. The selection of the informative Dye-EVOH@ sensors per each PLS model is performed based on the loading and the logK_a values after functionalisation. It must be underlined that a neat separation between the PLS models should be avoided while a partial overlap of the pH subintervals leads to a better result, in particular for those samples at the boundary between the two models. For each cluster, the limits of pH subinterval and the informative Dye-EVOH@ sensors are listed in Table 4.14

Table 4.14: pH subintervals limit and informative Dye-EVOH@ sensors for each cluster identified by PCA

Cluster/Model	Min. pH	Max. pH	Informative Dye-EVOH@ sensors
A	1	5	From **1**-EVOH@ to **8**-EVOH@
B	3	10	From **7**-EVOH@ to **11**-EVOH@
C	9	13	From **1**-EVOH@ to **4**-EVOH@ and from **10**-EVOH@ to **12**-EVOH@

4.3.14 CLT: pH calculation by PLS

Once defined the pH subintervals and the corresponding informative Dye-EVOH@ sensors, PLS is applied, using the training samples RGB triplets as input data, and three PLS models are developed to predict pH value from Dye-EVOH@ sensors array colours. The models are then validated predicting the test samples and comparing the experimental value with the calculated one.

In Table 4.15, number of components used to build the model, the % explained variance in CV, Root Mean Square Error in CV (RMSECV), the test samples used for validation, labelled as reported in Table 4.5, and the corresponding error (RMSEP) for models are reported for each model.

Table 4.15: n° components, % explained variance in CV, RMSECV, test samples for validation and RMSEP for PLS models

Model	n° comp.	% Exp. Var. CV	RMSECV	Test samples	RMSEP
A	2	87.36%	0.4907	*a,d*	0.4903
B	2	95.56%	0.4687	*a-i*	0.5536
C	1	95.67%	0.2937	*c,f*	0.3312

For Models A and B, the minimum global RMSECV is obtained considering 2 components while, for Model C, the best model is obtained considering only 1 component; in all cases, the % explained variance in CV is definitely high, more than 87% for Model A and 95% for Models B and C. As for RMSECV, they are around 0.5 units for Model A and B and a bit lower, around 0.3 unit, for Model C: these values are definitely high if compared with the pH-meter performances but the main contribution is represented by the intrinsic variability of Dye-EVOH@ sensors obtained from the lab-scale synthetic procedure. In fact, also for the prediction of test samples, similar errors are obtained meaning that the models' performances are affected neither by ionic strength nor by the buffering agent or, at least, that their effect is much lower than the Dye-EVOH@ sensors variability's one.

Finally, in Figure 4.20, the plots reporting the experimental vs fitted values for each model are shown. As we can see, for all the models, there is a good agreement between experimental and fitted values and no significant difference is observed between training and test samples, confirming the models' robustness towards the type of buffering agent and ionic strength. To further improve the models' accuracy and to reduce the RMSEs, Dye-EVOH@ sensors reproducibility should be improved, mainly in terms of sensors thickness.

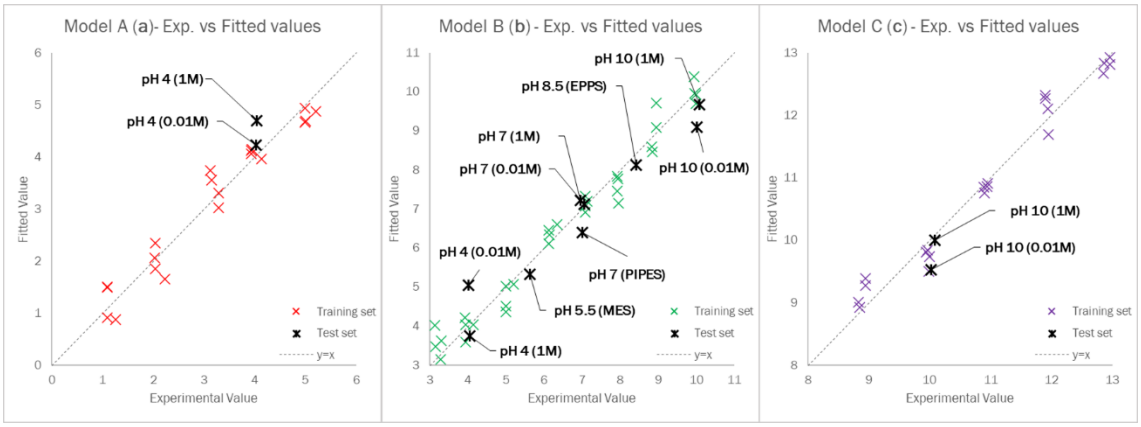

Figure 4.20: Experimental vs. Fitted plot for training (coloured *x*) and test (black stars) samples for Model A (a), B (b) and C (c).

4.3.15 CLT: Dye-EVOH@ sensors dye release

In Figure 4.21, UV-Vis spectra registered during release experiments in the case of **3**-EVOH@ (Figure 4.21**a**) and **7**-EVOH@ (Figure 4.21**b**) are reported. Similar behaviour is observed for these two dyes and BCP in concentrated samples, described in Section 4.3.11, suggesting that all the dye have similar behaviour and the specific dye does not influence release kinetic which is mainly determined by the polymeric support.

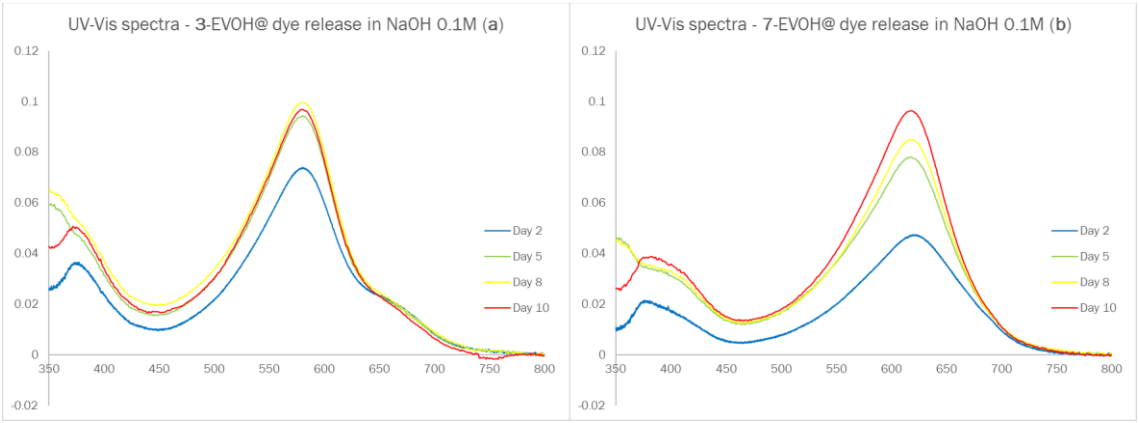

Figure 4.21: UV-Vis spectra of solutions registered during release experiments in the case of 3-EVOH@ (a) and 7-EVOH@ (b)

In Table 4.16, dyes concentration in solution (μM) and dyes release, expressed as μmol per Dye-EVOH@ g, are reported. Considering the estimated value of 0.1 mmol/g of dye content in Dye-EVOH@, dye release ranges from 0.8% to 1% for **3**-EVOH@ and from 0.4% to 0.8% for **7**-EVOH@ of total dye content in 10 days. As already discussed in Section 4.3.11, the low amount of dye released, the slow release kinetic and the equilibrium reached in the last days suggest that only dye molecules not covalently bound to EVOH are released in these experiments. This issue can be solved by improving the washing step during the synthetic procedure.

Table 4.16: Absorbance value at maximum absorption wavelength, dye concentration in solution (μM) and dye release (mmol/g) for release experiments in the case of 3-EVOH@ and 7-EVOH@

Time (d)	**3-EVOH@**			**7-EVOH@**		
	A (596nm)	[Dye] (μM)	Dye release (μmol/g)	A (617nm)	[Dye] (μM)	Dye release (μmol/g)
Day 2	0.065	3.2	0.79	0.047	1.6	0.39
Day 5	0.082	4.0	1.01	0.078	2.7	0.67
Day 8	0.087	4.3	1.08	0.085	2.9	0.73
Day 10	0.084	4.2	1.04	0.096	3.3	0.83

4.3.16 CLT: logK_a shift estimation after functionalisation

In Table 4.17, the results of the preliminary investigation about logK_a shift are summarised. As for dyes in solution, the logK_a values reported in literature [64, 65] is confirmed for Dye n°3 while a slightly higher value is found for Dye n°7. As for Dye-EVOH@, the logK_a shift hypothesized from UV-Vis spectra and sensors optical behaviour is confirmed: for **3**-EVOH@, the experimental logK_a' value is 9.7(1), considering the theoretical dye amount of 0.002 mmol, or 10.2(1), refining the dye amount at 0.003 mmol. For **7**-EVOH@, logK_a' is calculated only for the theoretical dye amount, obtaining 6.2(1) while it is not possible to refine the dye amount value.

Table 4.17: logK_a value reported in literature and calculated for dye n°3 and 7, both in solution and after covalent functionalisation to EVOH, considering the theoretical and refined dye amount, for Dye-EVOH@

Sample	logK_a	Dye amount (mmol) (theoretical)	Exp. logK_a	Dye amount (mmol) (refined)	Exp. logK_a
3 in solution	8.9	0.002	9.01(6)	--	--
***3**-EVOH@*	--	0.002	9.7(1)	0.003	10.2(1)
7 in solution	4.35	0.002	4.74(2)	--	--
***7**-EVOH@*	--	0.002	6.2(1)	--	--

These preliminary results confirm both the logK_a shift previously assumed and the dye amount linked to EVOH, estimated from EDX analyses. Further investigations could be performed on this aspect but, at the moment, it is out of the purpose of our research.

4.4 Conclusions

To conclude, the main issue encountered using EVOH (32% ethylene) as solid support, which was the delay in spoilage detection during chilled storage, has been successfully solved by changing the solid support and, as a consequence, the choice of receptors was optimised for each specific application.

Spoilage monitoring, both by naked-eye and multivariate data elaboration, was verified for various solid protein foods and milk types and also the applicability as Chemometric-assisted Litmus Test was demonstrated. For all these prototypes, a large-scale synthesis need to be optimized but they can be easily implemented on sales packages and used either as smart labels for food freshness monitoring or for specific applications alongside the entire food supply chain, as it could be for both solid and liquid foods continuous monitoring anywhere it is needed.

The main disadvantage of these devices was represented by the plastic nature of the solid support used, which is not in line with the new trends, in general, and in food packaging, in particular, mainly focused on biocompatible and biodegradable materials. For this reason, bio-based materials were also tested for smart labels production, as described in Chapter 5.

To conclude, the results discussed in this Chapter were presented in two oral communications at the "XXVII Congresso Nazionale Della Società Chimica Italiana" (Milano, 2021), at the "International Symposium on MEtal Complexes" (Białystok, 2021), and as poster communication, at "RETASTE: RETHINK FOOD WASTE Conference 2021" (Athens, 2021). As for data publication, a paper focused on the application for milk spoilage monitoring has been recently accepted for publication on Talanta (Elsevier) while manuscripts containing the results for protein foods freshness monitoring and for chemometric-assisted litmus test are still under preparation.

5. CMC-based devices

In this chapter, the CMC-based devices are discussed. Firstly, the state of art is presented providing a brief description of the recent literature on this topic. The selection of the receptors, the synthetic pathway, the physicochemical and optical characterization are described and the related results are presented. For this solid support, two different deposition strategies were tested: in both cases, the optimisation of the preparation procedure by Design of Experiments is described in detail. For the first deposition strategy, the sensing performances and the applicability of the sensors for food freshness monitoring was also investigated. Eventually, the main conclusions are driven, the publications on this topic are summarised and the insights for further development are discussed.

5.1 State of art

In recent years, the environmental concerns surrounding conventional petroleum-based materials have stimulated the research on natural macromolecules which guarantee biodegradability and sustainability [90]. This trend has been particularly followed in the field of food packaging, both for flexible and rigid packages, due to the always increasing volume of waste generated by the extensive disposal of food packaging [90]. For this reason, many biodegradables, renewable and even edible materials have been proposed to partially replace petroleum-based plastics, ranging from polysaccharides to proteins [90, 91, 92, 93, 94, 95].

These materials have been also widely investigated for active packaging solutions in which the packaging materials act as a carrier for antimicrobial or antioxidant species and several strategies have been tested to integrate bioactive compounds in biodegradable packaging materials [91, 92, 93, 94, 95]. On the other side, biodegradable materials are also exploited for intelligent packaging solutions, thanks to their versatility towards chemical modification or functionalization [96].

Among the wide variety of natural macromolecules and derivatives, our choice fell on carboxymethylcellulose (CMC), a cellulose derivative in which some of the hydroxyl groups of the glucopyranose units are substituted by sodium carboxymethyl groups (−CH2COONa) [97, 98]. In Figure 5.1 the chemical structure of CMC and a picture of CMC powder commercially available are shown. CMC guarantees both large availability (production around 583.782 ton/y) and appealing properties like biodegradability, biocompatibility, improved solubility in aqueous or organic solvents, and presence of reactive functions [97, 98]. Thanks to its unique features, this material has been widely exploited both as an additive to improve mechanical properties of biodegradable films containing starch [92, 99, 100], PVA [100, 101, 102] and others [91, 94, 95] and as a substrate for chemical modifications. In fact, the presence of reactive carboxyl groups onto a CMC backbone paves the way toward its further chemical modification, currently performed mainly by amidation and esterification reactions, in the presence of carbodiimides as coupling reagents [97, 98].

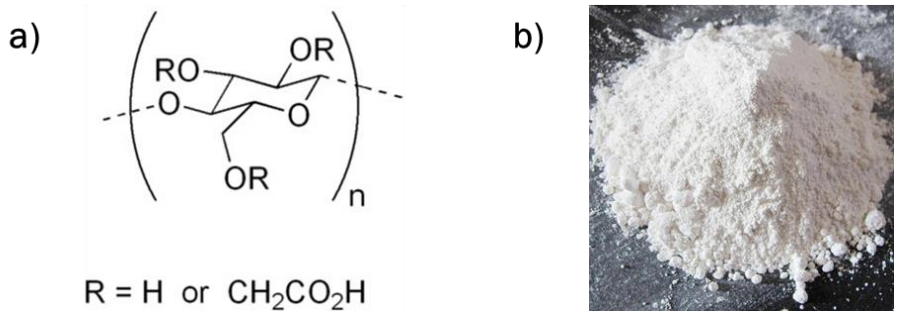

Figure 5.1: Chemical structure of CMC (a) and CMC powder, as commercially available.

All the experiments were performed using Carbocel MM250, provided by Lamberti Spa. The synthetic pathway, firstly developed for EVOH functionalisation, was successfully adapted to CMC functionalisation [11, 13] and two different deposition strategies were investigated, applying tailored ED techniques: *drop* and *film casting deposition*.

5.2 Materials and methods

5.2.1 Receptors

CMC is firstly functionalised with the panel of pH indicators already tested with EVOH(32% ethylene):*m*-cresol purple (**1**), *o*-cresol red (**2**), bromothymol blue (**3**), thymol blue (**4**), chlorophenol red (**5**) and bromophenol blue (**6**), described in Section 3.2.1. Then, for protein foods freshness monitoring, in light of the interesting results obtained with **CR**-EVOH@ dual sensors device, described in Chapter 4, *o*-cresol red (CR) is selected as sensing unit; the acid-base behaviour of this molecule has been already discussed in Section 4.2.1.

5.2.2 Synthesis of Dye-CMC@

The synthetic pathway previously developed for EVOH covalent functionalisation and internationally patented, [10, 11, 13, 12] is adapted for CMC.

The first step of dye activation is performed as described in Section 3.2.2. In the second step, unlike the EVOH functionalisation procedure, the covalent anchoring is performed without CMC dissolution: CMC powder is poured in toluene at 65 °C, under stirring, and a freshly prepared sulfonyl chloride toluene solution is added dropwise to the powder dispersion. After 3 h at 65 °C, the reaction mixture is evaporated to reduce by half the toluene volume, then cooled at room temperature and in an ice bath. The functionalized powder is filtered under vacuum, washed with DCM and left to dry overnight.

After the synthesis, the functionalized CMC comes in the form of coloured powder (Figure 5.2**a**) and needs to be dissolved in water with proper additives (Figure 5.2**b**) to perform both *drop* (Figure 5.2**c**) and *film casting deposition* (Figure 5.2**d**).

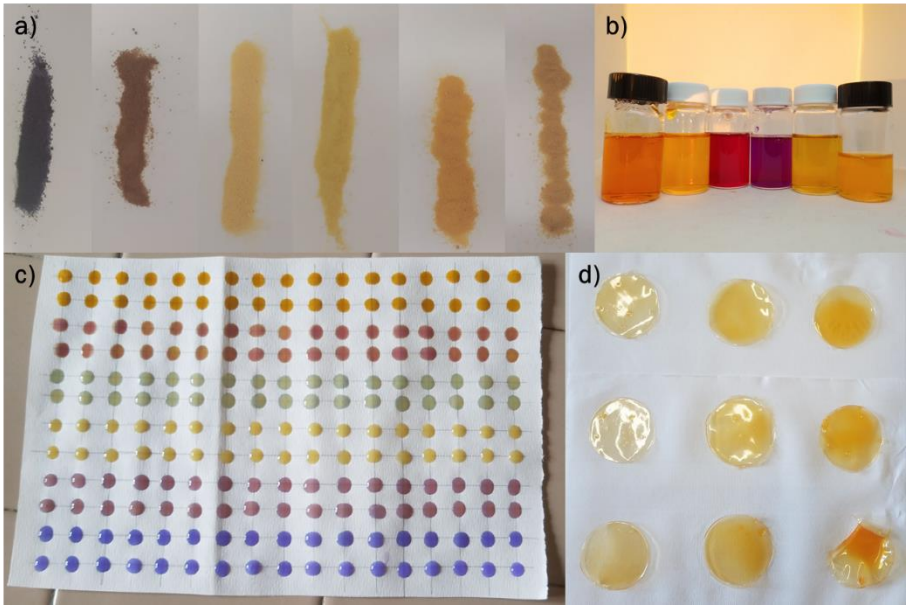

Figure 5.2: Dye-CMC@ in powder, as obtained after synthesis (a), aqueous mixtures of Dye-CMC@ and additives (b), Dye-CMC@ based sensors obtained by *drop* (c) and *film* (d) *casting deposition.*

5.2.3 Dye-CMC@ powder characterisation

The powder characterization is performed on **CR**-CMC@, being the final sensitive material for real samples monitoring.

Physicochemical measurements

Differential scanning calorimetry (DSC) analyses are performed by heating the samples (~5 mg) from −20 to 250 °C at a rate of 5 °C/min under a N_2 atmosphere. The heating process is preceded by an isothermal to remove the sorbed humidity.

Fourier transform infrared (FT-IR) spectra are acquired using a spectrometer equipped with an attenuated total reflectance (ATR) sampling accessory in the range from 4000 to 650 cm^{-1}.

Optical measurements

UV−vis spectra of **CR**-CMC@ solutions 0.5% (w/V) in 0.1 M HNO_3, phosphate buffer at pH 7.00, and 0.1 M NaOH are acquired and compared with the corresponding spectra of the dye dissolved in the same media (~10 μM).

5.2.4 Dye-CMC@ drop-casting deposition optimisation

Dye-CMC@ *drop-casting deposition* is optimised by Design of Experiments, applying a tailored model for the variables under investigation: glycerol and starch amount, drop volume and type of cellulose-based support. The selection of variables and the development of the tailored design are deeply discussed in Section 5.3 while the experimental matrixes are reported in Appendix IV.

Sensors' preparation general procedure

Dye-CMC@ concentration in aqueous solutions is fixed at 5% (w/V) and the solutions are obtained by pouring Dye-CMC@ powder and additives in 10 mL, under heating and stirring till complete dissolution. Then a defined volume of solution is collected by a positive displacement pipette and dropped on the cellulose-based support. The drop-deposited sensors are finally dried at RT for 2 hours before the application

SEM characterisation

SEM analyses of the drop-deposited Dye-CMC@ sensors, (dd)Dye-CMC@, on different cellulose-based supports are performed by an EVO MA10 scanning electron microscope (SEM). The sensors are supported on graphite bi-adhesives fixed on Al stubs and subsequently transferred into the SEM chamber.

Response collection

The aim of this design is the optimisation of (dd)Dye-CMC@ sensors' sensing performances in terms of sensitivity, colour change rate and colour homogeneity over the sensors' surface. These performances can not be quantified by a single measurable parameter therefore colour change kinetics are performed in defined conditions. For this specific experiment, chlorophenol red (**5**) is used as receptor since it is less sensitive than *o*-cresol red towards alkaline volatile molecules thus more efficient sensors can be easily distinguished even using synthetic samples.

(dd)**5**-CMC@ sensors on each support, equilibrated at acid pH by addition of 10 µL of HNO_3 0.1 M, are exposed to vapours generated by 20 mL NH_3 0.005M in a sealed box (V=125 mL). The boxes are stored at RT and pictures of the sensors are acquired at defined times.

Based on preliminary experiments, drop deposited sensors may present an inhomogeneous colour change, starting from the border and moving to the middle of the sensor. To control this issue, per each sensor, deposited on different supports and analysed at different times, three different RGB triplets are acquired, taking into account different fractions of the sensor's surface, as displayed in Figure 5.3, to evaluate colour homogeneity [61]:

- Average RGB (Figure 5.3**a**): the entire surface area is investigated, as usually performed in the previously described experiments
- Border RGB (Figure 5.3**b**): only the border of the drop-deposited sensor is analysed
- Middle RGB (Figure 5.3**c**): the border is excluded from the selection which comprehends only the middle

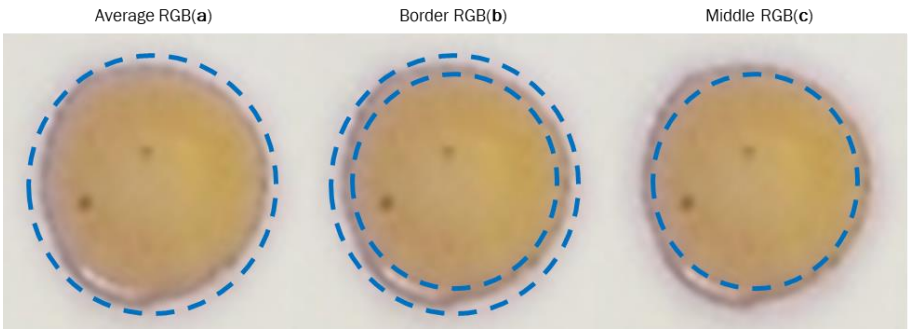

Figure 5.3: Sensor's surface fraction selected to acquire Average (a), Border (b) and Middle (c) RGB triplets

The overall dataset is then submitted to 3-Way PCA to check if it was possible to rationalise the colour change kinetic and reduce the dataset dimensionality to one informative parameter. This approach is followed to overcome response selection issue, which is of paramount importance in every Experimental Design. Depending on the results, the loading values could summarise the information of interest and thus could be exploited as response for the Experimental Design.

Model validation

The model, developed applying Experimental Design, is validated preparing three replicates at the point [0 0 0 D], registering and analysing colour change kinetics performed in the same conditions. The average experimental response value is finally compared with the calculated value.

5.2.5 (dd)Dye-CMC@ stock aqueous solutions preparation for drop deposition

Once defined the ideal mixture composition for (dd)Dye-CMC@ sensors preparation, stock aqueous solutions are prepared dissolving 1 g glycerol, and 1 g Dye-CMC@ powder in 20 mL H_2O, under heating and stirring till complete reagent dissolution. The aqueous mixtures are then stocked in a closed bottle away from direct light.

5.2.6 (dd)Dye-CMC@ sensing performances

Sensing performances of (dd)Dye-CMC@ sensors array need to be evaluated before the final application. These experiments are performed on drop-deposited sensors made of each Dye-CMC@ but, for brevity's sake, only the results for CR-CMC@ are reported, being this last the final sensor for protein food freshness monitoring.

(dd)Dye-CMC@ sensors "titration"

Per each (dd)Dye-CMC@ sensor at each acid-base form, the stoichiometric amount of strong acid or base to obtain the complete conversion of the entire sensor's surface is determined by dropwise addition of increasing amounts of HNO_3 or NaOH to sensors replicates. Each addition consists of 10µL of HNO_3 or NaOH, either 0.01 M or 0.1 M and sensors are left drying and equilibrating before new additions. The final acid or base amount added is reported as mmol H^+ or OH^-. A picture of each sensor is acquired after the addition and the stoichiometric amount is determined by naked-eye evaluation.

Reproducibility

To evaluate sensors reproducibility, for each (dd)Dye-CMC@, 10 independent drop-deposited sensors are equilibrated by the addition of the proper amount of strong acid or base in 10 mL, as reported in Table 5.1, and analysed by photo acquisition. The reproducibility is assessed, based on the RGB values collected and compared.

Table 5.1: Equilibration conditions used to test sensors reproducibility for each drop-deposited Dye-CMC@

(dd)Dye-EVOH@	Equilibration A	Equilibration B	Equilibration C
1-CMC@	4 µmol HNO_3	1 µmol NaOH	No addition
2- CMC @ (CR-CMC@)	4 µmol HNO_3	1 µmol NaOH	No addition
3- CMC@	No addition	1 µmol NaOH	---
4- CMC@	3 µmol HNO_3	1 µmol NaOH	No addition
5- CMC@	2 µmol HNO_3	1 µmol NaOH	---
6- CMC@	3 µmol HNO_3	No addition	---

5.2.7 Protein foods freshness monitoring by (dd)CR-CMC@ dual sensors device

Experimental setup

As previously described in Section 4.2.4, a dual sensors device is used, made of two (dd)**CR**-CMC@ sensors, previously equilibrated one at the completely deprotonated form (CR^-), from now called b-(dd)**CR**-CMC@, and one at the completely protonated one (H_2CR^+), from now defined a-(dd)**CR**-CMC@. Equilibrations are performed adding 10 µL NaOH 0.1M, for b-(dd)**CR**-CMC@, or 40 µL HNO_3 0.1 M, for a-**CR**-CMC@, resulting respectively in violet and pink sensors.

Chicken breast slices and codfish fillets are purchased at the local supermarket, choosing a tray containing similar weights of food, and are carried to the lab within 10 minutes. The plastic film is removed, the (dd)**CR**-CMC@ dual sensors device is taped to the bottom of the PP tray using 3M Magic Tape, as already discussed, and a new plastic film is fixed to seal the package. Samples are stored in a domestic fridge at 4 °C for 10 days, in the case of chicken, or for 6 days, for fish products.

Colour analysis & Chemometrics

At given times, photos of the device are acquired by a Nikon COOLPIX S6200 in a lightbox to ensure a constant and reproducible light exposition. To extract the RGB triplets for each sensing unit during freshness monitoring, GIMP software is employed [61].

For each food under investigation, Principal component analysis (PCA) is performed on RGB triplets, only centring the data because these indexes are intrinsically scaled from 0 to 255, to rationalize the colour evolution and visualize spoilage process. The open-source Chemometric Agile Tool (CAT) program was employed for multivariate data elaboration [60].

Training and test sets

Both for chicken breast slices and codfish fillets, the training set consists of five samples of similar mass, purchased the same day of the delivery from the supplier. Therefore, the input matrix has 6 columns (3 RGB indexes per 2 **CR**-CMC@ sensors) and respectively 135 and 70 rows in the case of chicken breast slices and codfish fillets (27 or 14 acquisition times per 5 replicates).

Then, to preliminary validate the model, one new sample of similar mass is projected as external test set, again purchased the same day of the delivery.

5.2.8 First attempts of CR-CMC@ film casting optimisation

Dye-CMC@ *film casting deposition* is optimised by Mixture and Process Design, applying a tailored model for the variables under investigation. The selection of variables and the development of the tailored design are deeply discussed in Section 5.3 while the experimental matrixes are reported in Appendix IV.

Sensors' preparation procedure

Also in this case, aqueous solutions of **CR**-CMC@ powder and additives are prepared, adapting the preparation procedure found in literature [99]. The water volume is fixed at 20 mL and the total reagent mass, **CR**-CMC@, starch and glycerol, is fixed at 2 g. The solutions are obtained by pouring

CR-CMC@ powder and additives in 20 mL, under heating and stirring till complete dissolution. Then 5 mL solution is poured into a plastic Petri dish (Ø =5.2 cm) and dried overnight at 65°C in a closed oven at constant humidity. After the drying step, films are left equilibrating at RT for 30 minutes and peeled from the mould.

Response collection

For this very first investigation, only a qualitative response is collected and the samples are classified as successful or unsuccessful. More in detail, films are considered successful when they can be easily peeled from the mould and handled, otherwise they are unsuccessful.

5.3 Results and discussion

5.3.1 Physicochemical and optical characterisation

DSC analyses are performed on **CR**-CMC@ powder, obtained after the synthesis. Due to CMC hydrophilicity, the heating process is preceded by an isothermal to remove the sorbed humidity. In Figure 8.12**a** e Figure 8.12**b** in Appendix V, the calorimetric profile of CMC and **CR**-CMC@ before the isothermal is reported as an example. After water removal, no significant transitions occur in the investigated range, analysing CMC powder before and after functionalisation, as clearly displayed by the profiles in Figure 8.12**c** e Figure 8.12**d** in Appendix V.

FT-IR spectra of the pH indicator powders, starting CMC, and **CR**-CMC@ powder are reported in Figure 8.13 in Appendix V. The same signals characterize the spectra of CMC before and after the functionalization, with different intensity, and it was not possible to confirm the successful covalent binding by this technique.

The optical behaviour of Dye-CMC@ is investigated by UV–Vis spectroscopy. Dye-CMC@ powders are solubilised in water at a fixed concentration of 0.5% (w/V) and UV-Vis spectra are registered. For each receptor under investigation, we want to compare the optical behaviour of the molecule in an aqueous solution and after functionalization at different pH values. In Figure 5.4, the results for **CR** (~10 μM) and **CR**-CMC@ (0.5% w/V) in solution are displayed: UV–Vis spectra and corresponding photographs after equilibration at acidic, basic, and neutral pH.

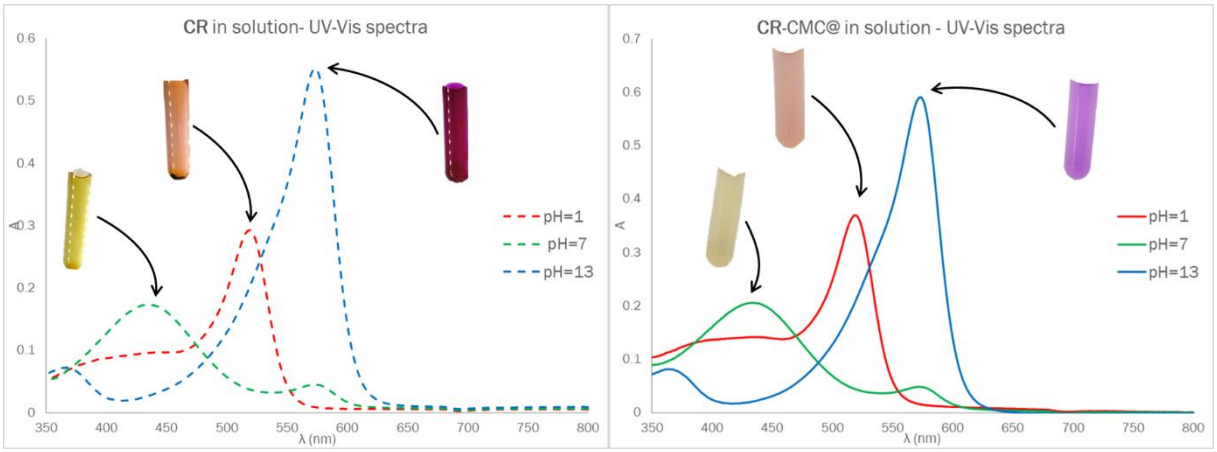

Figure 5.4: UV–Vis spectra and corresponding photographs of a ~10 μM CR solution (graphs on the left, dashed lines) and 0.5% (w/V) CR-CMC@ solution (graphs on the right, solid lines).

No significant differences in the optical behaviour are detected after dye anchoring in terms of maximum absorption wavelength. Assuming that the anchoring to CMC does not affect the molar absorption coefficient, CMC dye capacity, or CMC degree of functionalisation, is estimated from the absorbance value at 433 nm at pH=7: the estimated dye capacity turns out to be 0.002 mmol g^{-1}.

This value is much lower than EVOH dye capacity, estimated by EDX analysis (Section 3.3.2) and confirmed by potentiometric titration (Section 4.3.16). It must be underlined that the commercial CMC employed, named Carbocel MM250 and commercialised by Lamberti Spa, is characterised by an average degree of substitution (D.S.) between 0.75 and 0.95. The degree of substitution is the average number of carboxymethyl groups substituted per monomer unit, ranging from 0 to 3 with the remaining R = H. Considering that dye anchoring occurs on substituted carboxymethyl groups, the low starting degree of substitution results in low dye capacity. Furthermore, the functionalisation is performed on CMC powder, without solubilising the solid, thus decreasing the available sites.

Therefore, the difference between Dye-@EVOH and Dye-CMC@ IR spectra can be justified taking into account the different degree of functionalisation: for Dye-EVOH@, the higher degree of functionalisation makes visible the band corresponding to the formation of a sulphonic ester while, due to the lower number of functionalised sited in Dye-CMC@, the corresponding band is not visible in the spectra.

As already hinted in the case of EVOH (32%)- based devices, the UV-Vis spectra at different pHs allow to preliminary investigate any differences in the logK_a' values of the target dyes in solution and after functionalisation. Opposite to the previously described material, in this case a shift to higher logK_a' values is no longer observed after dye anchoring to CMC and the spectra registered for CR and **CR**-CMC@ solutions perfectly overlap. Nevertheless, it must be underlined that, in the case of Dye-EVOH@, the UV-Vis spectra were acquired directly analysing the films while, in this case, **CR**-CMC@ powder is soluble in water and the spectra of **CR**-CMC@ solution are analysed. Furthermore, in the case of Dye-EVOH@, the solid films used to register the spectra were the same from which Dye-EVOH@ final sensors were cut while, in this case, **CR**-CMC@ powder represents only the starting material for the deposition procedure, required to obtain the **CR**-CMC@ final sensors. Therefore, the absence of logK_a' shift in these spectra is not sufficient to claim that **CR**-CMC@ final sensors logK_a' values is equal to CR logK_a values in solution. Further investigation on this aspect will be conducted in the future.

5.3.2 Drop-casting deposition optimisation: Design setup

Variables and experiments selection

The drop-casting deposition is firstly optimised by Design of Experiments. When applying these chemometric techniques, the first step corresponds to variables selection. Based on preliminary experiments performed, Dye-CMC@ concentration is fixed at 5% (w/V) because this amount ensures sufficiently coloured and sensitive spots, making visible the colour evolution even at low concentrations of analytes.

Based on the literature [92, 99, 100], starch and glycerol are the most commonly employed additives to improve the mechanical and physical properties of CMC-based films. Therefore, the amounts of both these additives are set as quantitative variables, considering the absence of the additives as minimum level and a concentration of 5% (w/V), equal to Dye-CMC@ amount, as the maximum level. Also the drop volume is analysed as a quantitative variable, ranging from 10 µL to 20 µL as limits of

the experimental domain. The last variable under investigation is the type of cellulose-based support used for the deposition: common filter paper and three different papers, provided by Barbè SRL, are tested.

In Table 5.2 the quantitative variables under investigation and the corresponding levels are summarised, in Table 5.3 the qualitative variable's levels are defined.

Table 5.2: Level definitions for the quantitative variables

Variable		Upper level (+)	Lower level (-)
Glycerol (%gly)	x_1	5%	0%
Starch (%st)	x_2	5%	0%
Drop volume (V)	x_3	20	10

Table 5.3: Level definitions for the qualitative variable

Variable		Level A	Level B	Level C	Level D
Support (Supp)	x_4	Filter paper	Food grade paper	Paperboard	Pure cellulose

To build the experiment list, a Full Factorial Design 2^3, considering only the quantitative variables in the defined experimental domain, is performed per each support. The 32 (dd)**5**-CMC@ sensors prepared, named Xy with X referring to the support (A-D) and y to the composition (a-h), are listed in Table 8.2 in Appendix IV.

Model equation

Classical Factorial Design can not be applied for qualitative variables with more than two levels therefore a tailored model is developed. As for quantitative variables, both linear terms and two factors interactions are calculated while, for the qualitative variable, the only linear terms can be determined. It must be underlined that, for qualitative variables with *n* levels, only *n-1* independent factors can be defined and one of the levels is set as implicit, in this case support D. In Equation 5.1 the final model equation is reported.

$$Y = b_0 + b_1X_1 + b_2X_2 + b_3X_3 + b_{4A}X_{4A} + b_{4B}X_{4B} + b_{4C}X_{4C} + b_{12}X_1X_2 + b_{13}X_1X_3 + b_{23}X_2X_3$$

Equation 5.1: Model equation for Dye-CMC@ drop-casting deposition

5.3.3 Drop-casting deposition optimisation: SEM characterisation

Firstly, SEM characterisation of (dd)**5**-CMC@ sensors is performed to evaluate the interactions between the different supports and the drop deposited. Since no significant differences are observed analysing different compositions and drop volumes (samples *a-h*), in Figure 5.5, the SEM images only for sample *a* deposited on different supports, at different magnifications, are displayed.

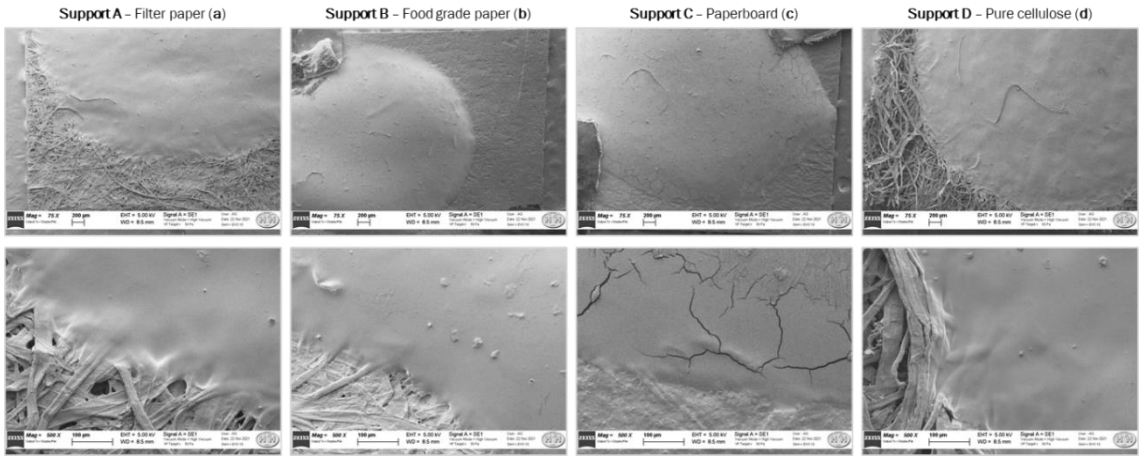

Figure 5.5: SEM images of (dd)5-CMC@ at 75X (top row) and 500X (bottom row) deposited on filter paper (a), food grade paper (b), paperboard (c) and pure cellulose (d)

In the images at a lower magnitude, shown in the top row of Figure 5.5, we can observe that support B and C present much more compact fibres than support A and D. In this last support, in particular, the fibres are not strictly assembled and present empty spaces in the lattice. The images at a higher magnitude, displayed in the bottom row of Figure 5.5, allow us to evaluate the interaction between support and drop and drop's homogeneity. Drops deposited on support A and D are sorbed by the cellulose-based material and partially penetrate within the support fibres. Opposite, drops deposited on support B and, even more, on support C are not sorbed and remain on the surface, without penetrating; they also look much less homogeneous and present some cracks on the drop surface, in particular in the case of support C. In conclusion, the interaction between support and drop seems to improve in the order C<B<A<D.

5.3.4 Drop-casting deposition optimisation: response collection

As already discussed in Section 5.2.4, the entire colour change kinetic in defined conditions, rationalised by 3-Way PCA, is exploited as response for this design since the final aim consists in the optimisation of the sensing performances, including sensitivity, sensing rate and colour homogeneity.

(dd)5-CMC@ colour change kinetic: colour evolution

In Figure 5.6, the colour evolution of the 32 (dd)**5**-CMC@ sensors, labelled as reported in Table 8.2 in Appendix IV, registered during the kinetic experiments described in Section 5.2.4, is displayed.

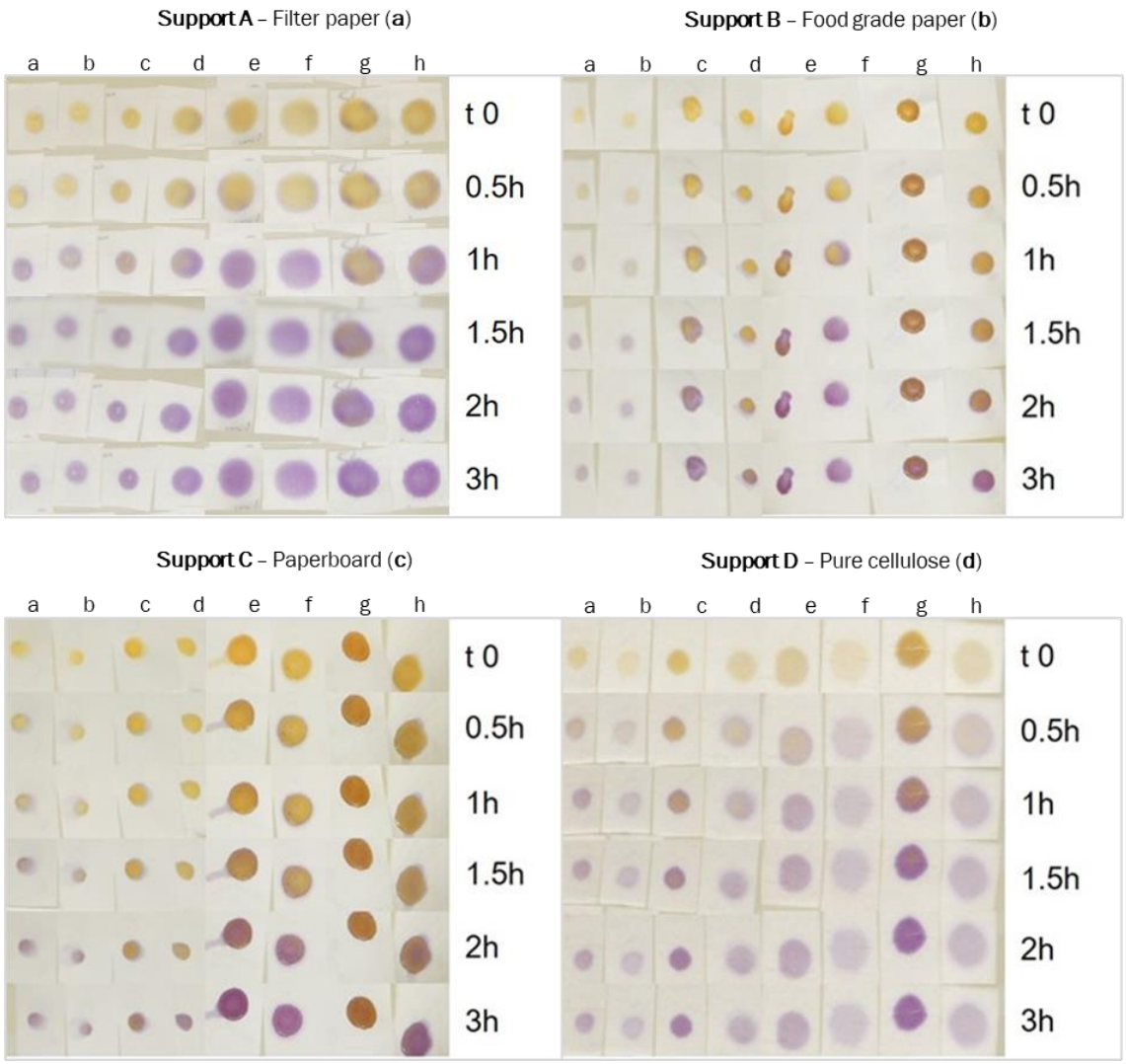

Figure 5.6: Colour evolution of (dd)5-CMC@ on support A (a), B (b), C (c) and D (d), previously equilibrated at the acidic form, registered during the exposition over 20 mL NH_3 0.005M in a sealed box (V=125 mL)

Some preliminary assumptions can be drawn by naked-eye analysis of the pictures reported in Figure 5.6. The higher colour change rate is observed for sensors deposited on support D, followed by those on support A while sensors on support B and C react slower. Analysing the quantitative variables, samples labelled as *c* and *g*, which contain only starch as an additive, present more intense colouration but slower kinetic than the other while no significant differences are highlighted by naked eye between lower and higher drop volumes.

(dd)5-CMC@ colour change kinetic: 3-Way PCA

The colour evolution shown in Figure 5.6 is rationalised by applying 3-Way PCA. This chemometric technique allows to jointly analyse the colour change process over time for the samples and to reduce the dataset dimensionality, ideally to one single informative parameter which can be used as response for the design.

As already discussed in previous cases, acquisition times (6), (dd)**5**-CMC@ sensors (32) and sensors RGB indexes, acquired as described in Section 5.2.4, (9) are labelled respectively as *conditions*, *objects* and *variables*. The first step in 3-Way PCA interpretation consists of comparing the cumulative % explained variance after unfolding, reported in Table 4.8, and the Tucker 3 model value (85.27%).

Table 5.4: Cumulative % explained variance after unfolding

Mode	PC1	PC1&2
Conditions	69.64%	94.13%
Objects	64.08%	86.76%
Variables	64.14%	94.76%

Both the cumulative % after unfolding and Tucker 3 model value are sufficiently high to assume that most of the information is taken into account by the model and, considering the common colour change process, only a small part of the overall information is lost.

As for interpretation is concerned, the loading values of *conditions*, *objects* and *variables* are jointly displayed in Figure 5.7. The *variables* are firstly discussed: (dd)**5**-CMC@ sensors, equilibrated at the acidic yellow form and exposed to ammonia vapours, undergo complete deprotonation and consequent conversion to the alkaline violet form. This colour transition increases B value, compared to R and G, in the sensors' RGB triplets; as a consequence, in the triplot, B loading values are separated from R and G. Alongside Axis 1, the *objects* are mainly separated and the B channel has the highest influence in their separation: *objects* with higher loading value in this Axis, which are mainly those deposited on support D and A, present higher B values, referred to the violet alkaline form, and better sensing performances. Analysing the three different RGB triplets acquired, the middle B value has the highest influence in *objects* separation and border B the lowest, confirming the tendency to change colour from the border to the middle, as hinted before. Opposite, the *conditions* are located alongside Axis 2, with a decreasing loading value during the kinetic experiment. Also in this case, B values are clearly divided by R and G, with negative loading values for B and positive for the other two channels, and middle B plays the most influent role in *conditions* separation. Therefore, the acquisition times are separated alongside Axis 2 depending upon the sensors' conversion from yellow to violet, occurring from the border to the middle.

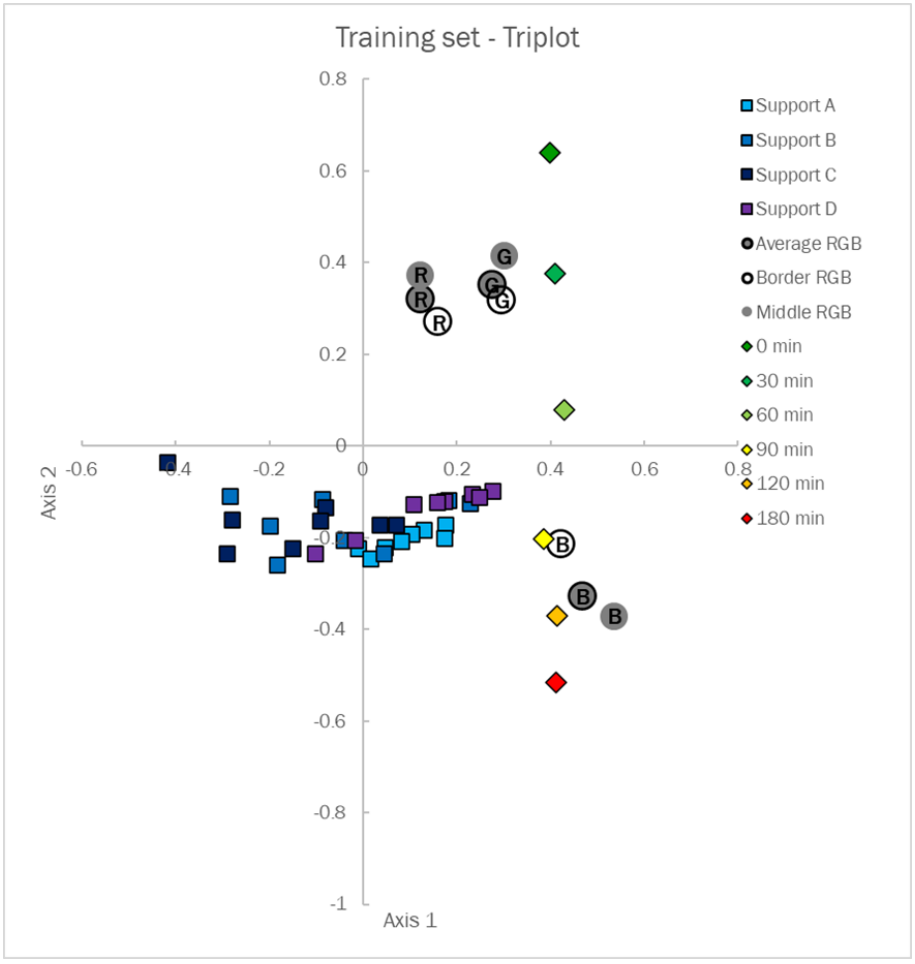

Figure 5.7: 3-Way PCA triplot reporting the loading values for *conditions* (diamonds), *objects* (square) and *variables* (spots) for 32 (dd)5-CMC@ sensors deposited on support A (light blue square), B (blue square), C (dark blue square) and D (violet square)

In conclusion, *objects* loading value on Axis 1 accounts for a sufficient percentage of the overall experimental variance, represents an informative parameter to characterise the drop deposited sensors in terms of sensing performances and present higher values for better sensors. For these reasons, it is selected as response to be maximised in the previously described design.

5.3.5 Drop-casting deposition optimisation: model solution and validation

Model solution

The model is calculated using 3-Way PCA *objects* loadings as response; the y value per each (dd)-5-CMC@ is reported in the last column of Table 8.2 in Appendix IV. In Table 5.5, the main statistics for the model are reported. The maximum leverage value in the experimental domain is 0.3125 and the model has 22 degrees of freedom. This value is definitely high because the number of experiments performed is much higher than the coefficients present in the model equation (Equation 5.1). D-Optimal Design could have been exploited to reduce the number of experiments but, requiring 32 depositions, an acceptable experimental effort, it was not performed in this case. Both % explained

variance in model calculation and cross-validation (CV) are sufficiently high and RMSECV is enough low to consider the model reliable for the specific application.

Table 5.5: Statistics for drop-casting deposition model

Statistic parameters	Value
Maximum leverage	0.3125
Degrees of freedom	22
% Explained Variance	71.87%
RMSECV	0.1127
% Explained Variance CV	60.54%

In Figure 5.8 the coefficients plot is shown while, in Table 5.6, the numerical values, semi-amplitude of confidence intervals and significance are listed. The significant parameters are, for quantitative variables, only the linear terms while, for the qualitative one, only support B and C. The addition of glycerol (%gly) has a positive effect on y while starch addition and drop volume have a negative effect. All the supports present a negative effect on the response compared to the implicit level (Support D), non-significant for Support A, while very significant for support B and C. Being the response maximisation the final aim of the design, glycerol amount has to be set at the higher value, starch and drop volume at the lower and either support A or D has to be used, with B and C abandoned.

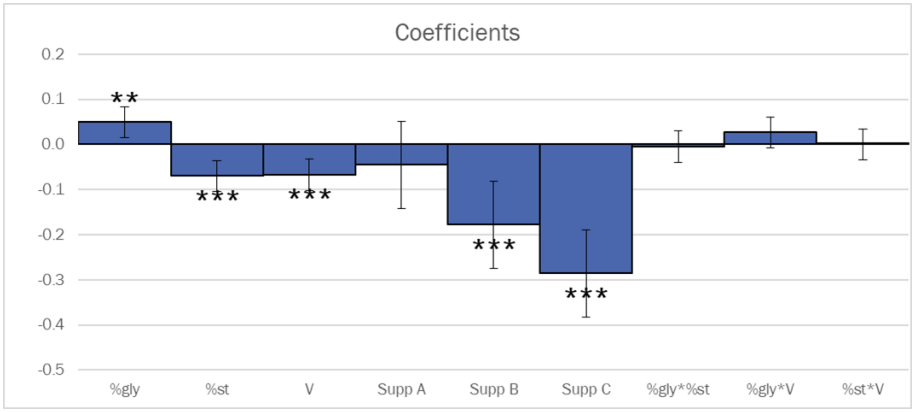

Figure 5.8: Coefficients plot for drop-casting deposition model

Table 5.6: Coefficients, semi-amplitude of confidence interval (CI) and significance (* p≤0.05, ** p≤0.01, *** p≤0.001) calculated for drop casting deposition model

Coefficients		Value	CI	Significance
	b_0	0.135	0.069	
Glycerol (%gly)	b_1	0.049	0.034	**
Starch (%st)	b_2	-0.070	0.034	***
Drop volume (V)	b_3	-0.068	0.034	***
Support A (Supp A)	b_{4A}	-0.045	0.097	
Support B (Supp B)	b_{4B}	-0.178	0.097	***
Support C (Supp C)	b_{4C}	-0.286	0.097	***
%gly%st*	b_{12}	-0.005	0.034	
*%gly*V*	b_{13}	0.026	0.034	
*%st*V*	b_{23}	0.001	0.034	

Model validation

To validate the model, three replicates at the point [0 0 0 D] are prepared and the colour change kinetic is registered in the same conditions of the training samples. At this point, a clarification is needed: 3-Way PCA allows to rationalise the colour change kinetic, reduce the dataset dimensionality without losing information and easily interpret the results obtained from the triplot. Nevertheless, this tool does not allow to project unknown samples, as PCA does, because only loading values are calculated and reported in the triplot instead of the score values typically showed for PCA. Similarly, when running PCA, it makes no sense to calculate the loading values for projected samples. Therefore, the test set used for model validation can not be projected in the triplot, shown in Figure 5.7, to obtain the *objects* loadings, used as response in the design.

Two strategies can be followed. Firstly, 3-Way PCA is run on the overall dataset, including both the training samples and three replicates of the centre point, and *objects* loadings are calculated. From a technical point of view, this strategy is not correct because the response for the training and test set are not completely independent, but they are jointly calculated by the same 3-Way PCA. Nevertheless, having verified that no significant differences are observed in the *objects* loadings of training samples, calculated with or without the test set included in 3-Way PCA, this strategy can be exploited for model validation.

As an alternative, 3-Way PCA can be replaced by PCA, differently organising the input dataset: the 32 (dd)5-CMC@ sensors are used as samples and the RGB triplets acquired at every acquisition time, ordered for increasing times, as variables. In the loading plot, the effect of RGB triplets, acquired considering different fractions of sensors' surface and at different times, is displayed while, in the score plot, the 32 experimental points are shown. At this point, the three replicates of the centre point can be here projected for validation purposes.

In Table 5.7, the results of validation performed according to the first strategy are reported: the predicted value fits into the confidence interval at 95% confidence level, thus the model is validated. Also applying the second strategy, model validation is successful but the interpretation is much more difficult and, for brevity's sake, these results are not presented.

Table 5.7: Model validation by three replicates at point [0 0 0 D]

	Y
Average value	0.10
Standard deviation	0.02
Upper bound CI	0.15
Lower bound CI	0.04
Predicted response	0.13

Selection of the optimised conditions

In Table 5.8, the optimised conditions for drop deposition casting of Dye-CMC@ sensors are summarised.

Table 5.8: Optimized parameters for Dye-CMC@ sensors drop deposition.

Parameter		Optimized level
Glycerol (%gly)	x_1	5%
Starch (%st)	x_2	0
Drop volume (V)	x_3	10 µL
Support (Supp)	x_4	Pure cellulose

5.3.6 Sensing performances: (dd)Dye-CMC@ sensors titration

Once defined the optimised conditions, the sensing performances are evaluated, starting from the sensors titration. The term "titration" refers to the determination of the amount of strong acid or base that has to be added to each sensor to convert Dye-CMC@ into the required acid-base form. This determination plays a crucial role in sensors development. In fact, differently from EVOH-based devices, whose low permeability and hydrophilicity allow to equilibrate the sensors by immersion in an excess of acid or base, CMC-based devices are highly hydrophile and prone to sorb humidity and water solutions. Meanwhile, the sorption of strong acid or base in excess will drastically decrease the sensors' sensitivity towards weak acids or bases since the analytes firstly react with the excess of strong acid or base and, only in a second time, the reaction with the receptor, and the consequent sensing, occurs.

The case of (dd)-**CR**-CMC@ is discussed as an example. In Figure 5.9, the pictures of 13 independent sensors after the addition of a specific amount of strong acid or base are displayed; the solutions' concentration and the added drop volume are set, respectively, at 0.1M and 10 µL, therefore the addition is performed multiple times to increase the added amount, waiting for complete drying between the additions. A uniform pink colouration is observed for acid additions equal or higher than 4 µmol, which is set as stoichiometric amount while, as for the violet form, the transition partially occurs for base additions of 0.5 µmol and is complete for additions equal or higher than 1 µmol, which is set as the stoichiometric amount.

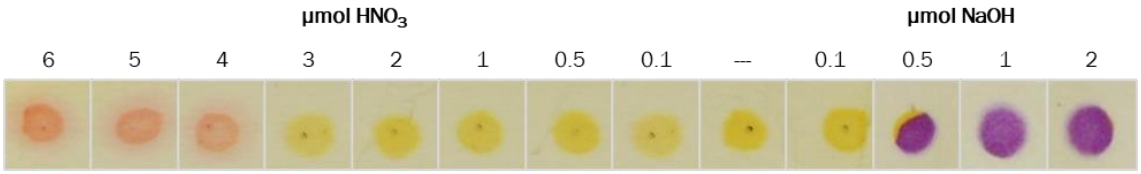

Figure 5.9: (dd)-CR-CMC@ sensors pictures after addition of increasing amount of strong acid (HNO_3) or base (NaOH).

These experiments are performed for all the Dye-CMC@ under investigation and the stoichiometric amounts, per each dye and each acid-base form, are those already reported in Table 5.1.

5.3.7 Sensing performances: (dd)Dye-CMC@ sensors reproducibility

Secondly, the reproducibility of the sensors is evaluated by equilibrating 10 independent sensors at each acid-base form, depending on the Dye-CMC@ under investigation, acquiring the photos of the sensors and analysing the RGB triplets.

In Figure 5.10 the case of (dd)**CR**-CMC@ is presented: the RGB reproducibility is judged to be satisfactory and no differences of colour shade are observed by naked-eye evaluation.

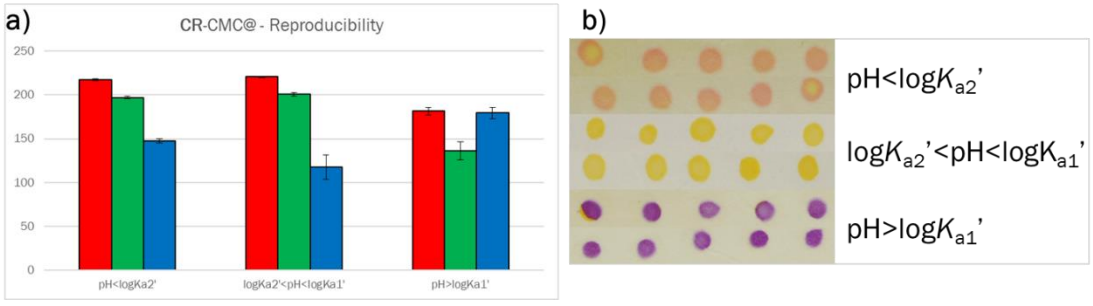

Figure 5.10: Bar plots representing the average value of RGB triplets acidic, neutral and basic form (a) and corresponding sensors picture (b) in the case of (dd)CR-CMC@.

5.3.8 Protein foods: (dd)CR-CMC@ dual sensors device colour evolution

While the synthesis and characterisation of drop deposited sensors are performed for all Dye-CMC@, only (dd)**CR**-CMC@ sensors are exploited for protein foods freshness monitoring, applying the same approach previously discussed for CR-EVOH@ dual sensors device. The colour evolution during the spoilage process of chicken breast slices and codfish, stored at 4 °C, is registered and the pictures of the training set are reported in Figure 5.11.

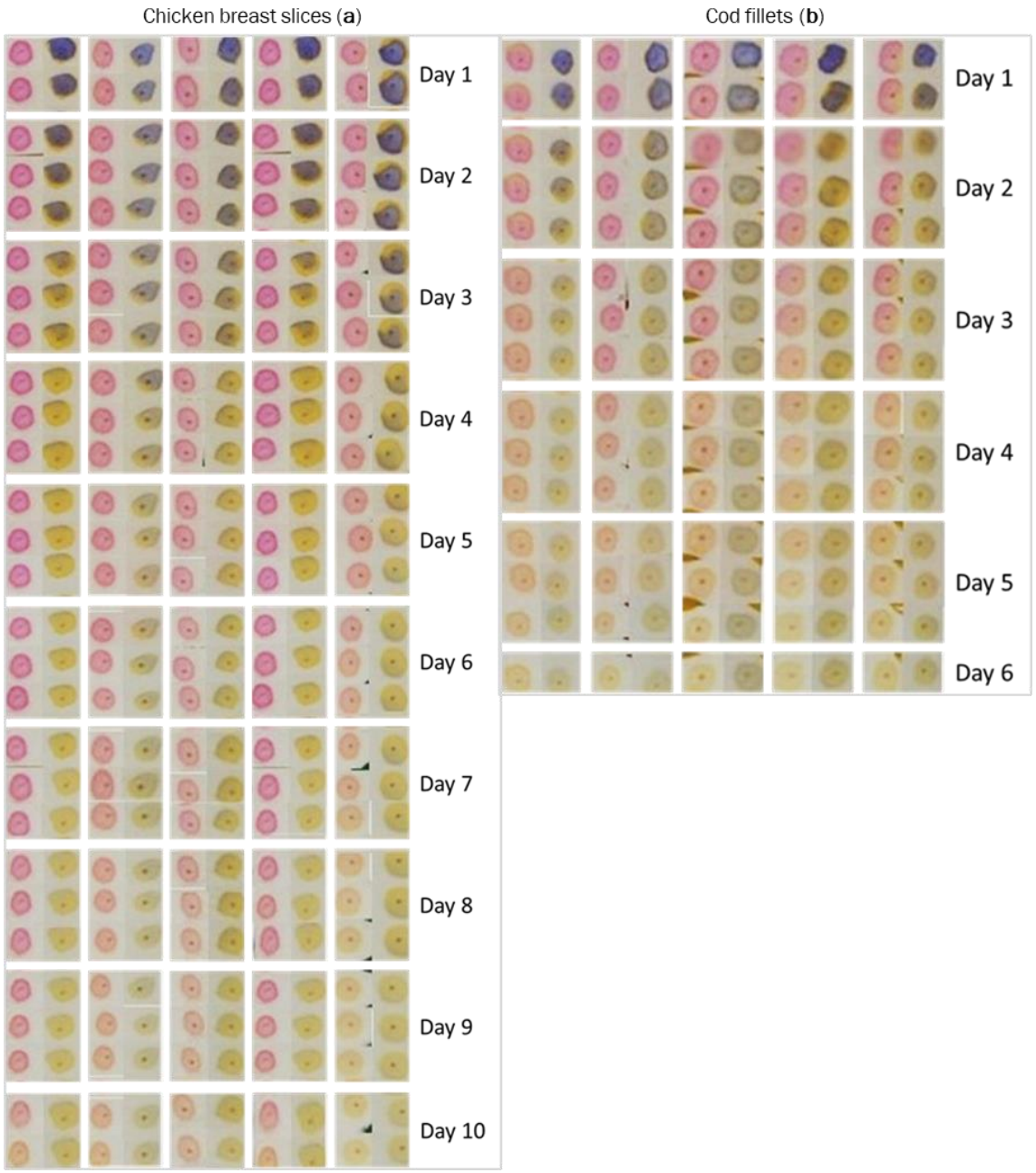

Figure 5.11: (dd)CR-CMC@ dual sensors device colour evolution over chicken breast slices (a) and codfish fillets (b), stored at 4 °C.

The colour evolution is very similar to the EVOH-based device ones. For both foods, in the "early spoilage", weak acid volatile by-products released by bacteria, are detected by the alkaline (dd)**CR**-CMC@ that turns its colour from violet to yellow. Then, in the second spoilage step, the so-called "spoilage", the bacterial release of thiols and amines, among which only a few are volatile in these conditions [52] results in a slight increase of pH, detected by acidic (dd)**CR**-CMC@ by its conversion from pink to yellow (HCR). These assumptions are rationalised by applying PCA to RGB triplets, as already discussed.

5.3.9 Protein foods: spoilage modelling by PCA

PCA is then performed on the RGB triplets of the sensors during degradation to visualise the degradation process of both foods training sets.

In both cases, the % explained variance on the first two components is satisfactory thus, these two components are selected for the final models. In Figure 8.9 in Appendix III: Loading and score plots the loading plots are shown while in Figure 5.12 the score plots, built on the training set and preliminarily validated by projecting the test set, for chicken breast slices and codfish fillets are reported.

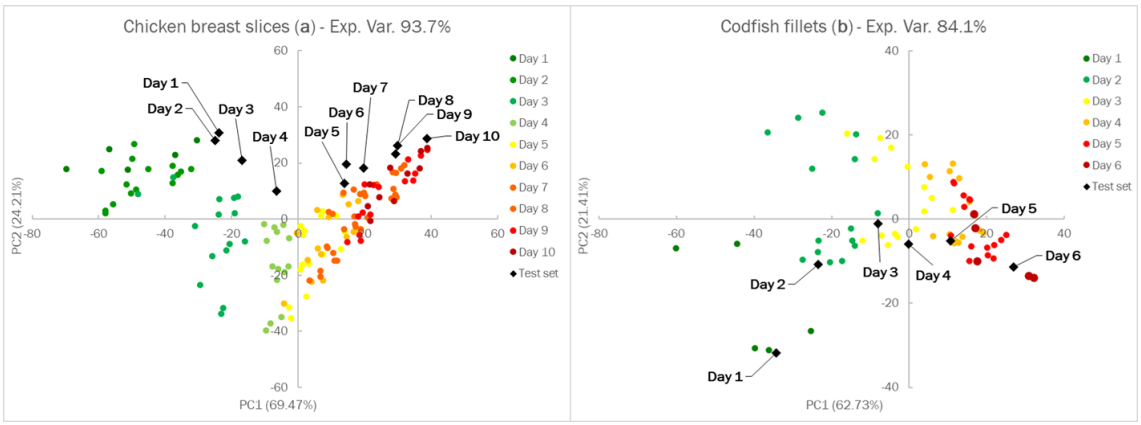

Figure 5.12: The score plots of the PCA models on the first two principal components, built on the training set and validated by projection of the test set, for chicken breast slices (a) and codfish fillets (b).

As for chicken breast slices (Figure 5.12**a**), the samples' score value on PC1 increases during the spoilage while, that on PC2 decreases during the early spoilage, from Day 1 to 4, and increases during the spoilage, from 5 to 10. Furthermore, in the first monitoring days, an higher variability among samples is observed while, after Day 5, all the samples present more similar behaviour. In general, once again the PCA score plot clearly rationalises the spoilage process, its characteristics, and samples behaviour.

The case of codfish fillets (Figure 5.12**b**) is easier: PC1, which accounts for the main % explained variance, represents the ongoing spoilage process, and the samples' score values on the *x*-axis

increase during spoilage. PC2 meaning, instead, accounts for the experimental variability which decreases during spoilage, as already observed for chicken breast slices.

As for test set projection, the new samples show a similar degradation process and are correctly located in the score plots in both cases.

5.3.10 Film casting deposition optimisation: Design setup

Variables' definition

Film casting deposition is secondly optimised by Design of Experiments. The variables' selection is performed differently from the previous optimisation since from literature and preliminary experiments, various Dye-CMC@ amounts lead to films with suitable properties. Therefore, in this case, the total amount of **CR**-CMC@ and additives is set at 2g, the water volume for mixture preparation at 20 mL and the mixture volume poured in the mould at 5 mL to obtain films with constant weight and thickness.

Also in this case, starch and glycerol are tested as additives to improve film properties [92, 99, 100], but, setting the total amount of reagents, the concentrations of the three compounds can not vary independently since the third compound amount is the difference between the total amount and the other two compound's quantity. From a chemometric point of view, this situation is named as "mixture" and has to be investigated by a suitable mixture design. 3-components mixtures, as in this case, are usually represented as triangles, with each component corresponding to one of the vertices.

In mixture design, the experimental domain can be set either by identifying the upper and lower level for each mixture variable or selecting a reference mixture composition and a variation range around this point. This second strategy is preferred since it leads to a triangular-shaped final domain with the vertices corresponding to the "pseudo components", from now labelled as PCn; opposite the first approach results in an irregular-shaped domain. The reference mixture, reported in the first row of Table 5.9 and highlighted as a star in Figure 5.13, is selected from literature [99] and verified by preliminary experiments; the components' amounts are reported as ratios, setting the total amount as 1. The semi amplitude of the variation range is set at 0.1 to determine the components' ratios in the pseudo components. It must be underlined that, in the reference mixture, **CR**-CMC@ amount is 0.1 and this value can not be further lowered since CR-CMC@ represents the sensitive part of the films. Therefore, instead of using the reference value as the centre of the variation range, for **CR**-CMC@ this value represents the lower amount. The pseudo components composition is reported in Table 5.9 and, in Figure 5.13, the final triangular-shaped experimental domain is displayed.

Table 5.9: Reference mixture and pseudo components composition for film casting deposition optimisation

Mixtures	Starch (x_1)	Glycerol (x_2)	CR-CMC@ (x_3)
Reference	0.6	0.3	0.1
PC1	0.7	0.2	0.1
PC2	0.5	0.4	0.1
PC3	0.5	0.2	0.3

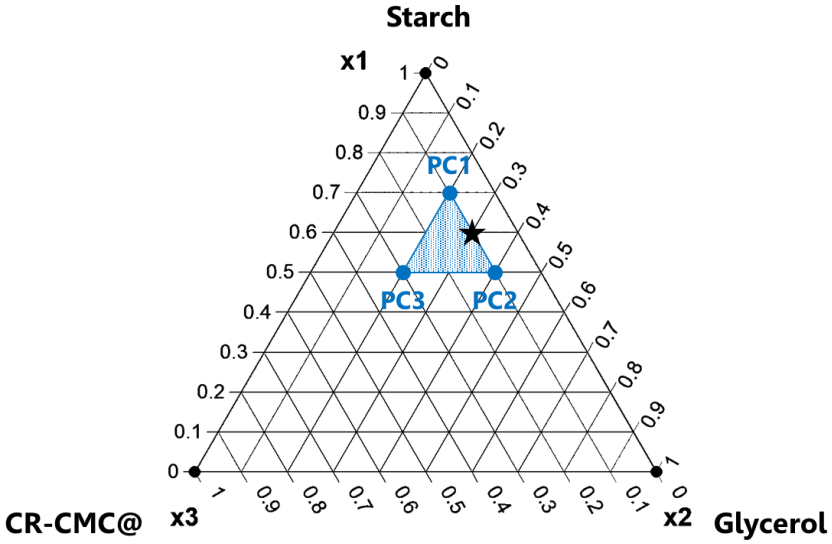

Figure 5.13: Experimental domain and pseudo components definition, referring to original mixture, for film casting deposition optimisation

In addition to mixture composition, other two qualitative variables are investigated: the presence of citric acid as cross-linker and the source of starch. Citric acid is reported in literature as a suitable crosslinker for starch-based films and its amount is usually set at 10% (w/w) of the starch quantity [99, 103]. Since the starch amount is not fixed, the presence of citric acid is considered a qualitative variable with the lower level corresponding to its absence and the upper to the addition in a fixed ratio to starch, as summarised in Table 5.10.

Table 5.10: Level definitions for qualitative variable "citric acid" film casting deposition optimisation

Variable		Lower level (-)	Upper level (+)
Citric acid	x_z	0	10% (w/w) starch

Finally, starch from different sources is characterised by widely different physical and mechanical properties [104, 105] which play a fundamental role in film production by casting deposition. For

this investigation, starches from four different sources are tested, as reported in Table 5.11; all these starches are commercially available, being used for alimentary purposes.

Table 5.11: Level definitions for the qualitative variable "starch source" film casting deposition optimisation

Variable		Level A	Level B	Level C	Level D
Starch source	x_x	Wheat	Corn	Potato	Rice

Model equation

In this case, "Mixture and Process Design" is applied to jointly evaluate the two classes of variables and a tailored model is developed. As for mixture variables, linear terms, two and three factors interactions are calculated while, for the qualitative variables, only linear terms can be determined and, as already hinted before, for starch source, level D is set as implicit. In Equation 5.2 the final model equation is reported in which, for simplicity, PCn are labelled as X_n.

$$Y = b_1X_1 + b_2X_2 + b_3X_3 + b_{12}X_1X_2 + b_{13}X_1X_3 + b_{23}X_2X_3 + b_{123}X_1X_2X_3 + b_zX_z + b_{xA}X_{xA} + b_{xB}X_{xB} + b_{xC}X_{xC}$$

Equation 5.2: Model equation for CR-CMC@ film casting deposition optimisation

Experiments definition and selection

To build the experiment list, a reduced cubical model, considering only the mixture variables in the defined experimental domain, is performed per each level of each qualitative variable, obtaining the 56 candidates (f)**CR**-CMC@ list reported in Table 8.3 in Appendix IV.

Performing all the experiments requires an excessive experimental effort so D-Optimal Design is applied to reduce the number of experiments for model development. This chemometric tool allows identifying the best balance between model reliability and experimental effort, selecting the most informative experiments. In this case, the 28-experiments solution, reported in Table 8.4 in Appendix IV represent the best experiment list.

In Mixture and Process design, diagrams, containing *n* triangular-shaped experimental domains for mixture variables, one per each level of each process variable. In Figure 5.14, 8 triangular-shaped experimental domains are displayed, the levels of "Starch source" qualitative variable are arranged in columns and the ones of "Citric acid" in rows. The 56 candidate points are highlighted as blue borderd circles and the 28 most informative experiments, selected by D-Optimal Design, are distinguished by full blue circles.

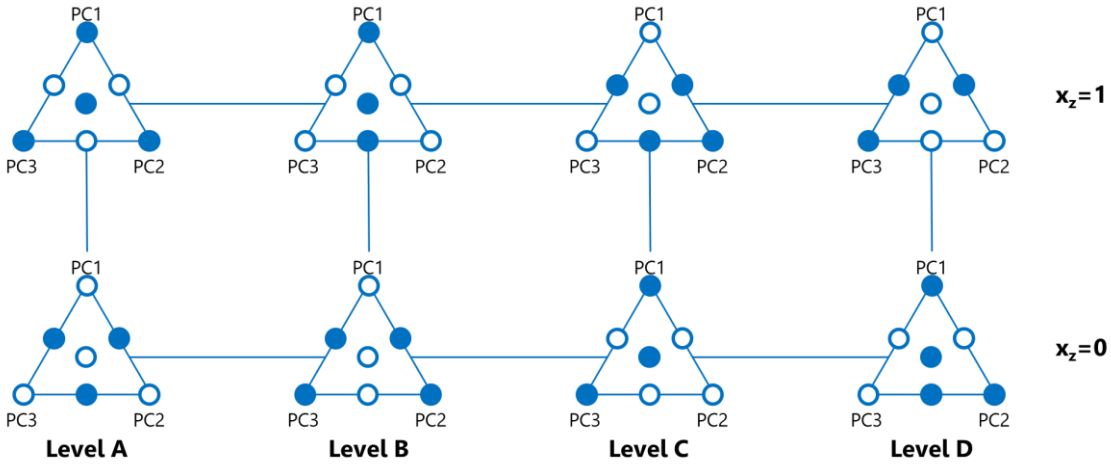

Figure 5.14: Summary diagram for Mixture and Process Design for film casting deposition optimisation. Candidate points (blue bordered circles) and experiments selected by D-Optimal Design (full blue circles) are highlighted.

Analysing Figure 5.14, we can observe that the distribution of the selected experiments is highly symmetrical: each mixture reduced cubical model point (7) is selected four times, each level for "citric acid" (2) fourteen times and each level for "starch source" (4) seven times.

5.3.11 Film casting deposition optimisation: response collection

As already discussed in Section 5.2.4, for this preliminary investigation only a qualitative response is collected, labelling the films as successful or unsuccessful. The successful films are easily peeled from the mould and are sufficiently resistant to be handled while the unsuccessful ones crack or crumble and are unusable. From a chemometric point of view, this response is classified as qualitative: for this type of response, specific designs have been developed but, being this a preliminary investigation, it is out of our purpose to model this response. In fact, this design aims to define a suitable experimental domain and refine the model in terms of influent variables and coefficients. After that, a refined design will be run and quantitative responses, as those described for drop-casting deposition, will be acquired.

For this reason, we assigned a fictitious numerical value as response, referred to the success in film formation, and we analysed the response as quantitative. In detail, Y=1 is assigned for successful films while Y=0 for the unsuccessful ones; the response for each performed experiment is reported in the last column of Table 8.4 in Appendix IV.

Overall, the successful films are 17 out of 28, highlighted as full dark blue circles in Figure 5.15. Analysing the diagram, we could observe that successful films are not homogeneously distributed in the experimental domain but twelve out of seventeen are located in the lower level of "Citric acid", which means in absence of citric acid. Also "Starch source" levels A and B seem to be more promising than the other two levels but this effect is less evident.

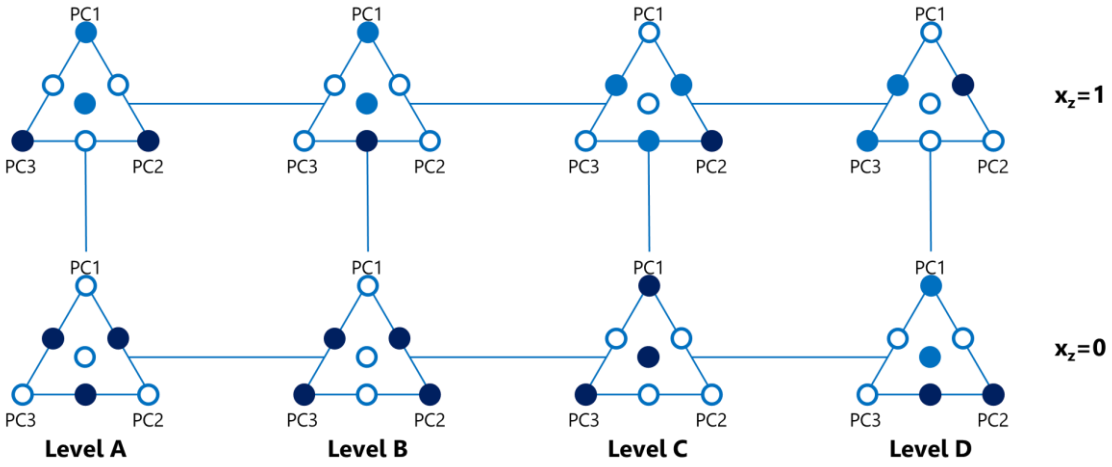

Figure 5.15: Summary diagram for Mixture and Process Design, including the response, for film casting deposition optimisation. Candidate points (blue bordered circles), experiments selected by D-Optimal Design (full blue circles) and successful films (empty dark blue circles) are highlighted.

5.3.12 Film casting deposition optimisation: model solution and refinement

Model solution

The model is calculated using the success in film formation as response; the Y value per each (f)-**CR**-CMC@ is reported in the last column of Table 8.4 in Appendix IV. In Table 5.12, the main statistics for the model are reported. The upper leverage value in the experimental domain is 0.4048 and the model has 17 degrees of freedom. The model performances are definitely not satisfying, both in terms of % explained variance in model calculation and cross-validation (CV) and RMSECV, mainly due to the type of response used and the codification exploited.

Table 5.12: Statistics for film casting deposition model

Statistic parameters	Value
Maximum leverage	0.4048
Degrees of freedom	17
% Explained Variance	40.62%
RMSECV	0.4939
% Explained Variance CV	1.38%

In Figure 5.16 the coefficients plot is shown while, in Table 5.6, the numerical values, semi-amplitude of confidence intervals and significance are listed. From the coefficients plot, shown in Figure 5.16, the significant variables can be identified for following model refinement. As for the Mixture part, pseudo components and linear terms will be kept unchanged since both PC2 and PC3 have a significant effect on the response while both two and three factors interactions will be excluded from the refined model being non-significant.

As for the Process part, “citric acid” has a significant negative effect on film formation thus it will be set at the lower level, which means that citric acid will not be used as a crosslinker. Opposite, the effect of different starch sources is non-significant in this model but, being the difference between the coefficients and the semi amplitude of confidence interval very small and considering the scarce performances of the model, this variable will be kept unchanged also in the refined model.

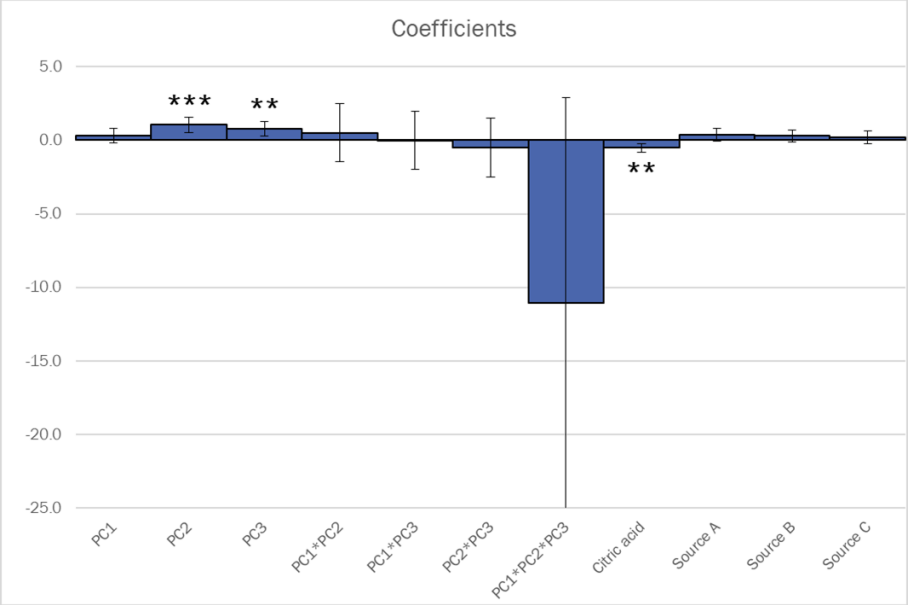

Figure 5.16: Coefficients plot for film casting deposition model

Table 5.13: Coefficients, semi-amplitude of confidence interval (CI) and significance (* p≤0.05, ** p≤0.01, *** p≤0.001) calculated for film casting deposition model

Coefficients		Value	CI	Significance
PC1	b_1	0.29	0.50	
PC2	b_2	1.05	0.50	***
PC3	b_3	0.79	0.50	**
*PC1*PC2*	b_{12}	0.5	2.0	***
*PC1*PC3*	b_{13}	0.0	2.0	
*PC2*PC3*	b_{23}	-0.5	2.0	
*PC1*PC2*PC3*	b_{123}	-11	14	
Citric Acid	b_z	-0.52	0.31	**
Source A	b_{4A}	0.36	0.43	
Source B	b_{4B}	0.29	0.43	
Source C	b_{4C}	0.22	0.43	

Model refinement

Model refinement is performed following two approaches: firstly, variables and coefficients already investigated are selected according to the preliminary assumptions described above. In particular, citric acid is no longer added as a crosslinker since it presents a significant negative effect on films formation, interactions are not calculated because never found significant, while the other variables are kept unchanged. Secondly, the total reagent amount (X_m) is included as process variable, since this value is strongly related to final films thickness, a crucial parameter for sensitive films. The refined model equation is reported in Equation 5.3, labelling PCn as X_n.

$$Y = b_1X_1 + b_2X_2 + b_3X_3 + b_{xA}X_{xA} + b_{xB}X_{xB} + b_{xC}X_{xC} + b_mX_m$$

Equation 5.3: Refined model equation for CR-CMC@ film casting deposition optimisation

5.4 Conclusions

To conclude, bio-based materials are successfully exploited to prepare smart labels for food freshness monitoring. Carboxymethylcellulose was used as solid support for the receptors, adapting the previously developed synthesis while other compounds, like glycerol, starch and citric acid, are used as additives. Functionalised CMC was characterised by performing physicochemical and optical measurements.

Differently from EVOH-based devices, these compounds require suitable deposition procedures to obtain solid materials with good physical and mechanical properties. Up to our knowledge, for the first time, advanced chemometric tools have been employed to model these processes and to optimise these materials preparation.

The first deposition procedure investigated was drop-casting deposition: the entire preparation workflow was optimised, the drop deposited sensors were characterised in terms of sensing performances and their application as smart labels for protein foods during chilled storage is demonstrated, obtaining similar results to the EVOH-based device. This type of CMC-based device represents a very interesting "proof of concept" in the development of printable compostable devices that will be investigated in the future.

The second deposition strategy is film casting deposition: despite its widespread distribution and apparent simplicity, many factors are involved in the casting deposition technique and must be controlled and optimised to obtain films with suitable properties and to develop a reproducible film preparation procedure. Also in this case for the first time, Mixture and Process Design was applied to casting deposition and a preliminary evaluation of the variables' effect is performed. Being the number of successful films too much low compared to the overall experiments performed, the preliminary results of this first model, together with background information, were exploited to refine the model, in terms of variables under investigation and coefficients calculated. In the future, the optimisation of film casting deposition will be performed, sensors will be cut from the films and characterised and their applicability as smart labels will be tested.

It must be underlined that, differently from EVOH-based devices, the solubility in water represents the main disadvantage for CMC-based materials. Both the deposition strategies were investigated to partially overcome this limit, but we are well aware that, in the final application as smart label, even for solid foods, these devices must be covered by a functional permeable barrier to avoid Dye-CMC@ leaching in contact with water or humidity.

To conclude, the results discussed in this Chapter were presented in an oral communication at "RETASTE: RETHINK FOOD WASTE Conference 2021" (Athens, 2021) and at the "Road to CAC2022" (Virtual Congress, 2021). As for data publication, the manuscript containing the results for (dd)**CR**-CMC@ dual sensors device is under preparation while the film casting deposition experiments are still ongoing.

6. Conclusions and perspectives

The last Chapter of this thesis is composed of two sections. In the "General conclusions", the key results obtained during the project are summarised and the features of the developed devices are compared to the main requirements for smart labels, listed in the Introduction. In the "Perspectives", the future experiments planned to complete or to wider the investigations are listed, divided according to the solid support.

6.1 General conclusions

The results of this research project, that I presented above, consists in a series of sensing devices that fulfil many of the requirements listed in the Introduction and here reported and commented:

- Low cost: the lab-scale production cost for all the devices is estimated to be below 0.10 € per sensing device.
- Naked-eye detection: relying on the PCA spoilage models, the average reference colours for each spoilage step were identified and the receptors that provide glaring colour changes were preferred among all.
- Suitability for untrained operators: the colour changes were judged enough glaring and clear to be easily detected by consumers with no technical background.
- Wide applicability: for all the devices, their applicability towards a wide panel of protein foods was verified, testing both meat and fish products or different milk types.
- Biocompatibility or compostability: only CC and CMC-based devices are made of environmentally friendly solid support while EVOH-based devices rely on a plastic material which, however, is widely used in food packaging for its good barrier properties.
- Efficiency during chilled storage: CC and EVOH (32%)-based devices were abandoned since not enough sensitive to immediately detect the spoilage during chilled storage and were substituted by EVOH (29%) and CMC-based devices, directly developed on chilled stored foods, which overcome this limitation.
- Scalable production: CC-based devices were discarded since their preparation procedure was definitely not scalable; this aspect was partially solved with EVOH-based device developing and patenting a synthetic procedure, easy to be scaled for industrial application. Even more appealing were the CMC-based devices since the synthetic procedure is even easier and their water solubility opens to various employment possibilities, such as printable devices.
- Ease to implement in packaging: EVOH-based devices could be implemented in common food packaging by heat sealing to the poly laminate film used to seal the package. Instead, (dd)CMC-based devices can be directly inserted in packages, both composed of plastic or compostable material, being a complete label.

Therefore, the presented results were definitely interesting both from an academic point of view, representing a clear improvement on the present literature, and from an industrial point of view, fulfilling almost all the requirements for smart labels suitable for large-scale implementation.

As regarding the first part, my three-years research production is summarised in six research articles, [7, 8, 9, 14, 15, 16] published on international peer review journals, and a book chapter; [52] I am the first author in all the research articles and the corresponding author for the last five published. [7, 8, 14, 15, 16] Other minor contribution of mine, always in the optical sensors field, are in four research papers [25, 27, 26, 73] and three reviews [62, 106, 107] written in collaboration with my research group during the COVID-19 lockdown period.

The encouraging results obtained with CC and EVOH-based devices and the interesting industrial application perspective led to the first Italian patent deposition in March 2019, [10] in which I am listed as author together with Raffaela Biesuz and Paolo Quadrelli. In the following years, the patent was extended to WIPO/PCT [11] and deposited in USA and Europe. [13, 12]

Moreover, I have had a consistent participation to Italian and International congresses, being the presenting author in oral and poster contributions concerning my research. The congresses participations are listed at the end of each Chapter.

As for the industrial application, an innovative start-up named SAFER Smart Labels was founded in July 2020 and I am one of the co-founder of this company. The main activity of the company is the investigation of the concrete possibility of our sensing devices implementation as smart labels, based on our findings, and the development of a scalable and implementable prototype for the food packaging marketing. [108]

6.2 Perspectives

Despite all the results obtained, some conclusive experiments are still to be done and further areas of application are planned to be tested. For simplicity, the perspectives will be distinguished between EVOH and CMC-based devices and other materials.

6.2.1 EVOH (29%)-based devices

As for this class of devices, the focus will be placed on the instrumental methods to validate the devices responses and the spoilage models and to apply supervised and predictive chemometric tools. Instrumental validation will be focused on solid protein foods since, in the case of milk, a complete validation was already performed and classification and multivariate calibration were successfully applied.

The very first validation will be performed calculating the TVB-N according to the European Standard methodology [56]; secondly, as already performed preliminarily, the composition of the solid food, in terms of BA, and of the headspace, in terms of VOCs and spoilage by-products, will be determined relying on standard methodologies. [8, 54, 55] In addition, specific microbiological assays will be performed to quantify the different bacterial populations forming the SSO and thus related to spoilage ongoing. The reference values acquired by one or more of these techniques will be exploited to build either classification or multivariate calibration models which allow, if validated, to predict the reference values for unknown samples.

To verify even wider applicability, EVOH-based devices will be tested for freshness monitoring of protein foods stored under modified atmosphere (MAP). Since the storage atmosphere strongly influences the spoilage process and the headspace composition [33], the receptors' selection will be updated for these conditions and the entire development process will be performed. The applicability towards MAP-stored foodstuffs will allow to further expand the panel of protein target foods like processed meat and salami.

6.2.2 CMC-based devices

As for this last class of the devices, first of all, the optimisation of the film casting deposition procedure will be completed relying on the refined model developed from the preliminary experiments described in the last part of Chapter 5. Once defined the main features for this device, the films will be characterised, the sensing performances will be evaluated and the applicability as smart label will be tested.

Then, while instrumental validation will be performed in parallel with EVOH-based devices, the possibility to prepare printable smart labels exploiting Dye-CMC@ water solutions as inks will be investigated. This innovative approach is highly appealing for industrial applications since printable devices have much lower costs and require simpler and cheaper machinery for their production and implementation.

6.2.3 Future devices

The reliable strategy for smart labels development, perfected during this project, can be applied to a wide panel of biological macromolecules, ranging from starches, cellulose-based derivatives and others. Therefore, the possible developments of this project are countless, considering the potential receptors, solid phases and deposition techniques that can be rationally investigated with a chemometric approach including the Design of Experiments for preparation procedure optimisation and Multivariate Data Analysis for data elaboration and spoilage modelling.

.

7. Bibliography

[1] J. J. Lavigne e E. V. Anslyn, «Sensing A Paradigm Shift in the Field of Molecular Recognition: From Selective to Differential Receptors,» *Angewandte Chemie International Edition,* vol. 40, pp. 3118-3130, 2001.

[2] K. L. Diehl e E. V. Anslyn, «Array sensing using optical methods for detection of chemical and biological hazards,» *Chemical Society Reviews,* vol. 42, p. 8596, 2013.

[3] Y. Fan, J. Li, Y. Guo, L. Xie e G. Zhang, «Digital image colorimetry on smartphone for chemical analysis: A review,» *Measurement,* vol. 171, p. 108829, 2021.

[4] P. H. Gonçalves Dias Diniz, «Chemometrics-assisted color histogram-based analytical systems,» *Journal of Chemometrics,* vol. 34, p. 3242, 2020.

[5] A. Dodero, A. Escher, S. Bertucci, M. Castellano e P. Lova, «Intelligent Packaging for Real-Time Monitoring of Food-Quality: Current and Future Developments,» *Applied Science,* vol. 11, p. 3532, 2021.

[6] P. Müller e M. Schmid, «Intelligent Packaging in the Food Sector: A Brief Overview,» *Foods,* vol. 8, p. 16, 2019.

[7] L. R. Magnaghi, G. Alberti, P. Quadrelli e R. Biesuz, «Development of a Dye-Based Device to Assess Poultry Meat Spoilage. Part I: Building and Testing the Sensitive Array,» *Journal of Agricultural and Food Chemistry,* vol. 68, n. 45, pp. 12702-12709, 2020.

[8] L. R. Magnaghi, G. Alberti, F. Capone, C. Zanoni, B. Mannucci, P. Quadrelli e R. Biesuz, «Development of a Dye-Based Device to Assess the Poultry Meat Spoilage. Part II: Array on Act,» *Journal of Agricultural and Food Chemistry,* vol. 68, n. 45, pp. 12710-12718, 2020.

[9] L. R. Magnaghi, F. Capone, C. Zanoni, G. Alberti, P. Quadrelli e R. Biesuz, «Colorimetric sensor array for monitoring, modelling and comparing spoilage processes of different meat and fish foods,» *Foods,* vol. 9, n. 5, p. 684, 2020.

[10] R. Biesuz, P. Quadrelli e L. R. Magnaghi, «Sensori per la Valutazione della Qualità di Prodotti Alimentari a Base di Carne.». Italia Brevetto 10201900000464, 19 March 2019.

[11] R. Biesuz, P. Quadrelli e L. R. Magnaghi, «Sensors for the Evaluation of the Quality of Meat-Based Food.». WIPO Brevetto PCT/IB2020/052998, 30 March 2020.

[12] R. Biesuz, P. Quadrelli e L. R. Magnaghi, «Sensors for the Evaluation of the Quality of Meat-Based Food». Europe Brevetto EURO-PCT 20721299, 4 March 2020.

[13] R. Biesuz, P. Quadrelli e L. R. Magnaghi, «Sensors for the Evaluation of the Quality of Meat-Based Foods». USA Brevetto 17599196, 28 September 2021.

[14] L. R. Magnaghi, G. Alberti, C. Milanese, P. Quadrelli e R. Biesuz, «Naked-Eye Food Freshness Detection: Innovative Polymeric Optode for High-Protein Food Spoilage Monitoring,» *ACS Food Science & Technology,* vol. 1, n. 2, pp. 165-175, 2021.

[15] L. R. Magnaghi, F. Capone, G. Alberti, C. Zanoni, B. Mannucci, P. Quadrelli e R. Biesuz, «EVOH-based pH-sensitive Optodes Array & Chemometrics: From Naked-eye Analysis to Predictive Modelling to Detect Milk Freshness,» *ACS Food Science & Technology,* 2021.

[16] L. R. Magnaghi, C. Zanoni, G. Alberti, P. Quadrelli e R. Biesuz, «Towards intelligent packaging: BCP-EVOH@ optode for milk freshness measurement».

[17] A. Hulanicki, S. Glab e F. Ingman, «Chemical Sensors: Definition and Classification,» *Pure & Applied Chemistry,* vol. 63, n. 9, pp. 1247-1250, 1991.

[18] G. Alberti, V. Amendola, G. Bergamaschi, R. Colleoni, C. Milanese e R. Biesuz, «Supramolecular receptors in solid phase: developing sensors for anionic radionuclides,» *Dalton Transactions,* vol. 42, pp. 6227-6234, 2013.

[19] R. Biesuz, G. Emma, C. Milanese, G. Dacarro, A. Taglietti, G. Alberti e V. M. Nurchi, «Novel DFO-SAM on mesoporous silica for iron sensing. Part I. Synthesis optimization and characterization of the material,» *Analyst,* vol. 139, pp. 3932-3939, 2014.

[20] G. Alberti, G. Emma, R. Colleoni, M. Pesavento, V. M. Nurchi e R. Biesuz, «Novel DFO-functionalized mesoporous silica for iron sensing. Part 2. Experimental detection of free iron concentration (pFe) in urine samples,» *Analyst,* Vol. %1 di %23940-3948, p. 139, 2014.

[21] G. Alberti, F. Quattrini, R. Colleoni, V. M. Nurchi e R. Biesuz, «Deferoxamine–paper for iron(III) and vanadium(V) sensing,» *Chemical Papers,* vol. 69, n. 8, pp. 1024-1032, 2015.

[22] G. Alberti, S. Re, A. M. Tivelli e R. Biesuz, «Smart sensory materials for divalent cations: a dithizone immobilized membrane for optical analysis,» *Analyst,* vol. 141, pp. 6140-6148, 2016.

[23] R. Biesuz, V. M. Nurchi, J. . I. Lachowicz e G. Alberti, «Unusual PLS application for Pd(ii) sensing in extremely acidic solutions,» *New Journal of Chemistry,* vol. 42, pp. 7901-7907, 2018.

[24] R. Biesuz, M. A. Santos, V. M. Nurchi e G. Alberti, «Development of a sensor for trivalent iron: AHP fixed on mesoporous silica,» *New Journal of Chemistry,* vol. 42, pp. 15237-15244, 2018.

[25] R. Biesuz, V. M. Nurchi, L. R. Magnaghi e G. Alberti, «Inexpensive Alizarin Red S-based optical device for the simultaneous detection of Fe(III) and Al(III),» *Microchemical Journal,* vol. 149, p. 104036, 2019.

[26] G. Alberti, V. M. Nurchi, L. R. Magnaghi e R. Biesuz, «A portable, disposable, and low-cost optode for sulphide and thiol detection,» *Analytical Methods,* vol. 11, pp. 4464-4470, 2019.

[27] G. Alberti, C. Zanoni, L. R. Magnaghi e R. Biesuz, «Low-cost, disposable colourimetric sensors for metal ions detection,» *Journal of Analytical Science and Technology,* vol. 11, n. 30, 2020.

[28] P. Oliveri, C. Malegori e M. Casale, «Chemometrics and Statistics | Multivariate Classification Techniques,» in *Encyclopedia of Analytical Science*, P. Worsfold, C. Poole, A. Townshend e M. Mirò, A cura di, Academic Press, 2019, pp. 481-486.

[29] R. Leardi, «Chemometrics: From Classical to Genetic Algorithms,» *Grasas y Aceites,* vol. 53, n. 1, pp. 115-127, 2002.

[30] . P. . V. Ajay, J. Printo, D. S. Kiruba, L. Susithra , K. Takatoshi e M. Sivakumar , «Colorimetric sensors for rapid detection of various analytes,» *Materials Science and Engineering C,* vol. 78, pp. 1231-1245, 2017.

[31] B. Kuswandi e A. Nurfawaidi, «On-package dual sensors label based on pH indicators for real-time monitoring of beef freshness,» *Food Control,* vol. 82, pp. 91-100, 2017.

[32] M. Miks-Krajnik, Y.-J. Yoon e H.-G. Yuk, «Detection of Volatile Organic Compounds as Markers of Chicken Breast Spoilage Using HS-SPME-GC/MS-FASST,» *Food Science and Biotechnology,* vol. 24, n. 1, pp. 361-372, 2015.

[33] G.-J. E. Nychas, P. N. Skandamis, C. C. Tassou e K. P. Koutsoumanis, «Meat spoilage during distribution,» *Meat Science,* vol. 78, pp. 77-89, 2008.

[34] K. Koutsoumanis e G.-J. E. Nychas, «Chemical and Sensory Changes Associated with Microbial Flora of Mediterranean Boque (Boops boops) Stored Aerobically at 0, 3, 7, and 10°C,» *APPLIED AND ENVIRONMENTAL MICROBIOLOGY,* vol. 65, n. 2, pp. 698-706, 1999.

[35] M. Miks-Krajnik, Y.-J. Yoon, D. O. Ukuku e H.-G. Yun, «Identification and Quantification of Volatile Chemical Spoilage Indexes Associated with Bacterial Growth Dynamics in Aerobically Stored Chicken,» *Journal of Food Science,* vol. 81, p. M2006–M2014, 2016.

[36] R. H. Dainty, «Chemical/biochemical detection of spoilage,» *International Journal of Food Microbiology,* vol. 33, pp. 19-33, 1996.

[37] F. B. Erim, «Recent analytical approaches to the analysis of biogenic amines in food samples,» *Trends in Analytical Chemistry,* vol. 52, p. 239.247, 2013.

[38] A. Poghossian, H. Geissler e M. J. Schoning, «Rapid methods and sensors for milk quality monitoring and spoilage detection,» *Biosensors and Bioelectronics,* vol. 140, p. 111272, 2019.

[39] S. Choudhary, B. Joshi, G. Pandey e A. Joshi, «Application of single and dual fluorophore-based pH sensors for determination of milk quality and shelf life using a fibre optic spectrophotometer,» *Sensors and Actuators B: Chemical,* vol. 298, p. 126925, 2019.

[40] M. Lu, Y. Shiau, J. Wong, R. Lin, H. Kravis, T. Blackmon, T. Pakzad, T. Jen, A. Cheng, J. Chang, E. Ong, N. Sarfaraz e N. S. Wang, «Milk Spoilage: Methods and Practices of Detecting Milk Quality,» *Food and Nutrition Science,* vol. 4, pp. 113-123, 2013.

[41] M. Lu e N. S. Wang, «Chapter 7 - Spoilage of Milk and Dairy Products,» in *The Microbiological Quality of Food*, A. Bevilacqua, M. R. Corbo e M. Sinigaglia, A cura di, Woodhead Publishing, 2017, pp. 151-178.

[42] S. T. Chan, M. W. Y. Yao, Y. C. Wong, T. Wong, C. S. Mok e D. W. M. Sin, «Evaluation of chemical indicators for monitoring freshness of food and determination of volatile amines in fish by headspace solid-phase microextraction and gas chromatography-mass spectrometry,» *European Food Research and Technology,* vol. 224, pp. 67-74, 2006.

[43] H. Chun, B. Kim e H. Shin, «Evaluation of a freshness indicator for quality of fish products during storage,» *Food Science and Biotechnology,* vol. 23, pp. 1719-1725, 2014.

[44] C. Rukchon, A. Nopwinyuwong, S. Trevanich, T. Jinkarn e P. Suppakul, «Development of a food spoilage indicator for monitoring freshness of skinless chicken breast,» *Talanta,* vol. 130, pp. 547-554, 2014.

[45] A. Casaburi, P. Piombino, G.-J. Nychas, F. Villani e D. Ercolini, «Bacterial populations and volatilome associated to meat spoilage,» *Food Microbiology,* vol. 45, pp. 83-102, 2015.

[46] G.-J. Nychas e C. C. Tassou, «Spoilage process and proteolysis in chicken as detected by HPLC,» *Journal of the Science of Food and Agriculture,* vol. 74, pp. 199-208, 1997.

[47] M. Alizadeh-Sani, E. Mohammadian, J.-W. Rhim e S. . M. Jafari, «pH-sensitive (halochromic) smart packaging films based on natural food colorants for the monitoring of food quality and safety,» *Trends in Food Science & Technology,* vol. 105, p. 93–144, 2020.

[48] S. J. Lee e A. Mijanur Rahman, «Intelligent Packaging for Food Products,» in *Innovations in Food Packaging*, 2014, pp. 171-209.

[49] R. Priyadarshi, P. Ezati e J.-W. Rhim, «Recent Advances in Intelligent Food Packaging Applications Using Natural Food Colorants,» *ACS Food Science and Technology,* vol. 1, pp. 124-138, 2021.

[50] C. Rodrigues, V. G. Lauriano Souza, I. Coelhoso e A. L. Fernando, «Bio-Based Sensors for Smart Food Packaging—Current Applications and Future Trends,» *Sensors,* vol. 21, p. 2148, 2021.

[51] E. Balbinot-Alfaro, D. Vieira Craveiro, K. Oliveira Lima, H. Leão Gouveia Costa, D. Rubim Lopes e C. Prentice, «Intelligent Packaging with pH Indicator Potential,» *Food Engineering Reviews,* vol. 11, pp. 235-244, 2019.

[52] R. Biesuz e L. R. Magnaghi, «Role of Biogenic Amines in Protein Foods Sensing: Myths and Evidence,» in *Meat and Nutrition*, C. L. Ranabhat, A cura di, IntechOpen, 2021.

[53] H. Peng, W. Chen, Y. Cheng, L. Hakuna, R. Strongin e B. Wang, «Thiol Reactive Probes and Chemosensors,» *Sensors,* vol. 12, pp. 15907-15946, 2012.

[54] V. Sirocchi, G. Caprioli, M. Ricciutelli, S. Vittori e G. Sagratini, «Simultaneous determination of ten underivatized biogenic amines in meat by liquid chromatography-tandem mass spectrometry (HPLC-MS/MS),» *Journal of Mass Spectrometry,* n. 49, p. 819–825, 2014.

[55] G. Sagratini, M. Fernández-Franzón, F. De Berardinis, G. Font , S. Vittori e J. Mañes, «Simultaneous determination of eight underivatised biogenic amines in fish by solid phase extraction and liquid chromatography–tandem mass spectrometry,» *Food Chemistry 132,* pp. 537-543, 2012.

[56] M. A.-T. L. M. Omayma, M. M. Hassouba e E. E.-M. Eman, «Effect of Methodology on the Determination of Total Volatile Basic Nitrogen as an Index of Quality of Meat and Fish,» *Egyptian Journal of Food Safety,* vol. 1, n. 2, pp. 23-34, 2013 .

[57] M. A. Fabro, H. V. Milanesio, L. M. Robert, J. L. Speranza, M. Murphy, G. Rodriguez e R. Castaneda, «Technical Note: Determination of Acidity in Whole Raw Milk: Comparison of Results Obtained by Two Different Analytical Methods,» *Journal of Dairy Science,* vol. 89, pp. 859-861, 2006.

[58] G. E. P. Box, J. S. Hunter e W. G. Hunter, Statistics for Experimenters: Design, Innovation, and Discovery, Wiley, 2005.

[59] G. Brereton, Chemometrics: Data Analysis for the Laboratory and Chemical Plant, Wiley, 2003.

[60] R. Leardi, C. Melzi e G. Polotti, «CAT, Chemometric Agile Tool software».

[61] «GIMP software,» [Online]. Available: https://www.gimp.org/.

[62] G. Alberti, C. Zanoni, L. R. Magnaghi e R. Biesuz, «Disposable and Low-Cost Colorimetric Sensors for Environmental Analysis,» *International Journal of Environmental Research and Public Health,* vol. 17, n. 22, p. 8331, 2020.

[63] I. Safarik, J. Prochazkova, E. Baldikova e K. Pospiskova, «Commercially available color-catching sheets for magnetic textile solid phase extraction of water-soluble dyes,» *Measurements,* vol. 172, p. 108877, 2021.

[64] R. Casula, G. Crisponi, F. Cristiani e V. M. Nurchi, «Characterization of the ionization and spectral properties of sulfonephtalein indicators. Correlation with substituent effects and structural features,» *Talanta,* vol. 40, n. 12, pp. 1781-1788, 1993.

[65] M. C. Aragoni, M. Arca, G. Crisponi, V. M. Nurchi e R. Silvagni, «Characterization of the ionization and spectral properties of sulfonephtalein indicators. Correlation with substituent effects and structural features. Part II,» *Talanta,* vol. 42, pp. 1157-1163, 1995.

[66] R. W. Sabnis, Handbook af Acid-Base Indicators, Oxfordshire, UK: Taylor and Francis Group, 2008.

[67] Q. Chen, Z. Hui, J. Zhao e Q. Ouyang, «Evaluation of chicken freshness using a low-cost colorimetric sensor array with AdaBoosteOLDA classification algorithm,» *LWT - Food Science and Technology,* Vol. %1 di %2502-507, p. 57, 2014.

[68] Y. Salinas, J. V. Ros-Lis, J.-L. Vivancos, R. Martínez-Máñez, M. D. Marcos, S. Aucejo, N. Herranz e I. Lorente, «A novel colorimetric sensor array for monitoring fresh pork sausages spoilage,» *Food Control,* vol. 35, pp. 166-176, 2014.

[69] K. Urmila, H. Li, Q. Chen, Z. Hui e J. Zhao, «Quantifying of total volatile basic nitrogen (TVB-N) content in chicken using a colorimetric sensor array and nonlinear regression tool,» *Analytical Methods,* vol. 7, p. 5682, 2015.

[70] H.-z. Chen, M. Zhang, B. Bhandari e C.-h. Yang, «Development of a novel colorimetric food package label for monitoring lean pork freshness,» *LWT - Food Science and Technology,* vol. 99, pp. 43-49, 2019.

[71] M. Sànchez-Chaves, C. Ruiz, M. L. Cerrada e M. Fernàndez-Garcìa, «Novel glycopolymers containing aminosaccharide pendant groups by chemical modification of ethylene–vinyl alcohol copolymers,» *Polymer,* vol. 49, pp. 2801-2807, 2008.

[72] C. Ruiz, M. Sanchez-Chaves, M. L. Cerrada e M. Fernandez-Garcia, «Glycopolymers Resulting from Ethylene–Vinyl Alcohol Copolymers: Synthetic Approach, Characterization, and Interactions with Lectins,» *J Polym Sci Part A: Polym Chem,* pp. 7238-7248, 2008(46).

[73] G. Alberti, C. Zanoni, L. R. Magnaghi, M. A. Santos, V. M. Nurchi e R. Biesuz, «DFO@EVOH and 3,4-HP@EVOH: Towards New Polymeric Sorbents for Iron(III),» *Chemosensors,* vol. 8, n. 4, p. 111, 2020.

[74] J. Du, Z. Dong, X. Yang e L. Zhao, «Facile fabrication of sodium styrene sulfonate-grafted ethylene-vinyl alcohol copolymer as adsorbent for ammonium removal from aqueous solution,» *Environmental Science and Pollution Research,* vol. 25, pp. 27235-27244, 2018.

[75] H. Salehi-Mobarakeh, A. Yadegari, J. Didehvar e F. Khakzad-Esfahlan, «Polyamide grafting onto ethylene-vinyl alcohol copolymer,» *Journal of Polymer Engineering,* vol. 33, n. 9, pp. 843-850, 2013.

[76] K. Xie, Z. Dong, Y. Wang, W. Qi, M. Zhai e L. Zhao, «Facile Preparation of EVOH-Based Amphoteric Ion Exchange Membrane Using Radiation Grafting Technique: A Preliminary Investigation on Its Technique: A Preliminary Investigation on Its Application for Vanadium Redox Flow Battery,» *Polymers,* vol. 11, p. 843, 2019.

[77] D. Xu, J. Lu, S. Yan e R. Xiao, «Aminated EVOH nanofiber membranes for Cr(VI) adsorption from aqueous solution,» *RSC Advances,* vol. 8, p. 742, 2018.

[78] C. Salgado, M. P. Arrieta, A. Chiloeches, A. Muñoz-Bonilla, L. Peponi, D. López e M. Fernández-García, «Development of photoresponsive coumarin-modified ethylene-co-vinyl alcohol copolymers with antifouling behavior,» *Reactive and Functional Polymers,* vol. 157, p. 104750, 2020.

[79] G. Bylund, Dairy Processing Handbook, 2nd Ed. a cura di, Tetrapak, 2003, p. 440.

[80] M. Decimo, M. C. Cabeza, J. A. Ordonez, I. De Noni e M. Brasca, «Volatile organic compounds associated with milk spoilage by psychrotrophic bacteria,» *International Journal of Dairy Technology,* vol. 71, n. 3, pp. 593-600, 2018.

[81] K. Seiler e W. Simon, «Theoretical aspects of bulk optode membranes,» *Analytica Chimica Acta,* vol. 266, pp. 73-87, 1992.

[82] G. J. Mohr e O. S. Wolfbeis, «Optical sensors for a wide pH range based on azo dyes immobilized on a novel support,» *Analytica Chimica Acta,* vol. 292, pp. 41-48, 1994.

[83] G. J. Mohr, T. Werner e O. S. Wolfbeis, «Synthesis of Reactive Vinylsulphonyl Azo Dyes for Application in Optical pH Sensing,» *Dyes and Pigments,* vol. 24, pp. 223-240, 1994.

[84] G. J. Mohr, H. Muller, B. Bussemer, A. Stark, T. Carofiglio, S. Trupp, R. Heuermann, T. Henkel, D. Escudero e L. Gonzalez, «Design of acidochromic dyes for facile preparation of pH sensor layers,» *Analytical and Bioanalytical Chemistry,* vol. 392, pp. 1141-1418, 2008.

[85] L. R. Magnaghi, C. Zanoni, G. Alberti, P. Quadrelli e R. Biesuz, «Freshness traffic light for various fish products: dual-optodes label to monitor fish spoilage in sales package».

[86] C. Maes, W. Luyten, G. Herremans, R. Peeters, R. Carleer e M. Buntinx, «Recent Updates on the Barrier Properties of Ethylene Vinyl Alcohol Copolymer (EVOH): A Review,» *Polymer Reviews,* vol. 58, n. 2, pp. 209-246, 2018.

[87] S. Song, C. Hao, X. Zhang, Q. Zhang e R. Sun, «Sonocatalytic degradation of methyl orange in aqueous solution using Fe-doped TiO2 nanoparticles under mechanical agitation,» *Open Chemistry,* vol. 16, pp. 1283-1296, 2018.

[88] F. Guacheron, «The minerals of milk,» *Reproduction Nutrition Development,* vol. 45, n. 4, pp. 473-483, 2005.

[89] A. Braibanti, G. Ostacoli, P. Paoletti, L. D. Pettit e S. Sammartano, «Recommended Procedure for Testing the Potentiometric Apparatus and Technique for the pH-metric Measurement of Metal-Complex Equilibrium Constants,» *Pure and Applied Chemistry,* vol. 59, n. 12, pp. 1721-1728, 1987.

[90] H. M. C. De Azeredo, M. F. Rosa, M. De Sà, M. Souza Filho e K. W. Waldron, «The use of biomass for packaging films and coatings,» in *Advances in Biorefineries*, K. Waldron, A cura di, Woodhead Publishing, 2014, pp. 819-874.

[91] M. Mohammadi, M. Hossein Azizi e A. Zoghi, «Antimicrobial activity of carboxymethyl cellulose–gelatin film containing Dianthus barbatus essential oil against aflatoxin-producing molds,» *Food Science & Nutrition,* vol. 8, p. 1244–1253, 2020.

[92] W. Tongdeesoontorn, L. J. Mauer, S. Wongruong, P. Sriburi e P. Rachtanapun, «Physical and Antioxidant Properties of Cassava Starch–Carboxymethyl Cellulose Incorporated with Quercetin and TBHQ as Active Food Packaging,» *Polymers,* vol. 12, n. 2, p. 366, 2020.

[93] H. M. S. Akhtar, A. Riaz, Y. S. Hamed, M. Abdin, G. Chen, P. Wan e X. Zeng, «Production and characterization of CMC-based antioxidant and antimicrobial films enriched with chickpea hull polysaccharides,» *International Journal of Biological Macromolecules,* vol. 118, p. 469–477, 2018.

[94] W. Lan, L. He e L. Yaowen, «Preparation and Properties of Sodium Carboxymethyl Cellulose/Sodium Alginate/Chitosan Composite Film,» *Coatings,* vol. 8, n. 8, p. 291, 2018.

[95] S. M. Martelli, C. Motta, J. Alberton, I. Casagrande Bellettini, A. C. Pinheiro do Prado, P. L. Manique Barreto e V. Soldi, «Edible carboxymethyl cellulose films containing natural antioxidant and surfactants: a-tocopherol stability, in vitro release and film properties,» *LWT - Food Science and Technology,* vol. 77, pp. 21-29, 2017.

[96] C. Rodrigues, V. G. Lauriano Souza, I. Coelhoso e A. L. Fernando, «Bio-Based Sensors for Smart Food Packaging—Current Applications and Future Trends,» *Sensors,* vol. 21, p. 2148, 2021.

[97] A. Pettignano, A. Daunay, C. Moreau, B. Cathala, A. Charlot e E. Fleury, «Sustainable Modification of Carboxymethyl Cellulose by Passerini Three-Component Reaction and Subsequent Adsorption onto Cellulosic Substrates,» *ACS Sustainable Chemistry & Engineering,* vol. 7, n. 17, pp. 14685-14696, 2017.

[98] A. Pettignano, A. Charlot e E. Fleury, «Carboxyl-functionalized derivatives of carboxymethyl cellulose: towards advanced biomedical applications,» *Polymer Reviews,* vol. 59, n. 3, pp. 510-560, 2019.

[99] B. Ghanbarzadeh, H. Almasi e A. A. Entezami, «Physical properties of edible modified starch/carboxymethyl cellulose films,» *Innovative Food Science and Emerging Technologies,* vol. 11, pp. 697-702, 2010.

[100] K. Gulati, L. Sohan e S. Arora, «Synthesis and characterization of PVA/Starch/CMC composite films reinforced with walnut (Juglans regia L.) shell flour,» *SN Applied Sciences,* vol. 1, p. 1416, 2019.

[101] S. R. Kanatt e S. H. Makwanab, «Development of active, water-resistant carboxymethyl cellulose-poly vinyl alcohol-Aloe vera packaging film,» *Carbohydrate Polymers,* vol. 227, p. 115303, 2020.

[102] J. Zhu, Q. Li, Y. Che, X. Liu, C. Dong, X. Chen e W. Chao, «Effect of Na2CO3 on the Microstructure and Macroscopic Properties and Mechanism Analysis of PVA/CMC Composite Film,» *Polymers,* vol. 2, n. 12, p. 453, 2020.

[103] R. Kumar, G. Ghoshal e M. Goyal, «Synthesis and functional properties of gelatin/CA–starch composite film: excellent food packaging material,» *J Food Sci Technol,* vol. 56, n. 4, pp. 1954-1965, 2019.

[104] L. Dai, J. Zhang e F. Cheng, «Effects of starches from different botanical sources and modification methods on physicochemical properties of starch-based edible films,» *Int. J. Biol. Macromol.,* vol. 132, pp. 897-905, 2019.

[105] D. Domene-López, J. C. García-Quesada, I. Martin-Gullon e M. G. Montalbán, «Influence of Starch Composition and Molecular Weight on Physicochemical Properties of Biodegradable Films,» *Polymers,* vol. 11, p. 1084, 2019.

[106] G. Alberti, C. Zanoni, V. Losi, L. R. Magnaghi e R. Biesuz, «Current Trends in Polymer Based Sensors,» *Chemosensors,* vol. 9, p. 108, 2021.

[107] G. Alberti, C. Zanoni, L. R. Magnaghi e R. Biesuz, «Gold and Silver Nanoparticle-Based Colorimetric Sensors: New Trends and Applications,» *Chemosensors,* vol. 9, p. 305, 2021.

[108] «SAFER Smart Labels,» [Online]. Available: http://www.safersmartlabels.com/.

8. Appendix

8.1 Appendix I: Materials

8.1.1 Reagents

Receptors

- *m*-cresol purple: CAS n°2303-01-7
- o-cresol red: CAS n°1733-12-6
- bromothymol blue: CAS n°34722-90-2
- thymol blue: CAS n°76-61-9
- chlorophenol red: CAS n°4430-20-0
- Ellman's Reagent, 5,5-dithio-bis-[2-nitrobenzoic acid] (DTNB): CAS n°69-78-3
- bromophenol blue: CAS n° 33551-92-7
- bromocresol purple: CAS n° 115-40-2
- phenol red: CAS n° 143-74-8
- methyl orange: CAS n° 547-58-0
- Congo red: CAS n°573-58-0
- bromocresol green: CAS n°76-60-8
- alizarin red S: CAS n°130-22-3
- alizarin yellow R: CAS n°2243-76-7
- Clayton yellow: CAS n°1829-00-1

Solid supports and additives

- Colour Catcher®, Grey
- Ethylene vinyl alcohol (EVOH) copolymer (32% ethylene content) provided by Industria Termoplastica Pavese (ITP)
- Ethylene vinyl alcohol (EVOH) copolymers (DT2904, D2908, AT4403 and A4412) provided by Nippon Goshei
- Carboxymethylcellulose (CMC) (Carbocel MM250), provided by Lamberti Spa
- Filter paper, provided by Whatman
- Food grade paper, Paperboard and Pure cellulose, provided by Barbè Srl
- Corn, Potato, Rice and Wheat starch, food grade commercial product by Paneangeli©, Cameo Spa

Chemicals

- Nitric acid ultrapure 65%: CAS n°7697-37-2
- Sodium hydroxide: CAS n°1310-73-2
- Ammonium hydroxide solution 28%: CAS n°1336-21-6
- Acetic acid glacial: CAS n°64-19-7

- N,N-Dimethylacetamide: CAS n°127-19-5
- Thionyl chloride solution in DCM (1M): CAS n°7719-09-7
- Dichloromethane: CAS n°75-09-2
- Toluene: CAS n°108-88-3
- Potassium hydrogen phthalate: CAS n°877-24-7
- Sodium carbonate: CAS n°497-19-8
- Sodium hydrogen carbonate: CAS n° 144-55-8
- Sodium hydrogen phosphate: CAS n° 7558-79-4
- Sodium dihydrogen phosphate: CAS n°7558-80-7
- Citric acid: CAS n°77-92-9
- 2-(N-morpholino)ethanesulfonic acid (MES): CAS n°126615-59-1
- piperazine-N,N′-bis(2-ethanesulfonic acid) (PIPES): CAS n°5625-37-6
- N-(2-Hydroxyethyl)piperazine-N′-(3-propanesulfonic acid) (EPPS): CAS n°16052-06-5
- Glycerol: CAS n°56-81-5

8.1.2 Instruments

- Smartphone Samsung Galaxy S7
- NIKON COOLPIX S6200
- Portable led lightbox (23x23x23 cm), equipped with 20 LEDs (550LM, colour temperature 5500K) (PULUZ, Photography Light Box, Shenzhen Puluz Technology Limited).
- Jasco V-750 spectrophotometer equipped with UCB-710 Rectangular Cell Holder and FLH-740 film Holder
- Orion 420 pH meter with a combined glass electrode
- Analytical balance ORMA mod. BCA 120, capacità 120 g, n° serie 32340
- Ultra-Turrax S 18N-10G homogenizer (IKA-Werke Gmbh & Co., Germany)
- Potentionmetric titration equipment: pH meter Orion EA 940; combined microelectrode Metrohm 6.0234.100, automatic burette Hamilton with 500 µL microsyringe Hamilton; titration vessel with thermostat jacket Metrohm and circulation thermostat Lauda L100
- Differential Scanning Calorimeter Q2000 interfaced with a TA 5000 data station (TA Instruments)
- FT-IR iS10 spectrometer Nicolet (Madison, WI) equipped with an attenuated total reflectance (ATR) sampling accessory (Smart iTR with a diamond plate)
- EVO MA10 scanning electron microscope (SEM) equipped with X-max 50 mm2 probe (Oxford Instrument)
- KLA Tencor P-6 Stylus Profiler
- Laboratory equipment

8.2 Appendix II: Abbreviations

Abbreviation	Meaning
3-Way PCA	3-Way Principal Component Analysis
ATR	Attenuated Total Reflectance
BA	Biogenic Amines
BCP	BromoCresol Purple
CACHAS	Chemometrics-Assisted Colour Histogram-based Analytical Systems
CAT	Chemometric Agile Tool
CC	Colour Catcher
CI	Confidence Interval
CLT	Chemometrics-assisted Litmus Test
CMC	CarboxyMethyl Cellulose
CMYK	Cyan, Magenta, Yellow, BlacK colour model
CR	*o*-Cresol Red
CSI	Chemical Spoilage Index
CV	Cross Validation
DCM	DiChloroMethane
DIC	Digital Imaging Colourimetry
DMA	N,N-DiMethylAcetamide
DSC	Differential Scanning Calorimetry
EBT	Eriochrome Black T
ED	Experimental Design
EDX	Energy Dispersive X-ray analysis
EVOH	Ethylene Vinyl Alcohol copolymer
FQI	Food Quality Indicator
FT-IR	Fourier-Transform Infrared Spectroscopy
GC/MS	Gas Chromatography–Mass Spectrometry
HSSPME	HeadSpace Solid-Phase MicroExtraction
HSV	Hue Saturation Value colour model
KNN	k-Nearest Neighbour algorithm
L*a*b*	LAB colour model or CIELAB
LAB	Lactic Acid Bacteris
LC-MS/MS	Liquid Chromatography with tandem Mass Spectrometry
LDA	Linear Discriminant Analysis
LOD	Limit Of Detection
MAP	Modified Atmosphere Packaging
MFR	Melt Flow Rate
MLR	Multiple Linear Regression

PAN	1-(2-pyridylazo)-2-naphthol
PC	Pseudo Component Principal Component
PCA	Principal Component Analysis
PCR	Principal Component Regression
PDMS/DVB	PolyDiMethylSiloxane/DiVinylBenzene
PEG	PolyEthylene Glycol
PLS	Partial Least Squares regression
PLS-DA	Partial Least Squares Discriminant Analysis
PVA	PolyVinyl Alcohol
RGB	Red Green Blue colour model
RMSECV	Root Mean Square Error in Cross Validation
RMSEP	Root Mean Square Error in Prediction
RT	Room Temperature
SEM	Scanning Electron Microscope
SIMCA	Soft Independent Modelling by Class Analogy
SSO	Specific Spoilage Organism
TCA	TriChloroAcetic acid
VOC	Volatile Organic Compound
XYZ	XYZ colour model or CIEXYZ

8.3 Appendix III: Loading and score plots

8.3.1 CC-based devices

Sensitivity evaluation: loading plots

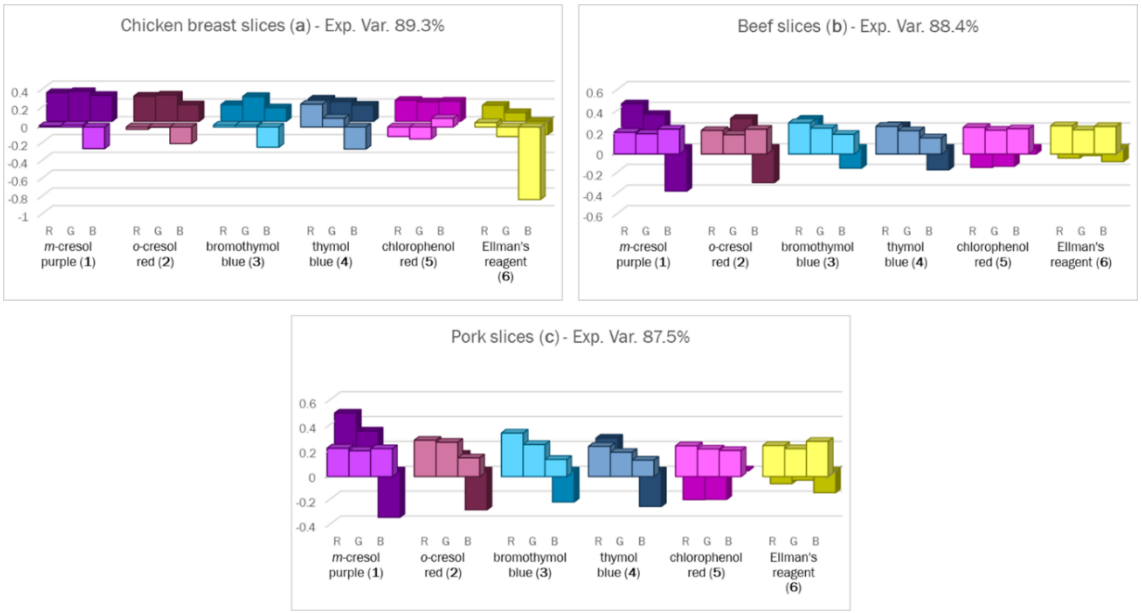

Figure 8.1: The loading plots of the PCA models on the first two principal components, built on the sensitivity dataset for chicken breast slices (a), beef slices (b) and pork slices (c). The loading values on PC1 are in the foreground, the ones on PC2 in the background.

8.3.2 EVOH (32%)-based devices

Protein foods spoilage modelling: loading plots

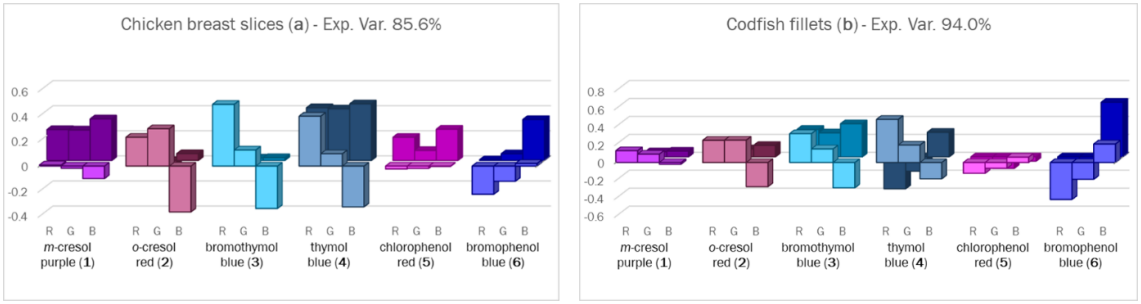

Figure 8.2: The loading plots of the PCA models on the first two principal components, built on the training set for chicken breast slices (a) and codfish fillets (b). The loading values on PC1 are in the foreground, the ones on PC2 in the background.

Milk spoilage modelling: loading plots

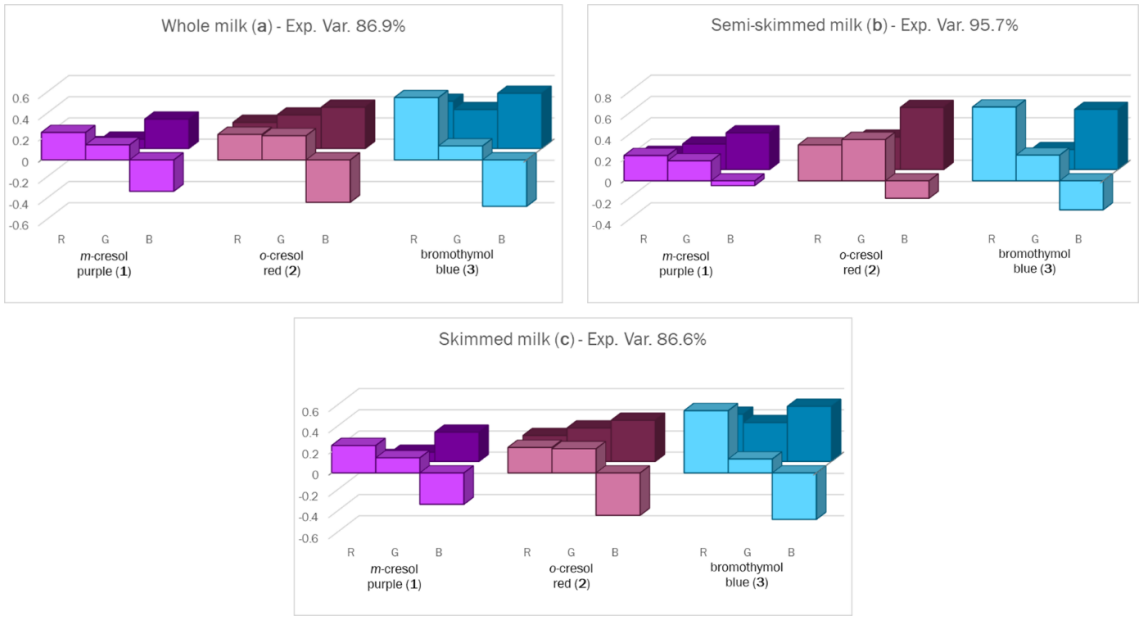

Figure 8.3: The loading plots of the PCA models on the first two principal components, for whole (a), semi-skimmed (b) and skimmed (c) milk. The loading values on PC1 are in the foreground, the ones on PC2 in the background.

8.3.3 EVOH (29%)-based devices

BCP-EVOH@ thickness selection: loading plot

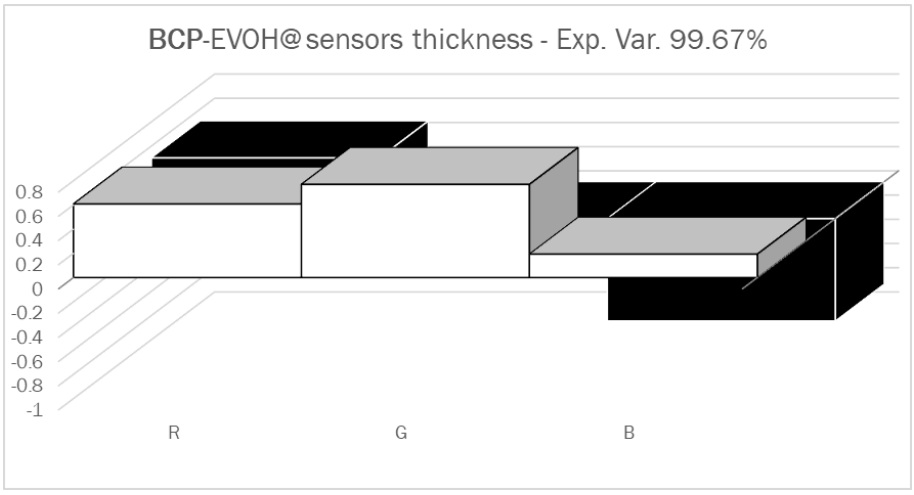

Figure 8.4: The loading plots of the PCA model on the first two principal components, built on the training set, for BCP-EVOH@ sensors thickness selection. The loading values on PC1 are in the foreground, the ones on PC2 in the background.

Protein foods spoilage modelling: loading plots

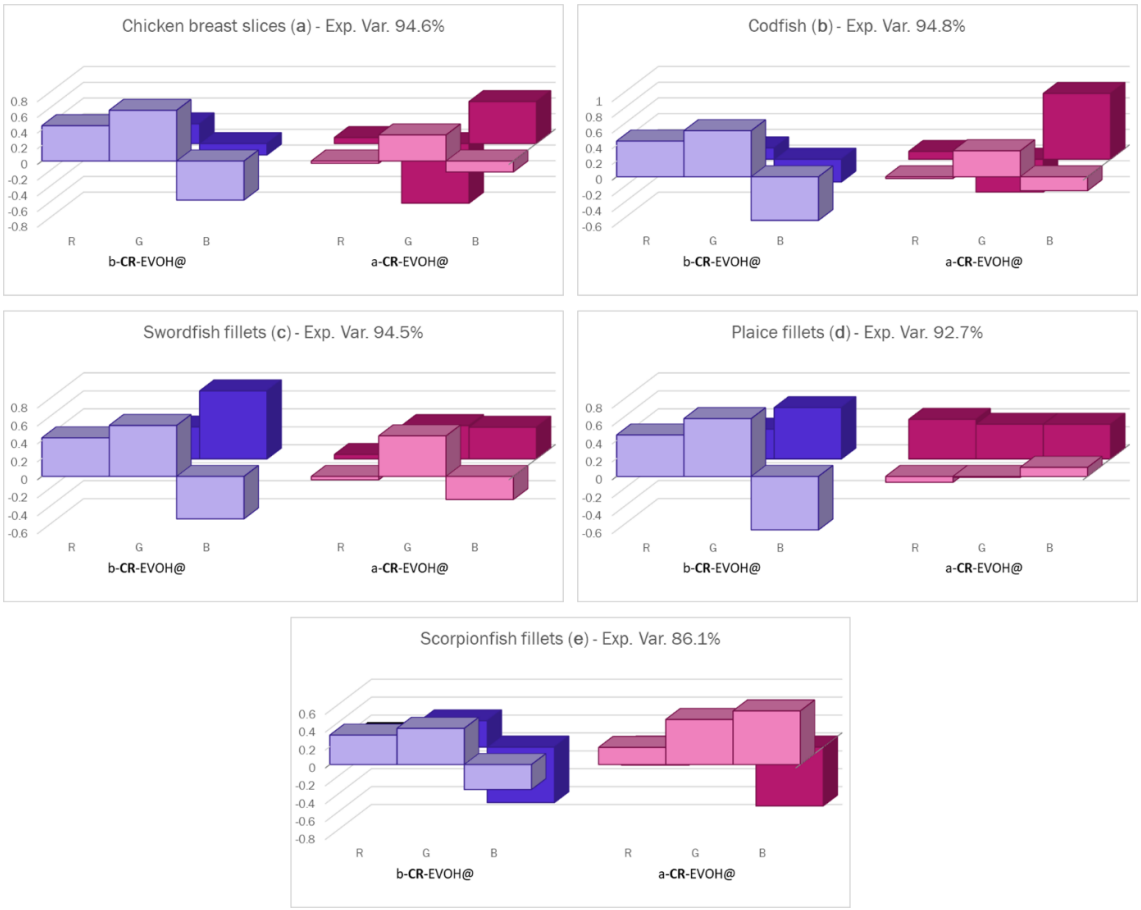

Figure 8.5: The loading plots of the PCA models on the first two principal components, built on the training set for chicken breast slices (a), codfish fillets (b), swordfish fillets (c), plaice fillets (d) and scorpionfish fillets (e). The loading values on PC1 are in the foreground, the ones on PC2 in the background.

Protein foods spoilage modelling: score plots

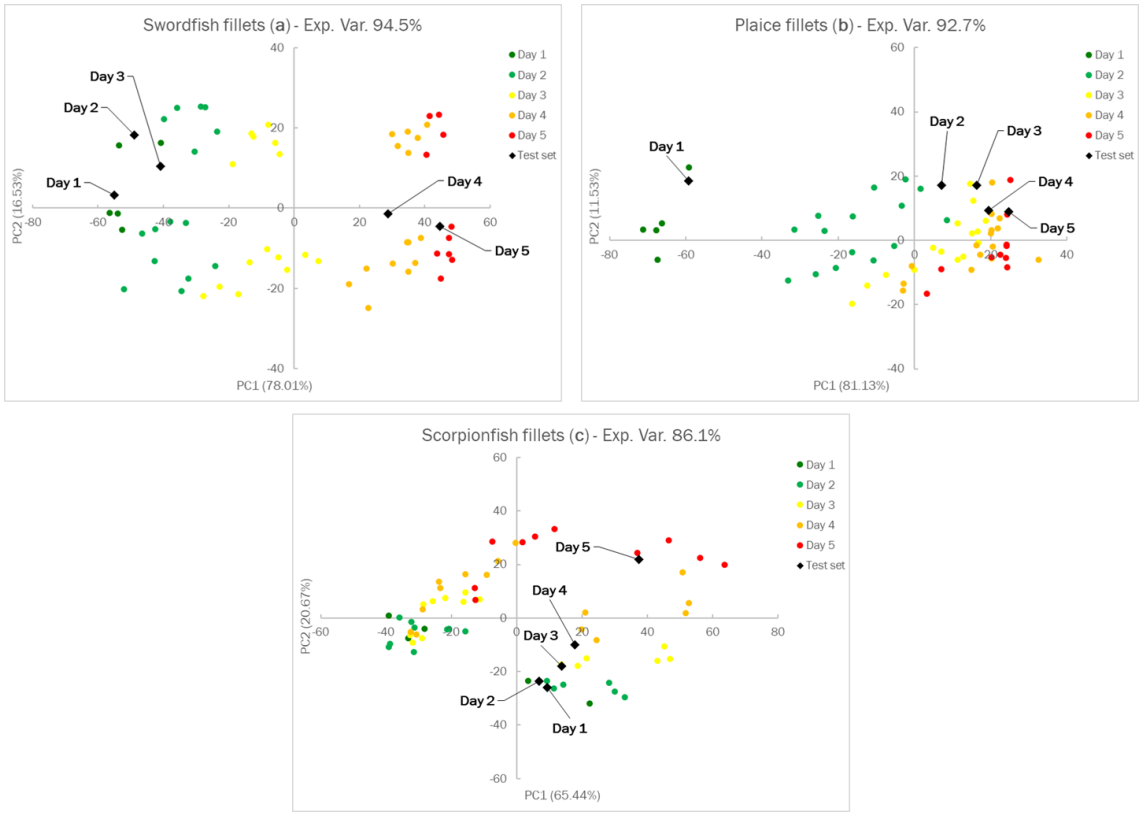

Figure 8.6: The score plots of the PCA models on the first two principal components, built on the training set and validated by projection of the test set, for swordfish fillets (a), plaice fillets (b) and scorpionfish fillets (c).

Milk spoilage modelling: loading plots

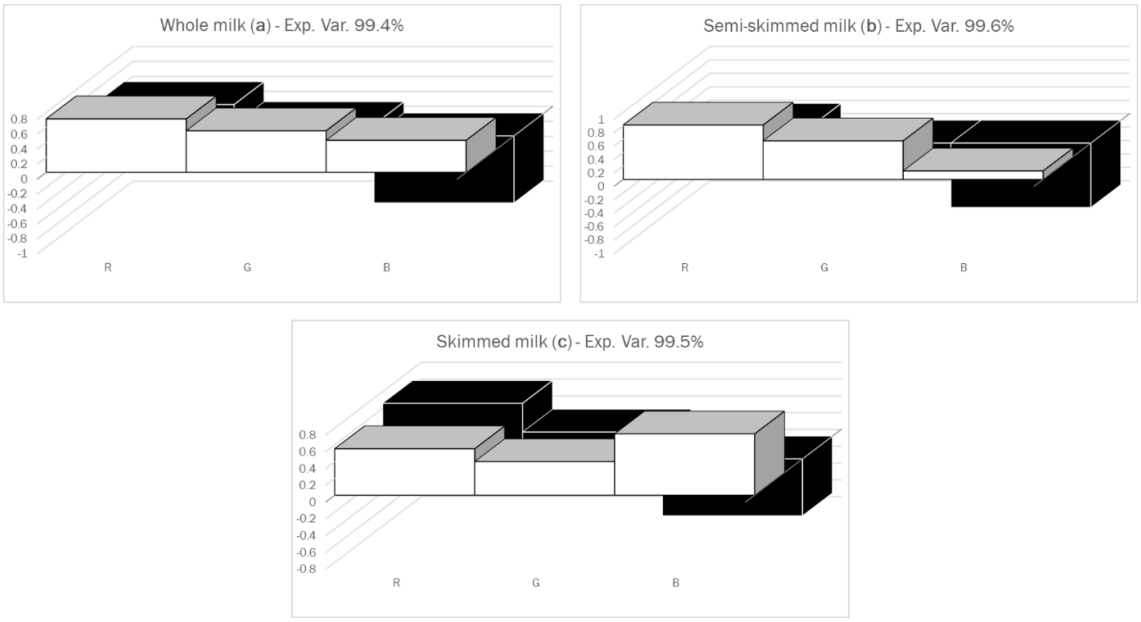

Figure 8.7: The loading plots of the PCA models on the first two principal components, for whole (a), semi-skimmed (b) and skimmed (c) milk. The loading values on PC1 are in the foreground, the ones on PC2 in the background.

Milk spoilage modelling: score plots

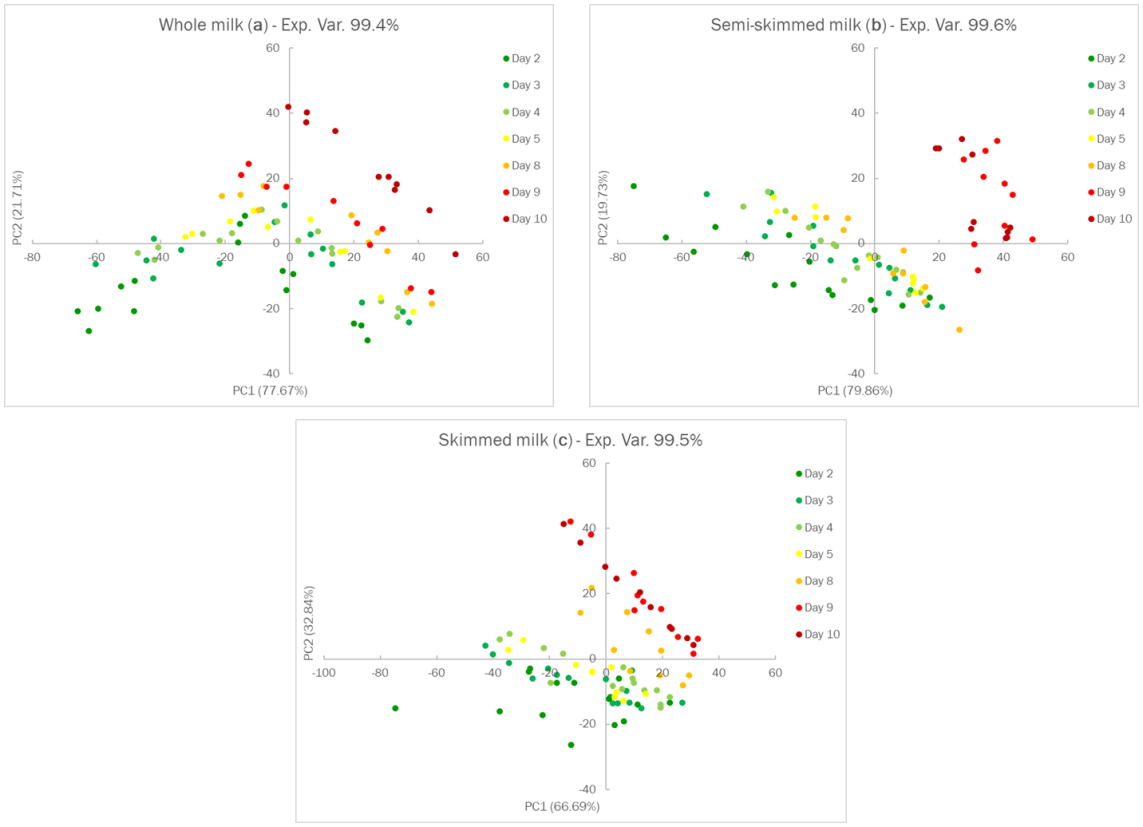

Figure 8.8: The score plots of the PCA models on the first two principal components, for whole (a), semi-skimmed (b) and skimmed (c) milk.

8.3.4 CMC-based devices

Protein foods spoilage modelling: loading plots

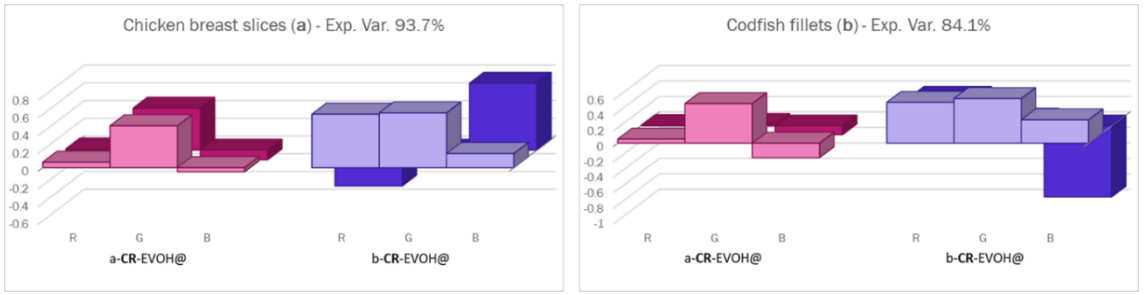

Figure 8.9: The loading plots of the PCA models on the first two principal components, built on the training set for chicken breast slices (a) and codfish fillets (b). The loading values on PC1 are in the foreground, the ones on PC2 in the background.

8.4 Appendix IV: Experiments lists

8.4.1 Dye-EVOH@ pressing procedure optimisation

Table 8.1 : Experimental matrix for Dye-EVOH@ pressing procedure optimisation and responses collected per each experiment

Experiment	Variables				Responses	
	x_1	x_2	x_3	x_4	y_1	y_2
1	1	1	1	1	4	25
2	-1	1	1	1	3	22
3	1	-1	1	1	3	20
4	-1	-1	1	1	3	18
5	1	1	-1	1	1	6
6	-1	1	-1	1	3	9
7	1	-1	-1	1	3	0
8	-1	-1	-1	1	3.5	14
9	1	1	1	-1	4.5	29
10	-1	1	1	-1	5	23
11	1	-1	1	-1	5	31
12	-1	-1	1	-1	4.5	19
13	1	1	-1	-1	4	12
14	-1	1	-1	-1	4.5	14
15	1	-1	-1	-1	2	9
16	-1	-1	-1	-1	4	19

8.4.2 Dye-CMC@ drop-casting deposition optimisation

Table 8.2 : Experimental matrix for Dye-CMC@ drop-casting deposition optimisation and response collected per each experiment

Experiment	Variables				Response
	x_1	x_2	x_3	x_4	y_1
Aa	-1	-1	-1	A	0.129
Ab	1	-1	-1	A	0.176
Ac	-1	1	-1	A	0.102
Ad	1	1	-1	A	0.082
Ae	-1	-1	1	A	0.047
Af	1	-1	1	A	0.174
Ag	-1	1	1	A	-0.011
Ah	1	1	1	A	0.015
Ba	-1	-1	-1	B	0.183
Bb	1	-1	-1	B	0.227
Bc	-1	1	-1	B	-0.042
Bd	1	1	-1	B	-0.087
Be	-1	-1	1	B	-0.185
Bf	1	-1	1	B	0.043
Bg	-1	1	1	B	-0.284
Bh	1	1	1	B	-0.200
Ca	-1	-1	-1	C	0.036
Cb	1	-1	-1	C	0.071
Cc	-1	1	-1	C	-0.081
Cd	1	1	-1	C	-0.092
Ce	-1	-1	1	C	-0.292
Cf	1	-1	1	C	-0.150
Cg	-1	1	1	C	-0.419
Ch	1	1	1	C	-0.281
Da	-1	-1	-1	D	0.108
Db	1	-1	-1	D	0.233
Dc	-1	1	-1	D	-0.016
Dd	1	1	-1	D	0.173
De	-1	-1	1	D	0.158
Df	1	-1	1	D	0.275
Dg	-1	1	1	D	-0.102
Dh	1	1	1	D	0.248

8.4.3 CR-CMC@ film casting deposition optimisation

Candidate points matrix

Table 8.3 : Candidate points matrix for CR-CMC@ film casting deposition optimisation

Experiment	Variables				
	x_1	x_2	x_3	x_4	x_5
1	1	0	0	0	A
2	0	1	0	0	A
3	0	0	1	0	A
4	0.5	0.5	0	0	A
5	0.5	0	0.5	0	A
6	0	0.5	0.5	0	A
7	0.33	0.33	0.33	0	A
8	1	0	0	1	A
9	0	1	0	1	A
10	0	0	1	1	A
11	0.5	0.5	0	1	A
12	0.5	0	0.5	1	A
13	0	0.5	0.5	1	A
14	0.33	0.33	0.33	1	A
15	1	0	0	0	B
16	0	1	0	0	B
17	0	0	1	0	B
18	0.5	0.5	0	0	B
19	0.5	0	0.5	0	B
20	0	0.5	0.5	0	B
21	0.33	0.33	0.33	0	B
22	1	0	0	1	B
23	0	1	0	1	B
24	0	0	1	1	B
25	0.5	0.5	0	1	B
26	0.5	0	0.5	1	B
27	0	0.5	0.5	1	B
28	0.33	0.33	0.33	1	B
29	1	0	0	0	C
30	0	1	0	0	C
31	0	0	1	0	C
32	0.5	0.5	0	0	C
33	0.5	0	0.5	0	C

34	0	0.5	0.5	0	C
35	0.33	0.33	0.33	0	C
36	1	0	0	1	C
37	0	1	0	1	C
38	0	0	1	1	C
39	0.5	0.5	0	1	C
40	0.5	0	0.5	1	C
41	0	0.5	0.5	1	C
42	0.33	0.33	0.33	1	C
43	1	0	0	0	D
44	0	1	0	0	D
45	0	0	1	0	D
46	0.5	0.5	0	0	D
47	0.5	0	0.5	0	D
48	0	0.5	0.5	0	D
49	0.33	0.33	0.33	0	D
50	1	0	0	1	D
51	0	1	0	1	D
52	0	0	1	1	D
53	0.5	0.5	0	1	D
54	0.5	0	0.5	1	D
55	0	0.5	0.5	1	D
56	0.33	0.33	0.33	1	D

28-experiments D-Optimal Design solution

Table 8.4 : 28-experiments D-Oprimal Design solution for CR-CMC@ film casting deposition optimisation and response collected per each experiment

Experiment	Variables					Response
	x_1	x_2	x_3	x_4	x_5	y_1
4	0.5	0.5	0	0	A	1
5	0.5	0	0.5	0	A	1
6	0	0.5	0.5	0	A	1
8	1	0	0	1	A	0
9	0	1	0	1	A	1
10	0	0	1	1	A	1
14	0.33	0.33	0.33	1	A	0
16	0	1	0	0	B	1
17	0	0	1	0	B	1
18	0.5	0.5	0	0	B	1
19	0.5	0	0.5	0	B	1
22	1	0	0	1	B	0
27	0	0.5	0.5	1	B	1
28	0.33	0.33	0.33	1	B	0
29	1	0	0	0	C	1
31	0	0	1	0	C	1
35	0.33	0.33	0.33	0	C	1
37	0	1	0	1	C	1
39	0.5	0.5	0	1	C	0
40	0.5	0	0.5	1	C	0
41	0	0.5	0.5	1	C	0
43	1	0	0	0	D	0
44	0	1	0	0	D	1
48	0	0.5	0.5	0	D	1
49	0.33	0.33	0.33	0	D	0
52	0	0	1	1	D	0
53	0.5	0.5	0	1	D	1
54	0.5	0	0.5	1	D	0

8.5 Appendix V: Physicochemical measurements

8.5.1 EVOH and Dye-EVOH@ DSC profiles

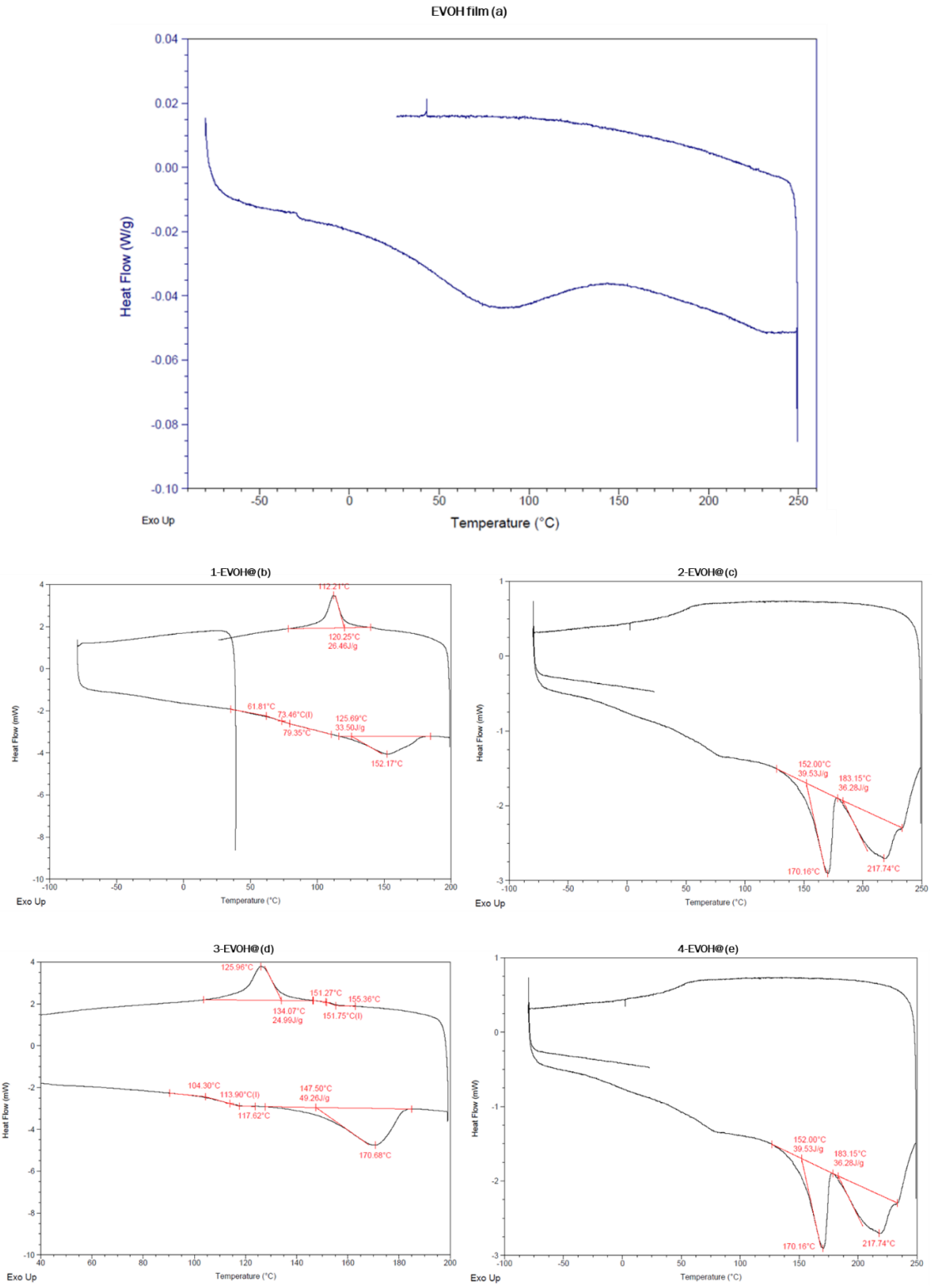

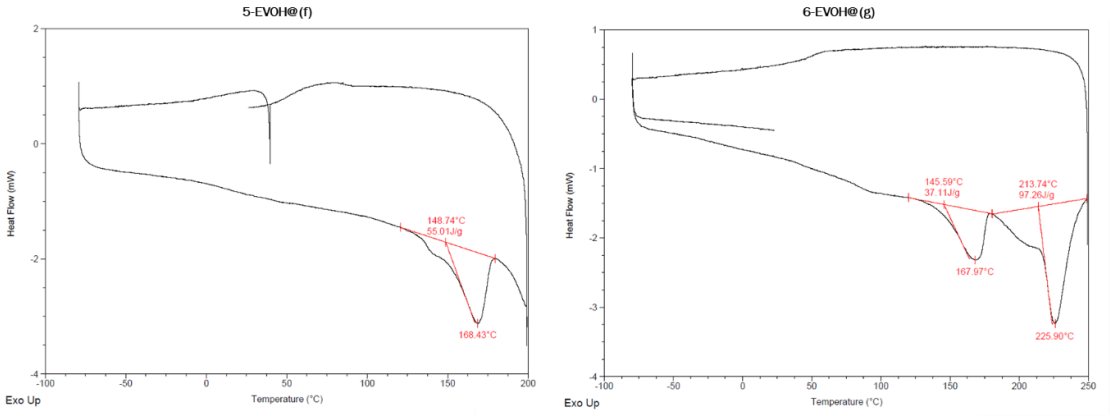

Figure 8.10: DSC profiles of EVOH (a), 1-EVOH@ (b), 2-EVOH, (c), 3-EVOH@ (d), 4-EVOH@ (e), 5-EVOH@ (f) and 6-EVOH@

8.5.2 EVOH, dyes and Dye-EVOH@ IR spectra

EVOH film (a)

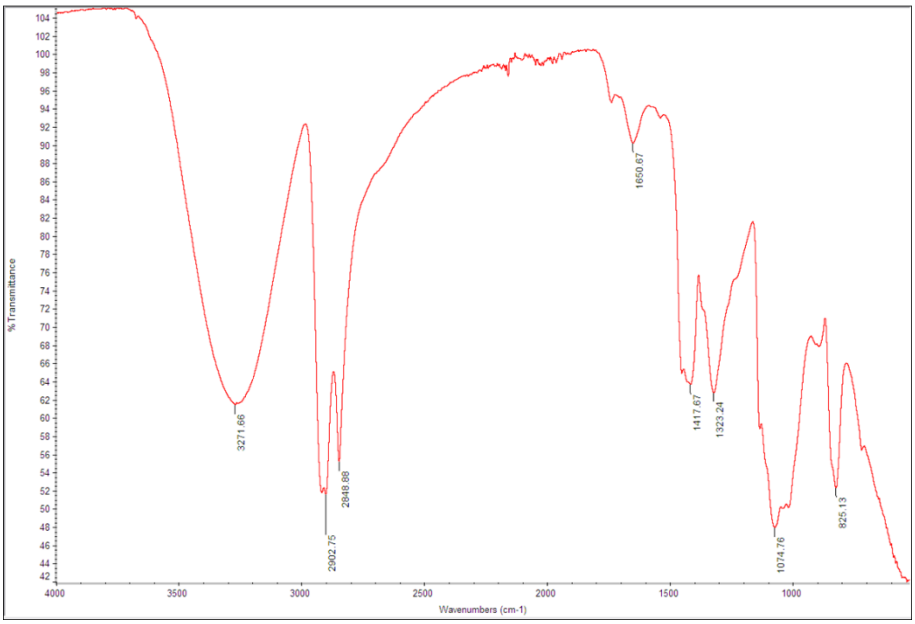

Dye 1 powder (b)

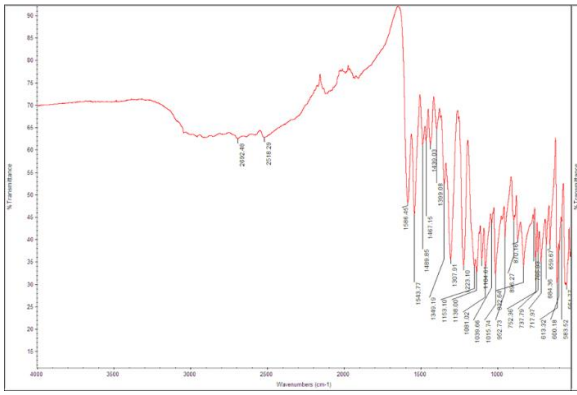

1-EVOH@film (c)

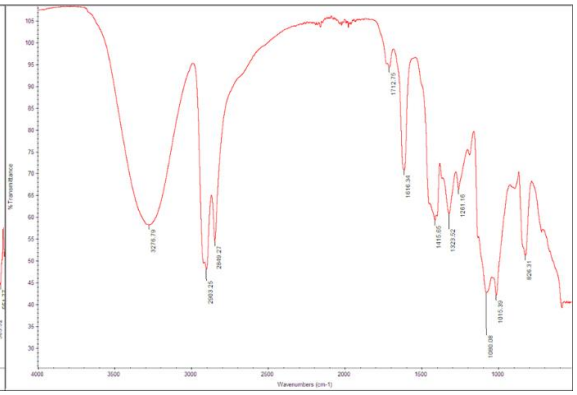

Dye 2 powder (d)

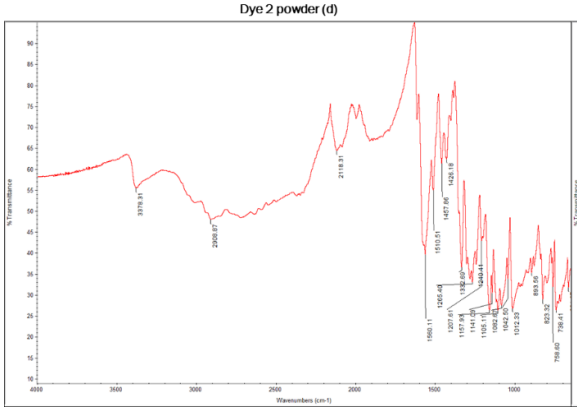

2-EVOH@film (e)

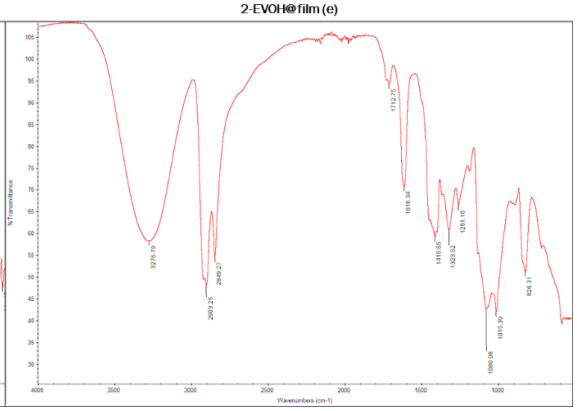

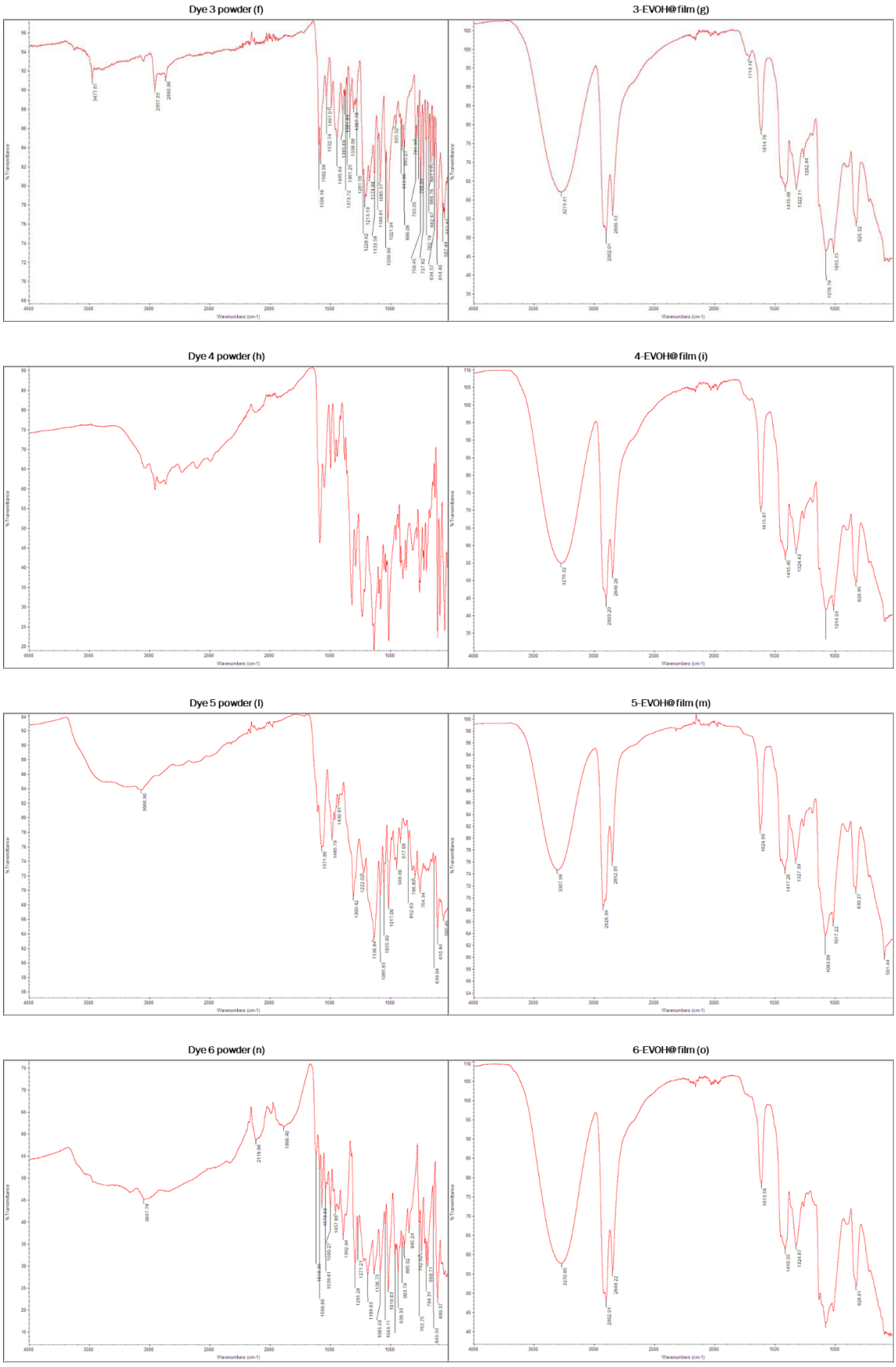

Figure 8.11: IR spectra of EVOH film (a), dye 1 in powder (b) and 1-EVOH@ film (c), dye 2 in powder (d) and 2-EVOH@ film (e), dye 3 in powder (f) and 3-EVOH@ film (g), dye 4 in powder (h) and 4-EVOH@ film (i), dye 5 in powder (l) and 5-EVOH@ film (m), dye 6 in powder (n) and 6-EVOH@ film (o).

8.5.3 CMC and CR-CMC@ DSC profiles

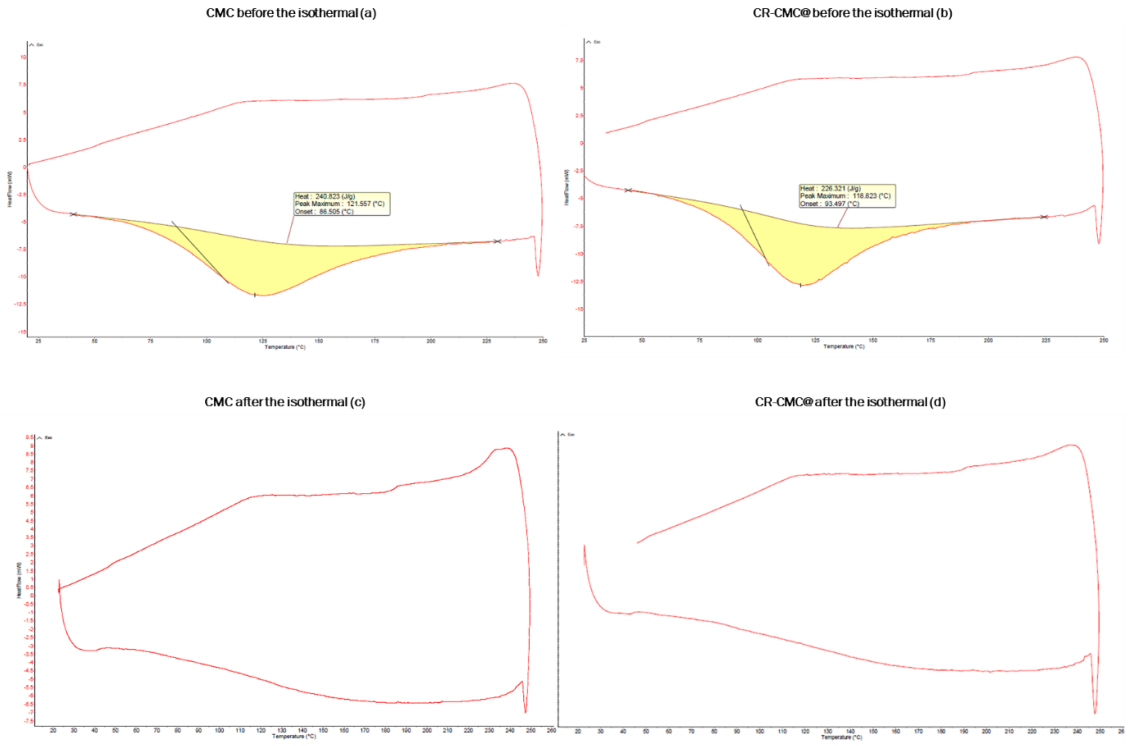

Figure 8.12: DSC profiles of CMC and CR-CMC@ before (a,b respectively) and after the isothermal (c,d)

8.5.4 CMC and CR-CMC@ IR spectra

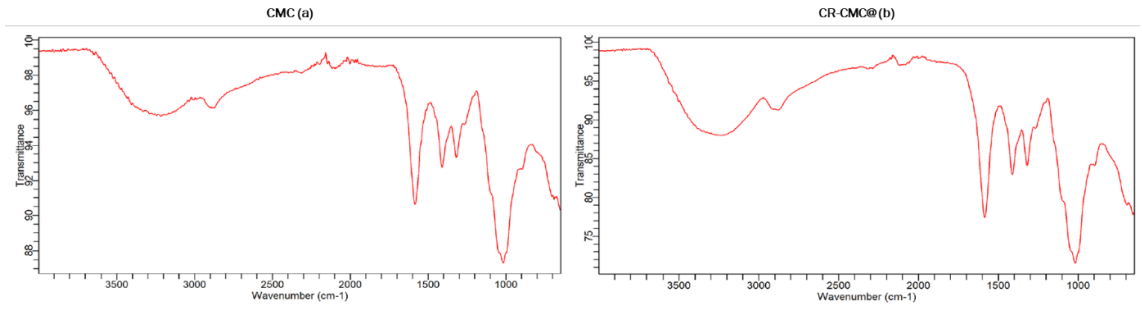

Figure 8.13:IR spectra of CMC (a) and CR-CMC@ (b)

8.6 Appendix VI: CR-EVOH@ sensors thickness selection

8.6.1 b-CR-EVOH@

Loading and score plots

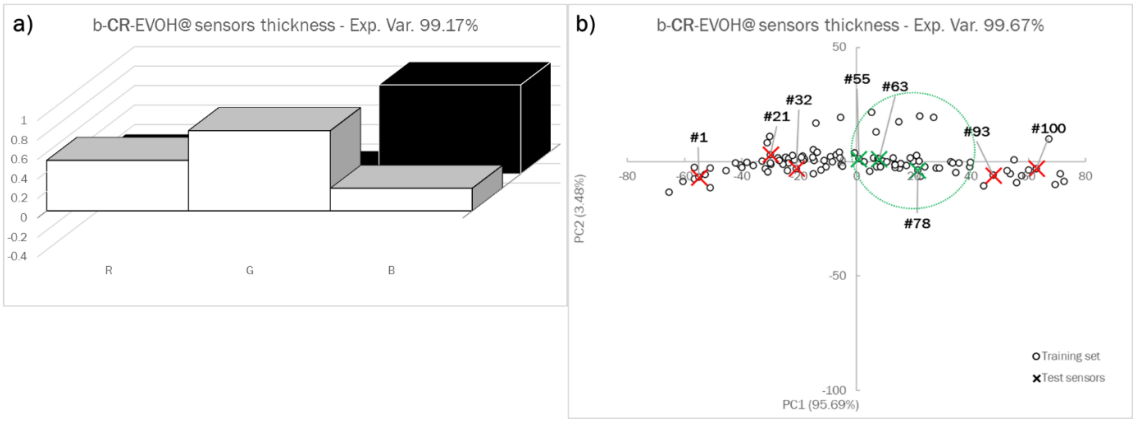

Figure 8.14: PCA loading (a) and score (b) plots on the first two components based on RGB triplets of 104 b-CR-EVOH@ sensors of various thicknesses (white circles); the sensors tested for real samples monitoring are highlighted with green and red x, and the suitable thickness range is identified by the green oval. The loading values on PC1 are in the foreground, the ones on PC2 in the background.

Pictures of b-CR-EVOH@ sensors ordered at increasing PC1 score

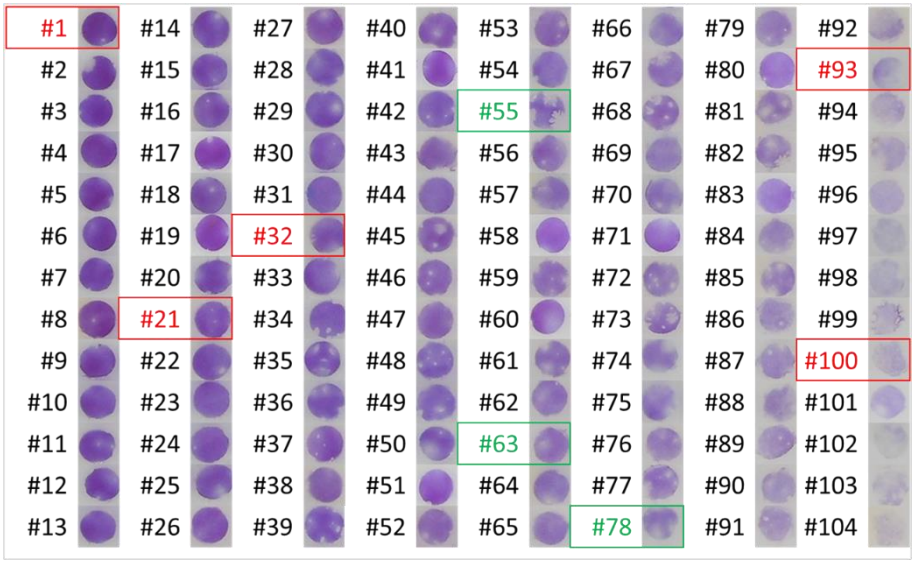

Figure 8.15: Pictures of the 104 sensors used to build the PCA model. The sensors tested for protein foods monitoring are highlighted in green and red.

8.6.2 a-CR-EVOH@

Loading and score plots

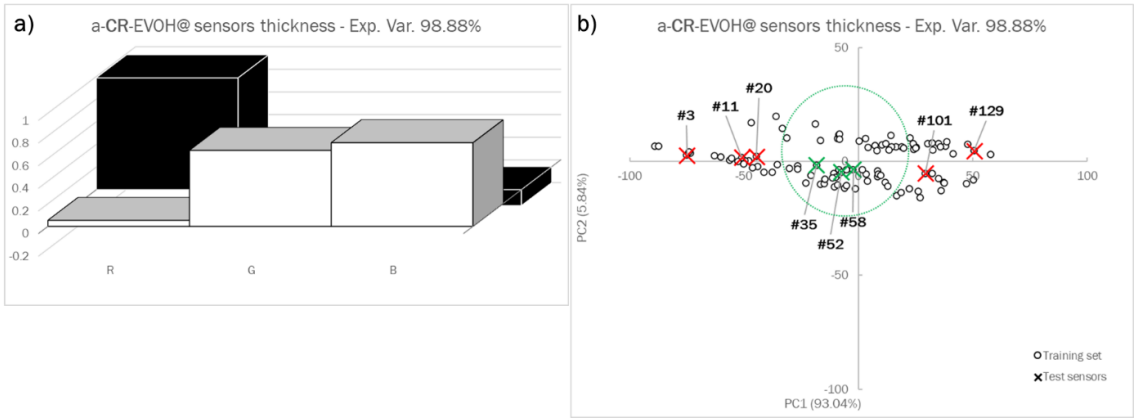

Figure 8.16: PCA loading (a) and score (b) plots on the first two components based on RGB triplets of 132 a-CR-EVOH@ sensors of various thicknesses (white circles); the sensors tested for real samples monitoring are highlighted with green and red x, and the suitable thickness range is identified by the green oval. The loading values on PC1 are in the foreground, the ones on PC2 in the background.

Pictures of a-CR-EVOH@ sensors ordered at increasing PC1 score

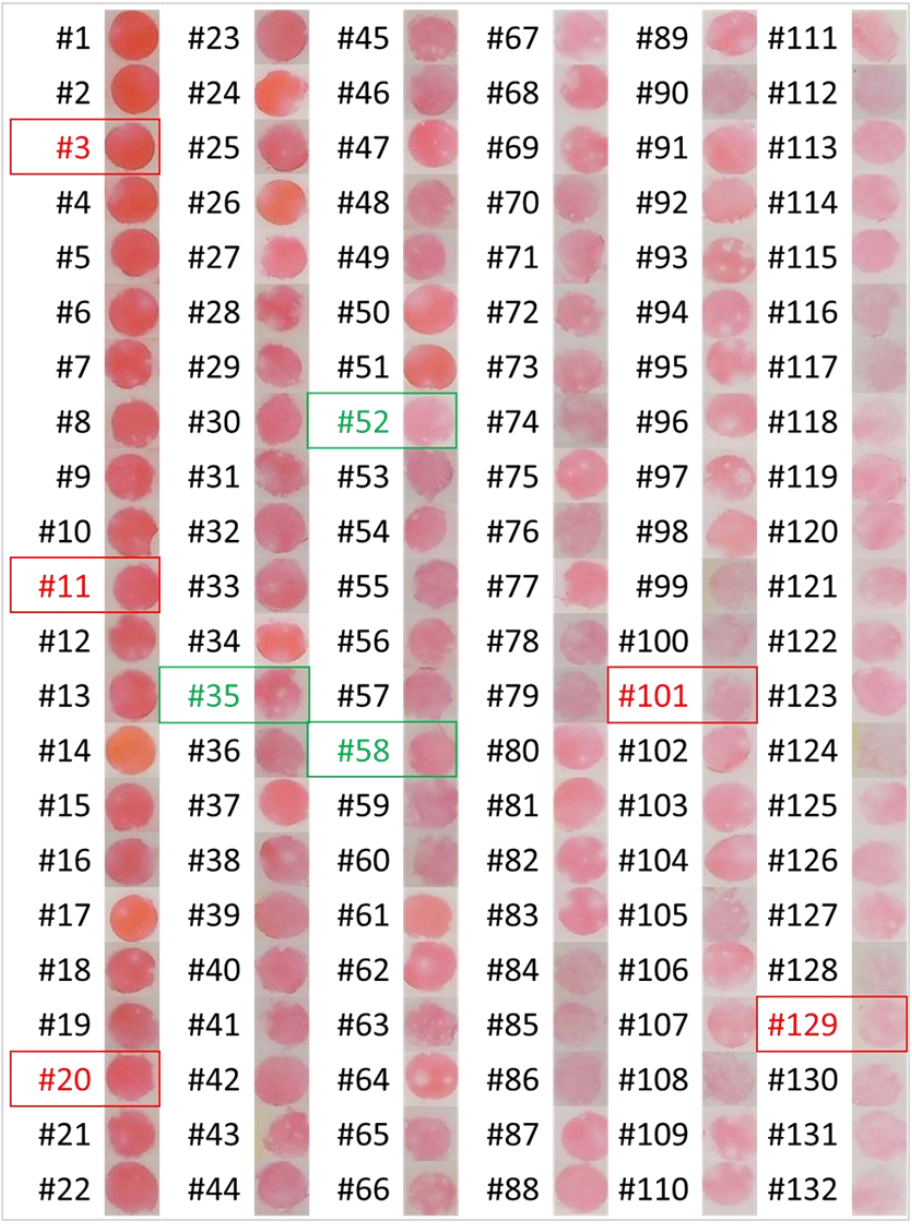

Figure 8.17: Pictures of the 132 sensors used to build the PCA model. The sensors tested for protein foods monitoring are highlighted in green and red.

9. Ringraziamenti